A theoretical and practical investigation of stress distribution in metal plates subject to various loads

A THEORETICAL AND PRACTICAL INVESTIGATION OF STRESS DISTRIBUTION IN METAL PLATES SUBJECT TO VARIOUS LOADS

by

G.M.S. GORDON

THESIS Submitted in partial fulfilment of the requirements for the award of Master of Technology of Loughborough University of Technology

SUPERVISORS J.N. Butters, Ph.D., A.Inst.P., Reader, Loughborough University of Technology

B.P. Helownia, M.Sc., Lecturer, Loughborough University of Technology

November, 1969

Copy Number 3.

ABSTRACT

Dynamic relaxation is used to calculate the stress distribution in a flat plate with a small circular hole at the centre and loaded by forces in the plane of the plate. The results are compared with those of an analytical solution. The deflection of a flat circular plate, simply supported, under transverse loading is measured using holographic interferometry. The deflection and stress distribution in the plate is determined using dynamic relaxation. The holographic and dynamic relaxation results are compared with an analytical solution. The methods and procedures used to analize these simple objects, are extended to the analysis of a geometrically complex plate; the plate is a flame plate from a large diesel engine.

TABLE OF CONTENTS

Appendices Page

SYMBOLS

a	constant
b	constant
c	velocity of normal-stress wave propagation, in./sec.
d	displacement vector, inches
E	modulus of elasticity, lb./in.^{2}
g	gravitational constant, in./sec.^{2}
G	shear modulus, lb./in.^{2}
I,J,K	subscripts denoting spatial location
k	damping constant
k_{cr}	critical damping constant
L	constant
p,q	normal-stresses on a boundary, lb./in.^{2}
r	iterative time step, radius, inches
$t, \Delta t$	time, time increment, seconds
T	temperature or temperature difference, $^\circ$F
u,v,w	resolved components of displacement vector "d"
$\dot{u},\dot{v},\dot{w}$	velocity, in./sec.
r,θ,z	cylindrical coordinates
x,y,z	rectangular coordinates
λ,μ	Lame' constants, lb./in.^{2}
λ	wavelength of light, He-Ne = 6328Å
ν	Poisson's ratio
α	coefficient of linear thermal expansion, in./in./$^\circ$F
ω_n	fundamental frequency of vibration, radians/sec.
ϕ',ϕ	angles of viewing and illumination relative to the surface
θ',θ	angles of viewing and illumination relative to the displacement vector "d"
σ	normal stress, lb./in.^{2}
ϵ	normal strain, in./in.
τ	shear stress, lb./in.^{2}
γ	shear strain, in./in.
ρ	mass density lb-sec^2/in^4

INTRODUCTION

In this thesis, the stress distribution in a water cooled flame plate from a large diesel engine is investigated. The engine is a recent development of Ruston-Hornsby Limited, Lincoln, England and is capable of developing 500 horse-power per cylinder. The flame plate is essentially a flat, thin, circular plate which is complicated by valve ports, fuel injector hole, and internal cooling passages. In addition to being geometrically three dimensional, the plate is subject to complex thermal gradients in three dimensions and thus a three dimensional analysis is required.

The geometry of the plate lends itself to a cylindrical coordinate system and thus the problem is to obtain a solution of the following partial differential equations.

$$\frac{\partial \sigma_r}{\partial r} + \frac{1}{r}\frac{\partial \tau_{r\theta}}{\partial \theta} + \frac{\partial \tau_{rz}}{\partial z} + \frac{\sigma_r - \sigma_\theta}{r} = 0$$

$$\frac{\partial \tau_{r\theta}}{\partial r} + \frac{1}{r}\frac{\partial \sigma_\theta}{\partial \theta} + \frac{\partial \tau_{z\theta}}{\partial z} + 2\frac{\tau_{r\theta}}{r} = 0$$

$$\frac{\partial \tau_{rz}}{\partial r} + \frac{1}{r}\frac{\partial \tau_{z\theta}}{\partial \theta} + \frac{\partial \sigma_z}{\partial z} + \frac{\tau_{rz}}{r} = 0$$

The solution of the above equations which define equilibrium, must also satisfy the following thermo-elasticity equations.

$$\sigma_r = (\lambda+2\mu)\frac{\partial u}{\partial r} + \lambda\frac{u}{r} + \frac{\lambda}{r}\frac{\partial v}{\partial \theta} + \lambda\frac{\partial w}{\partial z} - (\lambda+2\mu)\alpha T$$

$$\sigma_\theta = (\lambda+2\mu)\frac{1}{r}\frac{\partial v}{\partial \theta} + (\lambda+2\mu)\frac{u}{r} + \lambda\frac{\partial u}{\partial r} + \lambda\frac{\partial w}{\partial z} - (\lambda+2\mu)\alpha T$$

$$\sigma_z = (\lambda+2\mu)\frac{\partial w}{\partial z} + \lambda\frac{\partial u}{\partial r} + \frac{\lambda}{r}\frac{\partial v}{\partial \theta} + \lambda\frac{u}{r} - (\lambda+2\mu)\alpha T$$

$$\tau_{r\theta} = \mu\left(\frac{1}{r}\frac{\partial u}{\partial \theta} - \frac{v}{r} + \frac{\partial v}{\partial r}\right)$$

$$\tau_{rz} = \mu\left(\frac{\partial u}{\partial z} + \frac{\partial w}{\partial r}\right)$$

$$\tau_{z\theta} = \mu\left(\frac{\partial v}{\partial z} + \frac{1}{r}\frac{\partial w}{\partial \theta}\right)$$

Generally, these equations can only be solved analytically in cases where the geometry of the object and of the loading and support configuration is simple. For geometrically complex objects or loading conditions, numerical and/or experimental methods must be used.

In formulating the problem for solution by numerical methods, certain simplifying assumptions may have to be made to the geometry of the object or to the loading or support configurations and as a result the accuracy of the results may be questionable. In such cases, it is considered good practice to accompany a numerical solution with an experimental solution or at least with a few experimental values with which one can compare the theoretical or numerical solution and estimate the credibility of the numerical solution. The experimental work need not be carried out under the actual working conditions of the object as for example in the case of the flame plate being investigated in this thesis, it was not considered feasible to attempt to simulate engine conditions in the laboratory nor was it considered feasible to attempt an experimental solution with the plate in "situ". It was however reasoned that if the plate could be analized both experimentally and theoretically under a set of conditions compatible with the engine conditions and if the results of both solutions agreed favourably with each other, then substituting the actual working conditions into the arithmetic of the theoretical solution should produce a set of results in which one could be confident.

The methods chosen for the analysis of the flame plate are dynamic relaxation and holographic interferometry. The method of dynamic relaxation is described in Chapter 1. with the aid of simple

examples and again in Chapter 3 by the analysis of a flat plate with a small circular hole at the centre and loaded by forces in the plane of the plate. The results are compared with those from an analytical solution.

In Chapter 4, the transverse deflection of a simply supported flat circular plate subject to a transverse mechanical load is determined using holographic interferometry and dynamic relaxation. Dynamic relaxation is also used to determine the stress distribution in the plate. The results of the holographic and dynamic relaxation analyses are compared with the results from an analytical solution.

In Chapter 5, the procedures developed in the analysis of the geometrically simple objects described above, are extended to the analysis of the flame plate. The analysis of the flame plate is in two parts. The first part consists of a holographic and dynamic relaxation analysis of the flame plate under a transverse mechanical load. Using the holographic results as a basis for comparison, the dynamic relaxation solution was refined to improve the accuracy. The second part of the analysis consists of substituting the engine or working conditions of the plate into the arithmetic of the dynamic relaxation solution. The temperature distribution in the plate which constitutes the thermal loading in the plate was determined by dynamic relaxation; however the temperature information available for the thermal analysis is somewhat limited hence the results are questionable.

In Chapter 6, on the basis of the overall work done throughout this thesis, comments and conclusions with regard to accuracy and application of the methods of dynamic relaxation and holographic interferometry are given. Suggestions for future work on the flame plate and for development of the methods of dynamic relaxation and holographic interferometry are given.

In the following section, preceding Chapter 1., a brief survey of current numerical and experimental methods is given.

SURVEY OF NUMERICAL AND EXPERIMENTAL METHODS

Numerical Methods

The numerical methods in current use for solving problems in elasticity can be classified into two groups namely finite difference methods and finite element methods. The finite difference methods will be dealt with first.

In general, a number of finite difference methods exist however with digital computers being a common place item to-day the number can be reduced to four. These are the Jacobi iterative, the Gauss-Siedel iterative, successive over relaxation, and more recently, dynamic relaxation. These methods are classed as follows:

1. Jacobi (J.I.) - simultaneous basic relaxation
2. Dynamic Relaxation (D.R.) - simultaneous accelerated relaxation
3. Gauss-Siedel (G.-S.) - successive basic relaxation
4. Successive Over Relaxation (S.O.R.) - successive accelerated relaxation.

These methods are compared by Otter and Hobbs in (3), again by Otter in (17), and by Wood in (18). In comparing these methods, the workers cited above looked at Poissons equation and compared the speed of convergence from a mathematical point of view. One might also compare the methods from a point of view of ease of application or ease of programming and accuracy. Until D.R. was developed, S.O.R. offered the best approach since it is much faster than G.-S. which in turn is faster than J.I., and is equally easily applied. Dynamic relaxation is slower than S.O.R. and G.-S. but faster than J.I. and appears to be more difficult to programme because of the introduction of

auxilliary variables, which is fundamental to the method of D. R. The introduction of auxilliary variables requires greater storage space in the computer however it does reduce the second order Laplace or Poisson equation to three first order equations. It would appear then that S.O.R. is still the best choice as far as Poisson's equation is concerned however from Otter's experience in solving the partial differential equations which arise in elasticity problems, it is much simpler to use D.R. than S.O.R. and since S.O.R. is essentially derived from J.I. and G.-S. the same holds true for these methods. The reason for D. R. being simpler to apply or to programme in the case of elasticity problems is that one is involved with first order equations which makes the boundary conditions easier to specify than in the case of using S.O.R. where one is involved with second order equations or fourth order equations if the problem is formulated in terms of stress functions.

No direct comparisons of D. R. and S.O.R. with regards accuracy were found in the literature however simple illustrations of D.R. being used to solve the stress distribution in a tension member (2), (3), and the stress distribution in a tension member with a stress concentration (4), show D.R. to give a high degree of accuracy. S.O.R. being a well established method is also reputed to give accurate results. The accuracy of both methods is perhaps not the real question but rather the accuracy of the application, or the assumptions which go into the formulation of the problem. In addition it goes without saying that the accuracy of numerical solution will be enhanced by the fineness of the mesh. Dynamic relaxation is compared with the method of finite elements in (19); both methods are in good agreement with each other.

While the speed of convergence of S.O.R. and D.R. have not yet been compared for elasticity problems, it is believed that S.O.R. will be the quicker, hence one is faced with making a choice between speed and simplicity. If one is completely unfamiliar with both methods, D.R. being the simpler method to apply, appears to be the most attractive and may initially prove to be the quicker method.

The Finite Element Method

The method of finite elements originated in the field of civil engineering in the analysis of structures and is considerably different in concept from the finite difference methods. In finite difference methods, the partial differential equations which define equilibrium and stress-strain relationships are written in finite difference form and solved numerically using an iterative procedure. The finite element method does not seek a solution to these equations but rather to solve a set of simultaneous equations which have been formulated on the basis of the stiffness of the elements, into which the object has been divided, the displacement of the node points of the elements, and the forces which act at the node points of the elements. In the case of a structure this usually means solving the expression:

$$d = K^{-1} p$$

where "d" is the displacement vector of the node points, "p" is the force vector at the node points, and, "K" is the stiffness matrix of the elements.

The above procedure has been extended to continuous structures or elasticity problems and takes the form:

$$\sigma = Kd$$

For stress analysis, the stiffness matrix is formulated on the basis of energy methods, i.e. by equating the external work done on an element to the internal energy stored by the element. In order to determine the internal energy stored by the element, the strain or stress distribution within the element is assumed to be a function of the displacements at the node points and the geometry of the element.

In the finite element method, one is not confined to element shapes which are dictated by the coordinate system used as is the case in finite difference methods and one can take advantage of such element shapes as triangular, octagonal, rhombic, etc. The use of different shape elements often allows a better approximation to be made to the boundaries of an object. For example in the case of an object which

has both curved and straight boundaries which do not conveniently coincide with a conventional coordinate system, triangular elements can be made to fit the boundaries more closely than say rectangular or truncated triangles which result from rectangular coordinates and polar coordinates respectively.

The greatest difficulty in applying the method of finite elements is the formulation of the stiffness matrix and in practice this is usually left to the computer; programmes have been written such that one need only input the coordinates of the node points after having chosen the shape of the elemnts and having appropriately divided the object up into elements.

Without actually investigating the method of finite elements in detail and actually using it to solve a proble, one cannot competantly compare the method with finite difference methods and few comparisons were found in the literature. One comparison found, (19), looked at the accuracy of a finite element solution and a dynamic relaxation solution of an arch dam problem and as previously mentioned the two methods compared favourably with each other. Rushton, in (4), states that for the particular problem of the analysis of a stress concentration in a notched plate, the method of finite differences would be more accurate than a finite element solution and would be much simpler to programme.

In summarizing, it might be reasonable to assume that those who have a civil engineering background and who are experienced in matrix solutions of structural problems might choose the finite element method and those with a mechanical engineering background faced with the solution of partial differential equations might choose a finite difference method. It might also be assumed that no matter which method is chosen, the accuracy of the solution will depend on how well the method is applied.

Experimental Methods

A number of experimental methods have been developed and many books have been written on the subject. The job of the analyst

is to select the method or methods best suited to the problem at hand and in some cases prescribe a set of experiments from which useful information may be obtained. The name experimental stress analysis is somewhat of a misnomer since it implies that one measures stress and in practice one is involved in measuring displacements which when averaged over a finite distance give strains from which one can calculate stresses.

The methods available can be classified in two groups namely point methods and whole field methods. As the names imply, point methods give information at discrete points on the surface of the object while whole field methods give information over a large area of the surface. Point methods are confined to various forms of strain gauges; the electrical resistance type being the most widely used. Whole field methods include brittle coatings, grids, Moire' fringe, photoelasticity, and recently, holographic interferometry.

Electrical resistance strain gauges are designed to measure in-plane surface strains or average displacements over a gauge length. Gauge lengths of 0.2" to 2.0" are readily available. Under laboratory conditions, strains as low as 5 ~~micro-strains~~ microstrain can be accurately measured and special gauges are manufactured which can measure plastic deformations or strains in the region of 200,000 ~~micro-strains~~ microstrain. Temperature compensated gauges which exhibit low sensitivity to temperature change are available for use in thermal stress problems. To determine the magnitude and direction of the principal strains requires the use of at least three gauges; these are usually a combined gauge called a rosette. No information regarding the displacements normal to the surface of the object can be obtained from strain gauges unless the relationship between the normal displacements and the in-plane strain is known.

Generally, brittle coating methods give only the direction and relative magnitude of the principal strains and as with strain gauges, give no information regarding normal displacements of the surface. Brittle coating methods are often used in conjunction with strain gauges as an indicator of the location of stress concentration and as a guide for positioning the strain gauges.

Grid methods are used in cases where the displacements are

large for example in deep drawing operations; a coarse grid is applied to the object before the drawing operation. Grids are also used in analizing objects made from rubber and such like material.

The Moire' fringe method involves applying a high density grid to the surface of the object (100 to 2000 lines per inch). The grid on the surface of the object is aligned with a master grid located between the object and the observer. When the object is strained, the two grids are no longer in alignment and a fringe pattern is formed which is representitive of the displacements in the plane of the surface of the object. The fringes are loci of points having constant displacement. To determine the principal strains, the experiment has to be repeated with the grid on the surface of the object at different angles relative to the surface. Two or three patterns are required which can be differentiated to give the in-plane normal strains and shear strain or three in-plane normal strains respectively.

Measurement of normal or flexural displacements is possible with the Moire' but in general, the displacements must be large hence models are made from perspex or such like material which has a low modulus of elasticity. The method of measuring flexural displacements involves reflection of a grid off the surface of the object and making a double exposure photograph of the surface one before and one after the load has been applied.

Photoelasticity methods involve passing polarized light through a model of the object which is made from a photoelastic material. When the object is strained, the refractive index of the material is altered in accordance with the magnitude of the strain and interference fringes are formed on the projected image of the object. Two types of fringes are formed depending on the set-up used in the experiment. One type of fringe, referred to as an isoclinic, represents the loci of points having constant inclination or direction of principal strain. The second type of fringe referred to as an isochromatic, represents the loci of points having constant shear strain or difference of the two pricipal strains. Determination of the principal stresses at a free boundary is quite simple however for points inside the boundaries, determination of the principal stresses is much more difficult and requires the measurement of the change of thickness

of the object. The above description applies to plane stress problems. Three dimensional problems can be solved however the procedure is quite complicated and difficult. In three dimensional problems, a technique referred to as the frozen stress technique is used. This involves loading the object while at an elevated temperature and while maintaining the load, the object is allowed to cool thus as it were freezing the stress in. Slices are cut from the object and analized in a manner similar to a plane stress problem. Like strain gauges and brittle coating, no information can be obtained regarding normal or flexural displacements unless the relationship between the normal displacements and the in-plane strains is known.

Holographic interferometry offers an extremely sensitive and simple method ideally suited to the measurement of normal or flexural displacements. Very little work has been done in applying holographic interferometry to the measurement of in-plane displacements although a number of methods have been proposed. These methods will be investigated in this thesis.

In selecting a suitable experimental method, one might begin by deciding whether point or whole field information is required. Obviously whole field methods provide a more complete picture of the stress distribution on the surface of the object or of the deflected shape of the object however if one has a before hand knowledge of the stress distribution and requires only a few specific values to complete the analysis quantitatively, then point measurements may suffice.

A second consideration to be made is whether or not one can work directly on the part or is a model required. If a three dimensional analysis is required, then usually a model is required in which strain gauges can be imbedded or a photoelastic model is required with which one can apply frozen stress techniques. A model may also be required if the actual object is too large to accomodate in the laboratory or in the early design stages when the actual component is not available and an analysis is required to complete the design.

A third point to consider is whether or not the experimental solution will be the only solution or will it be used to collaborate a numerical or theoretical solution. If the experimental results are

to be used in support of a numerical solution, then it may not be neccessary for the experimental solution to be a detailed or complete solution. In such cases one may be more interested in the characteristics of the object. For example if the operating conditions under which the part is to function are too complex or too difficult to reproduce in the laboratory or the economics of producing them are prohibitive, then one might seek a numerical solution but at the same time require some experimental results with which to compare the numerical solution. It is inevitable that the numerical solution will be based on certain simplifying assumptions which will limit its accuracy hence it is good practice to accompany a numerical solution with some experimental results. One might reason that if the part is analized both numerically and experimentally using a set of conditions that are compatible with the actual operating conditions but easily produced in the laboratory, and the results of both analyses are in good agreement with each other, then substituting the actual conditions into the arithmetic of the numerical solution should produce a set of results in which one can be confident.

While each of the above experimental methods differ considerably in concept, their aim is the same which is to provide information from which one can calculate the magnitude and direction of surface stresses or in some cases to determine the deflected shape of an object. In general only surface stress information can be obtained however for many problems especially those which involve mechanical loads, the surface stresses are the largest stresses in the object hence one can neglect or not be concerned with internal stresses.

In summarizing, one might assert that experimental methods apply more to a specific type of problem, hence the experimental stress analyst must be skilled in all methods and may often have to resort to more than one method to obtain a set of useful results for a given problem.

CHAPTER ONE

DYNAMIC RELAXATION

1.1 Introduction

Dynamic relaxation was devised by A.S. Day at Rendel, Palmer and Tritton, Consulting and Designing Chartered Civil Engineers. Historically, the method evolved from calculations made in 1958-60 on tidal flow in the Thames estuary and in the North Sea. Since that time, the method has been extended by Day, Otter, et. al., to include stress analysis, (2)(3)(4), analysis of structures, (1), plate bending, (1)(5)(6), shell analysis, (7), and to solve problems in heat conduction, (2). Fundamentally, dynamic relaxation is a digital computer method of obtaining a numerical solution for a number of partial differential equations which arise in engineering problems. The prime requisite for the use of dynamic relaxation is a large core-storage digital computer.

This chapter describes the method of dynamic relaxation as it is applied to solving problems in stress analysis and heat conduction.

1.2 Application to Stress Analysis

To solve the partial differential equations which arise in problems of stress analysis, the stress-equilibrium equations are written in damped wave form. These damped wave equations are then written in finite difference form using centred differences. The stress-strain

equations are differentiated with respect to time to provide a form of coupling with the damped wave equations and then written in finite difference form using centred differences. The use of centred differences results in the variables being specified on an interlacing net in time and space. The finite difference equations, with known boundary conditions, can be solved using an iterative procedure and provide values of stress, velocity, and displacement at any point in the object and at any time. Since the procedure is based on using a damped wave equation for the stress equilibrium equation, the values obtained by the iteration process are made to converge to a steady state condition by the selection of a suitable damping constant and in particular, the rate of convergence has been found to be a maximum when the damping is slightly less than critical or dead beat, (2). A simple problem will serve to illustrate the formulation of the finite difference equations and the iteration procedure.

Figure (1.1) represents a simple rectangular cross section bar held at one end and loaded by a tensile force, which produces a stress on the free end of "p" lb./in.^{2} The stress-equilibrium equation for this problem is:

$$\frac{\partial \sigma_x}{\partial x} = 0 \tag{1.1}$$

Writing this expression in damped wave form gives:

$$\frac{\partial \sigma_x}{\partial x} = \rho \frac{\partial^2 u}{\partial t^2} + K \frac{\partial u}{\partial t} \tag{1.2}$$

Writing Eq. (1.2) in finite difference form gives:

$$\frac{\sigma_x^r(I) - \sigma_x^r(I-1)}{\Delta x} = \dot{u}^{r+1}(I)\left(\frac{\rho}{\Delta t} + \frac{K}{2}\right) - \dot{u}^r(I)\left(\frac{\rho}{\Delta t} - \frac{K}{2}\right) \tag{1.3}$$

In practice it is more convenient to write the damping term in Eq. (1.2), with no loss in generality, in the form $\rho K/\Delta t$ thus Eq. (1.3) becomes:

$$\frac{\sigma_x^r(I) - \sigma_x^r(I-1)}{\Delta x} = \frac{\rho}{\Delta t}\left[\dot{u}^{r+1}(I)\left(1+\frac{K}{2}\right) - \dot{u}^r(I)\left(1-\frac{K}{2}\right)\right] \tag{1.3a}$$

The stress-strain relationship for this case is:

$$\sigma_x = E \frac{\partial u}{\partial x} \tag{1.4}$$

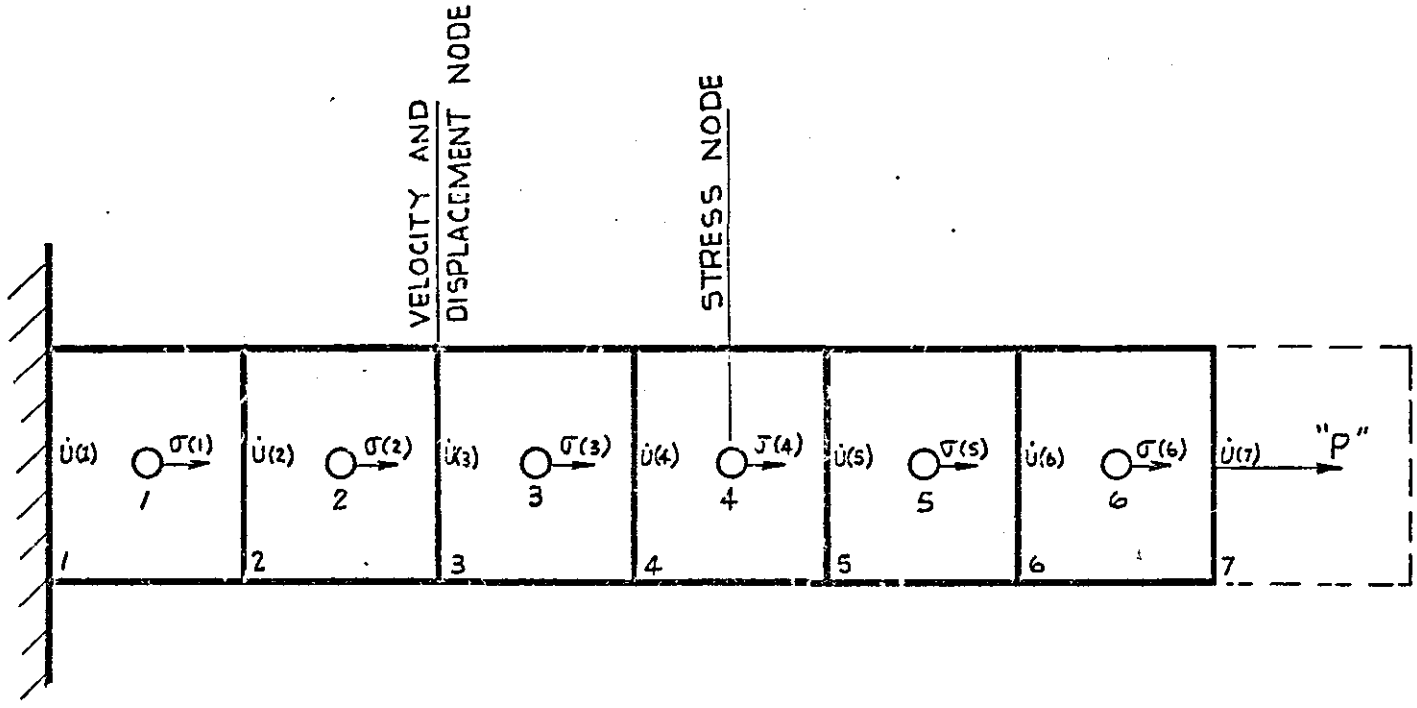
VELOCITY AND DISPLACEMENT NODE
STRESS NODE
$\dot{U}(1)$
$\sigma(1)$
1
$\dot{U}(2)$
$\sigma(2)$
2
$\dot{U}(3)$
$\sigma(3)$
3
$\dot{U}(4)$
$\sigma(4)$
4
$\dot{U}(5)$
$\sigma(5)$
5
$\dot{U}(6)$
$\sigma(6)$
6
$\dot{U}(7)$
"P"
1
2
3
4
5
6
7

FIGURE 1.1

Differentiating the stress-strain equation with respect to time gives:

$$\frac{\partial \sigma_x}{\partial t} = E \frac{\partial \dot{u}}{\partial x} \tag{1.5}$$

Writing Eq. (1.5) in finite difference form gives:

$$\frac{\overset{r+1}{\sigma_x}(I) - \overset{r}{\sigma_x}(I)}{\Delta t} = E \left[\frac{\overset{r}{\dot{u}}(I+1) - \overset{r}{\dot{u}}(I)}{\Delta x} \right] \tag{1.6}$$

Rearranging Eq's (1.3a) and (1.6), expressions for the new velocity and new stress value are obtained thus:

$$\overset{r+1}{\dot{u}}(I) = \overset{r}{\dot{u}}(I) \left[\frac{1 - K/2}{1 + K/2} \right] + \frac{\Delta t}{\rho(1+K/2)} \left[\frac{\overset{r}{\sigma_x}(I) - \overset{r}{\sigma_x}(I-1)}{\Delta x} \right] \tag{1.7}$$

$$\overset{r+1}{\sigma_x}(I) = \overset{r}{\sigma_x}(I) + E \Delta t \left[\frac{\overset{r}{\dot{u}}(I+1) - \overset{r}{\dot{u}}(I)}{\Delta x} \right] \tag{1.8}$$

The displacement at each mesh or node point is obtained by integrating the velocity with respect to time thus:

$$\overset{r+1}{u}(I) = \overset{r}{u}(I) + \overset{r+1}{\dot{u}}(I) \, \Delta t \tag{1.9}$$

In the above expressions, the subscript "I" refers to the position of the stress, velocity, or displacement in space and the superscript "r" refers to the postion in time.

Examining Eq. (1.7), a literal translation can be derived which states that " the new velocity is equal to the old velocity, multiplied by a term containing the damping constant, plus a velocity increment". The velocity increment is in the form of a force impulse (stress multiplied by the time interval) divided by the mass of the element and then multiplied by a term containing the damping constant. Similarily Eq. (1.8) can be stated as " the new stress is equal to the old stress plus a stress increment". The stress increment is simply the difference between the displacements at the two node points on either side of the stress node, divided by the length of the element, (the displacement being the velocity times the time interval) and then multiplied by the appropriate constant of elasticity. Looking at Eq. (1.7) again, it can be seen that as the velocity approaches zero,

the original equilibrium equation, Eq. (1.1), is satisfied.

As previously mentioned, the use of centred differences leads to the variables being specified on an interlacing net. This is illustrated in Fig. (1.1), and examining Eq'ns (1.7) and (1.8) a degree of physical significance in the equations can be observed. As shown in Fig. (1.1), the velocity and displacement node at the fixed end has been chosen to coincide with the boundary. Since Δx is constant then a velocity and displacement node occurs at the free end of the bar. In specifying the boundary condition at the fixed end the velocity at I = 1 is zero since the displacement is zero. The boundary condition at the free end is not so easily specified because the boundary coincides with the velocity and displacement node and the velocity and displacement are unknown. The stress at the boundary is known to be "p" however the stress at the first node point inside the boundary is not known. The stress on the end can be specified in terms of the stresses on each side of the boundary (the stress outside the boundary being imaginary or ficticious), by extrapolating linearly across the boundary thusly:

$$\sigma x(I-1) + \sigma x(I) = 2p \qquad (1.10)$$

In this expression , $\sigma x(I)$ is the ficticious stress outside the boundary. Adding $-2\sigma x(I-1)$ to both sides of Eq. (1.11) a term is obtained that can be substituted into the velocity equation.

$$\sigma x(I) - \sigma x(I-1) = 2\left(p - \sigma x(I-1)\right) \qquad (1.11)$$

Substituting Eq. (1.11) into Eq. (1.7), the velocity at the free end is:

$$\dot{U}(I) = \dot{U}(I)\left[\frac{1-K/2}{1+K/2}\right] + \frac{\Delta t}{\rho(1+K/2)} \cdot 2\left[\frac{p - \sigma x(I-1)}{\Delta x}\right] \qquad (1.12)$$

In this method of specifying the boundary condition at the free end the stress on the free end has been specified implicitly in the velocity equation and consequently for "N" velocity nodes there are N-1 stress nodes. The alternative method is to specify the ficticious stress in terms of the stress on the free end and the stress just inside the boundary. This means having "N" stress nodes instead of N-1 and consequently requires more storage space in the computer and

longer computer time.

For this simple problem, the stress nodes could have been chosen to coincide with the boundaries without any additional programming difficulties however in two and three dimensional problems it becomes more complicated to specify conditions on a boundary that coincides with a normal-stress node. This is because the shear stresses are specified on the corners of the mesh which forms a velocity node and in cases where one can take advantage of symmetry or in the case of a free surface, the shear stresses are zero and can be easily specified if the velocity node coincides with the boundary. Some further comments on specifying boundary conditions will be given in later chapters.

In addition to specifying the boundary conditions, the time increment, Δt, and the damping constant, "k", must be specified. The rate of convergence and hence the length of computer time required to obtain a solution, is dependant on both the time increment and the damping constant. In addition, the stability of the iterative process is dependant on the time increment.

The stability of the iterative process is based on the concept that the speed of the calculations, considered as a travelling wave, must be greater than the wave propagation in the actual physical problem. For stability, the following limit is applied to the time increment, (2).

$$\Delta t \leqslant \frac{\Delta X}{C} \tag{1.13}$$

In this expression, "c" is the speed of wave propagation in the physical problem and in the case of a one dimensional problem is given as:

$$C = \sqrt{\frac{E}{\rho}} = 2.02 \times 10^5 \text{ in./sec.} \quad \text{for steel} \tag{1.14}$$

For elasticity problems in more than one dimension, the speed of wave propagation is given by: (2)

$$C = \sqrt{\frac{\lambda+2\mu}{\rho}} = 2.35 \times 10^5 \text{ in./sec.} \quad \text{for steel} \tag{1.15}$$

Also, for problems in more than one dimension, the stability criterion

is given by: (2)

$$\Delta t \leq \frac{\Delta x}{c\sqrt{m}} \qquad (1.16)$$

where "m" is the number of dimensions of the problem. When the mesh size is not equal in all directions, the stability criterion is given by: (3)

$$\Delta t \leq \frac{1}{c}\left[\frac{1}{\Delta x_1^2} + \frac{1}{\Delta x_2^2} + \frac{1}{\Delta x_3^2}\right]^{-\frac{1}{2}} \qquad (1.17)$$

In practice, it has been found possible to deviate slightly from the values obtained from these stability criterion expressions however they do provide a good starting point from which to work. If the value of the time increment is too large, the solution will diverge instead of converge and if the time increment is too small in comparison with the optimum, the optimum being the largest value that can be used without the solution becoming unstable, then the convergence will be unduly slow. The procedure adopted to obtain an optimum time increment is to calculate the value from the above expressions and to run the programme with a value slightly larger. If after a few iterations the solution shows signs of diverging, then the time increment is reduced and conversely if the solution is converging, the time increment is increased until the solution diverges and is then reduced.

In any damped vibrating system, not under the action of external harmonic excitation, convergence to a static equilibrium condition is most rapid when the damping is critical or dead beat. The critical damping constant is related to the fundamental natural frequency of the system thus: (14)

$$K_{cr} = 2 m \omega_n \qquad (1.18)$$

For use with dynamic relaxation, this expression becomes: (2)

$$\frac{K_{cr}}{\Delta t} = 2\omega_n \qquad (1.19)$$

Equation (1.19) can be easily applied in the case of a simple rectangular bar where the natural frequency is known to be, for a bar held at one end:

$$\omega_n = \frac{c\pi}{2\ell} \qquad (1.20)$$

where "ℓ" is the length of the bar, however in the case of a geometrically complex object where the natural frequency is unknown, a trial and error method may have to be used. To estimate the critical damping constant by trial and error, the programme must be run for a few iterations and the convergence rate measured in terms of the rate of change in the values of the variables.

One measure of the rate and the degree of convergence is the change and value of the kinetic energy of the system. The sum of the squares of the velocity at every node point in the object is a measure of the energy of the object and as the solution converges to a steady state, so the sum of the squares of the velocity approaches zero. The procedure adopted in using the kinetic energy to measure the convergence is to calculate the sum of the squares of the velocity at each point in the object after each iteration and have the values printed out. The programme can be run for a few iterations and the effects of varying the damping constant can be determined after a few trial runs. The programme can then be restarted and allowed to run until the sum of the squares of the velocity reaches a low value.

As an alternative to using the kinetic energy as a measure of the convergence, the values of stress and displacement at a few points in the object can be printed out after each iteration and their progress towards a steady value watched. This method can be complicated by secondary harmonics in the early stages of the calculations but which are damped out as the calculations proceed. It is felt that the best method is to use both the kinetic energy and displacements or all three, i.e. kinetic energy, displacements, and stresses, to estimate when a solution has been reached and the rate at which it is reached.

Solving the problem of a simple tension member, consider a steel bar with unit cross sectional area, 4 -1/2" long, held at one end and subject to an axial tensile force of 500 lb. Dividing the bar into 9 parts gives 10 velocity nodes. The physical details are:

$$\Delta x = 0.5 \text{ in.}$$
$$E = 30 \times 10^6 \text{ lb./in.}^2$$
$$\rho = 0.732 \times 10^{-3} \text{ lb. sec.}^2/\text{in.}^4$$

Estimating the time increment from Eq. (1.13):

$$\Delta t = \frac{0.5}{2.02 \times 10^{5}} = 0.248 \times 10^{-5} \text{ sec.}$$

Estimating the critical damping constant from Eq. (1.19) and (1.20):

$$K_{cr} = 2\omega_n \Delta t = 2 \cdot \frac{c\pi}{2\ell} \cdot \frac{\Delta x}{c}$$

$$= \frac{\pi \Delta x}{\ell} = \frac{\pi}{9} = 0.349$$

A copy of the computer programme is given on page 245..

The programme was run with the time increment 5 percent larger than the above calculated value and the solution diverged. A time increment 3 percent smaller than the above calculated value was found to be satisfactory. Four damping constants were tried. These were, 0.44, 0.30, 0.20, and the critical damping value, 0.349. The value 0.30 gave the fastest rate of convergence and is approximately 85 percent of the critical value. The stress at point I = 3 is plotted against number of iterations in Fig. (1.2) for three values of damping and it can be seen that when k = 0.44 the solution is over damped, and when k = 0.20, the solution is underdamped. In all three cases of damping, a steady state solution is achieved however the length of time required varies by a factor of about two between the 0.30 damping constant and the 0.44 and 0.20 values.

Tables (1.1),(1.2),(1.3), and (1.4), give the stress at each node point after each iteration. The sum of the squares of the velocity is also given and the rate and degree of convergence can easily be compared for the four damping constants. Table (1.5) gives the displacement at each velocity node after each iteration for the 0.30 damping constant. The calculated deflection at the free end of the bar is:

$$U = \frac{\sigma_x}{E} \cdot \ell = 0.75 \times 10^{-4} \text{ in.}$$

and is complete agreement with the value obtained by dynamic relaxation.

For this simple problem, the accuracy of the solution is very good; the dynamic relaxation results are in complete agreement with the analytical results. The high degree of accuracy is attributed to

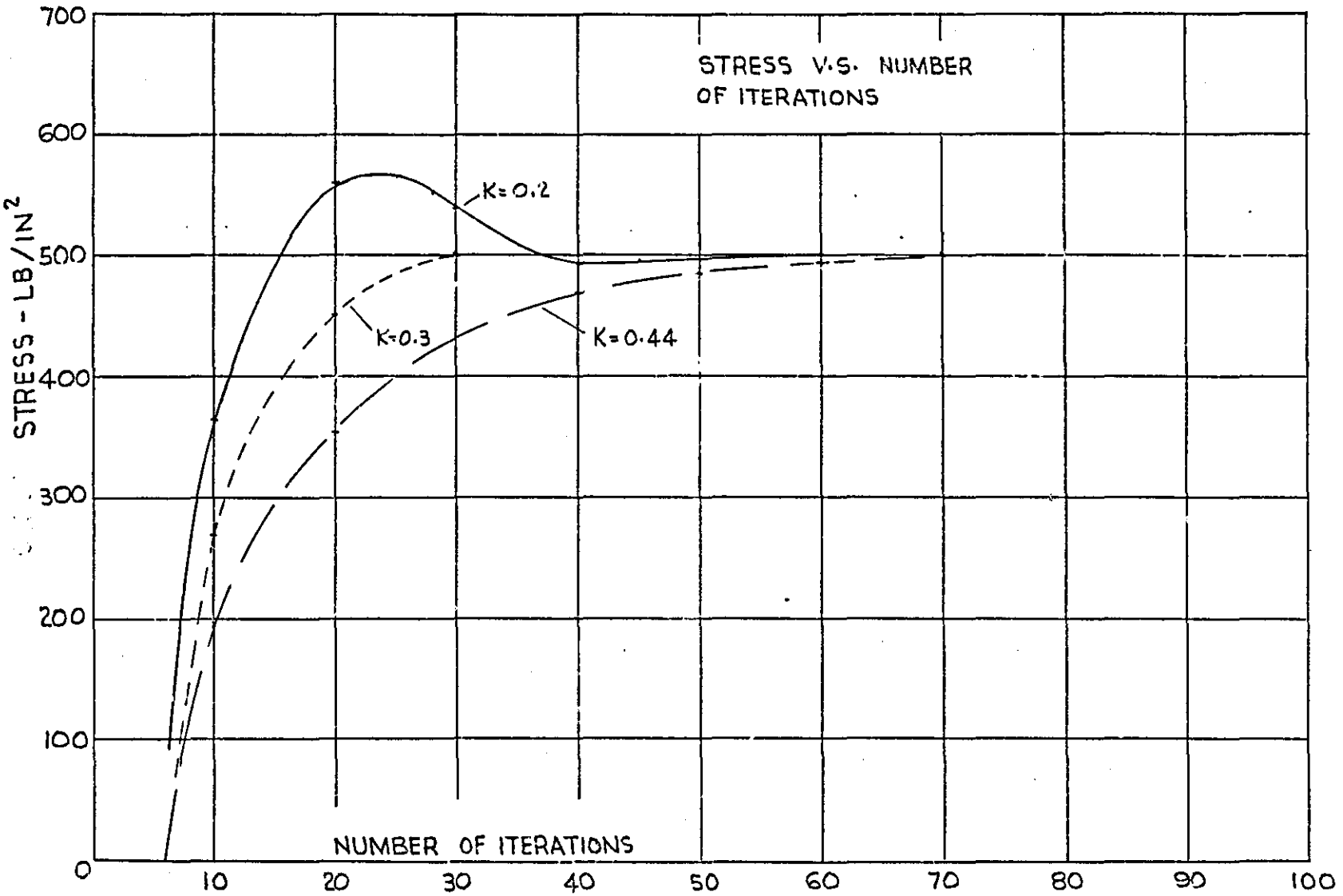
STRESS V.S. NUMBER OF ITERATIONS
STRESS - LB/IN^2
NUMBER OF ITERATIONS
K=0.2
K=0.3
K=0.44
0
100
200
300
400
500
600
700
10
20
30
40
50
60
70
80
90
100

FIGURE 1.2

the simplicity of the geometry of the object. In subsequent chapters where dynamic relaxation is used to analize more complex shaped objects, the accuracy of the solutions will be discussed.

1.3 Application to Thermal Stress Analysis

The application of dynamic relaxation to problems of thermal stress analysis is very simple. The effects of temperature are taken into account by the initial conditions. In the above example, the iteration process is begun with all values of stress, velocity, and displacement being made equal to zero. In the case of thermal stresses, one assumes that initially, the normal-stress at each node point is equal to the temperature stress that would exist if each element was completely constrained in all directions and the temperature of each was changed by "T" degrees, see App. (E). In any object this means knowing the temperature at each normal stress node point. To determine the temperature at each node point is a task in itself but fortunately dynamic relaxation is also adept at solving problems in steady state heat conduction or solving LAplace's equation; the procedure will be discussed in the following section.

1.4 Application to Heat Conduction

In applying the method of dynamic relaxation to elasticity problems, one is concerned only with first order partial differential equations, the reason being that there is a natural relationship between the damped wave equation and the stress-strain equation. In heat conduction, the breakdown of the second order partial differential equation in damped wave form, which defines equilibrium for heat conduction, is not directly obvious and requires the introduction of auxilliary variables. This can be demonstrated using a simple one dimensional problem.

For steady state heat conduction in a solid in which the conductivity is constant throughout the object and is constant over the temperature range in which one is working, the equilibrium equation is:

$$\frac{\partial^2 T}{\partial x^2} = 0 \qquad (1.21)$$

Writing Eq. (1.21) in damped wave form:

$$\frac{\partial^2 T}{\partial x^2} = \frac{\partial^2 T}{\partial t^2} + K\frac{\partial T}{\partial t} \tag{1.22}$$

An auxilliary variable "u" is introduced such that:

$$\frac{\partial u}{\partial x} = \frac{\partial T}{\partial t} \tag{1.23}$$

$$\frac{\partial u}{\partial t} + Ku = \frac{\partial T}{\partial x} \tag{1.24}$$

Equation (1.23) is similar to Eq. (1.5) when dot notation is used in Eq. (1.5) and, Eq. (1.24) is similar to Eq. (1.2) when dot notation is used in Eq. (1.2). The variable "u" is analogous to the quantity of heat flowing across a boundary of unit cross sectional area in an object having unit conductivity since under steady state conditons the derivative of "u" with respect to time will be zero hence the term "ku" must equal the temperature gradient which in turn is proportional to the heat flow. This concept can be taken advantage of when specifying conditions on a boundary, for example on a boundary which is insulated or a boundary which forms an axis of symmetry, the heat flow is zero hence one need only specify "u" as being zero.

Equations (1.23) and (1.24) are written in finite difference fomand rearranged to provide expressions for temperature in terms of the variable "u" and conversely "u" in terms of temperature "T". These equations are:

$$T^{r+1}(I) = T^{r}(I) + \frac{\Delta t}{\Delta x}\left[u^{r}(I+1) - u^{r}(I)\right] \tag{1.25}$$

$$u^{r+1}(I) = u^{r}(I)\frac{1-K/2}{1+K/2} + \frac{\Delta t}{1+K/2}\left[\frac{T^{r}(I) - T^{r}(I-1)}{\Delta x}\right] \tag{1.26}$$

The stability criterion for heat conduction problems is based on the same concepts as in the elasticity problems however since the conductivity, specific heat, and density have been eliminated by the right hand side of Eq. (1.21) being zero, the wave speed becomes equal to unity. For two and three dimensional problems, it is expected that the wave speed "c", will behave in a manner similar to elasticity problems and will therefore be slightly greater than unity.
The criterion for critical damping is also applicable to the heat conduction problem since the elasticity and heat conduction problem are

analogous.

To illustrate the method of dynamic relaxation as applied to a heat conduction problem, assume that the bar shown in Fig. (1.1) is insulated at the fixed end and on the edges, and that heat is applied to the free end such that the temperature on the surface at the free end is 500°F. The problem is one dimensional. The time increment and damping constant will be:

$$\Delta t = \Delta x = 0.5$$

$$K_{cr} = \frac{\pi \Delta x}{\ell} = 0.349$$

The commputer programme is given on page 246 and was run with damping constants of 0.30, 0.32, and 0.34, with the time interval calculated above. The 0.32 value for damping gave the fastest convergence. Increasing the time increment to 0.52 caused the solution to diverge. The results of the solution are given in table (1.6) for the 0.32 damping constant.

1.5 Closure

From the discussions and illustrations given above, the extension of dynamic relaxation to problems in two and three dimensions is straight forward. The finite difference equations for elasticity problems in cylindrical coordinates, for plane stress problems in polar coordinates and for problems in axisymmetric stress distribution, have been derived in the appendices of this thesis along with finite difference equations for heat conduction in cylindrical coordinates. In subsequent chapters of this thesis, the accuracy of the solutions obtained by dynamic relaxation in solving more complex problems will be discussed.

CHAPTER TWO

HOLOGRAPHIC INTERFEROMETRY

2.1 Introduction

The principles of holography were first demonstrated in 1948 by Dennis Gabor. Gabor showed that a sharply focused image of an object could be formed from a photographic record of its interference pattern. Virtually no development of the principle of holography took place until the laser came into being; the laser being the fundamental tool in holography because of its high temporal and spatial coherence and high intensity. Since the advent of the laser, holography has been developed by Leith and Upatnieks et. al. and a great many applications have been found including holographic interferometry. The use of holographic interferometry to measure surface deformations of strained objects is under current investigation and a number of workers in the field have already shown the possibilities, (9)(10)(11)

In this chapter, the holographic process is described briefly to provide the basic requirements for the understanding of holographic interferometry. The application of holographic interferometry to stress analysis is investigated.

2.2 The Holographic Process

The process by which a hologram is made and allows a three dimensional virtual image to be reconstructed in space can be described

briefly as follows.

Figure (2.1) represents a typical set up for making a hologram. A coherent light source, a laser beam in this case, is split by means of a beam splitter into a reference beam and an object beam. The reference beam, after passing through a lens which spreads the highly collimated laser beam, is allowed to fall directly onto a high resolution photographic plate. The object beam, also passing through a lens, is directed onto the object and the light which is scattered off the object is allowed to fall directly onto the same photographic plate. The light waves which make up the object and reference beams maintain a definite phase relationship with each other over a period of time and upon reaching the photographic plate, interfere with each other, the interference being recorded by the photographic plate. The recorded interference pattern is effectively a type of diffraction grating. If after the photographic plate is processed, it is illuminated by the reference beam incident on the plate at the same angle as when the hologram was made, the reference beam is diffracted into a number of components one of which has a wave front identical to that light which was scattered from the object with the exception of intensity and phase; the wave front being uniformly 180° out of phase with original wave front. Since the diffracted reference beam has a component which is identical to the original wave coming from the object, then a full three dimensional image is formed and is located in the same position that the object occupied during the making of the hologram. The process can be described mathematically as follows.

Let the light reflected off the object and incident on the photographic plate be described by:

$$U = a(x,y)\,\mathrm{Cos}\left[\omega t + \phi(x,y)\right] \tag{2.1}$$

where a(x,y) is the amplitude of the light and is a function of the coordinates "x" and "y" in the plane of the photographic plate, and $\phi(x,y)$ is a phase shift imposed on the object beam by the object. Similarily let the reference beam incident on the photographic plate be described by:

$$U_r = a_r\,\mathrm{Cos}\left[\omega t - \alpha x\right] \tag{2.2}$$

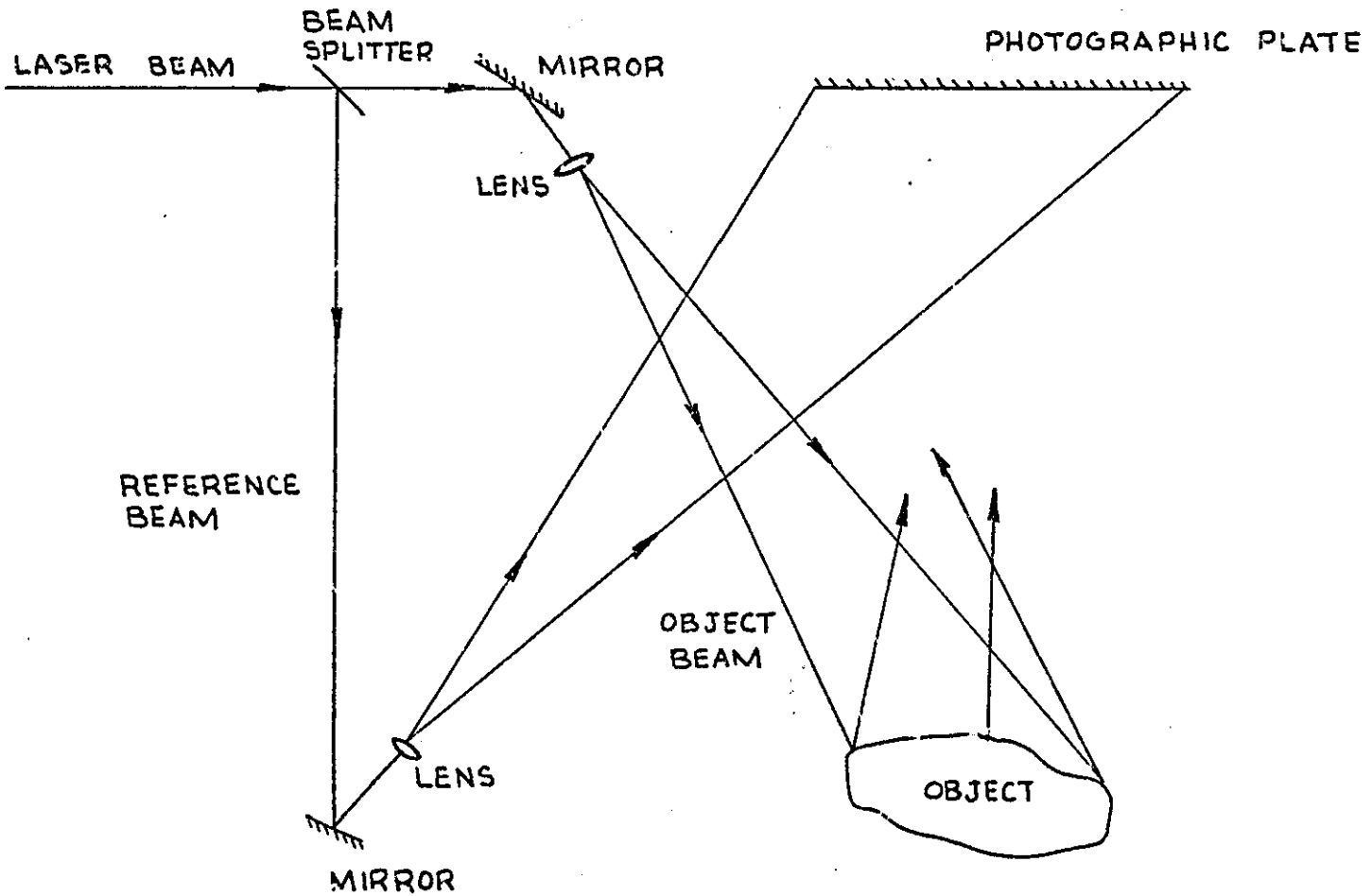
BEAM
SPLITTER
LASER BEAM
MIRROR
PHOTOGRAPHIC PLATE
LENS
REFERENCE
BEAM
OBJECT
BEAM
LENS
OBJECT
MIRROR

FIGURE 2.1

where a_r designates a uniform amplitude at the photographic plate and αx designates a linear phase shift across the photographic plate indicating that the reference beam strikes the plate at an oblique angle. The importance of the reference beam striking the plate at an angle will be discussed later on.

The total amplitude of the light falling on the plate is the sum of the amplitudes of the two beams thus:

$$U_t = a(x,y)\ \cos[\omega t + \phi(x,y)] + a_r \cos[\omega t - \alpha x] \qquad (2.3)$$

The photographic plate records the time averaged square of the total amplitude or the time averaged intensity of the light thus:

$$I = \frac{a_r^2 + a(x,y)^2}{2} + a_r\, a(x,y)\ \cos[\alpha x + \phi(x,y)] \qquad (2.4)$$

If the plate is processed and illuminated by the reference beam as previously described, the light transmitted by the plate is the product of the amplitude of the reference beam and the transmissivity of the plate. The transmissivity of the plate is proportional to the time averaged intensity of the light falling on it during the exposure time thus the transmitted light can be described by:

$$U_{tr} = a_r\frac{(a_r^2 + a(x,y)^2)}{2}\ \cos[\omega t - \alpha x] + \frac{a_r^2}{2}\, a(x,y)\ \cos[\omega t + \phi(x,y)]$$

$$+ \frac{a_r^2}{2}\, a(x,y)\ \cos[\omega t - 2\alpha x - \phi(x,y)] \qquad (2.5)$$

In Eq. (2.5), the first term represents that portion of the reference beam which passes directly through the plate at an angle α and which is attenuated by the overall darkening of the plate. The second term is indentical to the light scattered from the object as defined by Eq. (2.1) with the exception of the constant $a_r^2/2$. The third term represents a third wave which leaves the plate at an angle 2α and the negative sign in front of the term $\phi(x,y)$ in the argument of the Cos. indicates that the wave has a conjugate wave front or in other words, a conjugate image is formed in front of the photograhic plate. This conjugate image can be focused on a screen positioned in front of the plate without any optical apparatus. From this description it can be seen that if the reference beam does not strike the plate at an angle α then the conjugate wave will interfere with the wave which represents

virtual image and thus interfere with the viewing of the virtual image.

The above description of the holographic process is quite basic however it is sufficient to allow the principles of holographic interferometry to be discussed.

2.3 Holographic Interferometry

If a hologram is made as described above, and if after processing, it is put back in the exact same position as when it was made, in accordance with Fig. (2.1), and illuminated, the reconstructed virtual image will be superimposed exactly onto the object or in other words the rays coming from the object will coincide exactly with the rays which make up the reconstructed image. As previously mentioned, the reconstructed wave front is 180° out of phase with the actual wave front coming from the object hence the image will appear dark as compared with the image that would be produced in the absence of the object. The reason for the reconstructed wave front being 180° out of phase is that the hologram is effectively a "negative". If the object is displaced so that the two wave fronts are in phase then the object will appear bright. This change from dark to bright corresponds to an optical path length change of one half wave length of the light being used.

The brightening and darkening of the surface will be uniform over the entire surface if the angles of illumination and viewing are constant over the entire surface and every point on the surface moves by the same amount. As a simple example consider an object that is viewed and illuminated normal to the surface. As the object is displaced, the number of times the surface goes from dark to bright and back to dark again can be expressed as:

$$N = 2d/\lambda \qquad (2.6)$$

where "N" is the number of times the surface brightness changes or the number of fringes or fringe order number; λ is the wave length of light and "d" is the displacement of the object. For the general case where

the angles of viewing and illumination are not constant and where "d" is not constant over the surface, the fringe order number at a particular point on the surface is related to the displacement and the angles of viewing and illumination at that point thus, see Fig.(2.2):

$$N\lambda = d(\cos\theta + \cos\theta') \qquad (2.7)$$

where θ and θ' are the angles of illumination and viewing respectively, relative to the direction of the displacement "d".

The above description of the formation of interference fringes due to displacement of the object relative to the hologram is referred to as the live fringe technique since the fringes can be observed as they are formed. A second method of obtaining a fringe pattern representitive of the displacement of the object is referred to as the frozen fringe technique. The procedure for the frozen fringe technique is to make a hologram as described above with the exception that the exposure time is halved. Following the first exposure, the object is displaced and a second exposure made to complete the total exposure time. Effectively one has produced a double hologram and upon illuminating it after processing, two wave fronts are produced corresponding to the object in its initial and final position. These two wave fronts interfere to produce a frozen fringe pattern.

The advantage of the frozen fringe method over the live fringe method is that the hologram plate need not be accurately positioned or replaced in the exact same position, and, a permanent record of the interference fringes is made that can be examined at a later date.

2.4 Determination of Surface Displacements from a Fringe Pattern

To determine the displacement of the surface of an object, Eq. (2.7) is applicable however if the direction of the displacement is unknown, then the angles θ and θ' will be unknown hence it is impossible to solve Eq. (2.7) from a single fringe pattern or angle of viewing. Some simple cases exist that can be easily analized; these will be discussed in this section.

The displacement "d" can be considered as being made up from

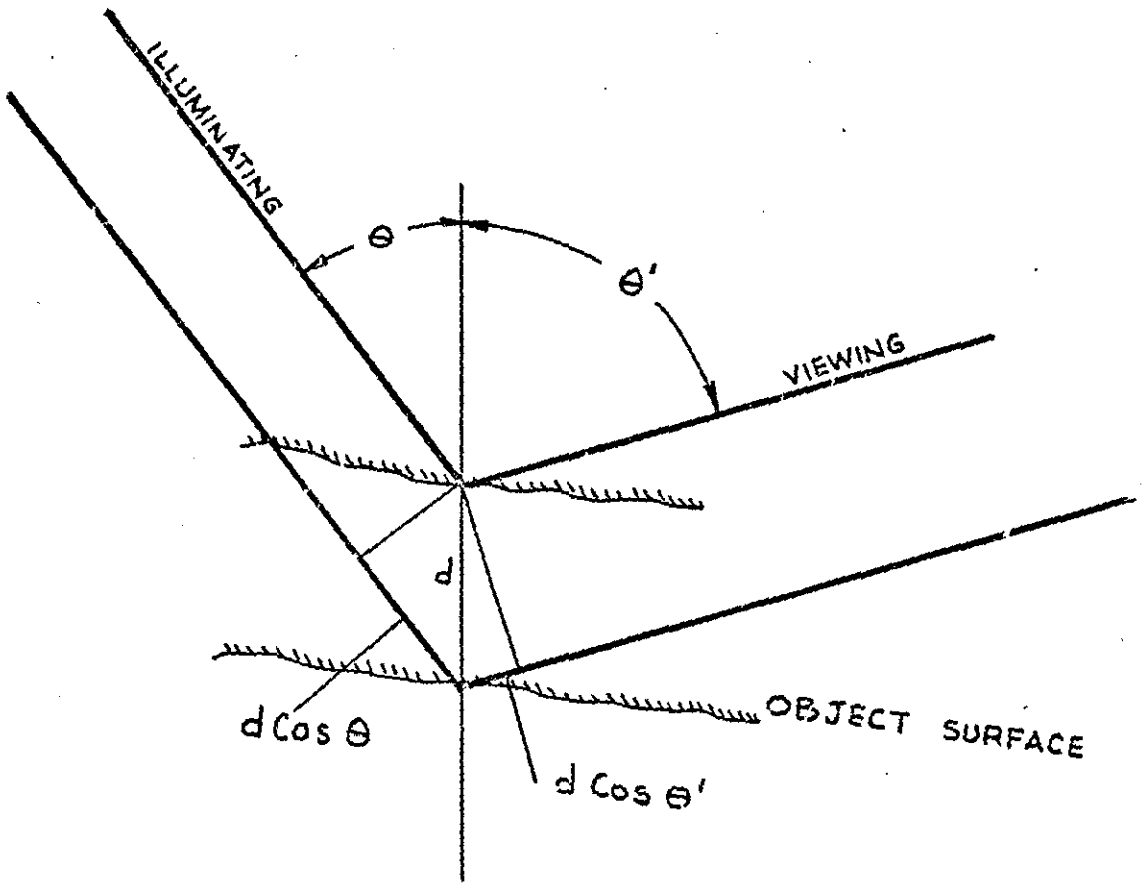

FIGURE 2.2

three components, two of which, "u" and "v", are in the plane of the surface, and the third component "w", normal to the plane of the surface. By illuminating and viewing the object parallel to one of the planes of the coordinates, an expression can be derived which includes only one of the in-plane components of displacement. For example if one were to view and illuminate in the x,z plane, then only the components "u" and "w" can contribute to a change in the optical path since displacements normal to the direction of viewing and illumination will not cause an optical path length change i.e. $w(\text{Cos } 90^{\circ}) = 0$. This argument assumes that the surface in question is small in comparison to the distance from which it is viewed and that the illuminating beam divergence is small so that effectively the angles of viewing and illumination are constant over the surface in the "y" direction and that the displacement in the "y" direction is of the same order of magnitude or less than the displacements in the "x" and "z" directions. From Fig. (2.3), the optical path length change for the illuminating beam is $u(\text{Cos } \phi) + w(\text{Sin } \phi)$ where ϕ is the angle the illuminating beam makes with the surface. Similarily for viewing, the optical path length change is $u(\text{Cos } \phi') + w(\text{Sin } \phi')$ from which the following expression is derived:

$$N\lambda = u(\cos\phi + \cos\phi') + w(\sin\phi + \sin\phi') \qquad (2.8)$$

Examining this expression, it is interesting to note that when $\phi'=\phi=90^{\circ}$, or when $\phi'=\phi+90^{\circ}$, displacements in the plane of the surface, i.e. "u", do not contribute to the change in optical path length. Also when $\phi'=\phi=90^{\circ}$, the sensitivity to normal displacement is a maximum. Unfortunately conditions for maximum sensitivity to in-plane displacements or conditions which are insensitive to normal displacement can not be realized since it is impossible to view and illuminate the surface at an angle of zero degrees. Thus while it is possible to set up a system which will detect only those displacements normal to the surface, it is impossible to have a system which detects only in-plane displacements. Again this assumes that the displacements are all of the same order of magnitude and that the angles of viewing and illumination are constant over the surface. From this argument, a useful expression can be derived for the analysis of flexural displacements of beams, plates, diaphrams etc. thus:

$$N\lambda = w(\sin\phi + \sin\phi') \qquad (2.9)$$

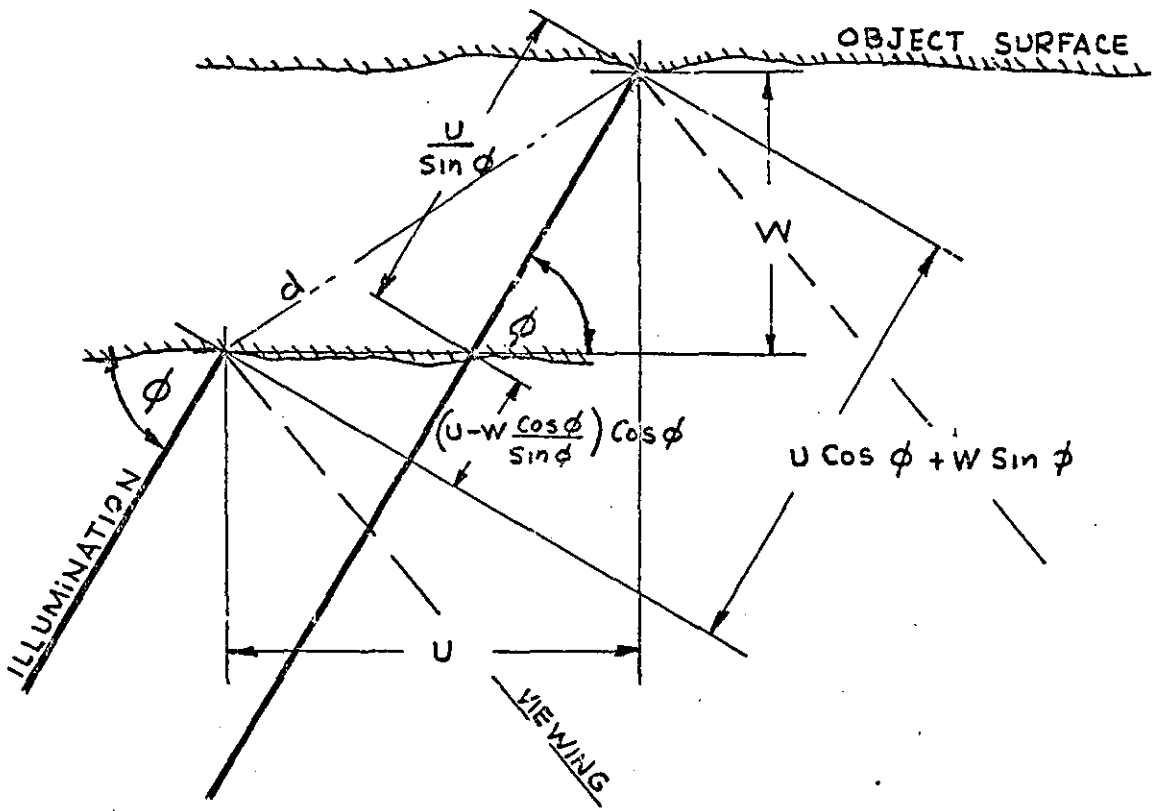
OBJECT SURFACE
U / Sin ϕ
W
d
ϕ
ϕ
(U-W Cos ϕ / Sin ϕ) Cos ϕ
U Cos ϕ + W Sin ϕ
ILLUMINATION
U
VIEWING

FIGURE 2·3

In flexural problems, the angles of viewing and illumination can vary over the surface and can easily be taken account of in the above expression; the contribution to the optical path length change by the in-plane displacements being neglected since for example in the case of a simply supported beam, the in-plane displacements are proportional to the first derivative of the normal displacement.

Using Eq. (2.8), and having a knowledge of the displacements that are imposed on the object, one can predict the general shape of the fringe patterns for some simple cases. For example, consider the case of pure rotation about the "y" axis. For small rotations, the normal displacement "w" at a distance "x" from the origin, will be $x\beta$ where β is the angle of rotation. Substituting for "w" in Eq. (2.8) and assuming that for small rotations the displacement in the "x" direction is negligible, gives:

$$N\lambda = x\beta(\sin\phi + \sin\phi')$$

For a given angle of rotation, and if the angles of viewing and illumination are constant over the surface, then the fringe order number is linear with respect to the distance "x", thus the fringe pattern will consist of a series of equally spaced fringes normal to the "x" axis. At the axis of rotation, the fringe order number is zero and represents a point on the surface with zero displacement. In the case of using the live fringe technique, the zero order fringe will be a dark band, whereas in the case of a frozen fringe pattern, the zero order fringe will be a bright fringe. If the location of the axis of rotation is unknown, it can be found by determining the location of the zero order fringe. This is done by changing the angle of viewing and observing the changing fringe order numbers over the surface i.e. the fringes move as one changes the direction of viewing. The fringe that does not move is the zero order fringe. One obvious problem which arises in analysis of rotation patterns is that if the direction of rotation is unknown, it can not be determined from the fringe pattern using a simple equation.

A pattern which is identical to the one described above is one due to constant in-plane strain. Consider a simple tension member subject to an axial load that induces a stress σx and a strain $\sigma x/E = \epsilon x$. The displacement in the "x" direction at a distance "x" from the fixed end is $u = x\epsilon x$. The lateral displacement, "w", is due to Poissons effect and assuming it is equal on both sides of the mid-plane of the

member, "w" is equal to $-\nu t\epsilon x/2$. Substituting for "u" and "w" in Eq. (2.8) gives:

$$N\lambda = \epsilon x\left[x(\cos\phi + \cos\phi') - \frac{\nu t}{2}(\sin\phi + \sin\phi')\right]$$

If the strain is constant along the length of the member and the angles of viewing and illumination are constant then as in the case of rotation, the fringe order number will be linear with respect to "x" and the pattern will consist of a series of equally spaced fringes, normal to the "x" axis. It may be noted that in this case ϕ' must not equal $\phi + 90^\circ$, and both ϕ' and ϕ must not simultaneously be equal to 90° or the sensitivity to in-plane displacement will be zero. The effects of the lateral displacement, "w", will be to cause a uniform phase shift over the entire surface since the contribution to the optical path length change will be the same at every point "x". One problem which arises in attempting to determine the strain from a fringe pattern as described above is that if the direction of the applied load is unknown, then one cannot tell from the pattern whether the strain is positive or negative i.e. tension or compression using a simple equation.

The fringe patterns described above for the case of solid body rotation and constant in-plane strain are identical and in a practical engineering problem, one can have any manner of displacements simultaneously in which case it would be impossible to tell from a single fringe pattern what is actually transpiring in the way of in-plane displacements. Methods have been developed which involve analizing the fringe patterns which have been obtained, by viewing the image from different angles. In effect one obtains a set of simultaneous equations which when solved will yield the three components of displacement. The most general of these methods is given in (11) and will now be described.

The basic problem is to solve Eq. (2.7) with the displacement vector "d" broken down into the three components; the two in-plane components, "u" and "v", and the normal component, "w". The procedure, for determining u,v, and w, given in (11) is as folows.

Consider a point on the surface of the object having coordinates x_o, y_o, z_o where the x,y axes are in the plane of the surface.

The illuminating beam comes from a point source located at coordinates x_i, y_i, z_i and the image is view through a point or small window in the hologram plate at coordinates x_1, y_1, z_1 as shown in Fig. (2.4). Letting the fringe order number of the fringe at the point in question on the surface of the object be N_1, Eq. (2.7) becomes:

$$N_1 \lambda = d(\cos\theta + \cos\theta_1') \tag{2.10}$$

By changing the viewing angle to correspond with point "2" on the hologram plate, the fringe order number of the fringe at the point in question is N_2 and Eq. (2.7) becomes:

$$N_2 \lambda = d(\cos\theta + \cos\theta_2') \tag{2.11}$$

Subtracting Eq. (2.10) from (2.11) gives:

$$(N_2 - N_1)\lambda = d(\cos\theta_2' - \cos\theta_1') \tag{2.12}$$

In Eq. (2.12), the angle that the illuminating beam makes with the displacement vector has been eliminated. Repeating the process for points "3" and "4" on the hologram plate gives three equations thus:

$$\begin{aligned}(N_2 - N_1)\lambda &= d(\cos\theta_2' - \cos\theta_1') \\ (N_3 - N_1)\lambda &= d(\cos\theta_3' - \cos\theta_1') \\ (N_4 - N_1)\lambda &= d(\cos\theta_4' - \cos\theta_1')\end{aligned} \tag{2.13}$$

The angle between the displacement vector "d" and the direction of viewing can be defined in terms of cosine directions thus:

$$\cos\theta_n' = L_o L_n + M_o M_n + P_o P_n$$

where: $L_o = \frac{u}{d}$ $M_o = \frac{v}{d}$ $P_o = \frac{w}{d}$

$$L_n = \frac{x_o - x_n}{r_n} \quad M_n = \frac{y_o - y_n}{r_n} \quad P_n = \frac{z_o - z_n}{r_n}$$

and:

$$r_n = \sqrt{(x_o - x_n)^2 + (y_o - y_n)^2 + (z_o - z_n)^2}$$

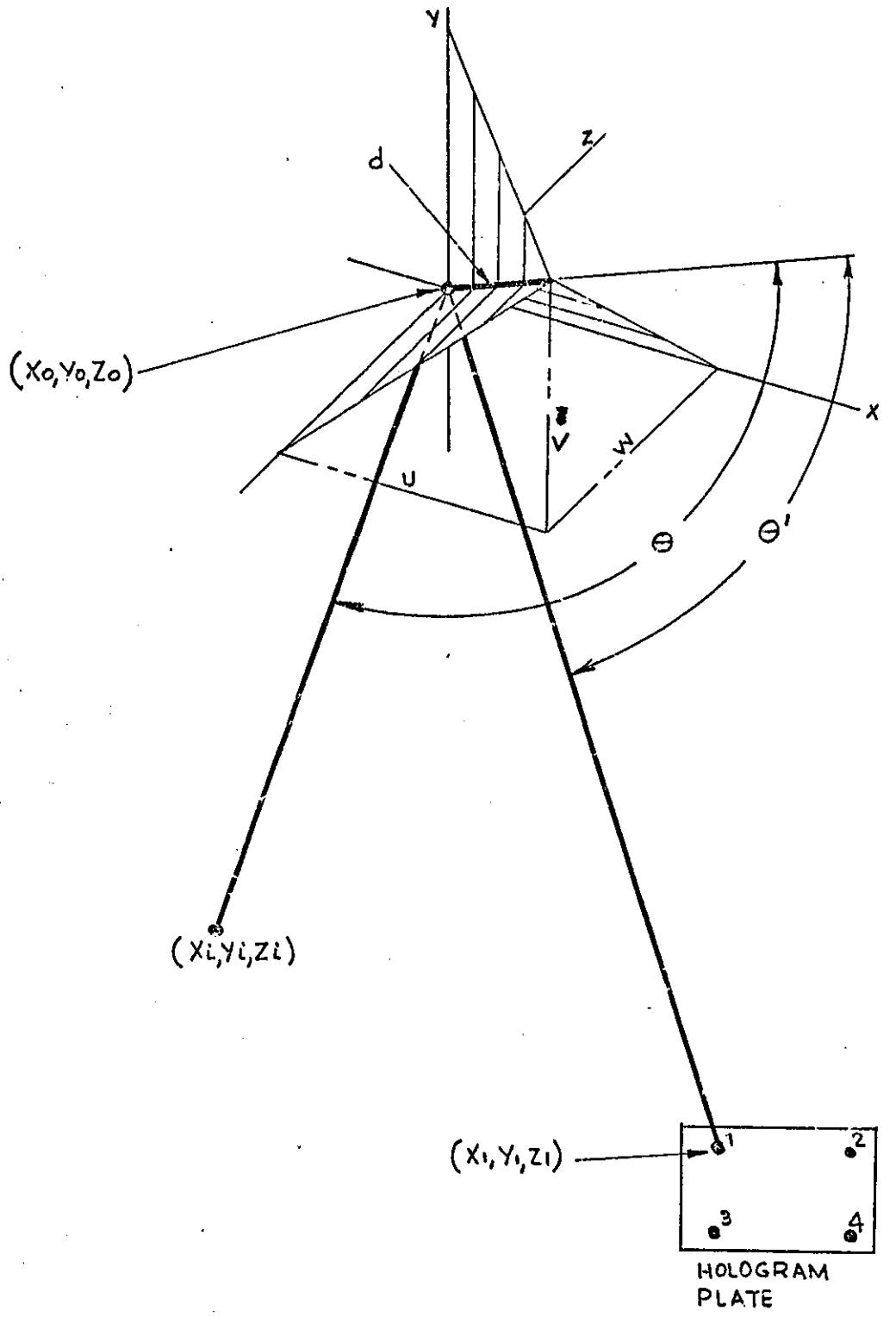

FIGURE 2·4

Substituting for Cos θ' in Eq. (2.13) gives:

$$(N_2-N_1)\lambda = u\left(\frac{x_o-x_2}{r_2}-\frac{x_o-x_1}{r_1}\right)+v\left(\frac{y_o-y_2}{r_2}-\frac{y_o-y_1}{r_1}\right)+w\left(\frac{z_o-z_2}{r_2}-\frac{z_o-z_1}{r_1}\right)$$

$$(N_3-N_1)\lambda = u\left(\frac{x_o-x_3}{r_3}-\frac{x_o-x_1}{r_1}\right)+v\left(\frac{y_o-y_3}{r_3}-\frac{y_o-y_1}{r_1}\right)+w\left(\frac{z_o-z_3}{r_3}-\frac{z_o-z_1}{r_1}\right) \qquad (2.14)$$

$$(N_4-N_1)\lambda = u\left(\frac{x_o-x_4}{r_4}-\frac{x_o-x_1}{r_1}\right)+v\left(\frac{y_o-y_4}{r_4}-\frac{y_o-y_1}{r_1}\right)+w\left(\frac{z_o-z_4}{r_4}-\frac{z_o-z_1}{r_1}\right)$$

In applying this approach to obtain the three displacement components one would view the image from position "1" and allocate a fringe order number to the fringe at x_o, y_o, z_o. The actual fringe number is not important since one is interested in determining differences in fringe order numbers. The direction of viewing is then changed to correspond to point "2" on the hologram plate and a fringe number assigned to the fringe at the same point on the surface of the object. From this process one can obtain $N_2 - N_1$. Repeating the procedure for points "3" and "4", one can obtain $N_3 - N_1$ and $N_4 - N_1$ and thus complete the L.H.S. of Eq. (2.14). If the zero order fringe position is known and one can see and count the fringes easily, then the process is straight forward however if the zero order fringe position is not known then the number of fringes which pass the point on the surface of the object as the viewing angle is changed, represents the difference between the fringe order numbers corresponding to the two viewing angles; viz. $\Delta N = N_2 - N_1$ etc. The value of ΔN can be positive or negative and one must adopt a convention for example fringes moving from left to right are positive and fringes moving from right to left are negative.

Having obtained the L.H.S. of Eq. (2.14) and by measuring the coordinates of the point on the object and the four points on the hologram, one has enough information to solve Eq. (2.14) and thus obtain the values of the three displacement components. Before looking into the methods of measuring in-plane displacements as described in (9) and (10), it is advantageous at this point to look at the application of the method described above to problems of stress analysis.

2.5 Application of Holographic Interferometry to Stress Analysis

The strain information that is required to calculate the

principal stress at a point on the surface of the object is the princi-strains ϵ_1 and ϵ_2. Generally the direction of the principal strains will be unknown hence the strains cannot be measured directly. They can however be calculated from the relatioship:

$$\epsilon_1, \epsilon_2 = \frac{\epsilon x + \epsilon y}{2} \pm \frac{1}{2}\sqrt{(\epsilon x - \epsilon y)^2 + 2\gamma x y^2} \qquad (2.15)$$

Measuring the normal strains ϵx and ϵy, is straight forward in the case of using strain gauges however the measurement of the shear strain, γxy, is impossible , in which case the strain in a third direction must be measured and the shear strain obtained by solving three simultaneous equations thus:

$$\begin{aligned}
\epsilon\alpha_1 &= \epsilon x \cos^2\alpha_1 + \epsilon y \sin^2\alpha_1 + \gamma xy \sin\alpha_1 \cos\alpha_1 \\
\epsilon\alpha_2 &= \epsilon x \cos^2\alpha_2 + \epsilon y \sin^2\alpha_2 + \gamma xy \sin\alpha_2 \cos\alpha_2 \\
\epsilon\alpha_3 &= \epsilon x \cos^2\alpha_3 + \epsilon y \sin^2\alpha_3 + \gamma xy \sin\alpha_3 \cos\alpha_3
\end{aligned} \qquad (2.16)$$

Using holographic interferometry, the shear strain can be obtained directly along with the strains ϵx and ϵy. To do this the in-plane displacements would be determined at four points which form a square mesh enclosing the point at which the principal strains are to be calculated. The strains at the centre of the mesh can be estimated using finite difference equations thus, see Fig. (2.5):

$$\epsilon x = \frac{1}{2}\left[\frac{U_2 - U_1}{\Delta x} + \frac{U_4 - U_3}{\Delta x}\right] \qquad \epsilon y = \frac{1}{2}\left[\frac{V_3 - V_1}{\Delta y} + \frac{V_4 - V_2}{\Delta y}\right]$$
$$\gamma xy = \frac{1}{2}\left[\frac{U_4 - U_2}{\Delta y} + \frac{U_3 - U_1}{\Delta y}\right] + \frac{1}{2}\left[\frac{V_4 - V_3}{\Delta x} + \frac{V_2 - V_1}{\Delta x}\right] \qquad (2.17)$$

Having the strains ϵx, ϵy, and γxy, one can calculate ϵ_1 and ϵ_2 from which the principal stresses σ_1, σ_2, and τ_{max} can be calculated thus:

$$\begin{aligned}
\sigma_1 &= \frac{E}{1-\nu^2}\left[\epsilon_1 + \nu\epsilon_2\right] \\
\sigma_2 &= \frac{E}{1-\nu^2}\left[\epsilon_2 + \nu\epsilon_1\right] \\
\tau_{max} &= \pm\frac{1}{2}\left[\sigma_1 - \sigma_2\right]
\end{aligned} \qquad (2.18)$$

The direction of the principal stresses can be determined from:

$$\tan 2\alpha = \frac{\gamma xy}{\epsilon x - \epsilon y} \qquad (2.19)$$

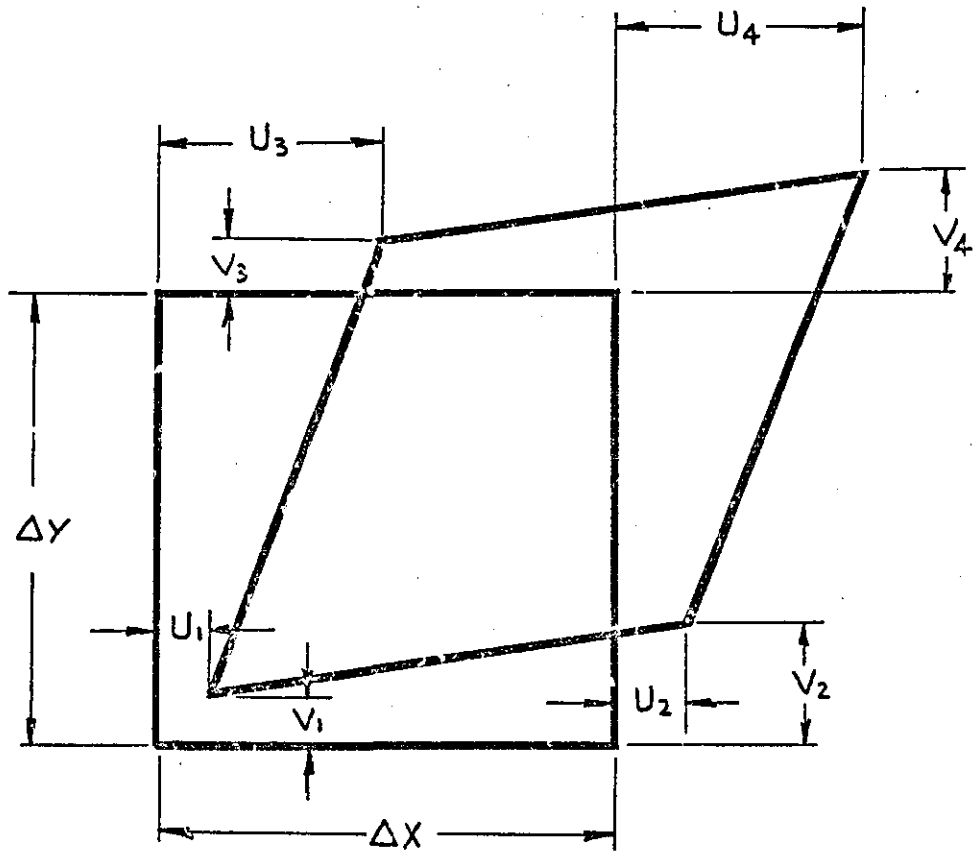

FIGURE 2·5

In considering the application of the method given in (11) to stress analysis, certain limitations become apparent. The most obvious undesireable feature is that unless one has a bench or set up with built in precision measuring equipment, it is very difficult to accurately measure the coordinates on the surface of the object and on the hologram plate. To determine the stress at a single point on the object requires the measurement of 12 coordinate points on the object and the solution of four sets of three simultaneous equations. Initially one must also measure the 12 coordinates of the 4 points on the hologram plate. The simultaneous equations could be assembled and solved by computer however to measure the coordinates associated with say ten points on the surface at which the principal stresses are required would be a formidable task and prone to error with out some form of built in measuring equipment. Another problem that is also expected to arise is that inevitably one would be required to estimate a fraction of a fringe order number and if the fringe spacing is large or if the spacing is changing rapidly, one cannot resolve by eye the variation in intensity between two dark fringes hence it would be possible to have large errors entering into the fringe order numbers especially if when counting the number of fringes which pass a point on the surface as the viewing angle is changed, the number of fringes is less than one or even in the region of two or three. In addition to these practical difficulties, one other obvious problem can be forseen and that is that if the problem under consideration is a flexural problem then the displacement "w" will most likely be much larger than "u" and "v" hence one is trying to solve a set of equations which involve large and small numbers which is a notoriously inaccurate process.

Another method developed for use in stress analysis is given in (9). This method uses a set up which eliminates one of the in-plane components of displacement by illuminating and viewing normal to the axis of one of the in-plane displacements. In this case one can make use of Eq. (2.8) and proceed as folows.

Two holograms are made in which the angle of illumination is common but the angles of viewing are different; see Fig. (2.6). From these two holograms one can obtain the following expressions:

$$N_1\lambda = u(\cos\phi + \cos\phi_1) + w(\sin\phi + \sin\phi_1)$$
$$N_2\lambda = u(\cos\phi + \cos\phi_2) + w(\sin\phi + \sin\phi_2)$$

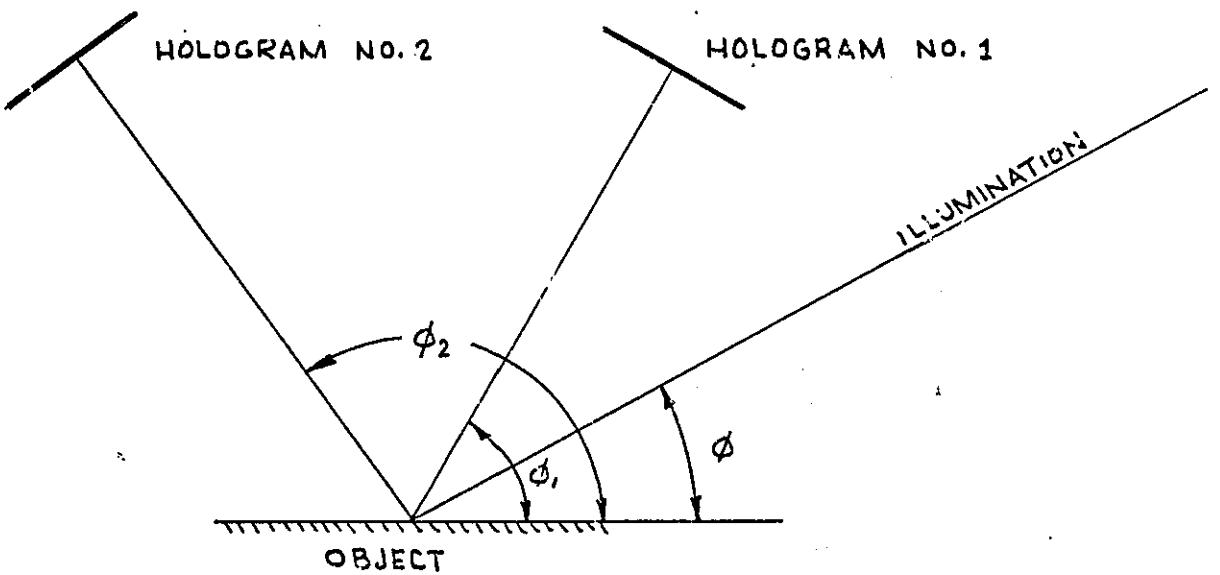
HOLOGRAM NO. 2
HOLOGRAM NO. 1
ILLUMINATION
ϕ_2
ϕ_1
ϕ
OBJECT

FIGURE 2.6

Eliminating the normal displacement "w" gives:

$$[N_2(\sin\phi + \sin\phi_1) - N_1(\sin\phi + \sin\phi_2)]\lambda = u[(\cos\phi + \cos\phi_2)(\sin\phi + \sin\phi_1) - (\cos\phi + \cos\phi_1)(\sin\phi + \sin\phi_2)] \quad (2.20)$$

The L.H.S. of the above equation can be written as $N_r\lambda$ where N_r can be thought of as the fringe order number corresponding to a pattern in which only the in-plane displacements have contributed to the optical path length change. If a grid were drawn on the surface of the object then one could calculate the value of N_r at each grid point and putting these values of N_r onto a duplicate of the grid drawn on the object, one could graphically construct a fringe pattern that represented in-plane displacements only. This pattern would cover the entire surface of the object and would correspond to loci of points having constant in-plane displacement similar to what one would expect from a Moire' experiment. To obtain the in-plane strain, one would have to plot a curve of the in-plane displacement and numerically differentiate the displacement with respect to a length increment; viz. $\epsilon x = du/dx$. To obtain the principal stress at a point on the object one would have to repeat the process at different angles say at 45° and 90° to the "x" axis and then use Eq. (2.16) to obtain the shear strain and subsequently the principal strains and stresses. In its simplest form, this method can be thought of as the graphical subtraction of two fringe patterns one of which is due to in-plane and normal displacements and the second due to normal displacements only. This case can exist if the second hologram is made with the angle of viewing equal to the angle of illumination plus 90°. If for the first hologram, the angle of viewing is equal to the angle of illumination and both are not 90°, then Eq. (2.20) becomes:

$$(N_1 - N_2)\lambda = 2u\cos\phi \quad (2.21)$$

In this case, subtraction of the two fringe order numbers at the same grid point yields the resultant in-plane fringe order number.

As with the previously described method the above method has practical limitations especially when it comes to a flexural problem. In a flexural problem one would have two fringe patterns which would be almost identical since the normal displacement would be large in com-

parison with the in-plane displacements. Effectively one would be involved in subtracting two large numbers to obtain a small number which again is prone to large errors. In addition one would again be faced with estimating a fractional fringe order number at a grid point and if the fringe order numbers were close to being equal on the two holograms, a great deal of error can be incurred in the subtraction of the two numbers. To illustrate the difficulty that would be encountered in trying determine the in-plane displacements in the case of a flexural problem consider a simple cantilever beam, loaded at the free end by a force "F". The lateral displacement "w" is defined by:

$$W = \frac{F}{EI}\left(L\frac{x^2}{2} - \frac{x^3}{6}\right)$$

The surface strain is given by $\epsilon x = t/2R = du/dx$ where "t" is the depth of the beam and "R" is the radius of curvature which is, for small deflection, approximately d^2x/dw^2. Thus the surface strain can be written as:

$$\frac{du}{dx} = \frac{t}{2}\frac{d^2W}{dx^2} = \frac{Ft}{2EI}(L - x)$$

The in-plane displacement at any point "x" from the fixed end is:

$$U = \int \frac{du}{dx}.dx = \frac{Ft}{2EI}\left(Lx - \frac{x^2}{2}\right)$$

At the free end, the lateral displacement "w" is $FL^3/3EI$ and the in-plane displacement is $FtL^2/4EI$. The ratio of lateral to in-plane displacement is $4L/3t$. If in a practical case, the length to thickness ratio was 10:1 and assuming that one was viewing and illuminating the cantilever at an angle of 45° so that the sensitivity to in-plane and lateral displacements was equal for both, then the normal or lateral displacement would contribute 40/43 or 93 percent of the number of fringes while the in-plane displacement would contribute only 7 percent. Thus if one made two holograms such that one contained a fringe pattern due to normal displacements only and the second, a fringe pattern due to in-plane and normal displacements, then one would be faced with trying to subtract 93 from 100, graphically, which is not likely to be very accurate.

The third method proposed for determining surface displacements is given in (10). This method appears to be rather complex and is not really understood by the author. Like the first method described it entails determining the three displacement components of "d" hence is likely subject to the same practical difficulties in application.

2.6 Closure

In surveying the literature on the use of holographic interferometry to determine surface displacements and in particular, application to stress analysis, only three methods were found. It is thus concluded that while in theory it is possible to determine in-plane displacements, in general application the methods are restricted to problems where the normal displacements are small or of the same order of magnitude as the in-plane displacements. In addition, to make the methods economically attractive, development of hardware which would allow rapid and accurate measurement of coordinates, angles, and fractional fringe order numbers is required.

The use of holographic interferometry to measure normal displacements of beams, plates, and diaphrams etc. has been demonstrated and is in current use. If one can conveniently relate the in-plane displacements to the normal displacements as is often the case in flexural problems, then the method of holographic interferometry is a very convenient method to apply since one can work directly on a component with very little preparation of the part. It is also a very sensitive method since one is working with wavelengths of light and perhaps in some instances it may be too sensitive however other methods such as Moire' fringe are in some instances not sensitive enough. This area of holographic interferometry is applicable the problem of the flame plate hence it is used in chapter four to determine the flexural displacements of a flat circular disc and again in chapter five to determine the flexural displacements of the Ruston Hornsby flame plate under a transverse mechanical load.

CHAPTER THREE

ANALYSIS OF A FLAT PLATE WITH A SMALL CIRCULAR HOLE

3.1 Introduction

In this chapter the stress distribution in a flat plate with a small circular hole at the centre and loaded by an axial tensile force in the "x" direction is analized by dynamic relaxation and the results compared with an analytical solution.

The analytical solution provides equations for the stress distribution based on a polar coordinate system. These expressions are fourth order polynomials and the stress values change rapidly near the hole in the centre of the plate. Using polar coordinates for the solution by dynamic relaxation requires the tangential stress on the hole boundary, which is unknown, to be extrapolated from values within the plate and it was suspected that using a simple linear extrapolation might not give accurate results. As a result, extrapolation based on a higher order variation in the tangential stress was used and the results compared for accuracy. For the mesh size used, the linear extrapolation gave good results and assuming a higher order polynomial did not affect the solution.

3.2 Analytical Solution

Figure (3.1) represents a flat plate of unit thickness subject to a tensile load in the "x" direction and having a small circular hole at the centre. The plate has the following geometrical

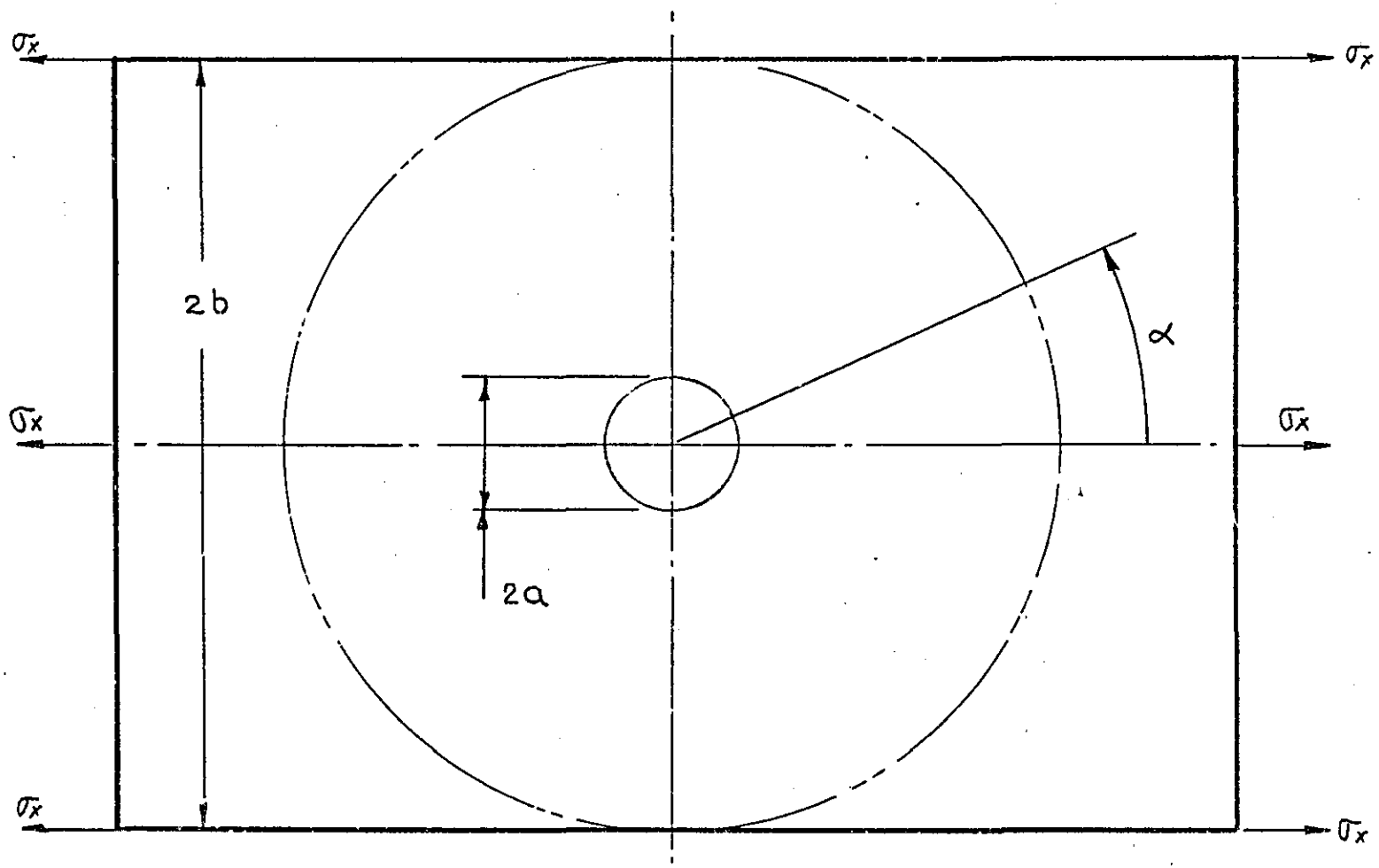

FIGURE 3·1

and physical properties:

$2a = 0.375$ in.

$2b = 2.25$ in.

$\rho = 0.732 \times 10^{-3}$ lb.-sec.^{2} /in.^{4}

$\nu = 0.3$

$E = 30 \times 10^6$ lb./in.^{2}

The stress distribution in the plate is affected by the hole however the effects are localized and if the hole is small in comparison to the width of the plate, the stress at the edge of the plate can be assumed to have the same value as if the hole did not exist. This assumption is based on the principle of Saint-Venant which effectively asserts that if the forces on the boundary of an elastic body are replaced by a statically equivalent system of forces but whose distribution is different, then the stress distribution at some distance from the point of application of the forces remains unchanged; the distance from the point of application of the load being of the same order of magnitude as the dimensions of the body. An analytical solution for this problem is given in (12) and the stress distribution, using a polar coordinate system with the centre of the hole as the origin, is given by the following expressions.

$$\sigma_r = \frac{\sigma_x}{2}\left(1 - \frac{a^2}{r^2}\right) + \frac{\sigma_x}{2}\left(1 + 3\frac{a^4}{r^4} - 4\frac{a^2}{r^2}\right)\cos 2\alpha \qquad (3.1)$$

$$\sigma_\theta = \frac{\sigma_x}{2}\left(1 + \frac{a^2}{r^2}\right) - \frac{\sigma_x}{2}\left(1 + 3\frac{a^4}{r^4}\right)\cos 2\alpha \qquad (3.2)$$

$$\tau_{r\theta} = -\frac{\sigma_x}{2}\left(1 - 3\frac{a^4}{r^4} + 2\frac{a^2}{r^2}\right)\sin 2\alpha \qquad (3.3)$$

The stress distribution along the "y" axis (i.e. when $\alpha = 90^\circ$) is given by:

$$\sigma_r = \frac{\sigma_x}{2}\left(3\frac{a^2}{r^2} - 3\frac{a^4}{r^4}\right) \qquad (3.4)$$

$$\sigma_\theta = \frac{\sigma_x}{2}\left(2 + \frac{a^2}{r^2} + 3\frac{a^4}{r^4}\right) \qquad (3.5)$$

$$\tau_{r\theta} = 0 \tag{3.6}$$

It can be seen from Eq. (3.5) that the tangential stress distribution along the "y" axis has a maximum at the edge of the hole and is equal to three times the stress at the edge of the plate. From Eq. (3.4) it can be seen that at the edge of the hole when r = a, the radial stress is zero and is again zero when "r" is large compared to "a". The stress distribution along the "x" axis (i.e. when $\alpha = 0^{\circ}$) is:

$$\sigma_r = \frac{\sigma_x}{2}\left(2 + 3\frac{a^4}{r^4} - 5\frac{a^2}{r^2}\right) \tag{3.7}$$

$$\sigma_\theta = \frac{\sigma_x}{2}\left(\frac{a^2}{r^2} - 3\frac{a^4}{r^4}\right) \tag{3.8}$$

$$\tau_{r\theta} = 0 \tag{3.9}$$

From Eq. (3.8) it can be seen that along the "x" axis the tangential stress is a maximum at the edge of the hole and is equal to the applied stress but with opposite sign. The radial stress is zero at the edge of the hole and when "r" is large compared with "a", the radial stress is equal to the applied stress.

Figure (3.3) shows the tangential stress distribution along the "y" axis and Fig. (3.4) along the "x" axis. The tangential, radial, and shear stresses are given in tables (3.1), (3.2), and (3.3). The values have been calculated at coordinates compatible with the mesh points used in the dynamic relaxation solution for comparison purposes.

3.3 Solution by the Method of Dynamic Relaxation

Because theplate and loading is symmetrical about the "x" and "y" axis, only one quarter is the plate need be considered as

shown in Fig. (3.2). The selection of the coordinate system for use with dynamic relaxation is not directly obvious. If a rectangular coordinate system is used, the hole will have to be approximated by a series of steps, however if the mesh were fine enough this would not likely be too great a disadvantage. One advantage of using rectangular coordinates for this problem is that no assumption would have to be made regarding the stress at the edge of the plate not being affected by the stress concentration at the hole. The assumption, based on the principle of Saint-Venant that the stress at the edge of the plate is unaffected by the stress concentration at the hole, will lead to large errors if the hole is not small. The limiting case for this particular problem is a plate width to hole diameter ratio of 5 : 1. The problem chosen for analysis has a ratio of 6 : 1 for this reason, hence, use can be made of the principle of Saint-Venant and it would appear that a polar coordinate system would be better in view of having to approximate the hole by a stepped boundary in the case of using rectangular coordinates.

Using polar coordinates, a pseudo-boundary can be formed by specifying the stress conditions on a radius "b" equal to one half the width of the plate. The stress on radius "b" specified in polar coordinates is obtained by transformation of coordinates thus

$$\sigma\alpha = \sigma x \cos^2\alpha + \sigma y \sin^2\alpha + 2 \tau xy \sin\alpha \cos\alpha \qquad (3.10)$$

$$\tau\alpha = -(\sigma x - \sigma y) \sin\alpha \cos\alpha + \tau xy (\cos^2\alpha - \sin^2\alpha) \qquad (3.11)$$

since the stress in the "y" direction at radius "b" is zero and the shear stress in the "x" and "y" direction is zero, then the stresses on radius "b" are:

$$\sigma r = \sigma x \cos^2\alpha \qquad (3.12)$$

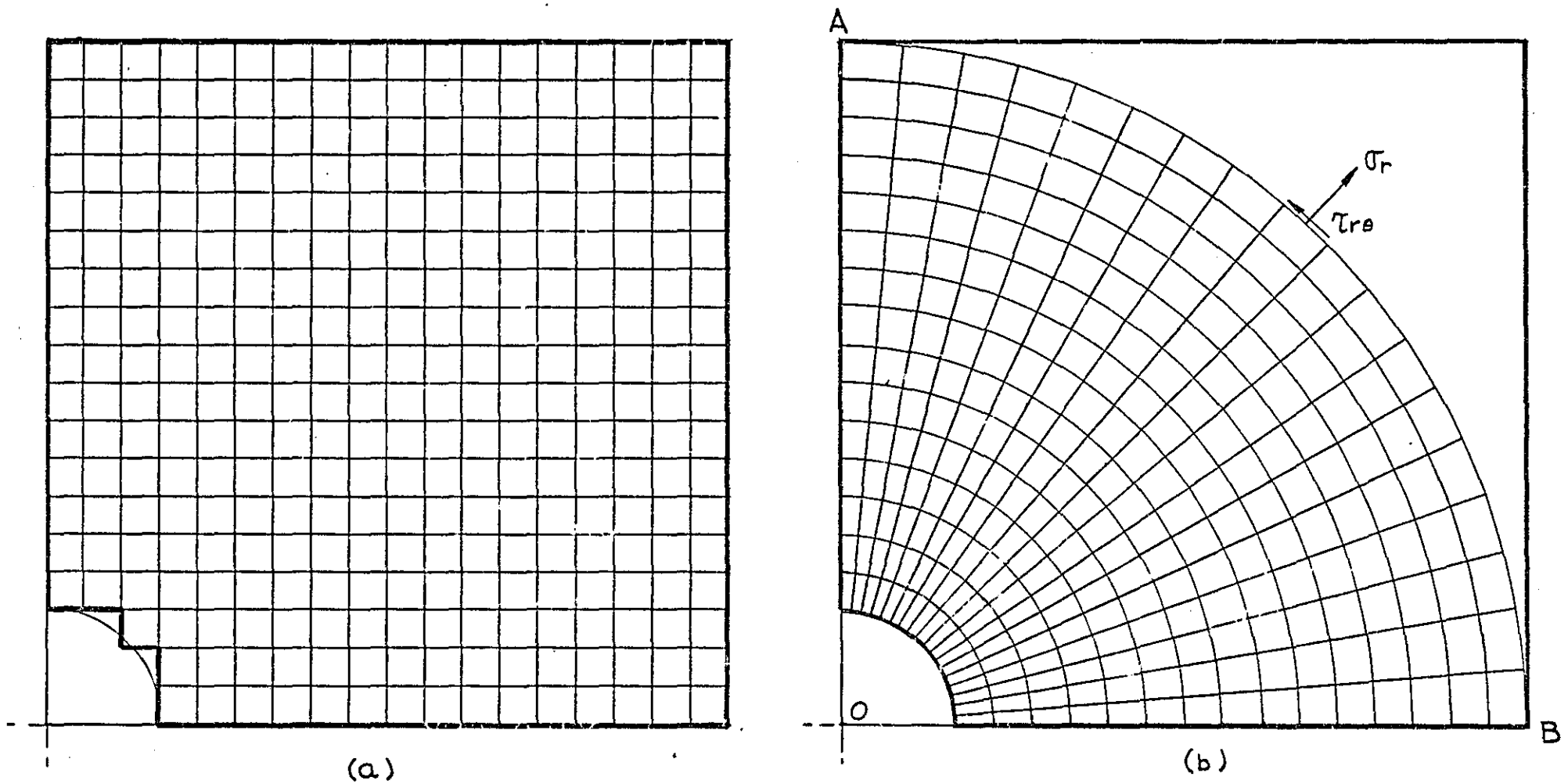

FIGURE 3·2

$$\sigma\theta = \sigma x \sin^2\alpha \qquad (3.13)$$

$$\tau r\theta = -\sigma x \sin\alpha \cos\alpha \qquad (3.14)$$

The problem now takes the form of a flat circular plate with a hole at the centre and loaded by forces at the outside diameter. These forces give rise to stresses defined by Eqs. (3.12), (3.13), and (3.14). The finite difference equations in polar coordinates for the case of plane stress are given in App. "B".

In specifying the boundary conditions, the procedure used in this thesis is to arrange the mesh points so that the velocity and shear nodes coincide with the boundaries and specify all boundary conditions in the velocity and shear equations. Examining Eq. (B.8) on the basis of the above procedure for specifying boundary conditions, the radial velocity on the outside diameter is given by:

$$\dot{U}(I,J) = \dot{U}(I,J)\frac{1-K/2}{1+K/2} + \frac{\Delta t}{\rho(1+K/2)}\left[\frac{2(P-\sigma r(I-1,J))}{\Delta r} + \frac{\tau r\theta(I,J+1)-\tau r\theta(I,J)}{\Delta\theta} + \frac{P-q}{r}\right] \qquad (3.15)$$

In this equation p, q, and α are:

$$P = \sigma x \cos^2\alpha$$
$$q = \sigma x \sin^2\alpha$$
$$\alpha = \Delta\theta\,(J-1/2)$$

On the inner or hole boundary, the radial velocity is:

$$\dot{U}(I,J) = \dot{U}(I,J)\frac{1-K/2}{1+K/2} + \frac{\Delta t}{\rho(1+K/2)}\left[\frac{2(\sigma r(I,J)-P)}{\Delta r} + \frac{P-q}{r}\right] \qquad (3.16)$$

In this equation, "p" is zero since there is no applied radial force in the hole. The tangential stress "q" is unknown, however it can be estimated by extrapolation of values calculated within the plate. Two extrapolation formulae have been derived in App. "F". Since the plate is being entered in the direction of advancing subscripts, then from Eq. (F.4), "q" can be expressed as:

$$q = \sigma\theta(I,J) - .5\left[\sigma\theta(I+1,J) - \sigma\theta(I,J)\right] + \frac{.75}{2}\left[\sigma\theta(I+2,J) - 2\sigma\theta(I+1,J) + \sigma\theta(I,J)\right] - \frac{1.875}{6}\left[\sigma\theta(I+3,J) - 3\sigma\theta(I+2,J) + 3\sigma\theta(I+1,J) - \sigma\theta(I,J)\right] + \cdots \quad (3.17)$$

If it is assumed that the tangential stress varies linearly in the radial direction, all terms in the above expression beyond the 2nd term vanish since 2nd and higher order differences are zero. Thus "q" becomes:

$$q = \sigma\theta(I,J) - .5\left[\sigma\theta(I+1,J) - \sigma\theta(I,J)\right] \quad (3.18)$$

Similarily if it is assumed that the stress varies as a 2nd order polynomial, then all terms beyond the third vanish and "q" is given by:

$$q = \sigma\theta(I,J) - .5\left[\sigma\theta(I+1,J) - \sigma\theta(I,J)\right] + \frac{.75}{2}\left[\sigma\theta(I+2,J) - 2\sigma\theta(I+1,J) + \sigma\theta(I,J)\right] \quad (3.19)$$

Assuming a 4th order polynomial "q" is given by:

$$q = \sigma\theta(I,J) - .5\left[\sigma\theta(I+1,J) - \sigma\theta(I,J)\right] + \frac{.75}{2}\left[\sigma\theta(I+2,J) - 2\sigma\theta(I+1,J) + \sigma\theta(I,J)\right] - \frac{1.875}{6}\left[\sigma\theta(I+3,J) - 3\sigma\theta(I+2,J) + 3\sigma\theta(I+1,J) - \sigma\theta(I,J)\right] + \frac{6.563}{24}\left[\sigma\theta(I+4,J) - 4\sigma\theta(I+3,J) + 6\sigma\theta(I+2,J) - 4\sigma\theta(I+1,J) + \sigma\theta(I,J)\right] \quad (3.20)$$

The shear stress on the outer boundary is given by Eq. (3.14) and since on the inner boundary there are no externally applied forces the shear stress is zero. These conditions are specified when working on the shear equations.

Specifying the conditions on the two radial boundaries is much simpler. Because of symmetry, no tangential displacement occurs on either boundary hence the tangential velocity is zero. Similarily because of symmetry the shear stresses are zero on both boundaries.

In selecting the mesh size, the accuracy and length of computer time required to achieve a steady state solution must be considered. The number of equations to be solved is directly proportional to the number of mesh points or inversely proportional to the product of the mesh dimension for a specific problem. In addition, the value

of the time increment is proportional to the mesh dimensions and in turn the number of iterations required for a solution is inversely proportional to the time increment; the number of iterations is related to the periodic time of oscillation thus, $N = T/\Delta t$ where T is the periodic time and N is the number of iterations in one oscillation. As an example, if in a given problem the mesh sizes are Δx and Δy, then the number of equations to be solved is proportional to $1/(\Delta x \Delta y)$. The time increment is proportional to $1/(1/\Delta x^2 + 1/\Delta y^2)^{-1/2}$. Since the length of time required is directly proportional to the number of equations to be solved and inversely proportional to the time interval, one can write:

$$\text{Length of computer time} \propto \frac{\sqrt{\Delta x^2 + \Delta y^2}}{\Delta x \Delta y} \cdot \frac{1}{\Delta x \Delta y}$$

or if N_x is the number of mesh points in the "x" direction and N_y is the number of mesh points in the "y" direction one can write:

$$\text{Length of computer time} \propto N_x N_y \sqrt{N_x^2 + N_y^2}$$

It can be seen that if one doubles the number of mesh points in both directions then the length of time to obtain a solution is increased eight times.

As in all numerical methods, the accuracy of the solution is enhanced by a fine mesh or large number of mesh points therefore it is desireable to have as fine a mesh as possible. It is obvious then that some sort of compromise must be made between computer time and accuracy. For the problem in this chapter, the mesh size chosen was 19x19. Since the plate width to hole diameter ratio is 6 : 1, the number of radial elements must necessarily be a multiple of 6 and in view of the fact that one would normally expect the stresses to be changing rapidly in the region of a stress concentration, a 19x19 net does not appear too extravagant. For this problem then, the mesh or element dimensions are:

$$\Delta r = 2.25/36 = 0.0625 \text{ in.}$$

$$\Delta \theta = 3.1416/36 = 0.0873 \text{ rad.}$$

The smallest mesh length is:

$$r \Delta \theta = 3.5 \times 0.0625 \times 0.0873 = 0.0191 \text{ in.}$$

Estimating the time interval using Eq. (1.17):

$$\Delta t = (1/\Delta r^2 + 1/(r\Delta\theta)^2)^{-1/2}/c$$
$$= 0.775 \times 10^{-7} \text{ sec.}$$

This value for Δt was found to be low; a value of 0.9×10^{-7} seemed to be about right. The damping constant was obtained by trial and error and a value of $k = 0.03$ gave rapid convergence. The computer programme is given on page 247.

Satisfactory convergence was achieved in 600 iterations which took approximately 25 minutes on the I.C.T 1905 computer; the sum of velocities squared decreased by approximately 8 orders of magnitude.

Two programmes were run. The first programme uses Eq. (3.18) to determine the tangential stress on the hole boundary; this equation assumes that the tangential stress varies linearly near the hole. The results of this solution are given in tables (3.4),(3.5), and (3.6). The tangential stress is plotted against radius in Fig's (3.3) and (3.4) for angles of $\alpha = 87.5^\circ$ and 2.5°. These two angles correspond to the mesh points near the "y" and "x" axis respectively and are sufficiently close to these axes to assume that the stress distribution along these radial lines, i.e. at 87.5 and 2.5°, is representitive of the stresses along the "y" and "x" axes respectively. The second programme uses Eq. (3.20) to specify the tangential stress on the hole boundary; this equation assumes that the tangential stress varies as a fourth order equation. The tangential and radial stresses for angles of 87.5° and 2.5° are given in table (3.7) and should be compared with the corresponding values in tables (3.4) and (3.5)

3.4 Discussion of Results

The main reason for using a numerical method to solve the differential equations which govern equilibrium conditions and define stress-strain relationships is that an analytical solution cannot be found or is too difficult to find because of the complexity of the geometry of the part or of the loading conditions. The results that are obtained from a numerical solution cannot therefore be checked against

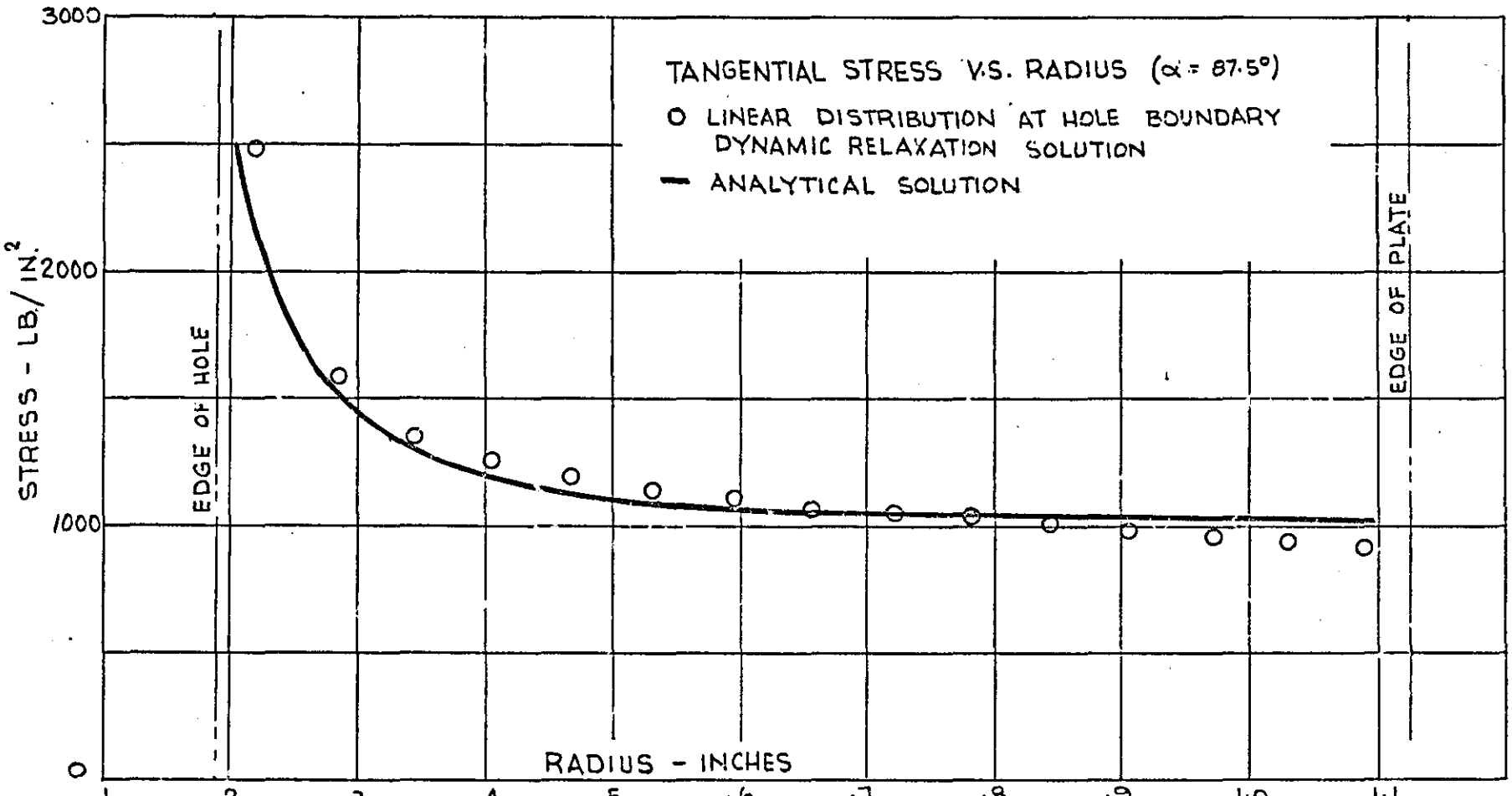
TANGENTIAL STRESS V.S. RADIUS (α = 87.5°)
O LINEAR DISTRIBUTION AT HOLE BOUNDARY DYNAMIC RELAXATION SOLUTION
— ANALYTICAL SOLUTION
STRESS - LB./IN.²
3000
2000
1000
0
EDGE OF HOLE
EDGE OF PLATE
RADIUS - INCHES
.1
.2
.3
.4
.5
.6
.7
.8
.9
1.0
1.1

FIGURE 3·3

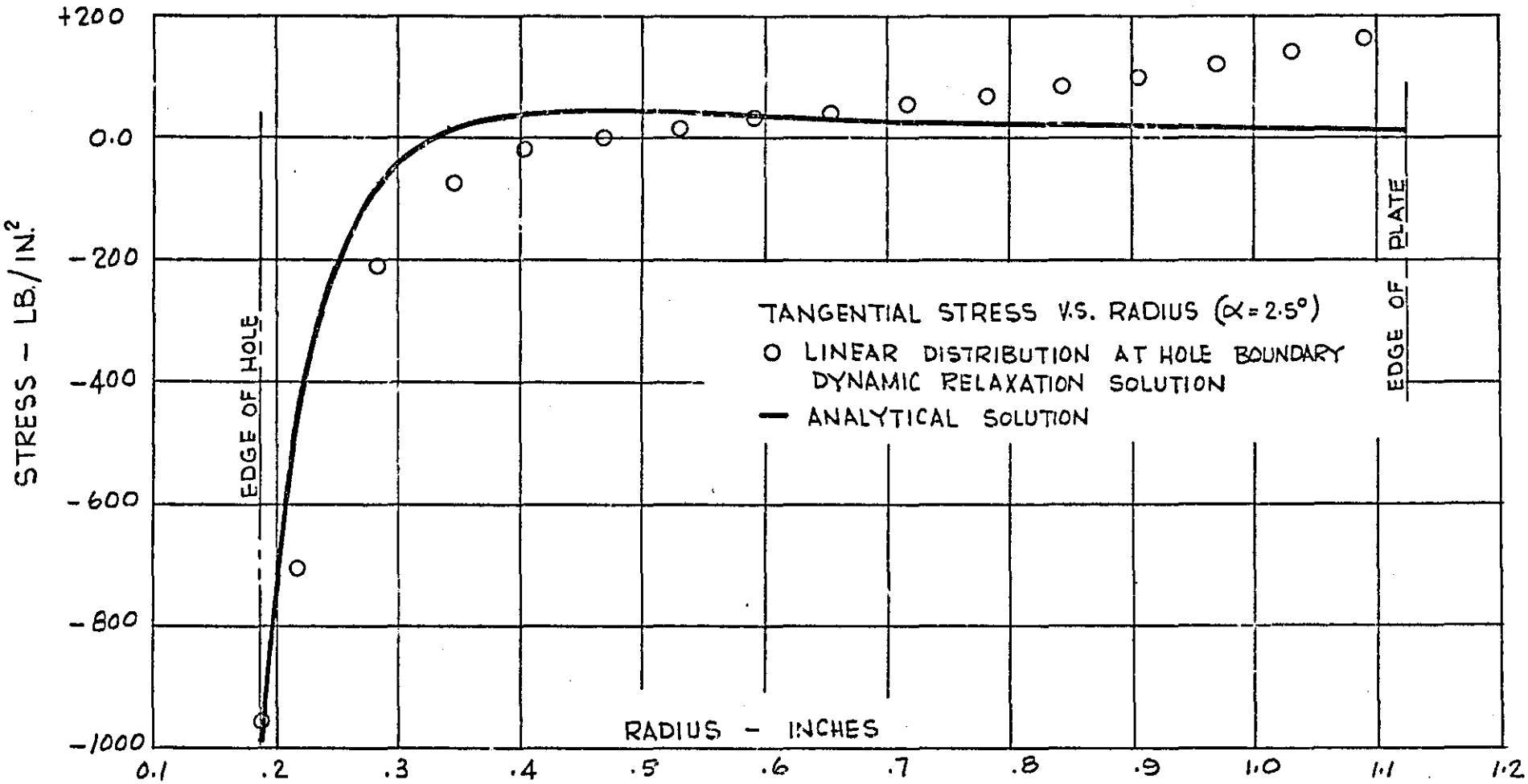
+200
0.0
-200
-400
-600
-800
-1000
STRESS - LB./IN.²
EDGE OF HOLE
EDGE OF PLATE
TANGENTIAL STRESS V.S. RADIUS (α = 2.5°)
O LINEAR DISTRIBUTION AT HOLE BOUNDARY
DYNAMIC RELAXATION SOLUTION
— ANALYTICAL SOLUTION
RADIUS - INCHES
0.1
.2
.3
.4
.5
.6
.7
.8
.9
1.0
1.1
1.2

FIGURE 3.4

an analytical solution (with the exception of cases such as in this chapter where the numerical method is being examined and a problem has chosen that has an analytical solution) however, certain checks can be made which will give the user confidence in the results. One check is the equilibrium of a portion of the object. This can be illustrated as follows.

The summation of the forces in the direction of the applied load must be zero. Taking the tangential stresses along the line O-A, Fig. (3.2), and multiplying these stresses by the respective areas upon which they act gives a load in the "x" direction of -1123.8 lb. The applied load is 1125.0 lb. The sum of the loads in the "x" direction is 1.2 lb. which in view of the magnitude of the applied load is negligible thus it is assumed that the plate is in equilibrium in the "x" direction or direction of the applied load. Similarily the summation of forces in the "y" direction must be zero. Multiplying the tangential stresses along line O-B by the corresponding areas gives 12.9 lb. Since there are no other forces acting in the "y" direction, this value of 12.9 lb. represents a certain amount of unbalance in the "y" direction however in the light of the applied load this unbalance is small thus it is assumed that the plate is in vertical equilibrium.

In addition to equilibrium in the "x" and "y" directions, the plate must be in equilibrium with regards moments about any point. Taking moments about the centre of the hole, the applied load produces a moment of -632.8 lb.-in. The tangential stress along line O-A produces a moment of 661.0 lb.-in. and along O-B, a moment of -30.4 lb.-in. Summing the moments gives -2.2 lb.-in. Again, while this indicates some unbalance, in view of the applied moments it is small thus it is assumed that the plate is in equilibrium with regards moments.

Another check that can be made is on the equilibrium of an individual element. This can be done using Eq. (B.1) and (B.2) in finite difference form. For equilibrium, the stress equilibrium equation must be zero and substituting the stresses obtained by dynamic relaxation into the finite difference form of the equilibrium equation will inevitably give a residual which is an indication of lack of equilibrium. In the early stages of the iteration process this residual will be large and as the solution converges the residual will dimin-

ish and approach a value orders of magnitude less than the maximum calculated in the early stages. Effectively, the velocity at the node points is measure of the residual and by calculating the sum of the squares of the velocity throughout the body, the overall internal equilibrium is measured. As the velocities throughout the body approach zero, the stress equilibrium equations are satisfied; viz. Eq. (B.1) and (B.2) in damped wave form as the velocities approach zero. This check has been made and for the first programme, i.e. the one using Eq. (3.18) for the tangential stress. Initially the sum of the velocities squared increased from zero to 0.304×10^{4} in the first 58 iterations, and then decreased to 0.825×10^{-4} in the remaining 542 iterations thus indicating that a high degree of equilibrium had been reached.

Without comparing the dynamic relaxation solution with the analytical solution, on the basis of the equilibrium checks both external and internal it would appear that a satisfactory solution has been achieved in as much as the programme has been correctly written and the boundary conditions are compatible with the finite difference equations and therefore one can be reasonably confident in the results. As for accuracy, this will depend at this stage, on the fineness of the mesh.

The final check by comparing the dynamic relaxation solution with the analytical solution will give an indication of the accuracy of dynamic relaxation solution. In Fig. (3.3), the tangential stress obtained from the first computer run is compared with the analytical solution along the radial line at an angle of 87.5°. The stress at the edge of the hole is obtained by extrapolation using Eq. (3.18) and is 2839 lb./in.^{2} The value obtained from the analytical solution is 2992 lb./in.^{2}; the value obtained by D.R. is low by about 5 percent. The remaining values obtained by D.R. follow the analytical curve reasonably well although a deviation of 13 percent occurs at the edge of the plate. Figure (3.4) compares the tangential stresses along a radius 2.5° from the "x" axis. At the edge of the hole, D.R. gives, by extrapolation, a stress of -956 lb./in.^{2} and the analytical solution gives -992 lb./in.^{2}; the value obtained by D.R. is low by about 4 percent. The remaining values obtained by D.R. follow the analytical curve but not as well as one would like and calculating percentage deviations indicates large errors especially where the stresses are

small or near zero. While the percentage deviations are large, the effects are not felt by the equilibrium since the forces associated with these small stresses must also be small hence from a point of equilibrium, one appears to be justified in overlooking large deviations in small stresses. From a mathematical point of view this appears to be unrealistic however from an engineering point of view it appears to be the only approach one can take.

Comparing the results of the two computer programmes, the use of a higher order equation to extrapolate the tangential stress at the hole boundary does not appear to improve the solution and in some areas of the plate the solution appears to be somewhat degraded. In problems where one is restricted to a coarse mesh, the use of higher order equations for the stress variation may improve the solution however for the mesh used in this problem a linear stress distribution appears to be a satisfactory assumption.

3.5 Closure

The results obtained by dynamic relaxation for the maximum stresses in the plate agree reasonably well with the analytical results and while large errors exist in areas where the stresses are small, these errors do not detract from the overall solution if looked at from an engineering point of view in the case of designing for strength. The use of higher order approximations for the unknown stresses on boundaries is not necessary if the mesh is fine enough although this point could be investigated further.

CHAPTER FOUR

ANALYSIS OF A SIMPLY SUPPORTED FLAT CIRCULAR PLATE SUBJECT TO A LATERAL CONCENTRIC LOAD

4.1 Introduction

In this chapter, the deflection of a simply supported flat circular plate subject to a lateral concentric load is determined using holographic interferometry and dynamic relaxation. The results are compared with an idealised analytical solution. A comprehensive analysis of the stress distribution and the in-plane displacements is also made using dynamic relaxation.

The practical case examined by holographic interferometry consists of a 4" diameter mild steel plate 5/16" thick supported by a flat steel ring, 3-3/4" inside diameter. The load is transmitted to the plate by means of a 1" diameter brass rod. The assumptions made to idealise the plate and loading condition are that the plate is supported at its outside edge and that upon deflecting, the rod through which the load is applied remains flat so that the load is concentrated on a circle of 1" diameter.

The analysis by dynamic relaxation is based on the idealised plate. The fundamental equilibrium and elasticity equations are used in place of the differential equations for bending of thin plates for reasons of interest only. Since the support is considered as acting over one mesh width, a degree of similarity exists with the experimental conditions.

4.2 Holographic Analysis

The experimental arrangement is shown in Fig's (4.1),(4.2), and (4.3). The loading mechanism consists of a hydraulic ram integral with the support ring. A dead weight tester is used to provide an accurate hydraulic pressure. The load is applied directly to the specimen by the hydraulic ram piston. The specimen was preloaded in the rig by a load of 114 lb. to ensure good contact with the support ring and to eliminate any possible extraneous movement.

The pertinent holographic dimensions are given in Fig. (4.3). Checking the angles of viewing and illumination, the maximum for both is 90°from the surface of the plate. The minimum viewing angle is:

$$\phi' = \tan^{-1}(23.5/2.63) = 83^\circ 36'$$

The minimum angle of illumination is:

$$\phi = \tan^{-1}(25.0/(\sqrt{1.75^2 + 0.75^2} + 1.875)) = 81^\circ 24'$$

For the maximum angles of viewing and illumination, the sensitivity is (Sin 90° + Sin 90°) = 2.0 and for the minimum angles of viewing and illumination the sensitivity is (Sin 83°36' + Sin 81°24') = 1.983; this value is not exactly correct since these two minimums do not occur simultaneously however it does serve to justify the assumption that the variation in sensitivity across the surface is negligible and that the angles of viewing and illumination are constant and equal to 90°.

Seven frozen fringe holograms were made with loads varying from 55.8 lb. to 156. lb. Photographs of the interference patterns are given in Fig's (4.4) to (4.10) inclusive. The deflected shape of the plate was determined from the fringe spacing which was measured on an enlarged photographic copy of the reconstructed image. Fringe order numbers were assigned to each dark fringe beginning at the edge of the support and the relative deflection at each fringe was determined using Eq. (2.9) thus:

$$N\lambda = w(\sin\phi + \sin\phi')$$

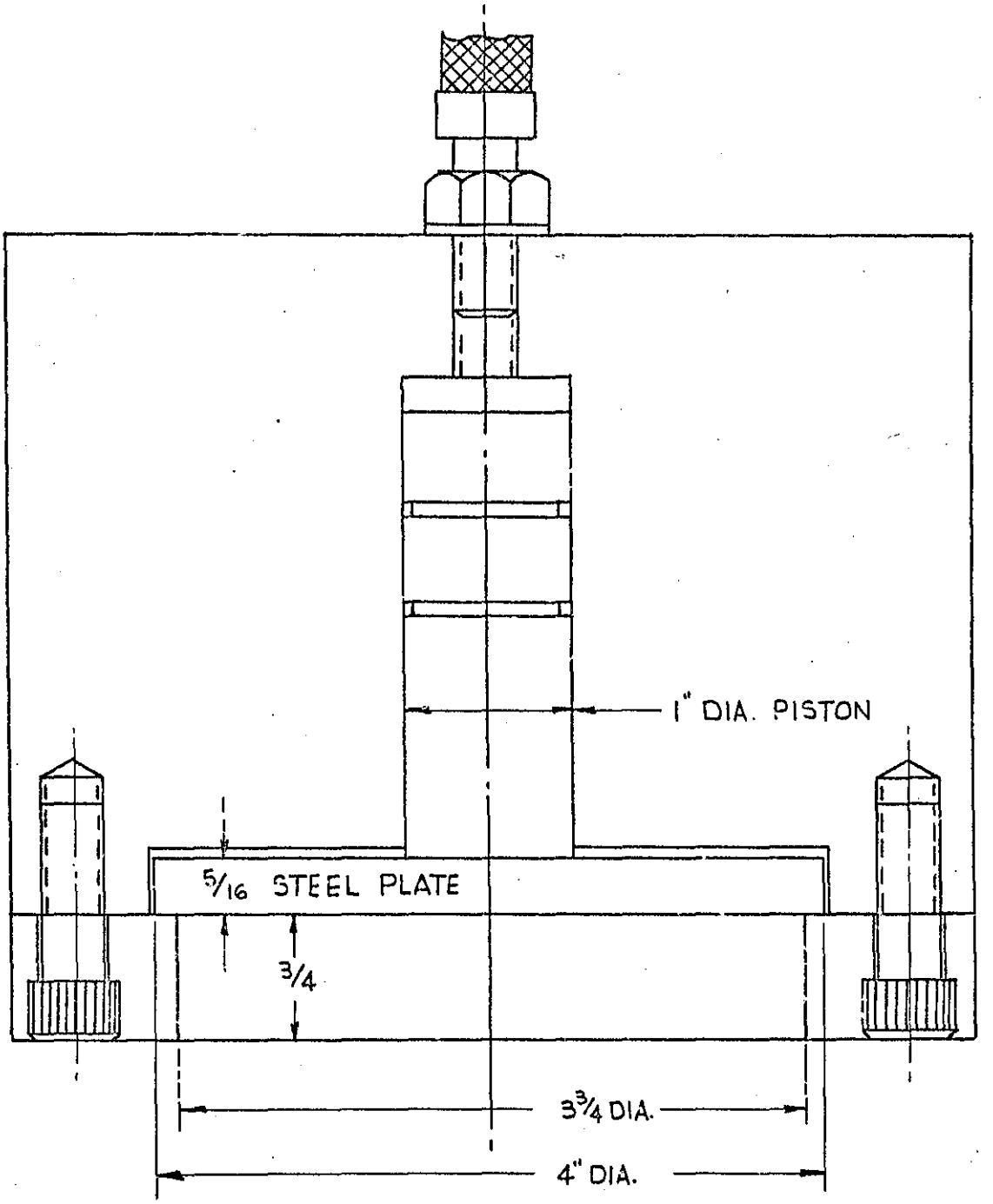

FIGURE 4.1

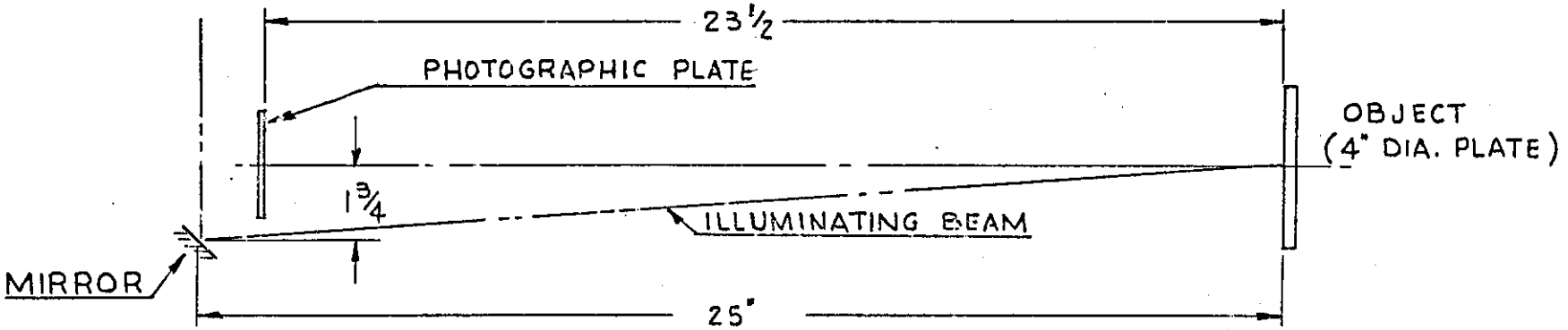

PLAN

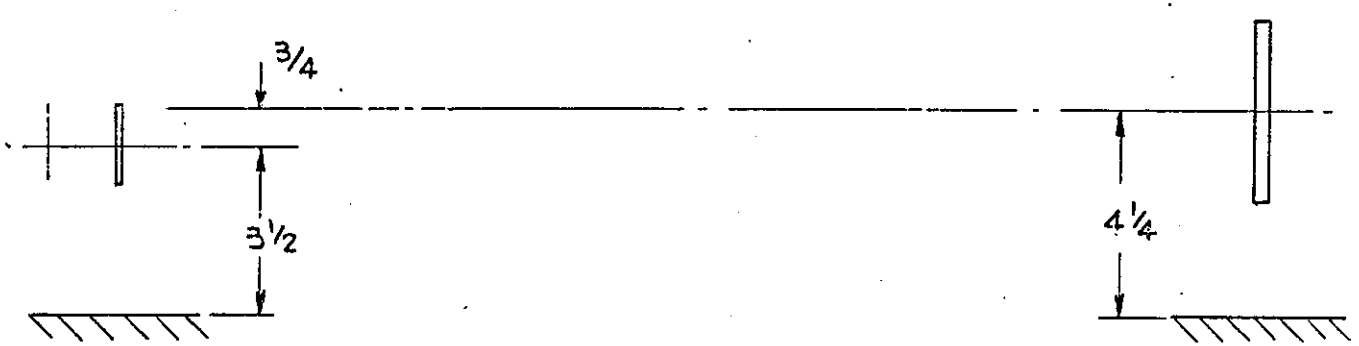

ELEVATION

FIGURE 4·2

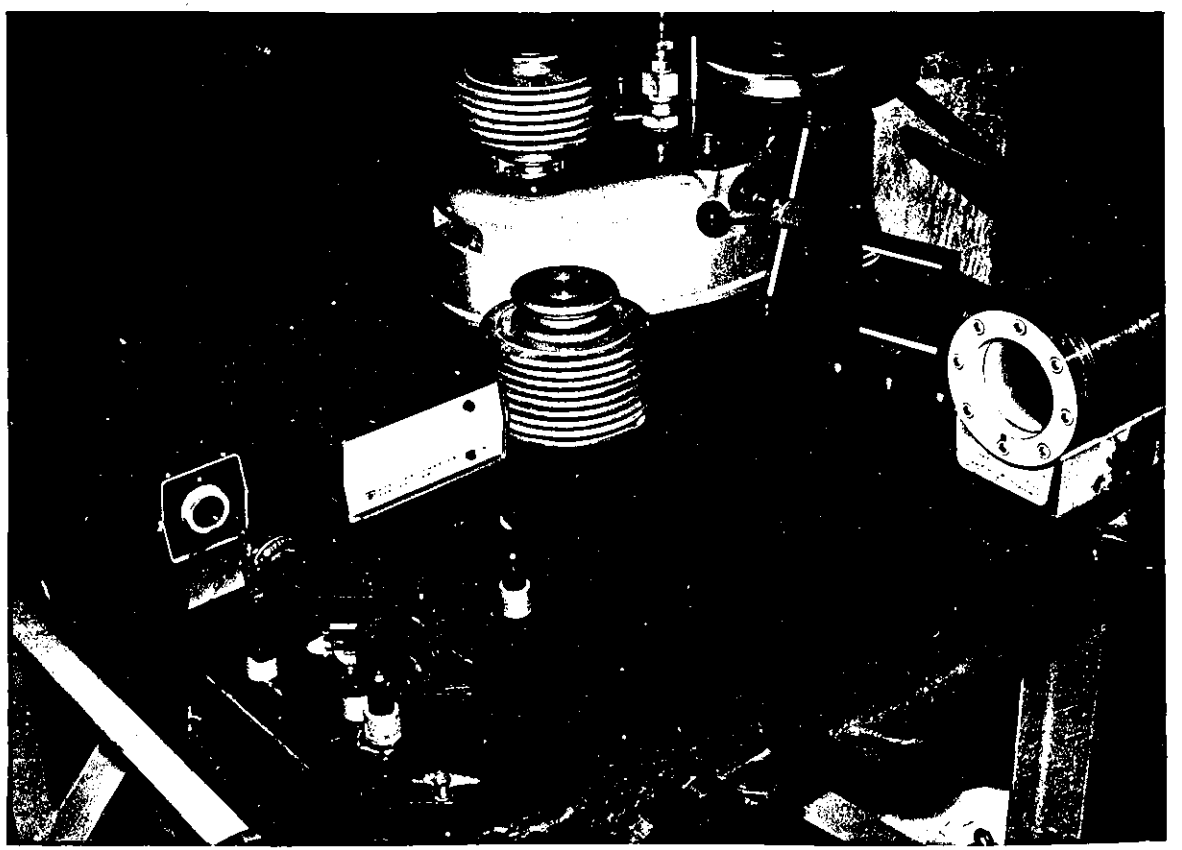

FIGURE 4.3

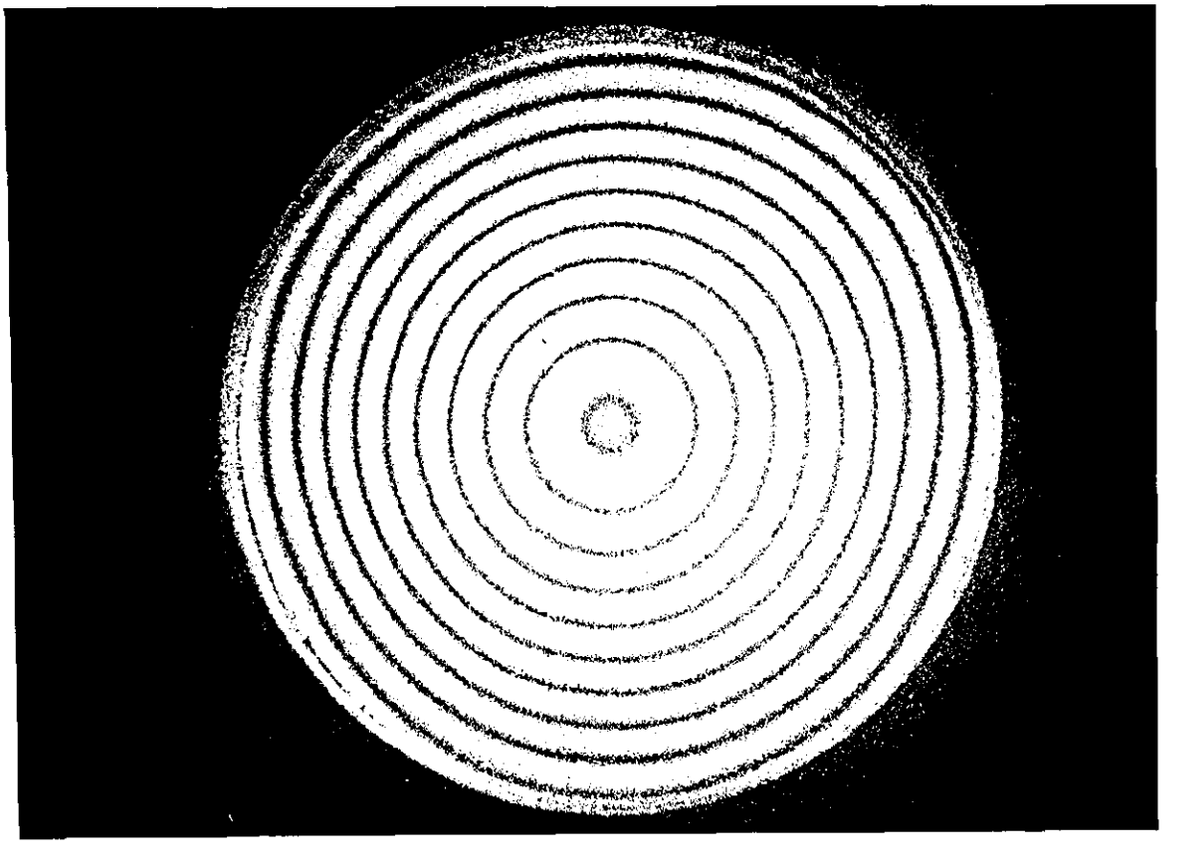

FIGURE 4.4
(Load 55.8 Lb.)

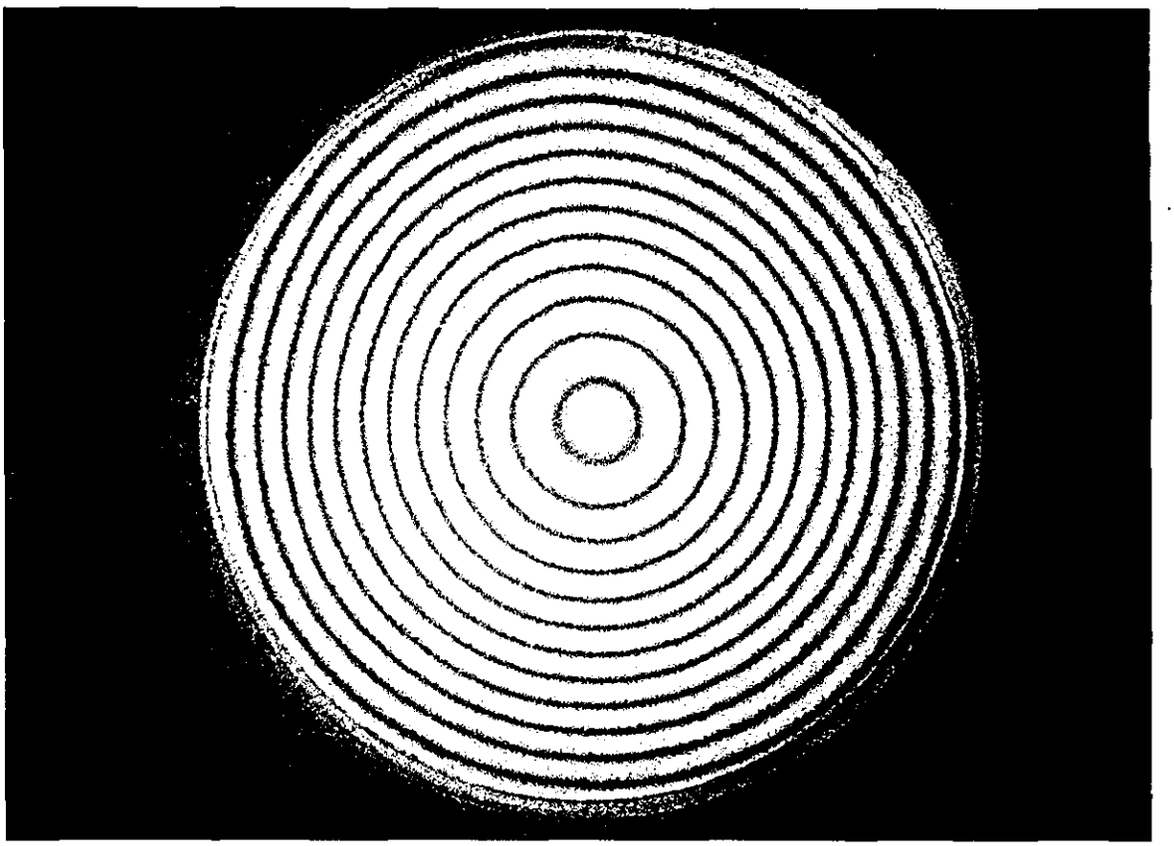

FIGURE 4.5
(Load 72.5 Lb.)

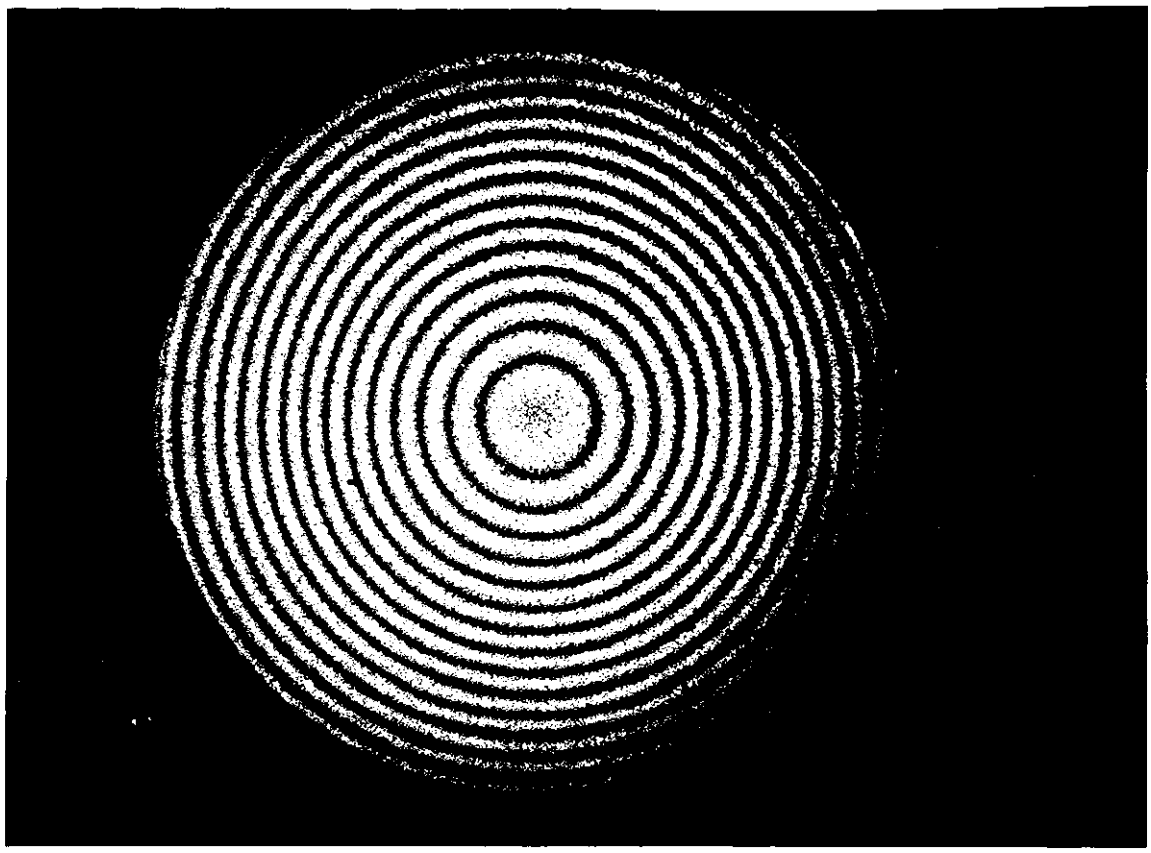

FIGURE 4.6

(Load 89.1 Lb.)

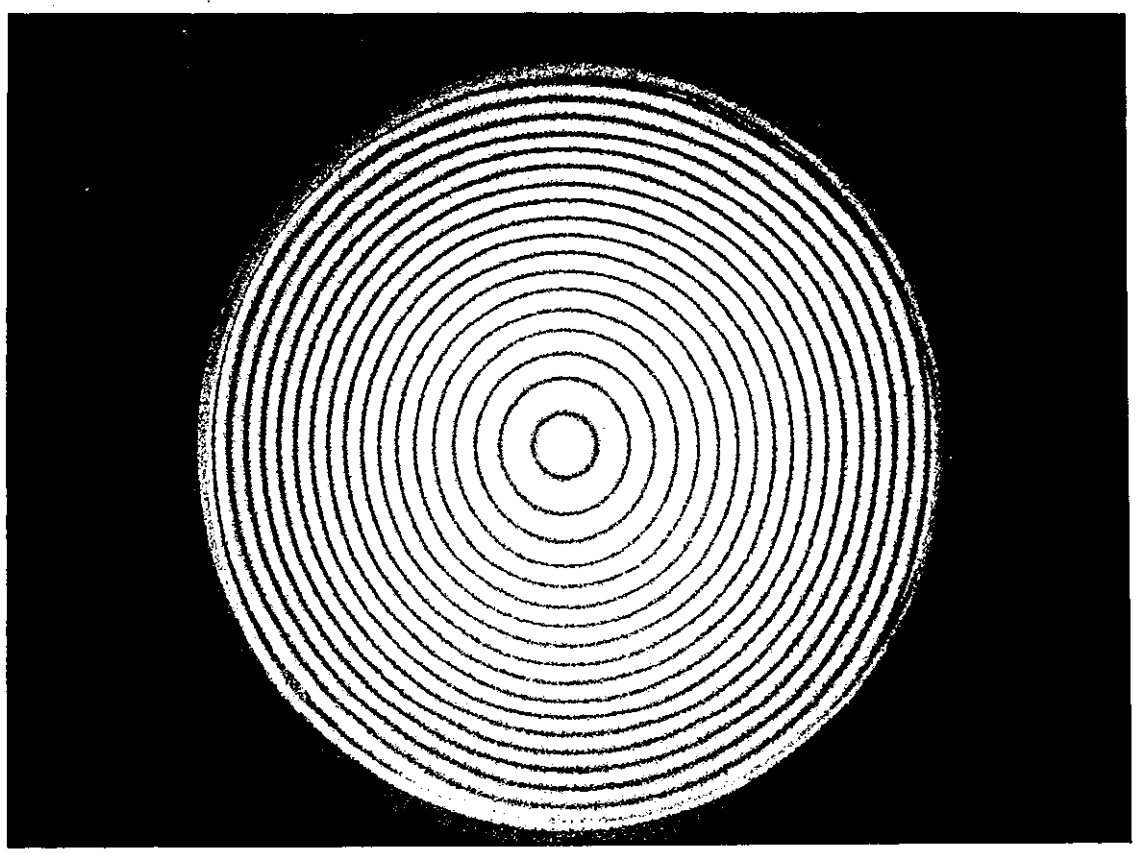

FIGURE 4.7

(Load 106 Lb.)

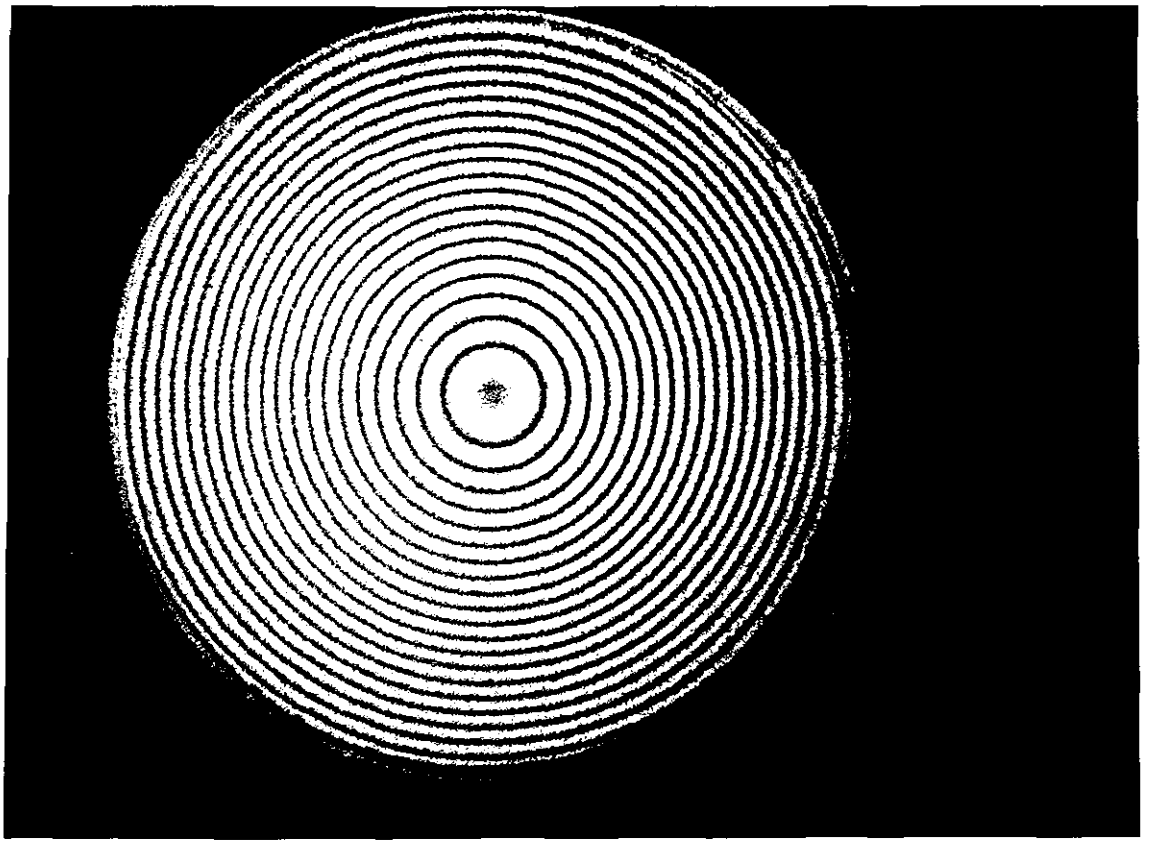

FIGURE 4.8

(Load 122 Lb.)

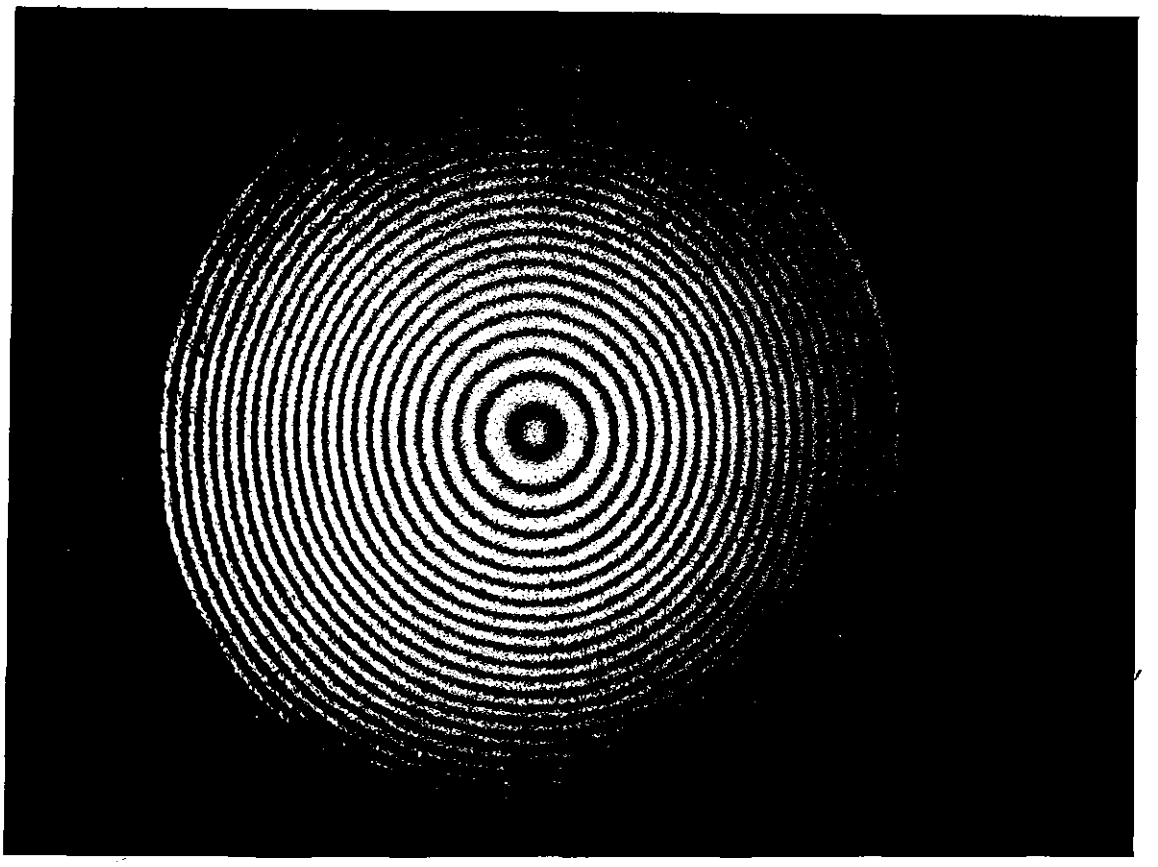

FIGURE 4.9

(Load 140 Lb.)

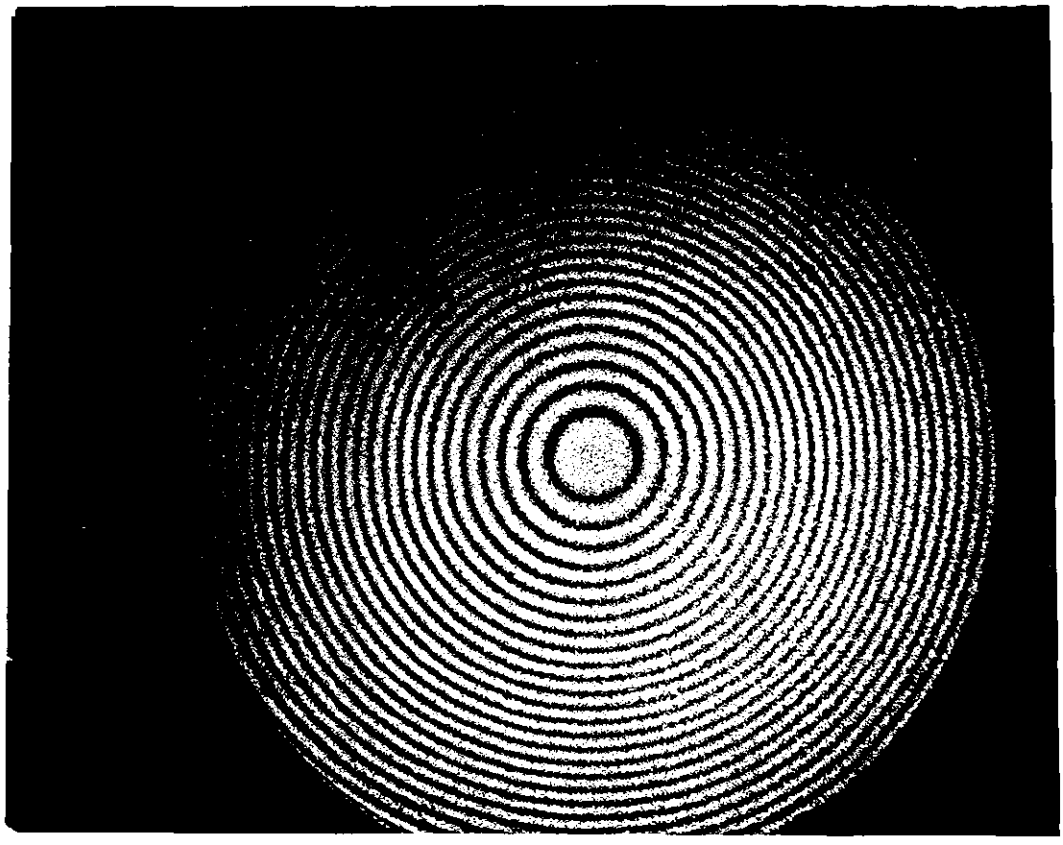

FIGURE 4.10
(Load 156 Lb.)

Using a helium-neon laser and for angles of viewing and illumination of 90°, the above expression reduces to:

$$W = 0.125 \times 10^{-4} N$$

Tables (4.1) to (4.7) give the fringe order number v.s. distance from the edge of the support and from the actual edge of the plate. The actual measurements of the fringe distances are multiplied by a scale factor relating the enlarged photographic copy of the fringe pattern with the actual size of the plate. The fringe pattern in each case seems to have some eccentricity and in order to enhance the accuracy of the analysis, the spacing was measured along three different radii and the results averaged. The results given in tables (4.1) to (4.7) are plotted in Fig's (4.11) to (4.17) along with the analytical results for comparison purposes.

4.3 Analysis by Dynamic Relaxation

The deflection, bending moments, and the resulting bending stresses in a thin plate can be obtained by dynamic relaxation using the differential equations for bending of thin plates, (5). This method does not take into account deflection due to shear or local effects of concentrated loads or support configuration. While these effects are generally negligible in thin plates they are not in thick plates where the diameter to thickness ratio is less than 4 : 1. The plate being analized in this chapter falls well within the category of thin plates and the loads being small will cause small deflections and stresses in the plate however from an interest point of view, the analysis has been based on the fundamental equilibrium and elasticity equations. To economise on computer time, the problem has been formulated using axi-symmetric stress distribution equations; the finite difference equations are given in App. C.

The mesh size was chosen arbitrarily as 16x6 and gives satisfactory results. The mesh dimensions are:

$$\Delta r = 0.1333$$
$$\Delta z = 0.0625$$

In specifying the boundary conditions, the support acts over one full mesh width thus for the mesh 15,1 the displacement is zero and therefore the velocity is zero. The applied load is specified as an axial stress acting on the surface of the plate over the mesh 4,6 and is incorporated in the velocity equation as in previous examples. The shear stress τ_{rz} is zero on the surface of the plate as is the axial stress except under the applied load. The zero axial stresses are specified in the velocity equation and the zero shear stresses in the shear equation. A copy of the programme is given on page 250.

The time increment was calculated using Eq. (1.17) and found to be 0.255×10^{-6} sec. A value of 0.270×10^{-6} was tried and the solution diverged. A value of 0.25×10^{-6} was used and found to be satisfactory. The damping constant was found by trial and error and a value of 0.010 gave a good rate of convergence.

Two computer runs were made, one with the load equal to 55.8 lb. and the second with the load equal to 156. lb. The first run was allowed to complete 2000 iterations and the second, 1100 iterations. Convergence was satisfactory at 1100 iterations and required just over 19 minutes on the I.C.T. 1905. The results are given in tables (4.8) to (4.17) and include radial stress, tangential stress, transverse shear stress, axial stress, transverse or lateral displacements, and in-plane displacements for both loading cases. The lateral displacements are plotted in Fig's (4.11) and (4.17) along with the results of the analytical solution and the holographic solution. The radial and tangential stresses being specified at mesh points below the surface of the plate have been extrapolated linearly to obtain the stresses on the surface of the plate. These values are plotted in Fig's (4.18),(4.19), (4.21) and (4.22) along with the analytical results. As a point of interest, the axial stress distribution through the thickness of the plate under the concentrated load is shown in Fig's (4.20) and (4.23). The transverse shear stress distribution through the thickness of the plate is given in Fig. (4.25) for the 156. lb. load and the bending stress distribution through the thickness of the plate is given in Fig. (4.24) for the 156 lb. load. These stress distributions through the thickness are under the concentrated load.

4.4 Analytical Solution

Equations which define the deflected shape of the plate based on an analytical solution are given in (13). Because the load is discontinuous, separate expressions are required for the two areas of the plate, i.e. the area inside and outside the load circle. The deflection of the plate within the load circle is defined by:

$$W = \frac{P}{8\pi D}\left[(b^2+r^2)\ln\frac{b}{a} + (a^2-b^2)\frac{(3+\nu)a^2-(1-\nu)r^2}{2(1+\nu)a^2}\right]$$

For the area outside the load circle, the deflection is defined by:

$$W = \frac{P}{8\pi D}\left[(a^2-r^2)\left(1+\frac{1}{2}\frac{(1-\nu)}{(1+\nu)}\frac{a^2-b^2}{a^2}\right) + (b^2+r^2)\ln\frac{r}{a}\right]$$

The radial and tangential stresses on the surface of the plate are defined by:

$$\sigma_r = \pm 6\frac{M_r}{t^2} \qquad \sigma_\theta = \pm 6\frac{M_\theta}{t^2}$$

where:
$$M_r = -D\left(\frac{d^2w}{dr^2} + \frac{\nu}{r}\frac{dw}{dr}\right)$$

$$M_\theta = -D\left(\frac{1}{r}\frac{dw}{dr} + \nu\frac{d^2w}{dr^2}\right)$$

and:
$$D = \frac{E t^3}{12(1-\nu^2)}$$

The radial and tangential stress distribution through the thickness of the plate is linear with both stresses being zero on the neutral axis or mid plane of the plate; the stress on the concave surface is negative and on the convex surface, positive. The transverse shear stress distribution is parabolic through the thickness of the plate with the maximum being at the mid-plane of the plate, and is defined by:

$$\tau_{rz} = \frac{12V}{t^3}\left(\frac{t^2}{8} - \frac{z^2}{2}\right)$$

where "V" is the shear force per inch in the tangential direction at radius "r", and "z" is measured from the mid-plane of the plate.

The deflection, radial stress and tangential stress have been

calculated at radii corresponding to the radial mesh points used in the dynamic relaxation solution. The deflection is determined for the loads used in the holographic experiments; the results are given in table (4.18). The stresses were calculated for the 55.8 and 156. lb. loads only; the results are given in table (4.19) for the stresses on convex surface. The tangential stress and transverse shear stress distribution through the thickness of the plate were calculated for the 156 lb. load; the calculations being simple, are not presented in the tables.

4.5 Discussion of Holographic Solution

The difficulty encountered in analizing the fringe patterns was the determination of the fringe order numbers or particularily the location of the zero order fringe. In the case of a frozen fringe hologram, the zero order fringe will be a bright band and of course will be loacated at the point of zero displacement. If the support ring did not move on the application of the load, the zero order fringe would be located at the edge of the support ring hence one would see a bright region at the edge of the support. In all of the patterns, a certain amount of eccentricity can be seen and in some cases a dark fringe can be seen very close to the support ring and in other cases, disappearing under the edge of the support. This would seem to indicate two possible conditions; 1, the plate and support are not flat relative to each other causing the support to be nonuniform and thus causing the plate to deflect nonuniformly, and 2, the support deflects on the edge. The first condition would explain the eccentricity of the fringe pattern and the second condition would explain the close proximity of a dark fringe to the edge of the support ring. A paper gasket was used between the plate plate and the support ring in an attempt to ensure an even distribution of the support reaction however it is still possible that the distrbution was not uniform. If the support has moved on application of the load, then it is difficult if not impossible to assign order numbers to the fringes however if the support moves uniformly all around then the total displacement will take the form of a constant added to the flexural displacement of the plate thus only the relative displacement of the plate is of interest. In other words, a normal displacement of the support ring will cause a uniform phase shift over the surface of

the plate which would have the effect of moving the dark fringes closer to the edge of the support ring.

To obtain the relative deflection curve of the plate, the actual fringe order numbers are not important and for this case the numbering system adopted was to number the first dark fringe as N = 1 beginning at the edge of the support and proceeding toward the centre of the plate, the fringes are numbered 2,3,4, etc. From the knowledge that the plate moves normally with the maximum deflection at the centre, the fringes can be numbered as described in increasing order. The reason for beginning at the edge of the support ring is to provide a reference point from which to work and since the fringe patterns are slightly eccentric, the fringe location was measured on three different radii and the results averaged.

Having the deflected shape of the plate relative to the first dark fringe and the location of the first dark fringe in relation to the outside diameter of the plate, the curve was extrapolated to the outside diameter of the plate and then superimposed onto the analytical so that the deflection at the edge of the plate was zero. Superimposing the holographic curve onto the analytical curve, effectively adds a constant to the holographic curve so that the deflection at the outside diameter is zero. Fig's (4.11) to (4.17) show the relative curve and the resulting curve which is obtained by matching the holographic curve and the analytical curve at the outside diameter. The deflection at the centre of the plate was obtained by extrapolation.

In all of the curves, the holographic results show a greater deflection at the centre than the analytical results. Two reasons for this have been postulated. First, it was noticed that a considerable amount of friction existed in the hydraulic ram and while reworking the piston removed some of the friction, it was not entirely eliminated. The procedure used to load the plate was to apply a load greater than that desired and then to remove the excess. This procedure would tend to cause the static friction force to act in the same direction as the hydraulic load and thus the load on the plate would be greater than anticipated. The friction force is not likely to be constant however it should constitute a smaller percentage of the hydraulic load at the higher loads consequently the deviation in the deflection of the plate

should be less at higher loads. The results tend to indicate this tendancy.

The second reason for the holographic results showing a greater deflection is that the hydraulic piston might not have remained flat on application of the load so that the load tended to be somewhat distributed towards the centre of the plate. The load being closer to the centre of the plate would cause the deflection to be greater. Some tendancy for this condition to exist can be seen in Fig's (4.13),(4.14),(4.15), and (4.17) where the holographic curve tends to be flatter in the region between the edge of the plate and approximately two thirds of the way in towards the centre of the plate.

One might expect the holographic results to indicate a lesser deflection since the plate is not supported at the edge but on a diameter which is about 6 percent smaller.

With the exception of the results shown in Fig's (4.11) and (4.16) the holographic results are reasonably good but could be improved. Improvements could be made to the loading mechanism to reduce the friction or if this were not possible, a thicker plate could be used so that the friction in the mechanism would be a much smaller fraction of the applied load. The support ring inside diameter could have been greater so that the plate would have been supported closer to the edge. Also the load could have been more concentrated; this could be achieved by undercutting the end of the piston where it contacts the plate. It is felt that these changes would improve the solution such that better agreement with the analytical would be achieved.

4.6 Discussion of Dynamic Relaxation Solution

The deflection curve obtained by dynamic relaxation deviates from the analytical curve towards the support. The most obvious reason for this is that the support is specified in the solution as acting over one full mesh width which in this case is 0.1333 in. If the curve obtained by dynamic relaxation were matched with the analytical curve at the edge of the plate as was done in the holographic solution, the dynamic relaxation curve would indicate a deflection at the centre

greater than the analytical curve by about 4.3 percent. Part of this discrepancy can be accounted for by the manner in which the load is applied; the load being spread over a mesh width whose centre is 0.47 in. from the centre of the plate instead of the actual 0.5 in. and is distributed instead of concentrated. Both the condition at the support and at the point of load application could be improved by using a finer mesh however the results for the mesh used are quite good.

The radial and tangential stresses obtained by D.R. are compared with the analytical results in Fig's (4.18),(4.19),(4.21), and (4.22) and show good agreement with the analytical results. The maximum error in the region of the highest stress does not exceed 6.5 percent for both loading cases and for both radial and tangential stress. The results obtained by D.R. show a higher stress at the centre of the plate; this is in agreement with the deflection being greater when the D.R. curve and analytical deflection curve are matched at the outside diameter.

Figure (4.24) compares the tangential stress distribution through the thickness of the plate for the 156 lb. load. The D.R. results are in good agreement with the analytical values. Figure (4.25) compares the transverse shear stress distribution through the thickness of the plate for the 156 lb. load. The point chosen for the comparison is directly under the applied load and some discrepancy exists towards the loaded surface. It is expected that this discrepancy is due to the load being concentrated and discontinuous in that region. In general the dynamic relaxation results are in good agreement with the analytical results.

From an interest point of view, the axial stress distribution through the thickness of the plate is given in Fig's (4.20) and (4.23), for the region under the concentrated load. It can be seen that the concentrated load which acts over one full mesh width is very localized and the effects effects are completely dispersed within one mesh width on either side of the load. The accuracy of the values is assumed to be reasonably good however since in practice the load is much more concentrated, the results cannot be considered applicable to the actual problem. The fact that the dynamic relaxation solution gives the axial stress distribution is, in this case, the interesting feature and illu-

strates the ease with which one can obtain a complete solution to a stress problem. If one wished to accurately determine the axial stress distribution under the load, that portion of the plate under the load could be isolated and a fine mesh used. The boundary conditions on the isolated portion would be the stresses calculated in the original solution of the plate taken as a whole.

4.7 Closure

With the exception of two sets of results, the holographic results agree well with the analytical solution for the deflection of the plate. The discrepancy of the holographic results in two out of seven cases is believed due to cumulative errors in the experimental technique which can be avoided by taking proper care.

The dynamic relaxation solution is also in good agreement with the analytical solution in both deflection analysis and stress distribution.

It is concluded that the procedures used in this chapter can be extended to the problem of the flame plate.

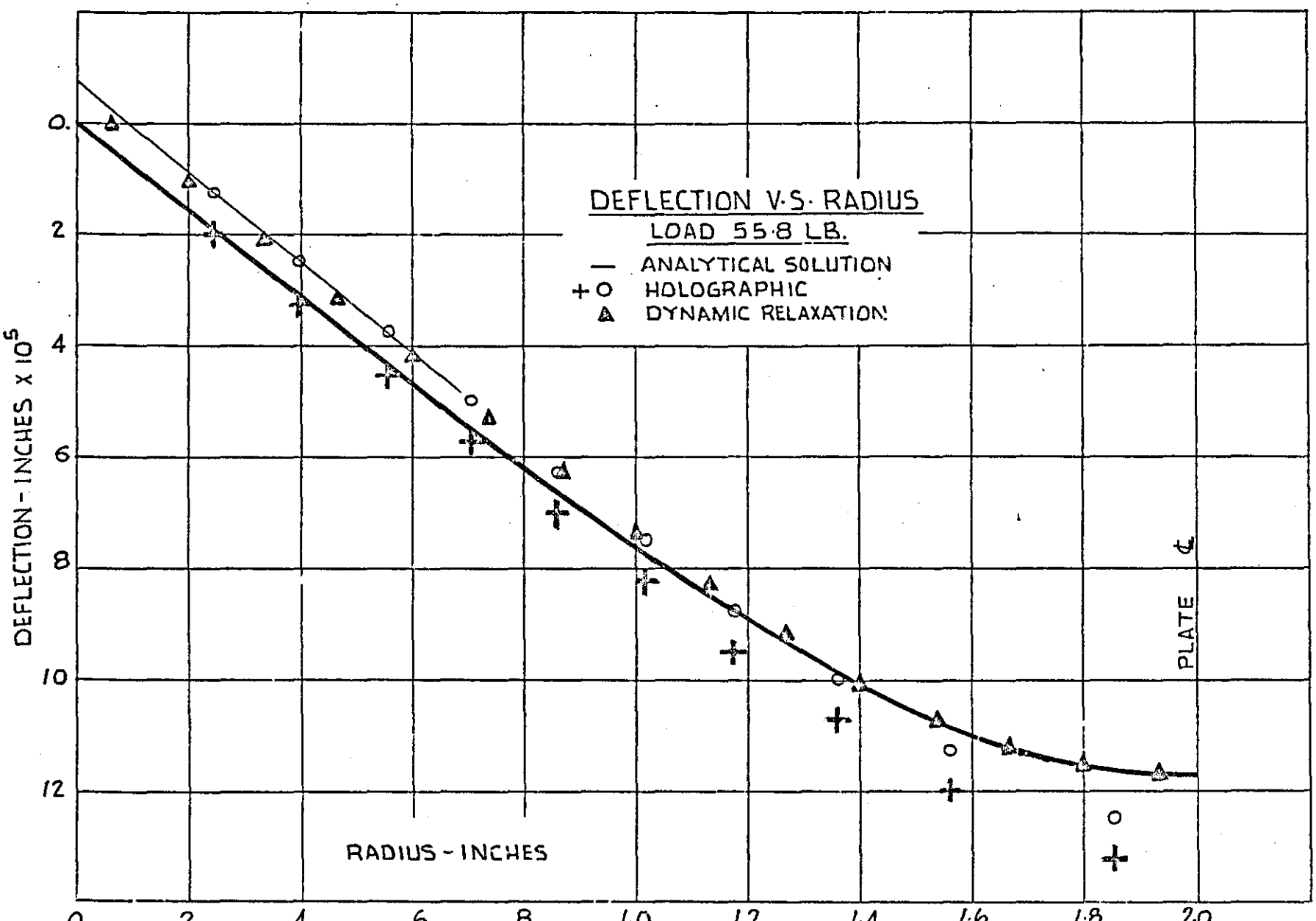
DEFLECTION V·S· RADIUS
LOAD 55·8 LB.
— ANALYTICAL SOLUTION
+ O HOLOGRAPHIC
△ DYNAMIC RELAXATION
DEFLECTION - INCHES X 10^5
0.
2
4
6
8
10
12
RADIUS - INCHES
0
.2
.4
.6
.8
1.0
1.2
1.4
1.6
1.8
2.0
PLATE ℄

FIGURE 4·11

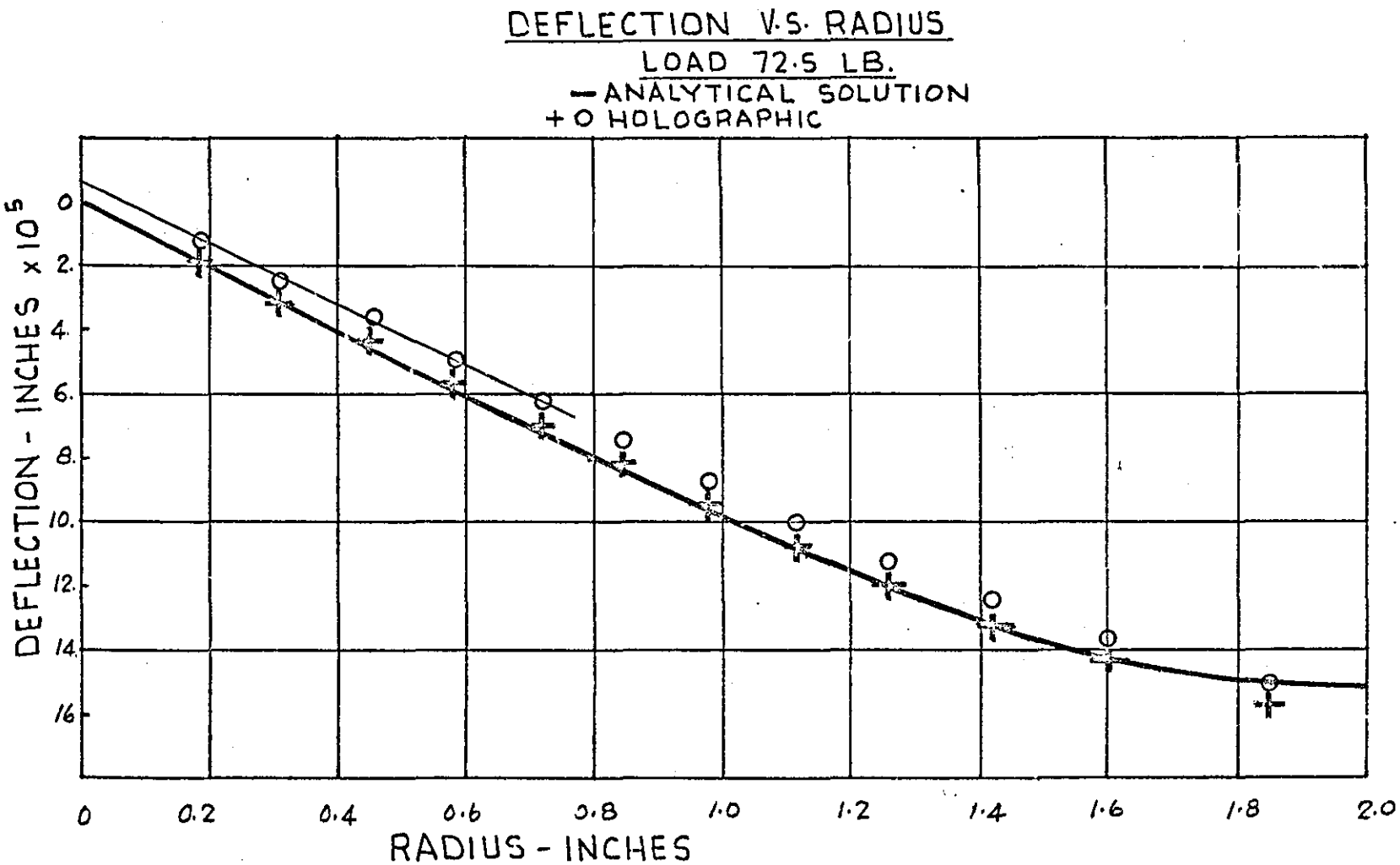
DEFLECTION V.S. RADIUS
LOAD 72.5 LB.
— ANALYTICAL SOLUTION
+ O HOLOGRAPHIC
DEFLECTION - INCHES x 10^5
0
2.
4.
6.
8.
10.
12.
14.
16
0
0.2
0.4
0.6
0.8
1.0
1.2
1.4
1.6
1.8
2.0
RADIUS - INCHES

FIGURE 4.12

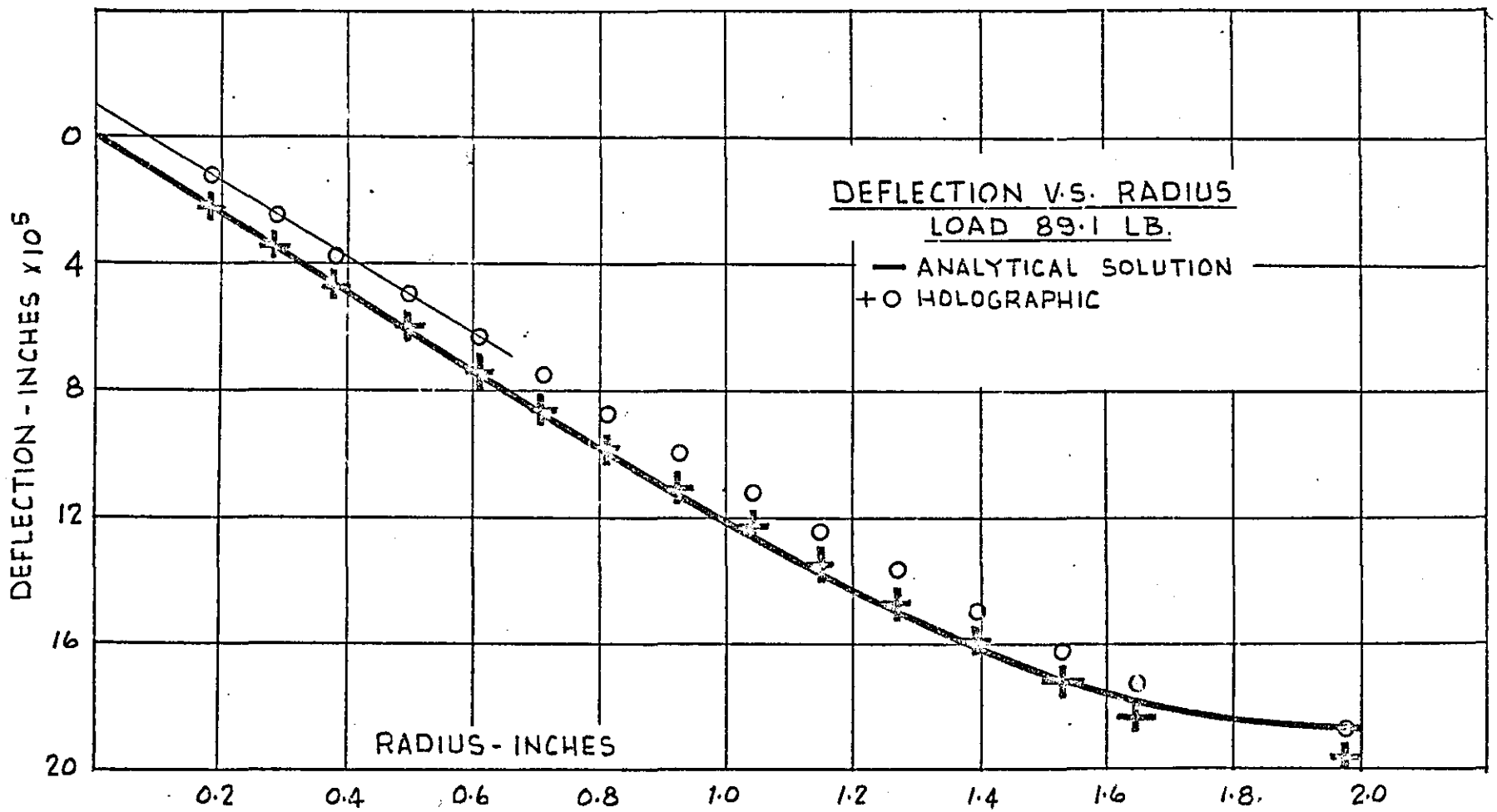
DEFLECTION V.S. RADIUS
LOAD 89.1 LB.
— ANALYTICAL SOLUTION
+O HOLOGRAPHIC
DEFLECTION - INCHES X10^5
RADIUS - INCHES
0
4
8
12
16
20
0.2
0.4
0.6
0.8
1.0
1.2
1.4
1.6
1.8
2.0

FIGURE 4.13

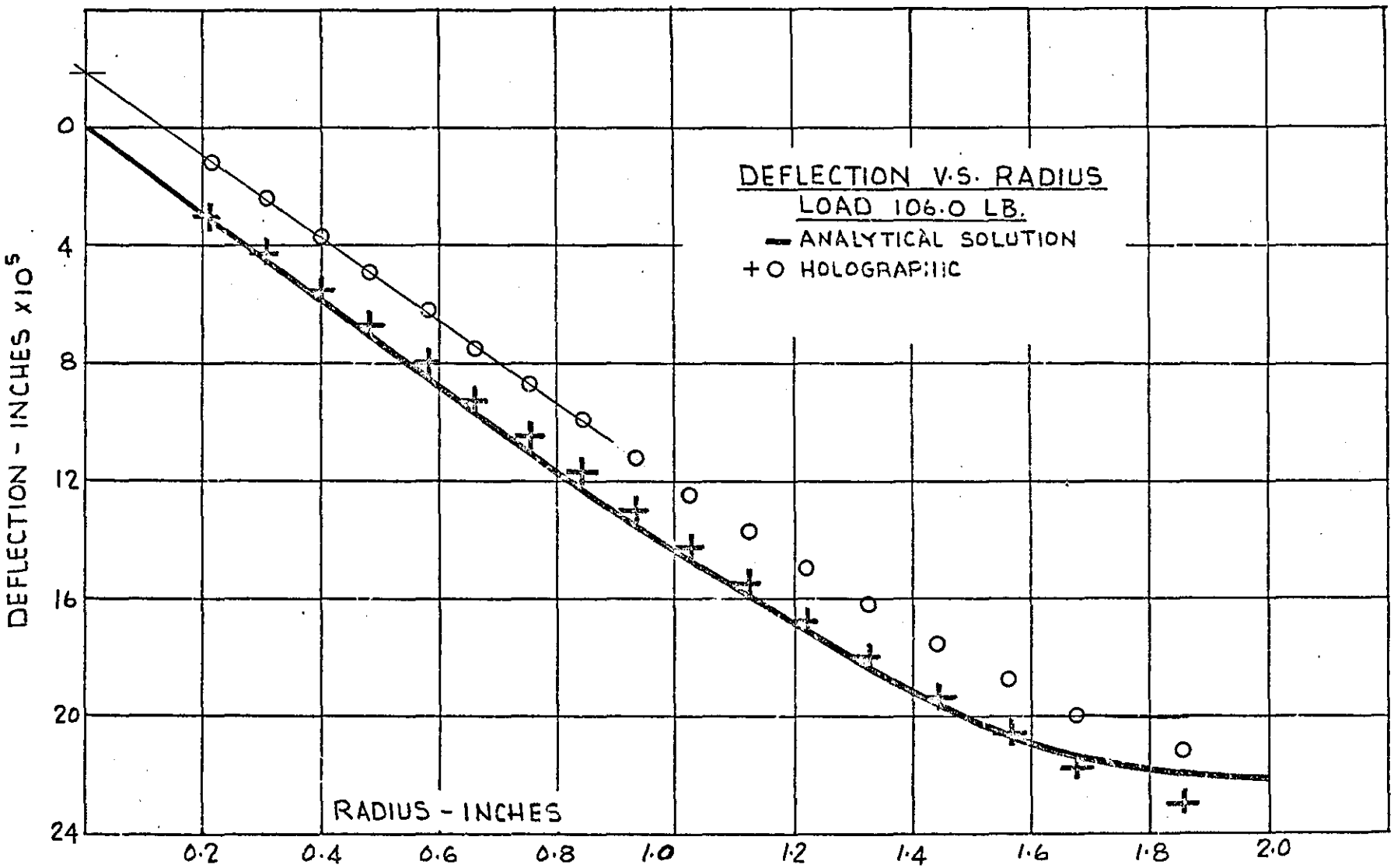
DEFLECTION V·S· RADIUS
LOAD 106.0 LB.
ANALYTICAL SOLUTION
+ O HOLOGRAPHIC
DEFLECTION - INCHES X10^5
RADIUS - INCHES
0
4
8
12
16
20
24
0.2
0.4
0.6
0.8
1.0
1.2
1.4
1.6
1.8
2.0

FIGURE 4.14

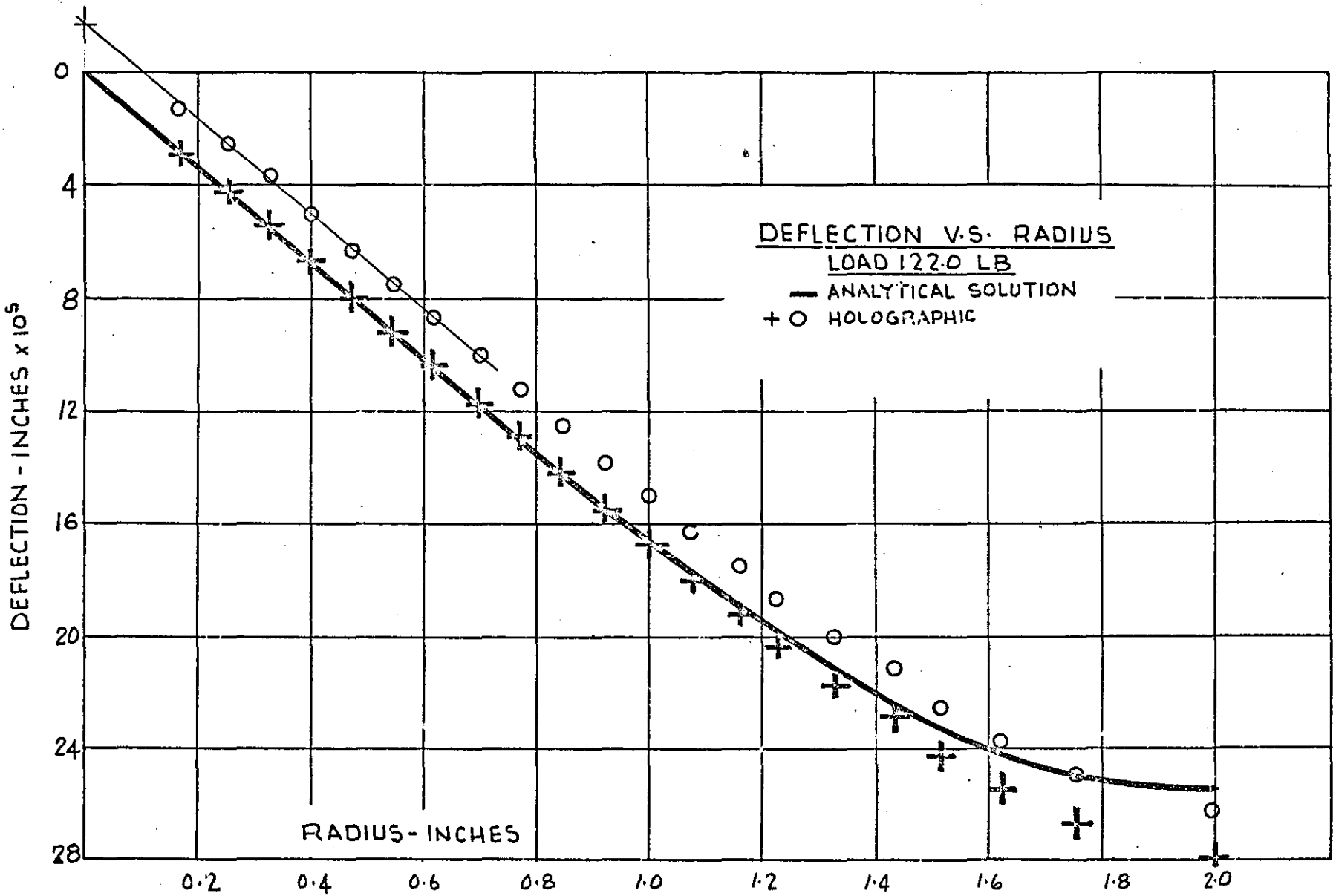
DEFLECTION V·S· RADIUS
LOAD 122·0 LB
ANALYTICAL SOLUTION
HOLOGRAPHIC
DEFLECTION - INCHES x 10⁵
RADIUS - INCHES
0
4
8
12
16
20
24
28
0·2
0·4
0·6
0·8
1·0
1·2
1·4
1·6
1·8
2·0

FIGURE 4·15

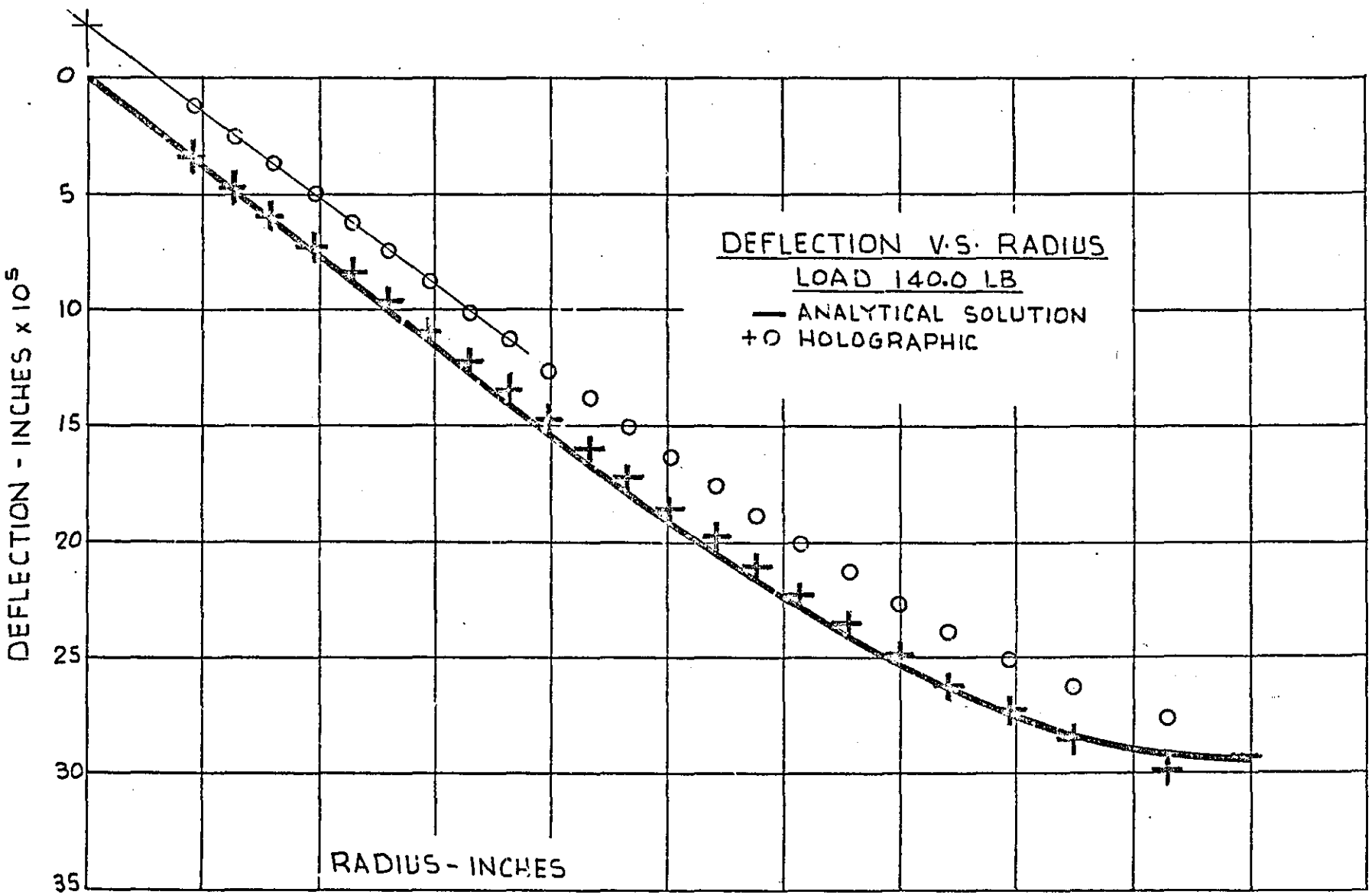
DEFLECTION V.S. RADIUS
LOAD 140.0 LB
ANALYTICAL SOLUTION
+O HOLOGRAPHIC
DEFLECTION - INCHES x 10^5
RADIUS - INCHES
0
5
10
15
20
25
30
35
0.2
0.4
0.6
0.8
1.0
1.2
1.4
1.6
1.8
2.0

FIGURE 4.16

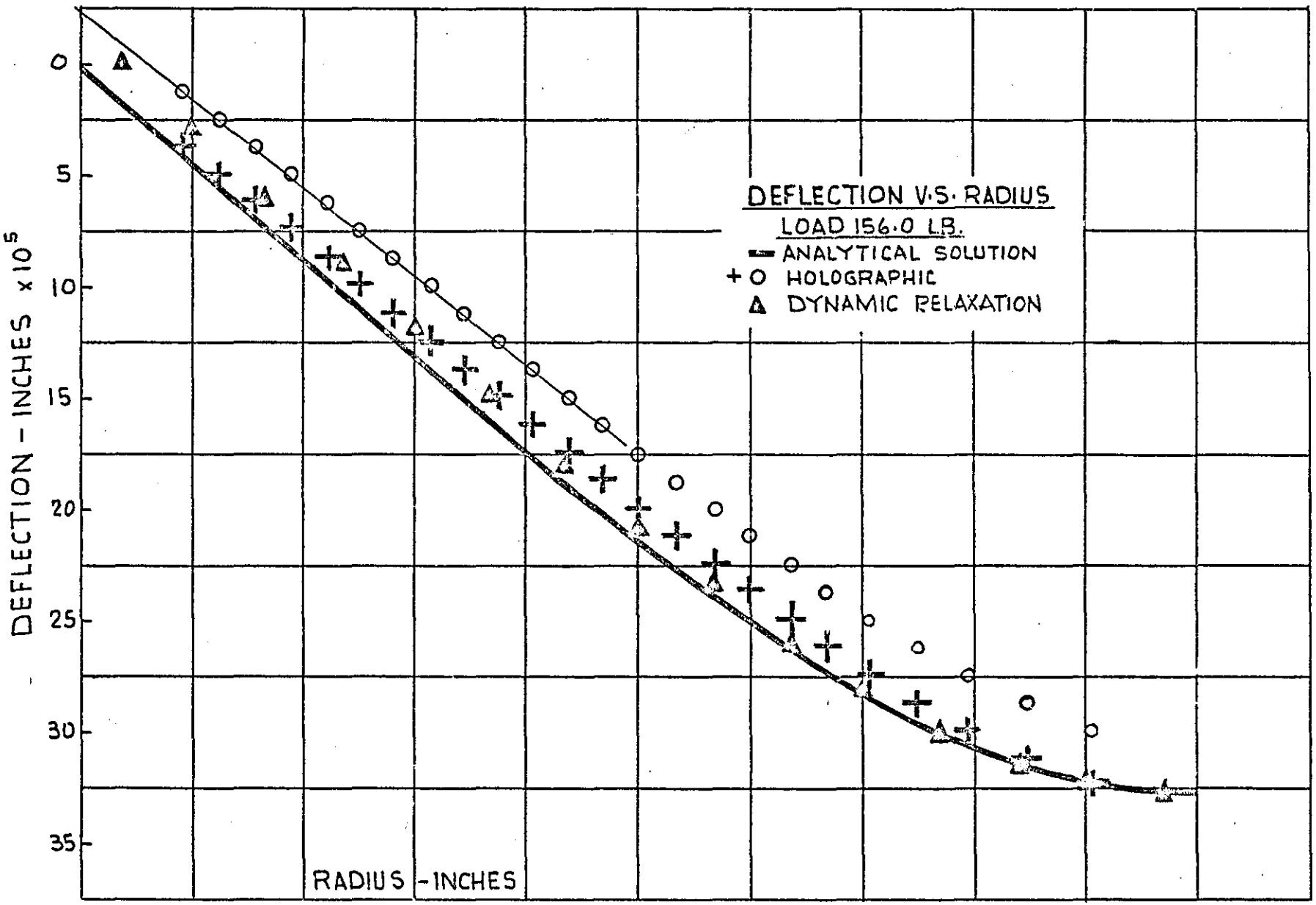
DEFLECTION V·S· RADIUS
LOAD 156·0 LB.
ANALYTICAL SOLUTION
HOLOGRAPHIC
DYNAMIC RELAXATION
DEFLECTION - INCHES x 10⁵
0
5
10
15
20
25
30
35
RADIUS - INCHES
0
0·2
0·4
0·6
0·8
1·0
1·2
1·4
1·6
1·8
2·0

FIGURE 4.17

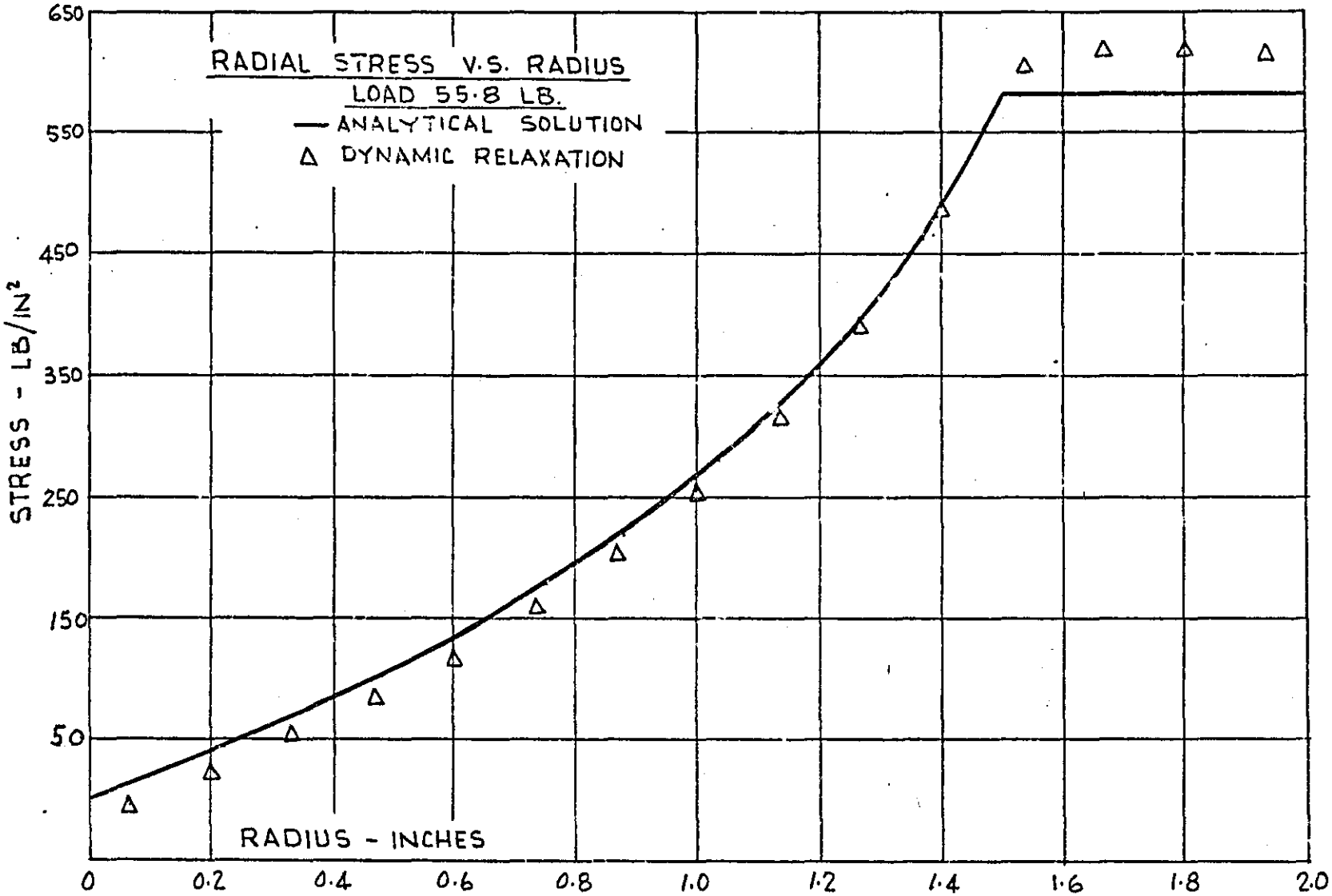
RADIAL STRESS V.S. RADIUS
LOAD 55·8 LB.
— ANALYTICAL SOLUTION
Δ DYNAMIC RELAXATION
STRESS - LB/IN²
650
550
450
350
250
150
50
RADIUS - INCHES
0
0.2
0.4
0.6
0.8
1.0
1.2
1.4
1.6
1.8
2.0

FIGURE 4.18

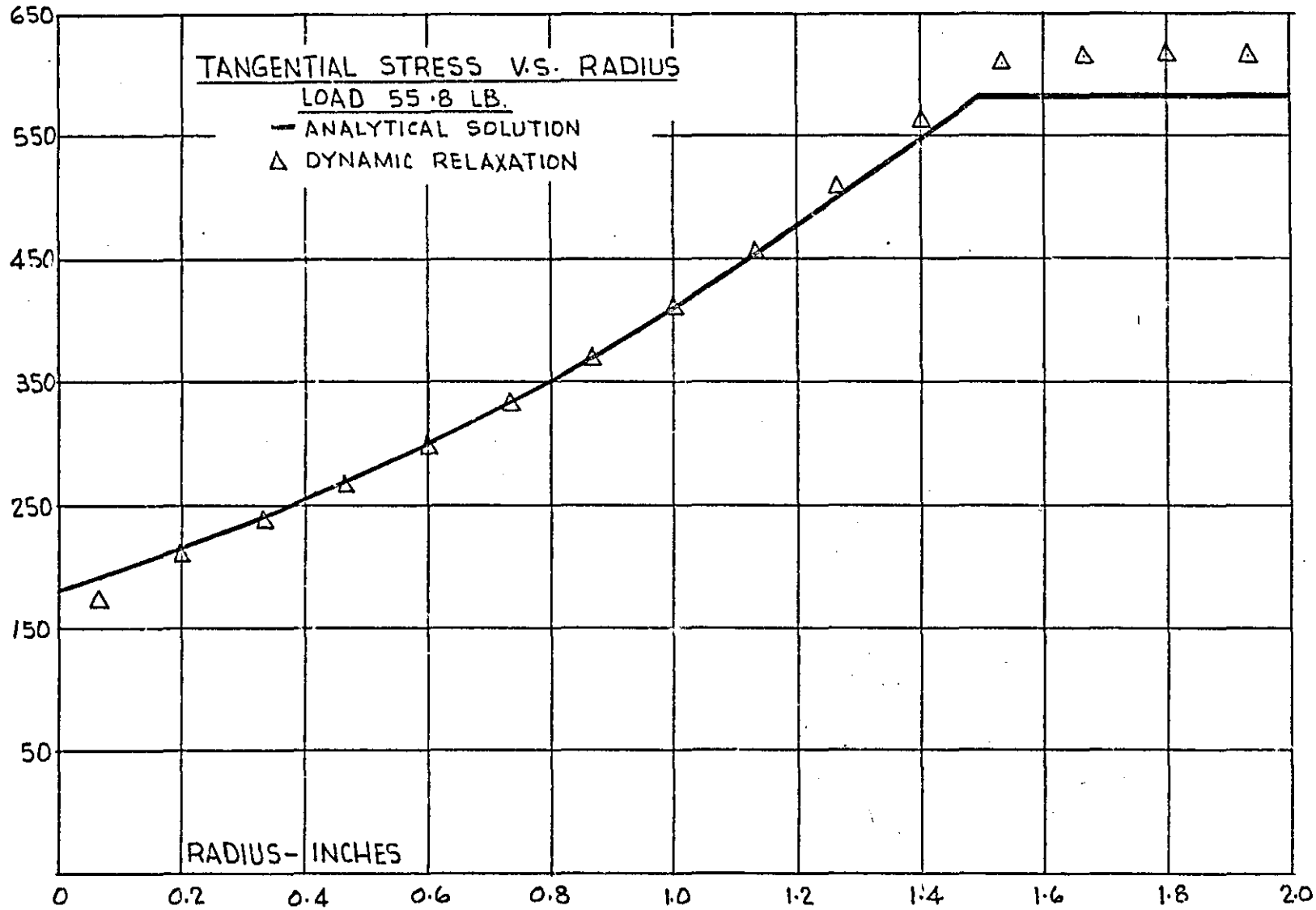
TANGENTIAL STRESS V.S. RADIUS
LOAD 55·8 LB.
ANALYTICAL SOLUTION
DYNAMIC RELAXATION
650
550
450
350
250
150
50
RADIUS- INCHES
0
0.2
0.4
0.6
0.8
1.0
1.2
1.4
1.6
1.8
2.0

FIGURE 4.19

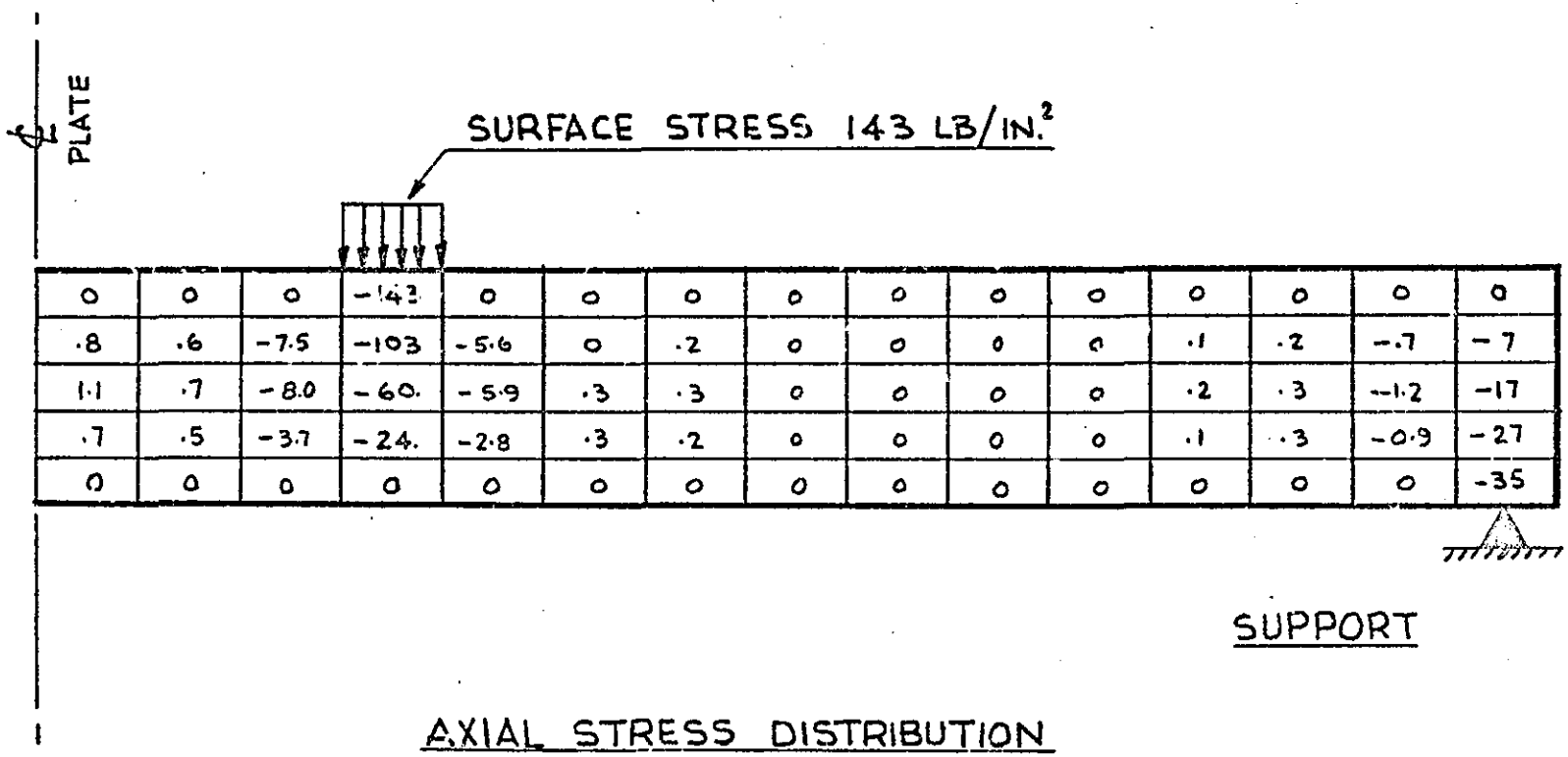

0	0	0	-143	0	0	0	0	0	0	0	0	0	0	0
.8	.6	-7.5	-103	-5.6	0	.2	0	0	0	0	.1	.2	-.7	-7
1.1	.7	-8.0	-60.	-5.9	.3	.3	0	0	0	0	.2	.3	-1.2	-17
.7	.5	-3.7	-24.	-2.8	.3	.2	0	0	0	0	.1	.3	-0.9	-27
0	0	0	0	0	0	0	0	0	0	0	0	0	0	-35

AXIAL STRESS DISTRIBUTION
IN FLAT CIRCULAR PLATE - LB/IN.²

FIGURE 4·20

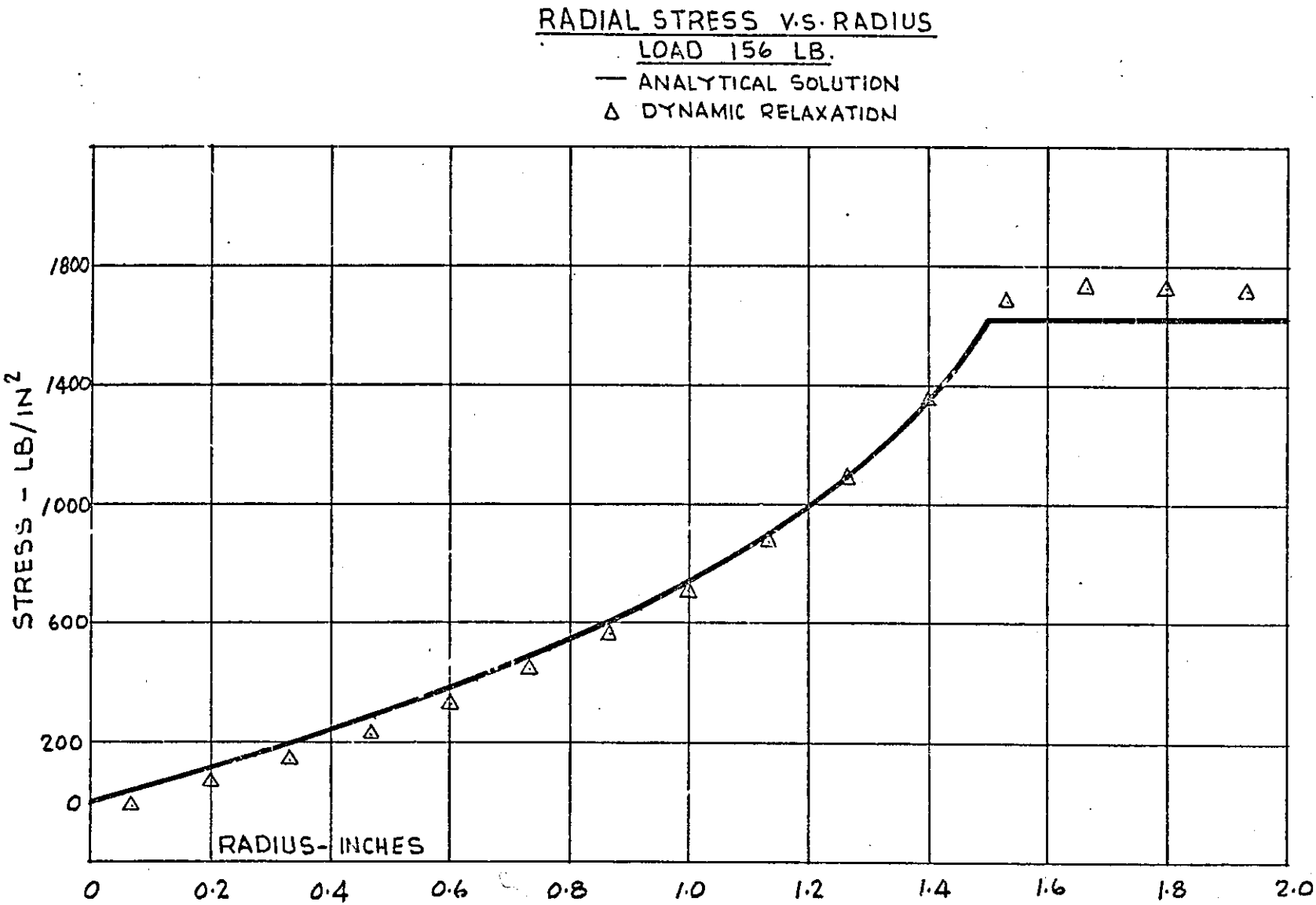
RADIAL STRESS V.S. RADIUS
LOAD 156 LB.
— ANALYTICAL SOLUTION
Δ DYNAMIC RELAXATION
STRESS - LB/IN²
1800
1400
1000
600
200
0
RADIUS - INCHES
0
0·2
0·4
0·6
0·8
1·0
1·2
1·4
1·6
1·8
2·0

FIGURE 4.21

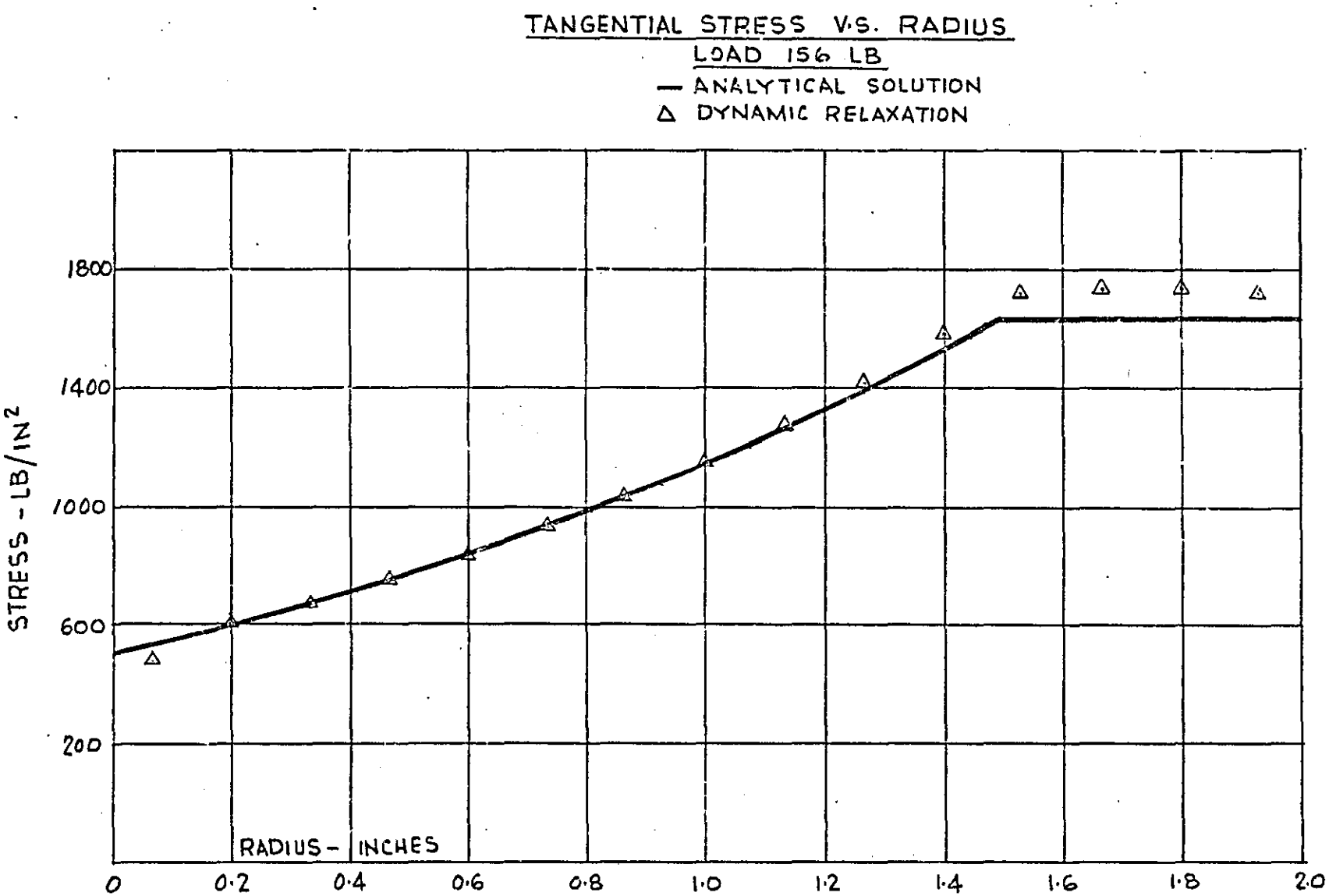
TANGENTIAL STRESS V.S. RADIUS
LOAD 156 LB
— ANALYTICAL SOLUTION
△ DYNAMIC RELAXATION
STRESS - LB/IN²
1800
1400
1000
600
200
RADIUS - INCHES
0
0·2
0·4
0·6
0·8
1·0
1·2
1·4
1·6
1·8
2·0

FIGURE 4·22

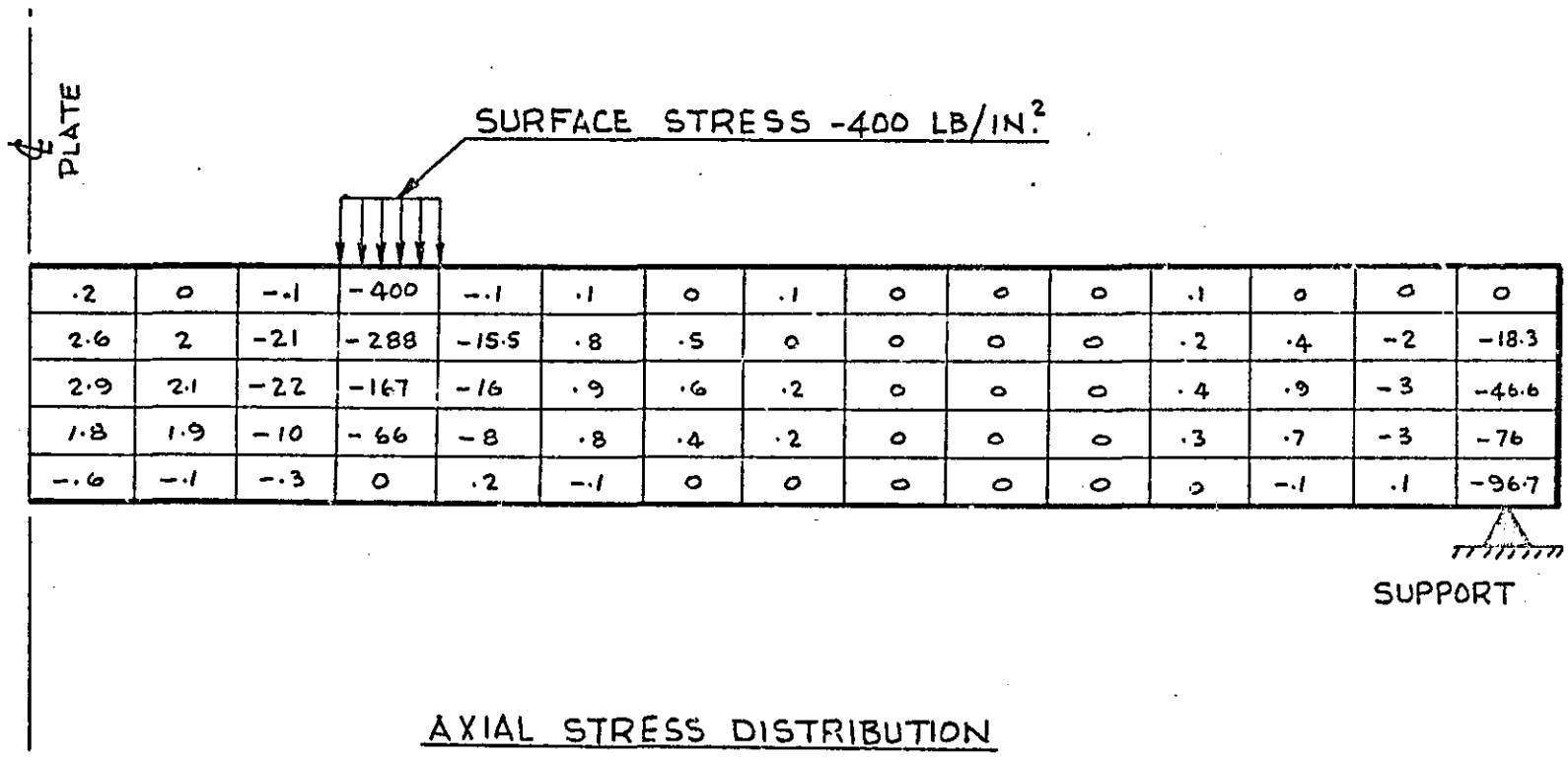

.2	0	-.1	-400	-.1	.1	0	.1	0	0	0	.1	0	0	0
2.6	2	-21	-288	-15.5	.8	.5	0	0	0	0	.2	.4	-2	-18.3
2.9	2.1	-22	-167	-16	.9	.6	.2	0	0	0	.4	.9	-3	-46.6
1.8	1.9	-10	-66	-8	.8	.4	.2	0	0	0	.3	.7	-3	-76
-.6	-.1	-.3	0	.2	-.1	0	0	0	0	0	0	-.1	.1	-96.7

AXIAL STRESS DISTRIBUTION
IN FLAT CIRCULAR PLATE LB/IN.²

FIGURE 4.23

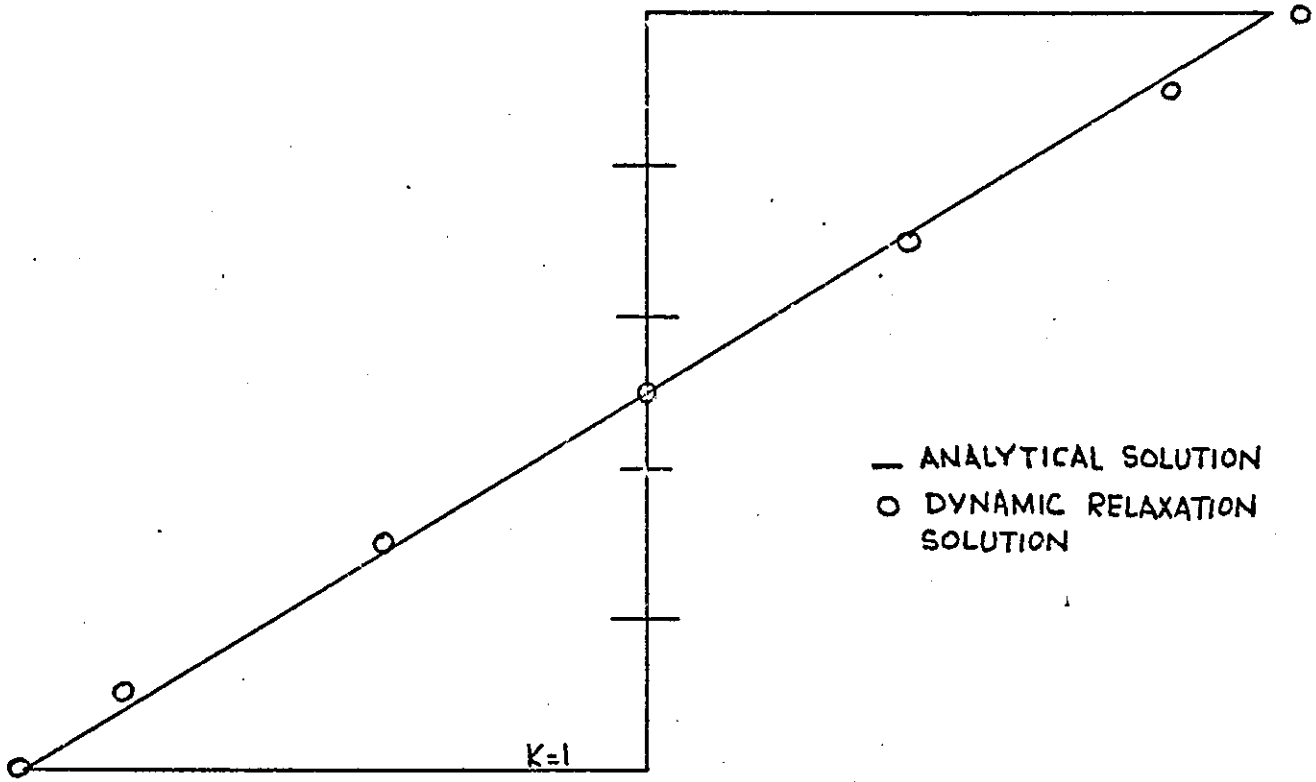

BENDING STRESS DISTRIBUTION
THROUGH PLATE 0.333" FROM ℄
LOAD 156 LB

FIGURE 4.24

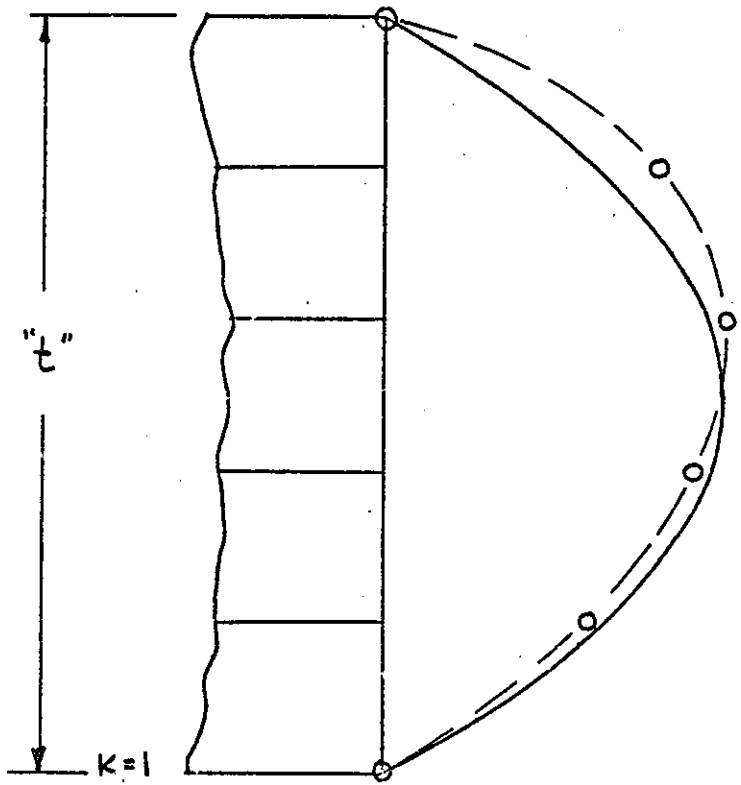

— ANALYTICAL SOLUTION
o DYNAMIC RELAXATION SOLUTION

TRANSVERSE SHEAR STRESS DISTRIBUTION THROUGH PLATE 0.4" FROM ℄ (LOAD 156 LB)

FIGURE 4.25

CHAPTER FIVE

ANALYSIS OF A FLAME PLATE FROM A LARGE DIESEL ENGINE

5.1 Introduction

In this chapter, the methods used in Chapter 4 to analize a flat circular plate are extended to the analysis of the flame plate from a Ruston-Hornsby "AO" engine. The analysis of the plate is in two parts. The first part consists of a holographic and dynamic relaxation analysis of the deflection of the flame plate under a transverse mechanical load. The results of the dynamic relaxation solution are compared with the results of the holographic solution to estimate the accuracy of the dynamic relaxation which in development required a number of geometric simplifications to be made to the plate. Using a coarse mesh, the dynamic relaxation solution was within 22 percent of the holographic solution. In an attempt to improve the dynamic relaxation solution, a finer mesh was used however no improvement was achieved. The coarse mesh solution required approximately 6 hours on the I.C.T. 1905 computer. For the fine mesh solution, the number of mesh points in the tangential direction was doubled. For this particular programme, doubling the number of mesh points in the tangential direction increases the time required for a solution by four thus requiring 24 hours and therefore in part two of the analysis the coarse mesh solution was used.

The second part of the analysis consists of substituting the

engine or working conditions of the plate into the computer programme written for the part one analysis. The thermal gradients in the flame plate which constitute part of the total loading conditions in the plate were determined by dynamic relaxation. The temperature data available for the analysis is somewhat limited consequently the results may not be entirely reliable however they do serve to illustrate certain tendancies particularily with regard to transverse deflections.

For a first approximation to the stress distribution in the plate, it was assumed that the plate is simply supported. Under this condition, two loading conditions were considered. One due to thermal gradients only, under which the plate deflects downward into the engine cylinder, and two, a combined thermal and gas pressure load under which the plate is pushed back upward to come into contact with the cylinder head; the cylinder head is assumed to act as a stiff but elastic foundation.

5.2 Details of Flame Plate

Details of the flame plate are shown in Fig's (5.1) to (5.4). Basically, the plate is a flat circular disc in which a number of holes have been machined. The four large holes or valve ports consist of a valve seat insert which is welded into the flame plate. The valve insert has a circumferential groove which forms an integral cooling passage with the flame plate. The hole in the centre of the plate or fuel injector hole, is made in a similar manner to the valve ports and also forms an internal cooling passage in the flame plate. The plate is cooled by the engine cooling water which flows through the four radially drilled holes at the mid plane of the plate and around the valve inserts. The cooling passage around the valve insert is connected to the cooling passage around the fuel injector insert. The cooling water leaves the plate via the four axial holes in the back or cold side of the plate. The large tapped hole near the rim of the plate is used for the air start valve. The flange on the rim of the plate has a number of small holes which are used to locate and bolt the flame plate to the cylinder head. The flange has a circumferential groove which is not shown in the detail drawings; the groove is used to house a sealing ring or "O" ring. The plate, valve insert, and fuel injector insert, are made from steel; the plate being made

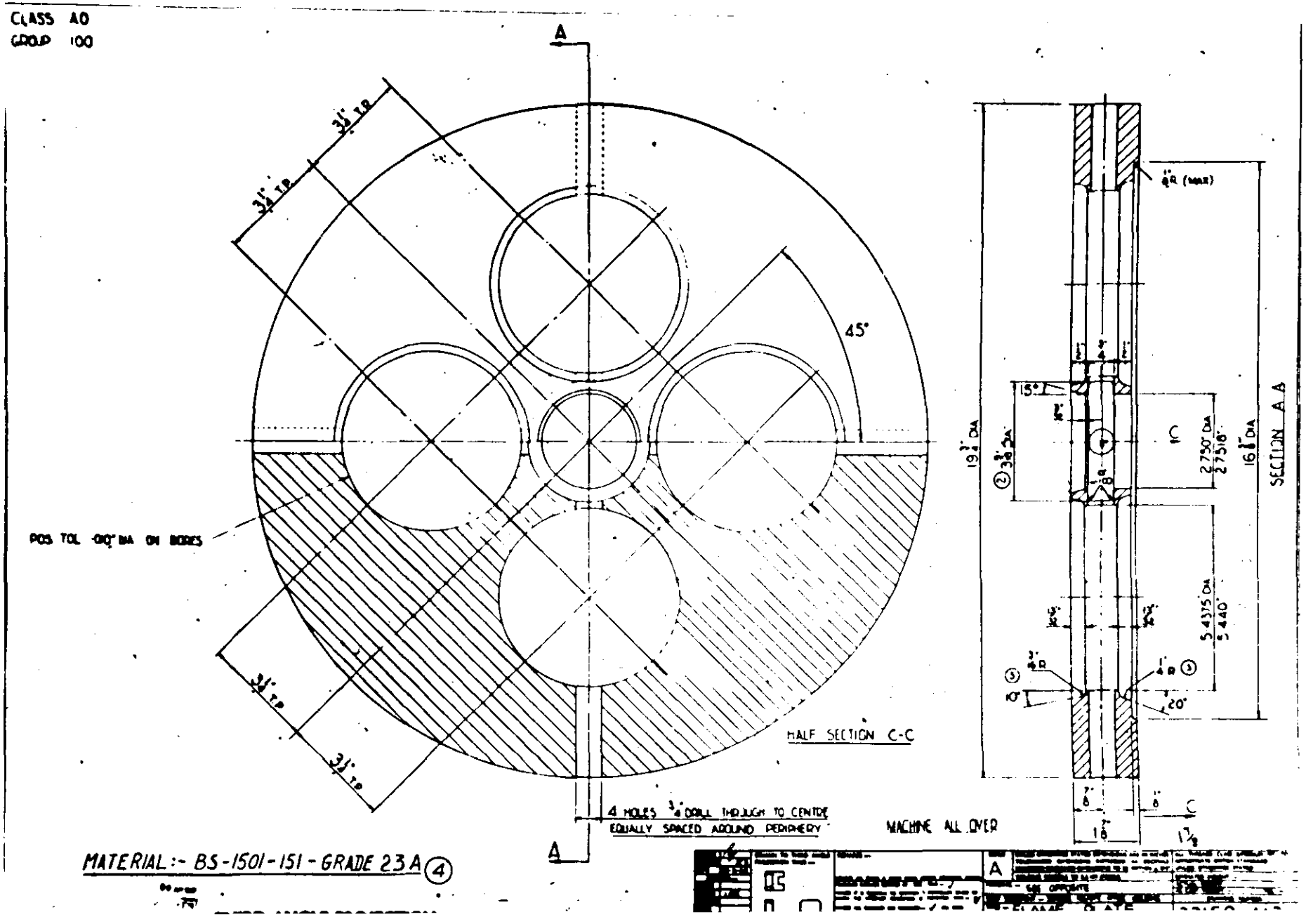
CLASS A0
GROUP 100
A
3¼" TP
3¼" TP
3¼" TP
45°
POS TOL ⌀0.1 M A ON BORES
3¼" TP
3¼" TP
HALF SECTION C-C
4 HOLES ¾ DRILL THROUGH TO CENTRE
EQUALLY SPACED AROUND PERIMETRY
A
MACHINE ALL OVER
MATERIAL :- BS-1501-151 - GRADE 23A (4)
SECTION A-A
15°
20°
2.750" DIA
2.7518"
5.4375" DIA
5.440"
16⅛" DIA
19¾" DIA

FIGURE 5.1

FIGURE 5.2.

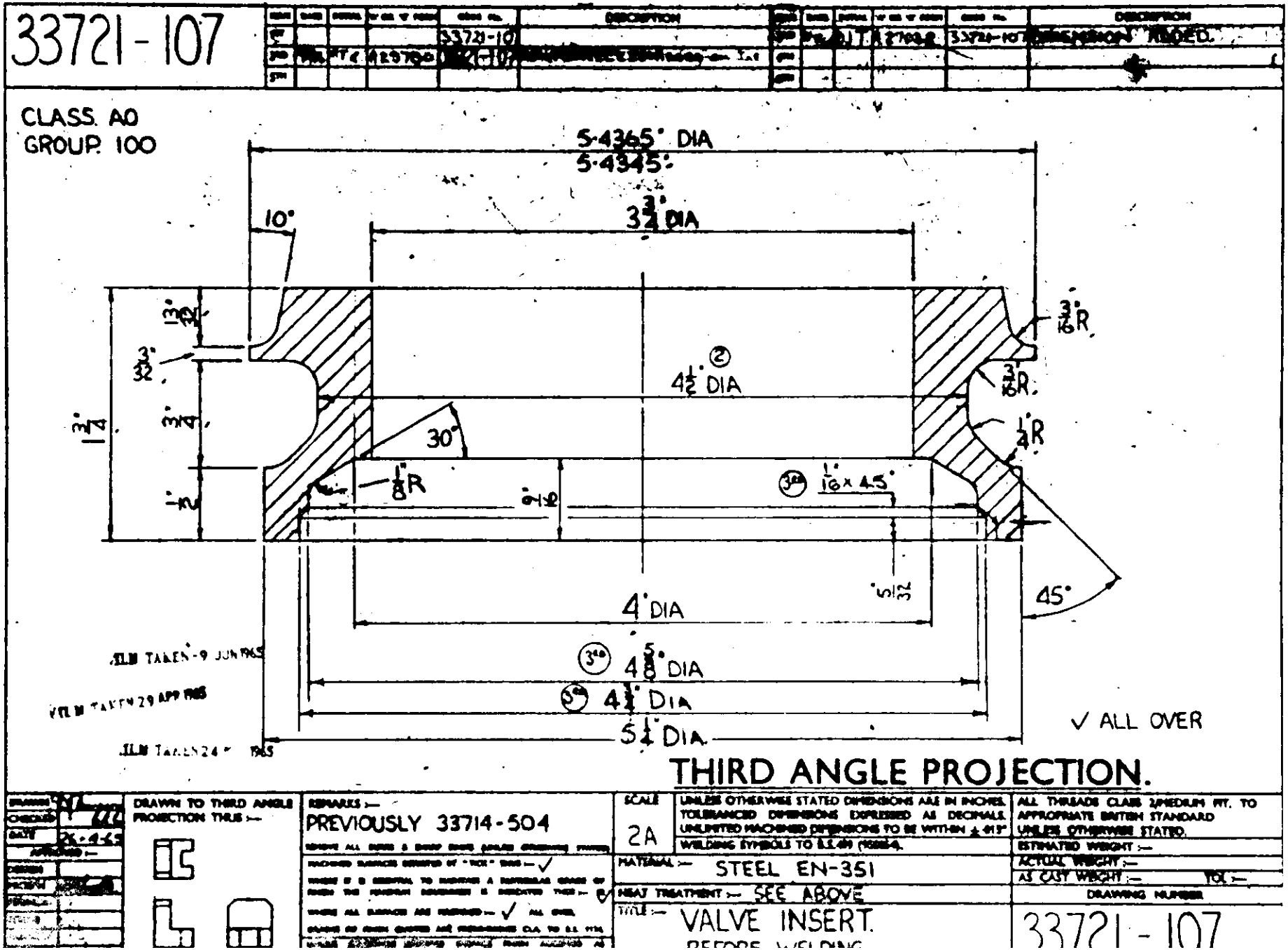
33721-107
CLASS. A0
GROUP. 100
5·4365" DIA
5·4345"
3½" DIA
10°
4½" DIA
30°
4" DIA
4⅞" DIA
4¾" DIA
5¼" DIA
45°
✓ ALL OVER
THIRD ANGLE PROJECTION.
PREVIOUSLY 33714-504
SCALE 2A
STEEL EN-351
SEE ABOVE
VALVE INSERT.
33721-107

CLASS AQ

GROUP 100

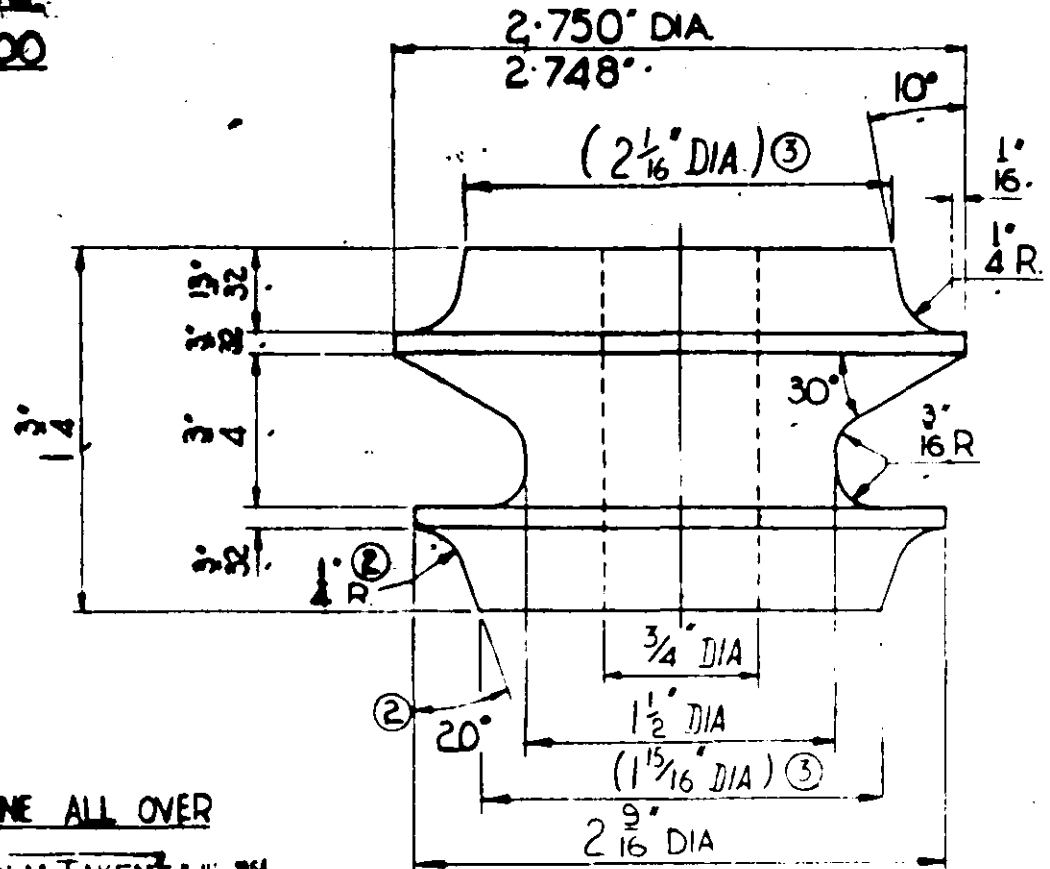

MACHINE ALL OVER

FILM TAKEN 5 JU... 1964

THIRD ANGLE PROJECTION.

DRAWN TO THIRD ANGLE PROJECTION THUS :—	REMARKS :—	SCALE D	UNLESS OTHERWISE STATED DIMENSIONS ARE IN INCHES. TOLERANCED DIMENSIONS EXPRESSED AS DECIMALS. UNLIMITED MACHINED DIMENSIONS TO BE WITHIN ± .015" WELDING SYMBOLS TO B.S.499 (1953).	ALL THREADS CLASS 2/MEDIUM FIT. TO APPROPRIATE BRITISH STANDARD UNLESS OTHERWISE STATED. ESTIMATED WEIGHT :—
		MATERIAL :— STEEL EN-31		ACTUAL WEIGHT :— AS CAST WEIGHT :— NO. :—
		HEAT TREATMENT :—		DRAWING NUMBER
		TITLE :— INJECTOR BOSS		32724-301

FIGURE 5·3

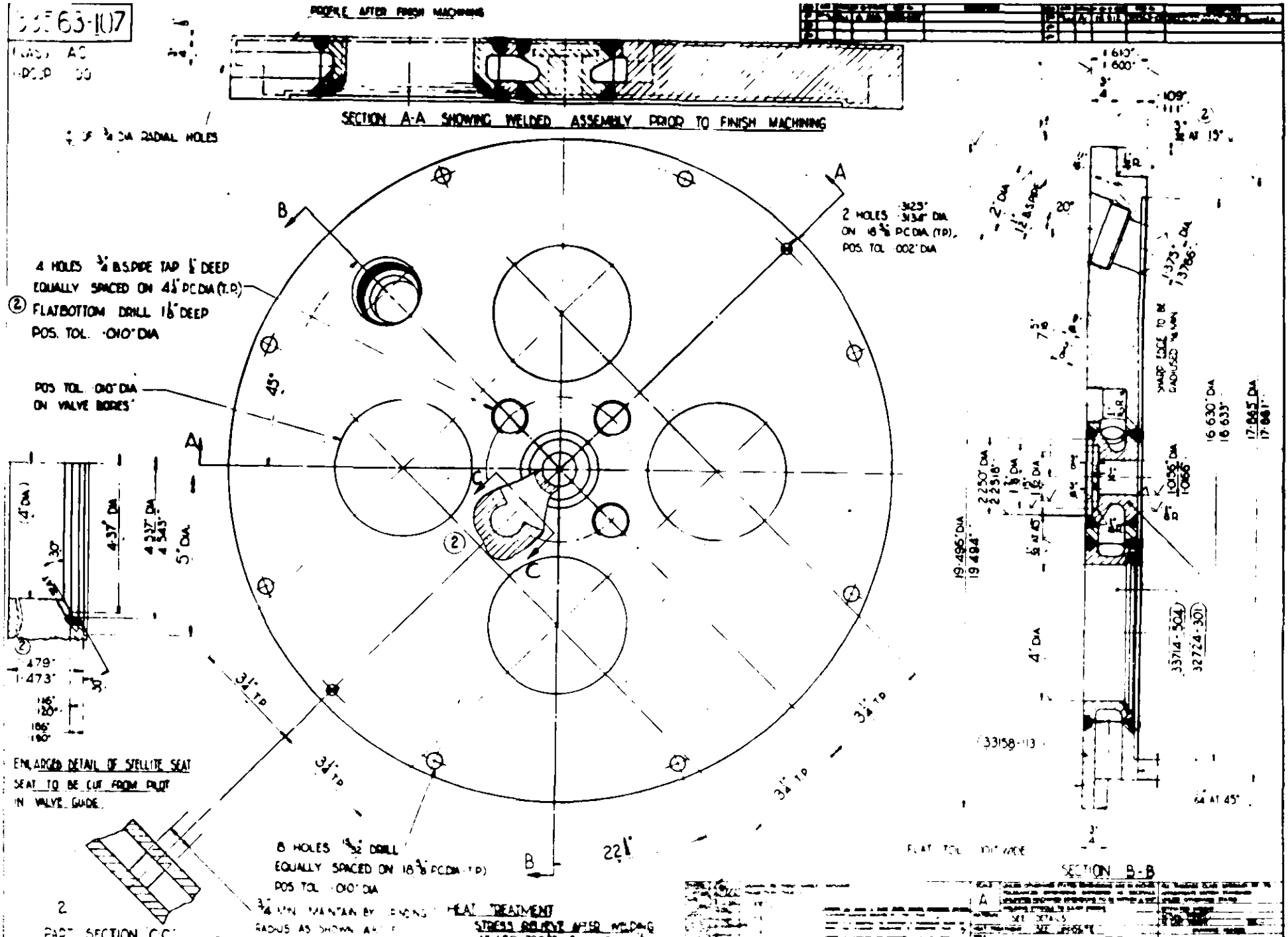
SECTION A-A SHOWING WELDED ASSEMBLY PRIOR TO FINISH MACHINING
4 HOLES ¾ B.S.PIPE TAP 1" DEEP EQUALLY SPACED ON 41" PC DIA (T.P.)
② FLATBOTTOM DRILL 1⅛" DEEP POS. TOL. ·010" DIA
POS TOL ·010" DIA ON VALVE BORES
2 HOLES ·3125" ·3134" DIA ON 18⅝ PC DIA (TP). POS. TOL ·002" DIA
8 HOLES ⅝ DRILL EQUALLY SPACED ON 18⅝ PC DIA (TP) POS TOL ·010" DIA
ENLARGED DETAIL OF STELLITE SEAT
SEAT TO BE CUT FROM PILOT IN VALVE GUIDE
PART SECTION C-C
SECTION B-B
HEAT TREATMENT
STRESS RELIEVE AFTER WELDING
33158-113
33714-504
32724-301

FIGURE 5·4

from B.S.-1501-151 grade 23A, and the valve insert and fuel injector insert from EN-351. The physical properties used in the dynamic relaxation solution are*:

$$E = 30 \times 10^{6} \text{ lb./in.}^{2}$$
$$\rho = 0.732 \times 10^{-3} \text{ lb.-sec}^{2}/\text{in.}^{4}$$
$$\nu = 0.3$$
$$\alpha = .64 \times 10^{-5} \text{ in./in./}^{\circ}\text{F}$$

5.3 Details of Support

Figures (5.5) and (5.6) show the flame plate and cylinder head assembly. When installed in the engine, the flame plate is sandwiched between the cylinder head and the copper head gasket; the head gasket is sandwiched between the flame plate and the cylinder. The boundary conditions at the edge of the plate will depend on whether one assumes a clamped edge or a simply supported edge. The plate being clamped between the head and the gasket could be assumed fixed at the edge however since the gasket is copper and comparatively soft, it is unlikely that the clamping or fixing at the edge will be 100 percent effective thus one might assume that the plate is simply supported. In actual operation, the plate will be partially clamped however with no knowledge of the slope at the edge one can only assume a clamped or a simple support. For a first approximation to the problem, a simply supported condition will be used. The simply supported condition only applies when the deflection is downward into the cylinder since as shown in Fig's (5.5) and (5.6), the cylinder head is capable of providing a continuous support for upward deflections. The effectiveness of the head in providing a continuous support is questionable if one considers the deflection of the plate under thermal gradients as follows.

Under transverse thermal gradients in which the flame side of the plate is at a higher temperature than the side next to the cylinder head, the flame plate will deflect away from the head**.

* Telephone conversation with I.N. Birchall of Ruston-Hornsby Ltd.
** if the plate is simply supported

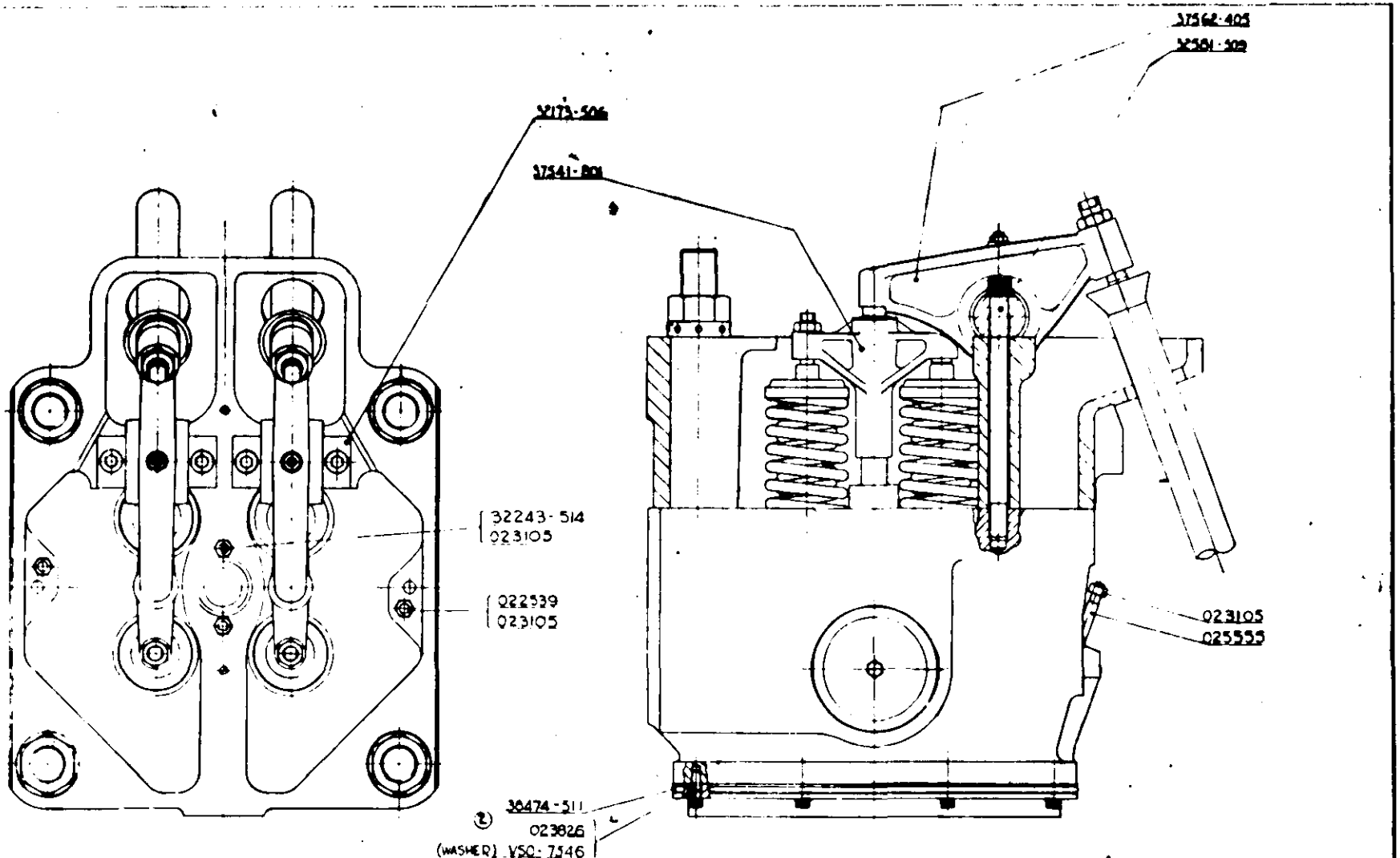

CYLINDER HEAD ASSEMBLY

THIRD ANGLE PROJECTION

DRAWING No. AQ-10000

FIGURE 5.5

FIGURE 5.6

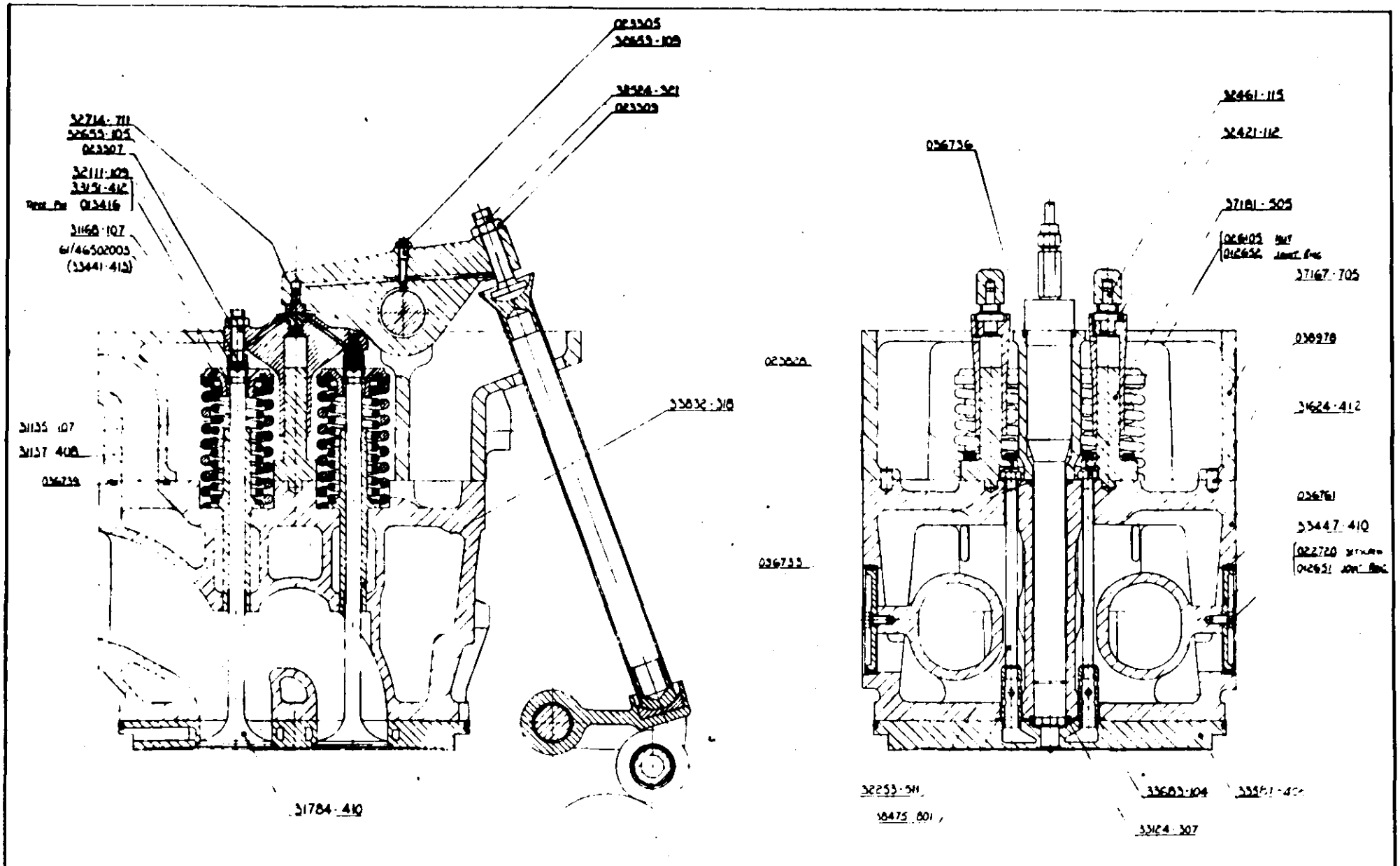
023305
30653-109
32714-711
30655-105
023307
32111-109
33151-412
Thrust Pin 023416
31160-107
61/46502005
(33441-413)
31135-107
31137-408
036739
33832-318
023626
036735
31784-410
32461-115
32421-112
036736
37181-505
026405 Nut
026652 Lockwasher
37167-705
036978
31624-412
036761
33447-410
022720 Screw
026951 Washer
32253-511
10475-801
33683-104
33124-307
CYLINDER HEAD ASSEMBLY
THIRD ANGLE PROJECTION
DRAWING No.
AO-10000
SHEET 1 OF 2

In this condition, the gas pressure load which occurs during the firpart of the engine cycle, will tend to push the flame plate back up towards the head; the plate is in contact with the cylinder head at its periphery. There will exist a gas pressure load which is just sufficient to force the plate to contact the head uniformly over the surface and if the firing pressure is less than this, then the head will not provide any support to the flame plate except at the outside diameter. If the gas firing pressure is greater than that which is just sufficient to push the plate up and contact the cylinder head, then the head will provide a support in the form of an elastic foundation. It appears then, that the plate will have to be analized under two conditions, one being the thermal load and the second condition being the combined thermal and gas pressure load. Details of these two analyses will be discussed in Section 5.7.

5.4 Loading Conditions In The Engine

The gas pressure load* during the firing stroke is 1500 lb/in.^{2} This pressure is assumed to act over the 16.630 in. diameter; the gasket load is exerted on the 0.606 in. gasket face.

The thermal loading or thermal gradients throughout the plate must be determined. The only information available with regards thermal conditions in the plate is the engine cooling water temperature**, 122 to 140 ^{o}F, and the temperature*** along a radial axis bisecting the valve ports; these temperatures were obtained using "Templugs", located about 3/16 in. below the surface of the plate, see Fig. (5.7). In order to determine the stress distribution due to thermal gradients, the temperature at each normal-stress node must be known. As illustrated in Chapter 1, dynamic relaxation can be used to solve problems of steady state heat conduction. To determine the temperature distribution the boundary conditions must be known and with the temperature information available a great deal of assuming had to be done. The assumptions made are as follows:

1. All of the heat enters the plate from the flame side and is carried away by the cooling water.
2. The surface temperature at the edge of the injector hole

*Letter from J.H. Worsfold, ref. RES/LHM/RM/293517, May 23, 1969

** Conversation with J.H. Worsfold

*** Ruston diagram No. RD 52551/66

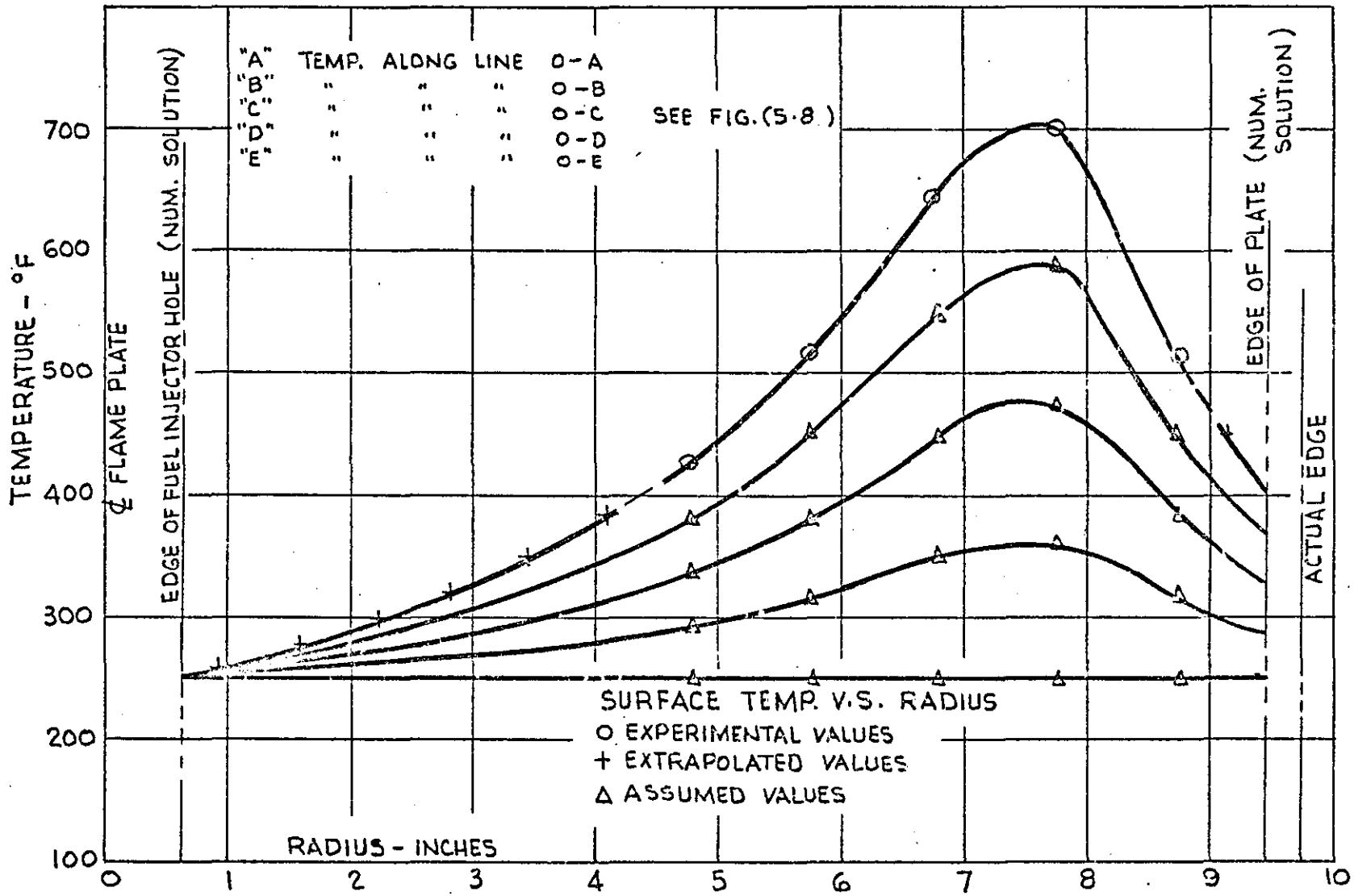
"A" TEMP. ALONG LINE O-A
"B" " " " O-B
"C" " " " O-C
"D" " " " O-D
"E" " " " O-E
SEE FIG.(5·8)
TEMPERATURE - °F
700
600
500
400
300
200
100
℄ FLAME PLATE
EDGE OF FUEL INJECTOR HOLE (NUM. SOLUTION)
EDGE OF PLATE (NUM. SOLUTION)
ACTUAL EDGE
SURFACE TEMP. V.S. RADIUS
O EXPERIMENTAL VALUES
+ EXTRAPOLATED VALUES
Δ ASSUMED VALUES
RADIUS - INCHES
0
1
2
3
4
5
6
7
8
9
10

FIGURE 5·7

and at the outside diameter of the flame plate, on the flame side of the plate, is obtained by extrapolation of the points given in Fig. (5.7).

3. The surface temperatures on the flame side vary linearly in the tangential direction from the hot axis, i.e. the axis bisecting the valve ports, to the axis which cuts through the valve port, see Fig. (5.7).
4. The temperatures on the edge of the plate in the injector hole, the radial cooling passage, and the outside diameter, are the extrapolated surface temperature at the edge of the injector hole, i.e. 260°F.

The basis of the first assumption is that the contact resistance between the cylinder head and the flame plate will be high relative to the convective film resistance in the cooling water channels particularily if the flame plate deflects away from the cylinder head thus the heat transfer to the head will be small. No real grounds for the remaing assumptions can be given except that of intuition and the authors past experience in heat transfer work. The 4th assumption puts the surface temperatures in the cooling passages above boiling which is perhaps optimistic in that it will tend to reduce the thermal gradients in the plate however with little information to go on, the situation is not inconceivable.

The above conditions are used in calculating the temperatures at the normal stress nodes. The solution will be described in Section (5.7) under the heading " Determination of Thermal Gradients".

5.5 Formulation of Dynamic Relaxation Solution

In examining the flame plate for analysis by dynamic relaxation, the possible mesh size in relationship to the size of the various features of the plate must first be considered. The problem could be treated as a thin plate since the diameter to thickness ratio is 13 : 1 and it could be assumed that the plate is symmetrical about its mid-plane, i.e. by neglecting the flange which is very much weakened by the "O" ring groove and transverse holes, thus making it possible to use the bending equations for thin plates however in view

of possible complex thermal gradients, it is neccessary to treat the problem as three dimensional. In a three dimensional analysis by dynamic relaxation, there are twelve variables for every mesh point. Each variable requires two "words" of core storage and the I.C.T 1905 computer in current use at Loughborough University has an available core storage of 23K words thus one is limited to less than 1000 mesh points. Disc storage is available but the access time to the disc would be prohibitive for an iterative process. Some reduction in storage requirements is realized in practice because of the interlacing net used in dynamic relaxation and in addition one may not require the displacements at every mesh point.

In trying to decide on a mesh size, it soon becomes evident that small details or features of the plate cannot be taken into account because they are of the same order of magnitude or smaller than the mesh dimensions. For example the small holes in the rim of the plate are about 1/20 of the radius thus to approximate these hole by one mesh would require 21 radial points, assuming that the mesh size is constant. In the tangential direction these holes represent about 1/120 of the circumference and assuming one analizes only 1/8 of the plate, then 16 tangential nodes would be required. Thus in two dimensions one would use up 336 points out of a possible 1000. This leaves only three point through the thickness of the plate which is in effect two normal stress nodes which is not enough. Thus a number of simplifying assumptions have to be made. These simplifications will undoubtedly affect the stress distribution and displacements in the plate and thus the accuracy of the results will be questionable. For this reason, it is neccessary to carry out an experimental analysis which, perhaps not as complete as the dynamic relaxation solution, will provide information which can be compared with the dynamic relaxation solution and an estimate of the accuracy of the dynamic relaxation solution made.

The first simplification made was to neglect the air start valve hole. This makes the plate symmetrical about axes 45° apart thus making it possible to analize one eighth of the plate. This simplification appears rather crude however without it one would have only one radial axis of symmetry and would have to analize one half of the plate which would require too many mesh points or conversely too coarse a mesh. The second simplification was to neglect the internal cooling

passages. The internal cooling passages affect the plate only locally and in terms of flexural stiffness of the plate, reduce the stiffness by only 12.5 percent, i.e. the ratio of the stiffness of the plate in the region of the cooling passage to the plate remote from the cooling passage is $(1.5^3 - .75^3)/1.5^3 = 7/8$.

Another simplification was made to the flange. The flange is weakened by the "O" ring groove and the transverse holes thus in part may be neglected. The diameter of the plate measured to the outside of the flange is 19.5 in. nominally, and the inside diameter of the flange is 17.863. In the final mesh chosen, the outside diameter of the plate is 18.90 in. and the flange is neglected. The final dimensions are a compromise which is more or less a result of fitting a constant radial mesh width to the valve port and outside diameter of the plate.

A third simplification made was to neglect the cooling water outlet holes. These holes are approximately equal to the mesh dimensions chosen and it is felt that since they are small they should not greatly affect the flexural stiffness of the plate. They most likely will give rise to stress concentration some of which will be carried by the water outlet nipple which is screwed into the plate. Finally, the 0.110 spigot which forms the gasket face is neglected.

Thus the plate has been considerably simplified and as mentioned, the results will be questionable. In theory, all of the features of the plate could be taken into account if the mesh were fine enough. It is possible that one might attempt to use a finer mesh in the region of discontinuities however this would very much complicate the solution and increase the storage requirements. Generally speaking, for a constant mesh size, only those features of the object which are of the same order of magnitude in size as the object itself can be taken into account.

Three mesh configurations were devised as shown in Fig's (5.8) to (5.10). Figure (5.8) shows a mesh 16 x 6 x 5. The fuel injector hole is approximated by one radial mesh width. The valve port in this case has been enlarged as indicated by the dotted line; the solid line represents the actual inside diameter of the valve port.

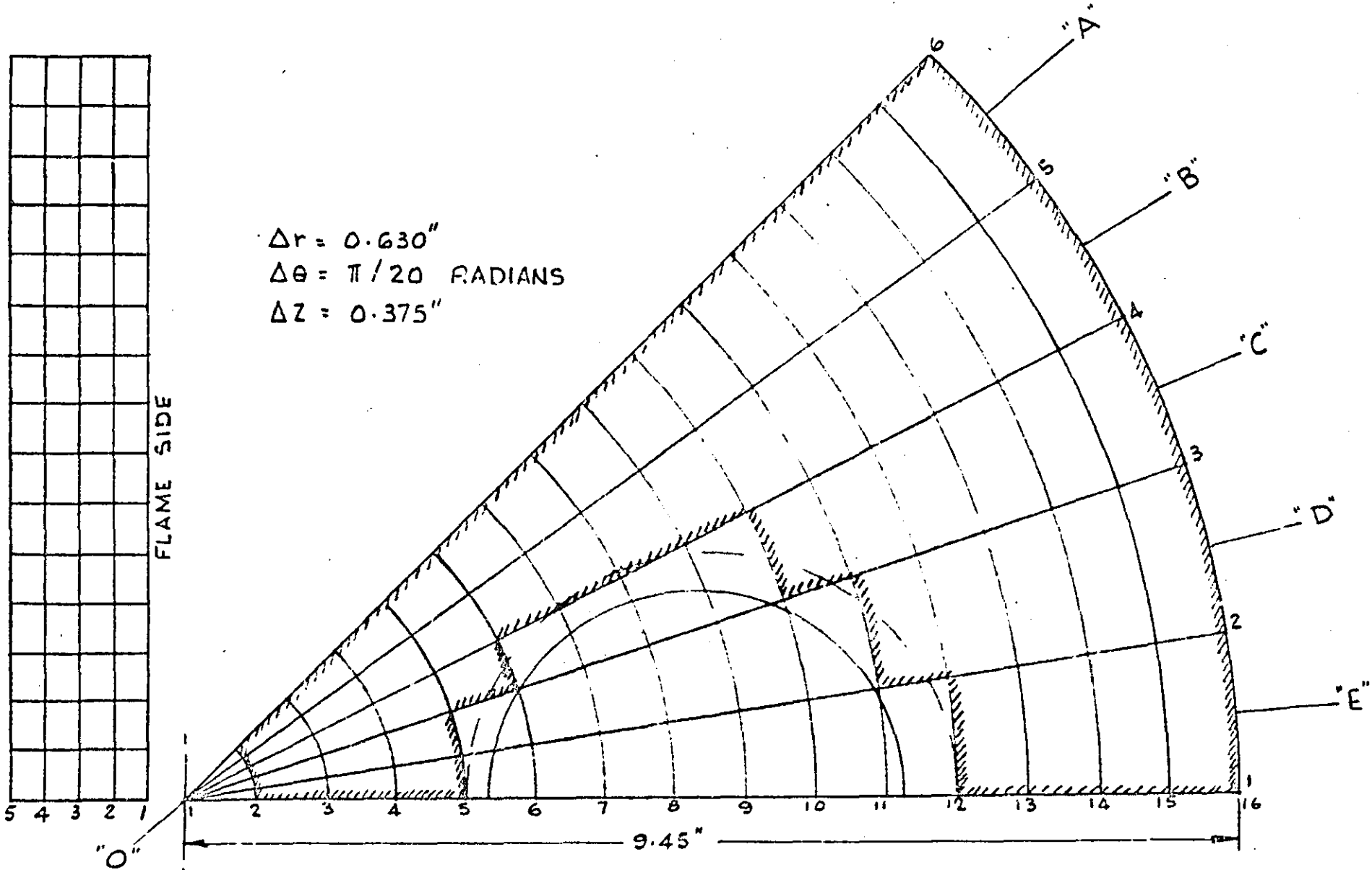
Δr = 0.630"
Δθ = π/20 RADIANS
ΔZ = 0.375"
FLAME SIDE
5 4 3 2 1
"O"
1 2 3 4 5 6 7 8 9 10 11 12 13 14 15 16
9.45"
"A"
"B"
"C"
"D"
"E"
6
5
4
3
2
1

FIGURE 5.8

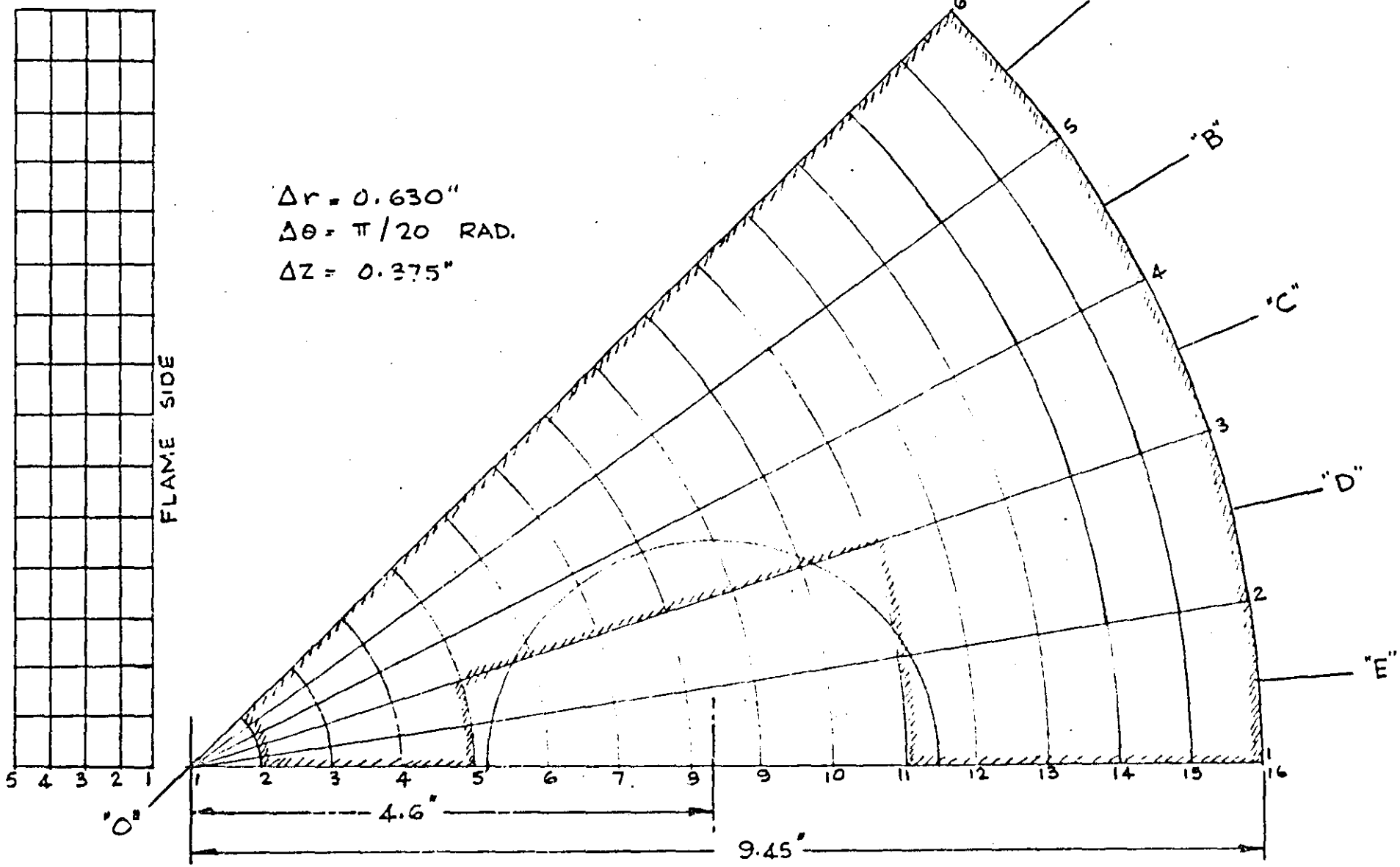
Δr = 0.630"
Δθ = π/20 RAD.
ΔZ = 0.375"
FLAME SIDE
5 4 3 2 1
"O"
1 2 3 4 5 6 7 8 9 10 11 12 13 14 15 16
4.6"
9.45"
"A"
"B"
"C"
"D"
"E"
6
5
4
3
2
1

FIGURE 5.9

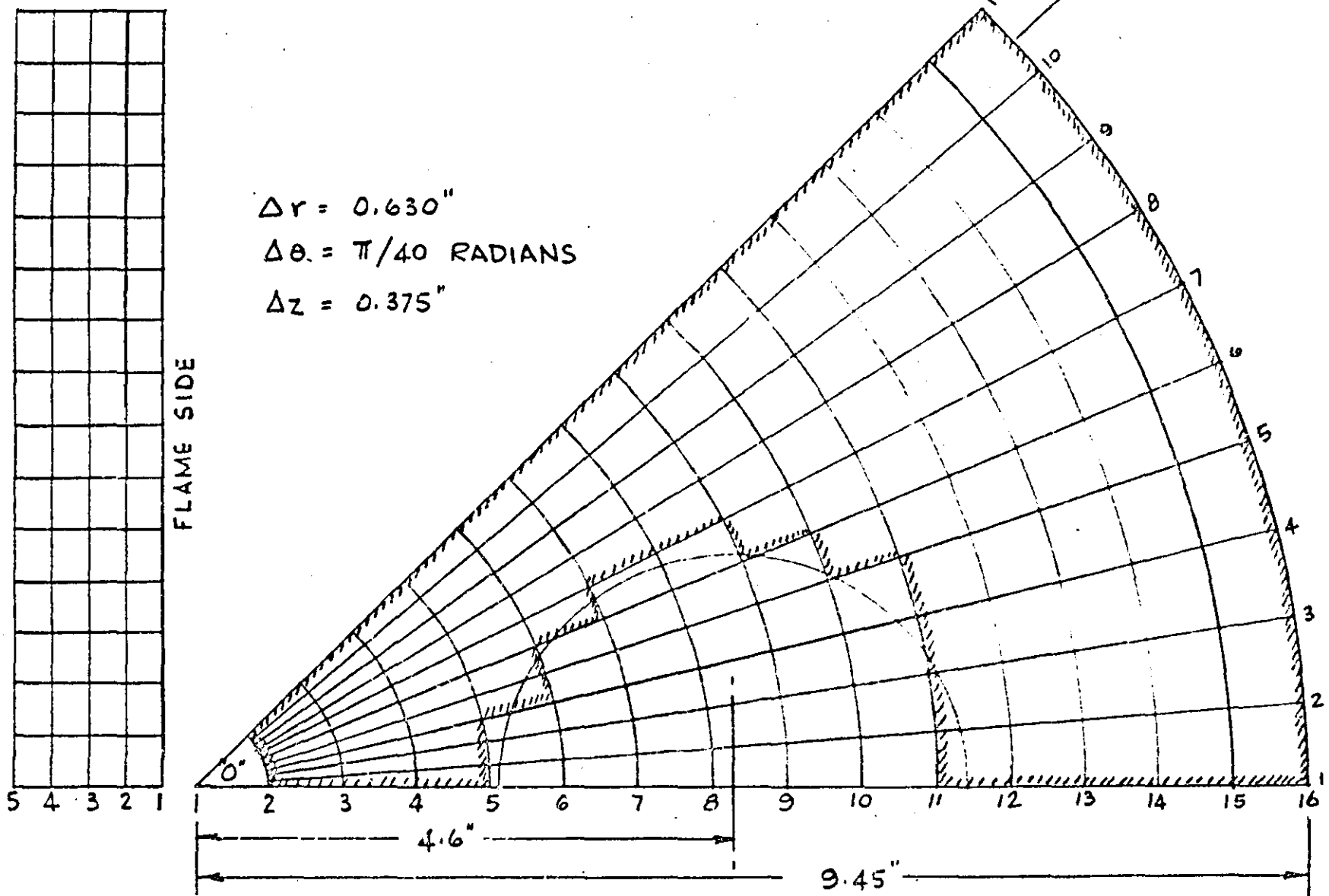
Δr = 0.630"
Δθ = π/40 RADIANS
Δz = 0.375"
FLAME SIDE
5 4 3 2 1
1 2 3 4 5 6 7 8 9 10 11 12 13 14 15 16
11 10 9 8 7 6 5 4 3 2 1
"A"
0°
4.6"
9.45"

FIGURE 5.10

The valve port is approximated by a series of steps. This mesh appears rather coarse however the solution requires about 6 hours for convergence and a storage requirement of 12.5K. Figure (5.9) shows an identical mesh size but the approximation of the valve port is much more crude. Figure (5.10) shows a mesh in which the number of meshes or elements in the tangential direction has been doubled. For this finer mesh, the time required to achieve a steady state condition is four times that of the two previous mesh configurations. The reason for the severe time increase is that doubling the number of points doubles the number of calculations to be made. In addition, the tangential mesh greatly controls the time increment and thus doubling the number of mesh points cuts the time increment by half in this particular instance.

The finite difference equations are given in App. A, for stress analysis and in App. D for heat conduction. The solutions will be described in more detail in the following sections.

5.6 ANALYSIS OF FLAME PLATE UNDER MECHANICAL LOAD

5.6.1 Holographic Analysis

The need for an experimental analysis has already been discussed. Also, it has been mentioned that it was not considered feasible to attempt to simulate engine conditions in the laboratory. It remains then to devise an experiment that is to some extent compatible with what one might expect to transpire in the plate under engine conditions. It seems reasonable to assume from the foregoing description of the engine conditions, that the flame plate will be subject to loads that will primarily cause transverse or flexural displacements. Thus a holographic interferometry analysis of the flexural displacements of the plate under transverse mechanical load was devised. The experimental arrangement is shown in Fig's (5.11) to (5.13).

The flame plate is simply supported, the support is assumed to act at the centre of the gasket face, and is loaded at the centre

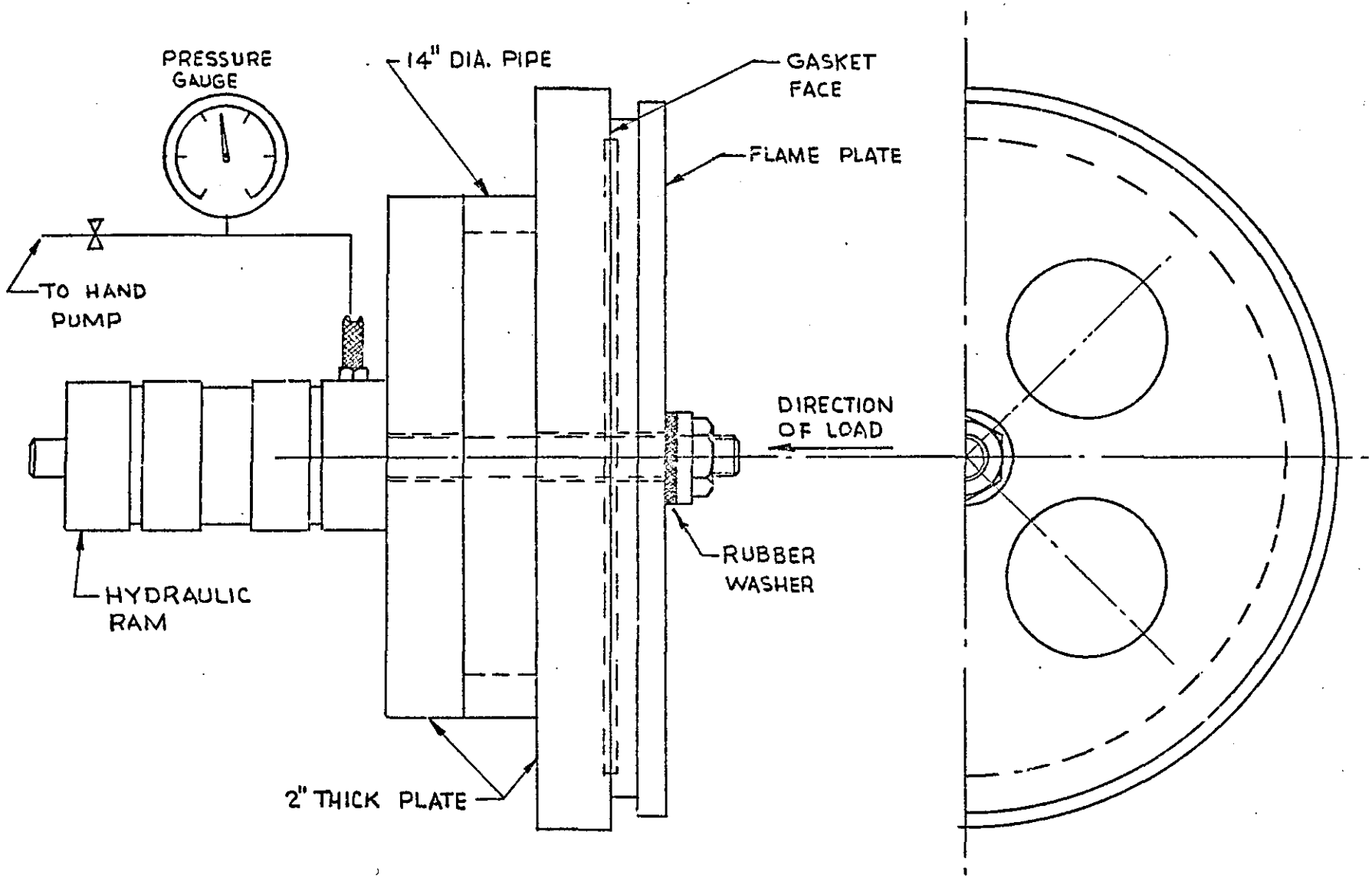
PRESSURE GAUGE
14" DIA. PIPE
GASKET FACE
FLAME PLATE
TO HAND PUMP
DIRECTION OF LOAD
RUBBER WASHER
HYDRAULIC RAM
2" THICK PLATE

FIGURE 5·11

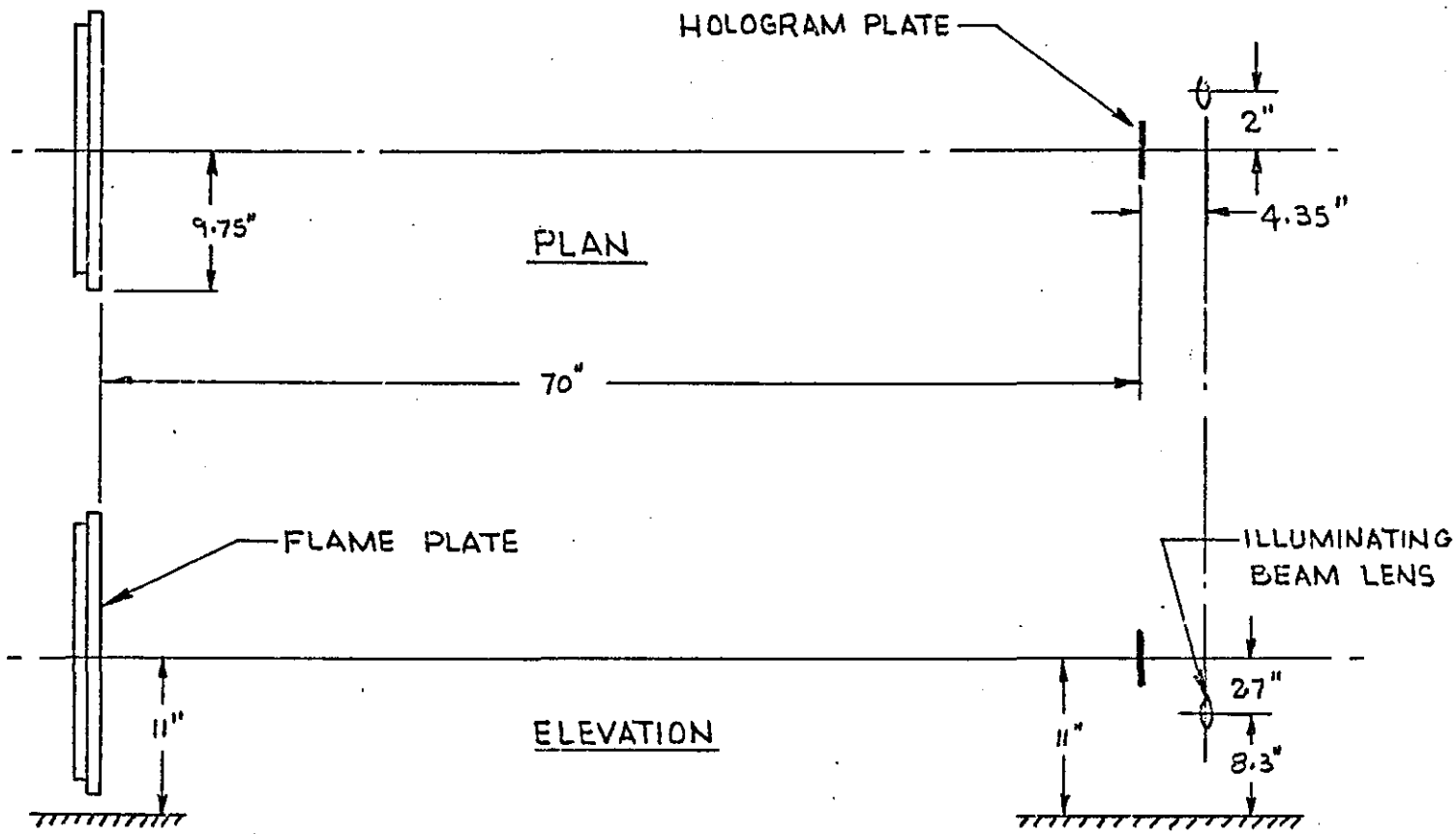
HOLOGRAM PLATE
2"
4.35"
9.75"
PLAN
70"
FLAME PLATE
ILLUMINATING
BEAM LENS
27"
11"
ELEVATION
11"
8.3"

FIGURE 5·12

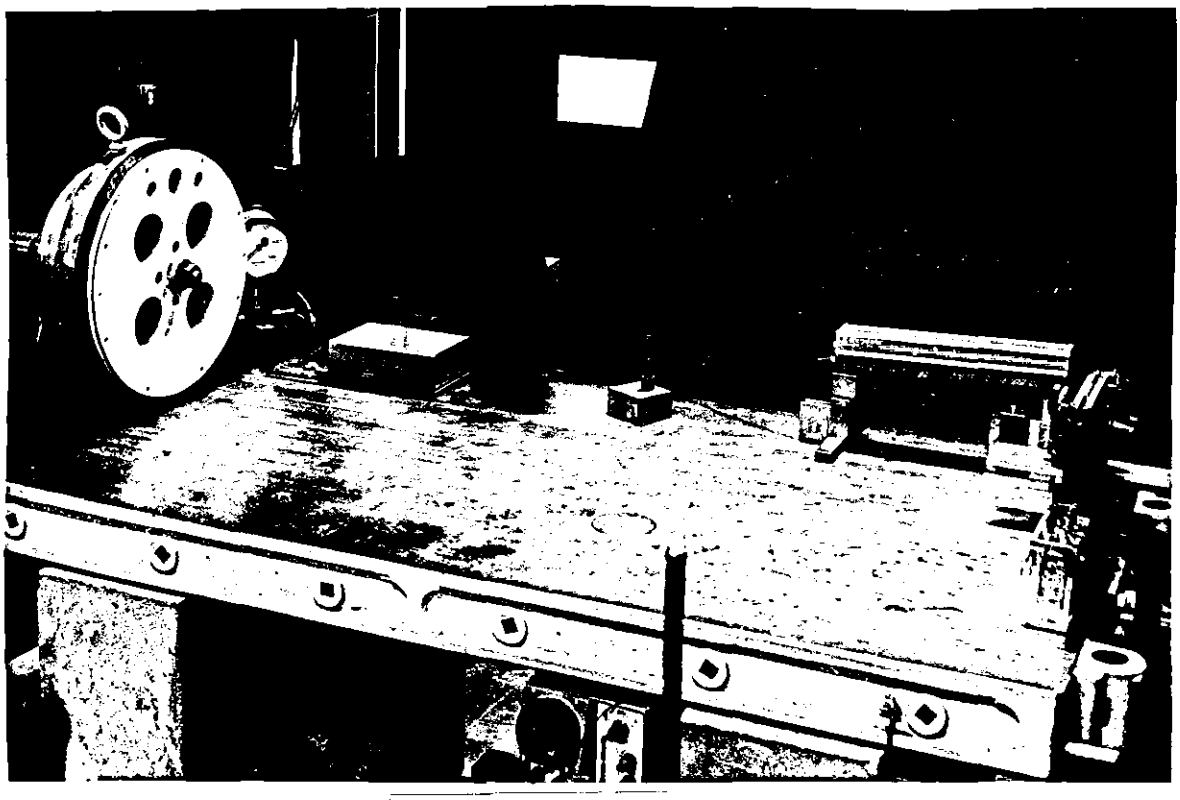

FIGURE 5.13

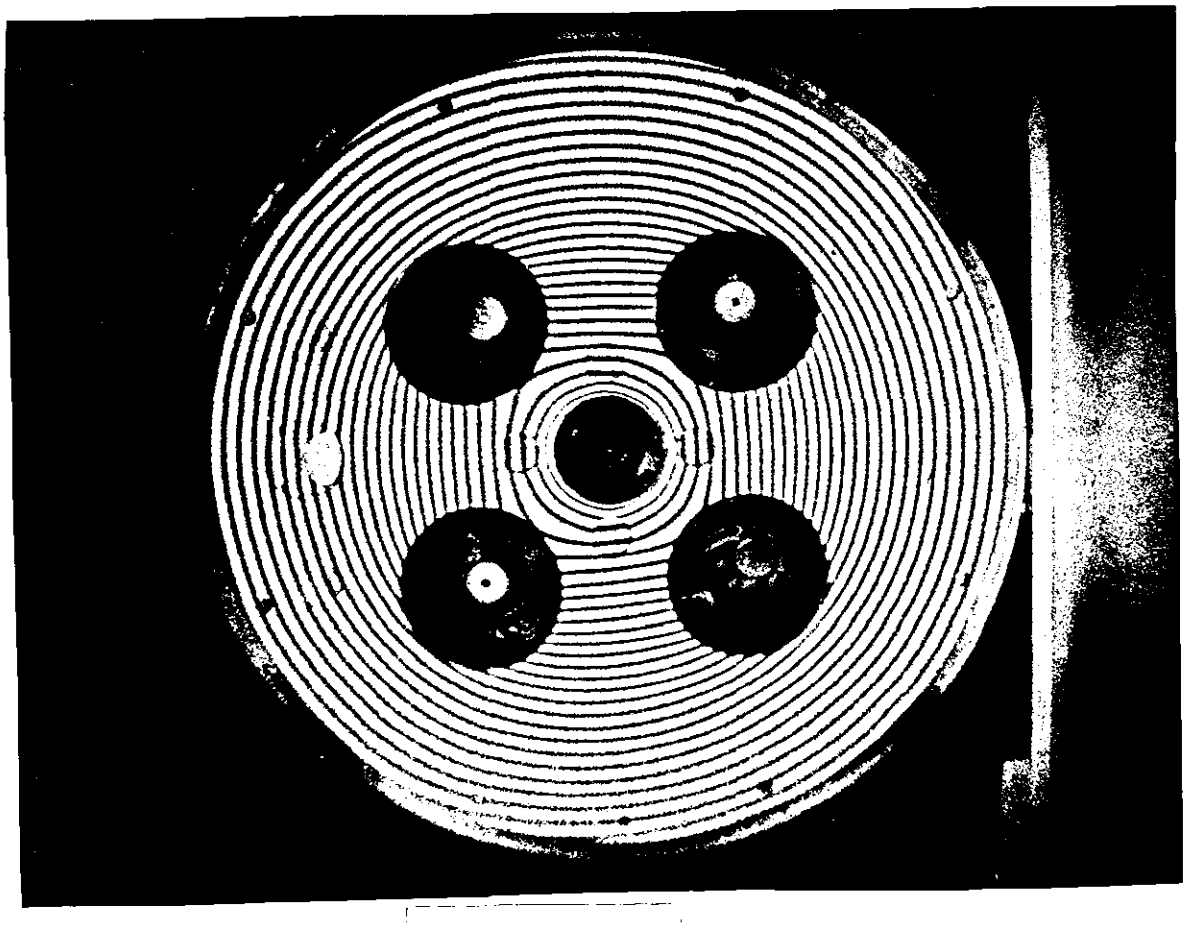

FIGURE 5.14

(LOAD 412 LB.)

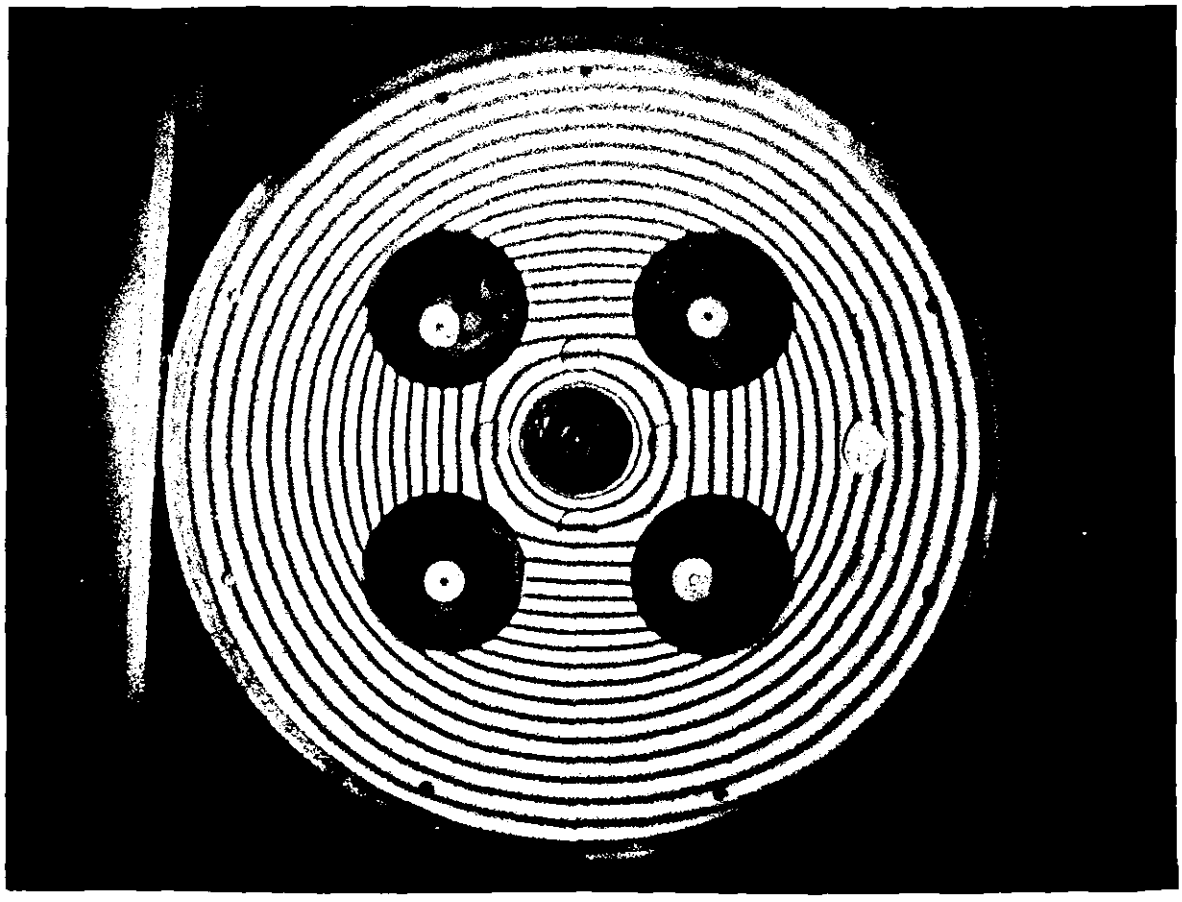

FIGURE 5.15

(LOAD 309 LB.)

by means of a hydraulic ram. The load acts over an annular diameter of $2\frac{1}{2}$" x $1\frac{1}{4}$" and to ensure that it is uniformly distributed, a canvas reinforced rubber washer was positioned between the flame plate and the washer under the nut on the end of the loading ram. The hydraulic pressure was obtained by means of a hand operated pump and measured using a 0-500 lb./in.^{2} pressure gauge graduated in 10 lb./in.^{2} increments. Before assembly, the gasket face on the flame plate was machined; a paper gasket was installed to ensure a uniform support reaction.

Four frozen fringe holograms were made, two with a load on the flame plate of 309 lb. and two with a load of 412 lb. Two were made at each load to ensure the accuracy and repeatabilty of the experiment. Figures (5.14) and (5.15) show two of the fringe patterns obtained. Enlarged photographic copies of Fig's (5.14) and (5.15) were used in measuring the fringe spacing from which the transverse deflections were obtained. The deflection of the flame plate was determined along the radial line O - A shown in Fig. (5.8). As was the case in the fringe patterns of Chapter 4, some eccentricity exists in the fringe patterns of the flame plate hence the fringe spacing was measured on two diametrically opposite radial lines corresponding to line O - A which in Fig's (5.14) and (5.15) is near the horizontal axis. Figures (5.14) and (5.15) are presented rotated 90° from the actual set up during the experiment. In measuring the fringe spacing or location, the dark fringes were numbered and their location measured from the centre of the flame plate. The locations were multiplied by an appropriate scale factor relating the enlarged photographic copy with the actual size of the flame plate.

Since the holographic set up views and illuminates normal to the plane of the surface, each dark fringe represents a relative displacement of 0.125×10^{-4} in. Assuming the deflection of the flame plate to be zero at a radius of 8.625 in. from the centre, which is the centre of the gasket face, the deflection curve for the plate along line O - A is obtained from the knowledge that each dark fringe represents a relative deflection of 0.125×10^{-4}, and by interpolating linearly, the displacement of the first dark fringe on either side of the zero displacement point, i.e. on either side of the 8.625 radius.

The results of the fringe measurements, the scaled measurements, and the deflection at each dark fringe is given in tables (5.1)

and (5.2). The deflection of the flame plate along line O - A is given in Fig's (5.16) and (5.17) along with the dynamic relaxation results for comparison purposes.

5.6.2. Dynamic Relaxation Analysis

The computer programme written for the analysis is given on pages 253-257. The boundary conditions of particular interest are as follows:

1. The axial or transverse deflection on the surface in contact with the support is zero, i.e. at I = 14 and K = 5 and for all values of J. This corresponds to the gasket face.
2. The load is applied over the second mesh on the reverse side of the plate, i.e. I = 2 and K = 1 and for all values J, in the form of a surface stress. The stress is equal to the applied load divided by the surface area of the mesh.

The method of dynamic relaxation requires the stress and velocity to be calculated at every node point in the structure however the deflection need not be determined since it is derived by integrating the velocity. The only deflections of interest in this particular solution are the transverse surface deflections on the side of the plate which was seen in the holographic solution. Three programmes were run corresponding to the mesh configurations shown in Fig's (5.8) to (5.10). Solution No. 1 refers to Fig. (5.8), No. 2 refers to Fig. (5.9) and No. 3 refers to Fig. (5.10). The deflections along the radial line O - A are given in table (5.3) for the three solutions. These deflections are also plotted in Fig's (5.16) and (5.17); solution No. 3 is not shown since it almost identical to No. 2 and the differences cannot be detected on the scale chosen for the plot.

5.6.3 Discussion of the Results of the Mechanical Load Analysis

Simply supporting the flame plate and applying a load near the centre of the plate provides a simple experiment that illustrates the

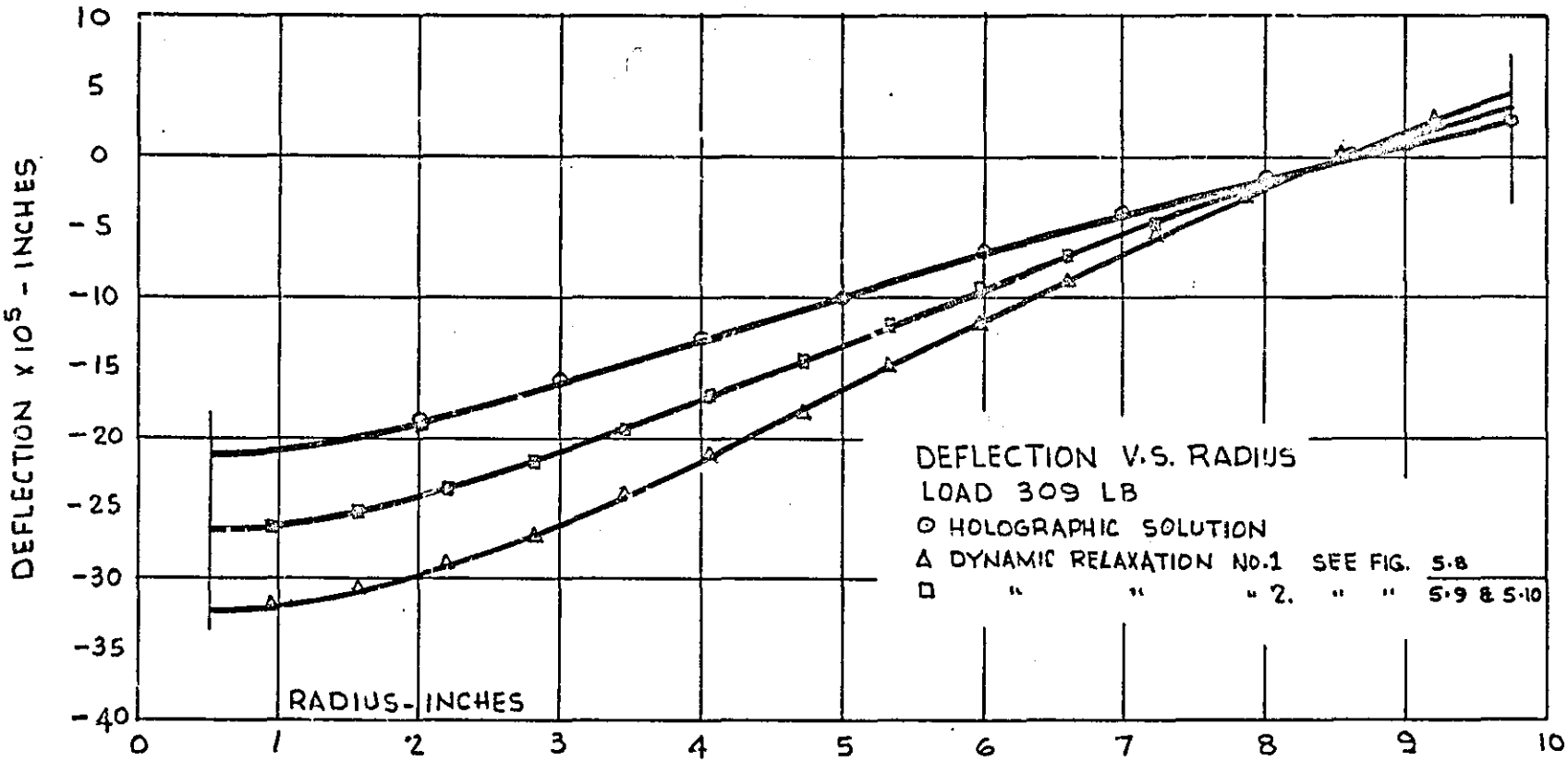
DEFLECTION X 10^5 - INCHES
10
5
0
-5
-10
-15
-20
-25
-30
-35
-40
0
1
2
3
4
5
6
7
8
9
10
RADIUS - INCHES
DEFLECTION V.S. RADIUS
LOAD 309 LB
⊙ HOLOGRAPHIC SOLUTION
Δ DYNAMIC RELAXATION NO.1 SEE FIG. 5.8
□ " " " 2. " " 5.9 & 5.10

FIGURE 5.16

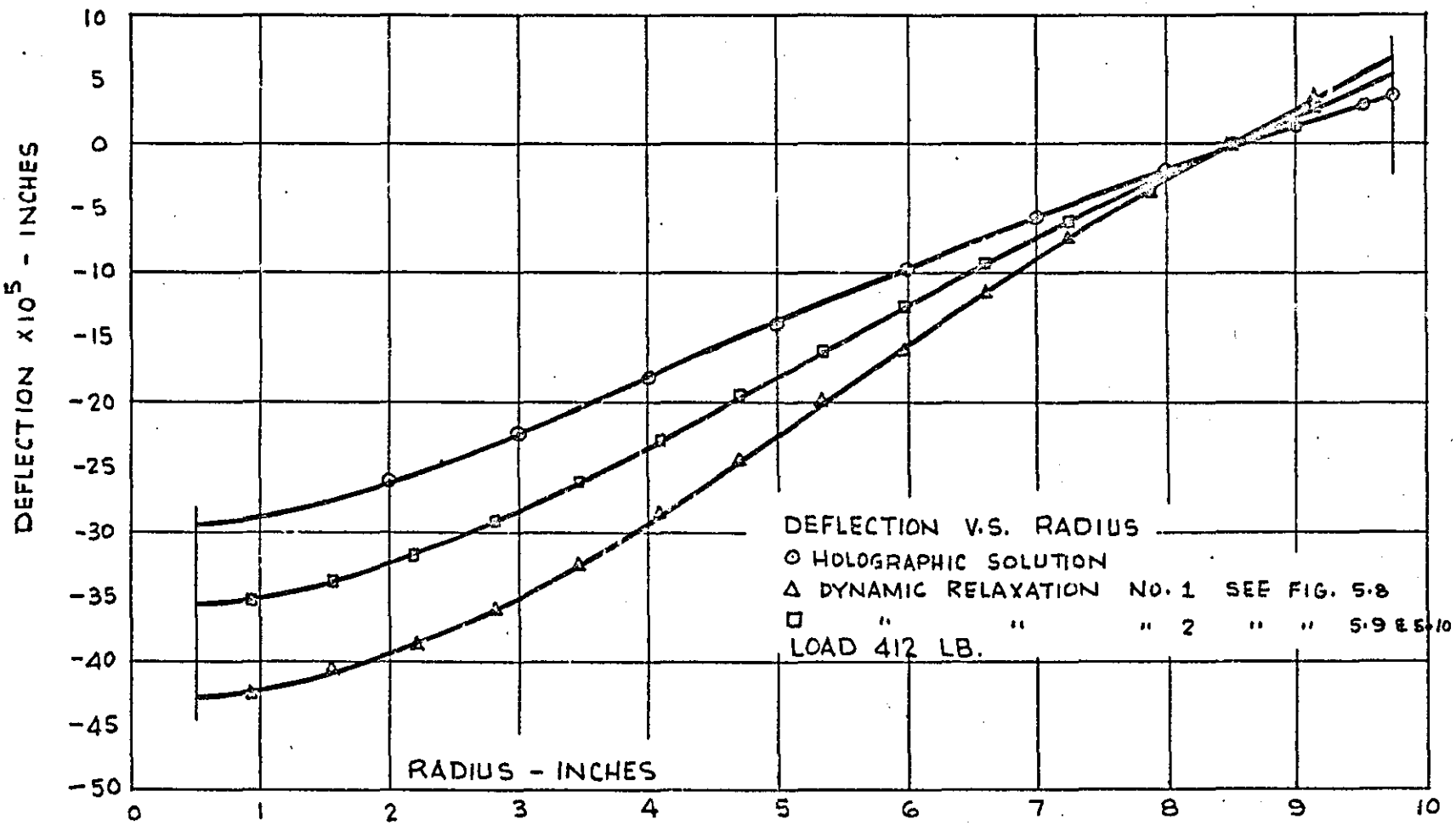
DEFLECTION X10^5 - INCHES
10
5
0
-5
-10
-15
-20
-25
-30
-35
-40
-45
-50
0
1
2
3
4
5
6
7
8
9
10
RADIUS - INCHES
DEFLECTION V.S. RADIUS
⊙ HOLOGRAPHIC SOLUTION
Δ DYNAMIC RELAXATION NO. 1 SEE FIG. 5.8
□ " " " 2 " " 5.9 & 5.10
LOAD 412 LB.

FIGURE 5.17

flexural characteristics of the plate. The deflection curve could be determined for a number of radial lines however from the fringe patterns it appears that the deflection does not vary greatly along other lines and that the deflection along line O - A is fairly representitive of the deflected shape.

Since the actual flame plate was used in the experiment, one does not need to consider inaccuracies that might be incurred if a model of the plate had been used. The use of holographic interferometry to determine normal displacements is basically simple and accurate. The holographic results corresponding to the two different loads are in good agreement with each other if one assumes that the deflection is linear with respect to the transverse load; the two sets of results are within 3.5 percent of each other. The two holograms made at the same load showed identical fringe patterns thus indicating that the experiment was repeatable (only one pattern at each load is presented in this thesis). The simplicity of the experiment and the good agreement between the two sets of results is felt to be sufficient justification to claim an accuracy within 5 percent. There is however one area in which a discrepancy might arise.

In the holographic analysis, it was assumed that the support acts at a radius of 8.625 in. Since the gasket face is flat and not a knife edge, it is possible that the support reaction occured on the inside diameter of the gasket face, i.e. at a radius 8.316 in. In the dynamic relaxation solution, the support acts at a radius 8.505 in. If the gasket face had been machined to a knife edge located at 8.505 in., then the support diameter would be increased by 0.189 in. and assuming that the central deflection is proportional to the square of the radius, which is the case for a solid flat circular plate with a load at the centre, then the deflection of the flame plate would increase by about 5 percent. It is felt that this may be pessimistic since the support reaction cannot act 100 percent on the edge of the gasket face. In any event, the holograhic results should form a reasonable basis with which the dynamic relaxation results can be compared.

The first dynamic relaxation solution, corresponding to Fig. (5.8) is in poor agreement with the holographic solution. This was believed due to the mesh being coarse. The running time for this solution

was approximately 6 hours and thus before attempting a fine mesh, a second programme was run in which the valve port hole was reduced in size. In the first solution, the valve port hole was deliberately made large to try and compensate for the internal cooling passage around the valve port which was being neglected. Thus the second solution is made to come closer to the holographic solution by effectively stiffening the plate, and, worsening the approximation of the boundary around the valve port. This approach of stiffening the plate can, to some extent, be justified since in areas remote from the valve port, the stress distribution will not be greatly affected by the shape of the port and thus by making the deflected shape come closer to the holographic solution, which is believed to be accurate, the stress distribution in areas remote from the valve port should be more realistic or accurate. This improved solution deviates from the holographic solution by approximately 22 percent based on the deflection at the edge of the injector hole.

Finally, a third programme was run based on the finer mesh configuration shown in Fig. (5.10). The programme was run for 22 hours and while the results had not completely converged to a steady state, the change in deflections indicated that the solution was not going to be significantly better than the second solution and in fact appeared to deviate slightly more from the holograhic solution. The fine mesh solution would undoutedly be much better than the first coarse mesh solution and while some of the improvement can be attributed to the valve port being made smaller, additional improvement must be the result of the mesh being finer. In view of the fact that the fine mesh solution would be about 22 percent from the holographic solution and requires in excess of 22 hours computer time, it was decided to proceed to the analysis of the plate under engine conditions using the second coarse mesh solution. It is possible that an even finer mesh, than used in the third solution, would improve the solution however even neglecting the length of time reqired, the storage requirements would exceed the core capacity of the I.C.T. 1905 in current use at Loughborough University, and if one is able to live with a 22 percent deviation in the results, then it is not practical to proceed to a finer mesh.

5.7 ANALYSIS OF FLAME PLATE UNDER WORKING CONDITIONS

5.7.1 Determination of Thermal Gradients

The boundary conditions with regard temperature and temperature gradients were described in Section 5.4 under the heading "Loading Conditions in the Engine". The geometrical boundaries used for the thermal analysis must be identical to those that will be used in the thermal stress analysis and of course the mesh configuration must be the same. The programme for the thermal analysis is given on pages 258 to 260 and is based on the mesh configuration shown in Fig. (5.9). The temperatures are calculated at each normal stress node. For use in stress analysis, it is not the temperature that is required but rather the temperature difference of a particular point relative to a reference temperature. The reference temperature will be the lowest temperature in the case of the object being heated or the highest temperature in the case of an object being cooled. For the flame plate, the reference temperature will be 260°F.

The output of the thermal programme gives the temperature differences at each normal stress node thus to determine the actual temperature at each point, 260°F must be added to each value at every point. The temperature differences are given in Fig's (5.18) to (5.21); Fig. (5.18) being the first layer begining on the flame side of the plate.

The initial conditions which are used in the thermal stress solution, are the normal stresses that would exist if each element in mesh was perfectly constrained in all directions and the temperature of each element was changed by an amount "T" corresponding to the temperature differences calculated in the thermal programme, see App. E. In the thermal programme, these stresses have been calculated and are stored on magnetic tape to be used as input data for the thermal stress programme.

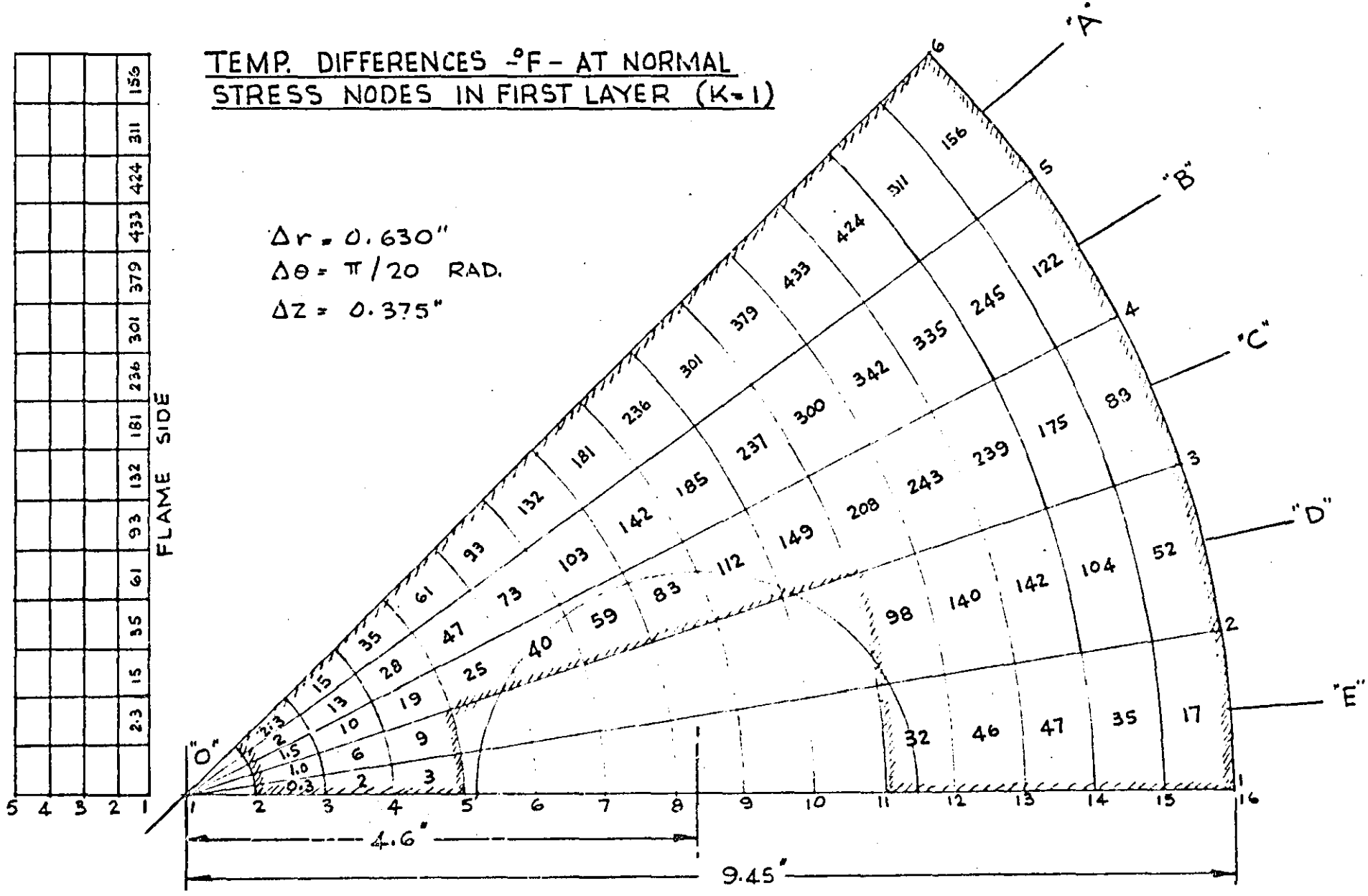
TEMP. DIFFERENCES °F - AT NORMAL
STRESS NODES IN FIRST LAYER (K=1)
Δr = 0.630"
Δθ = π/20 RAD.
ΔZ = 0.375"
FLAME SIDE
"A"
"B"
"C"
"D"
"E"
"O"
4.6"
9.45"

FIGURE 5.18

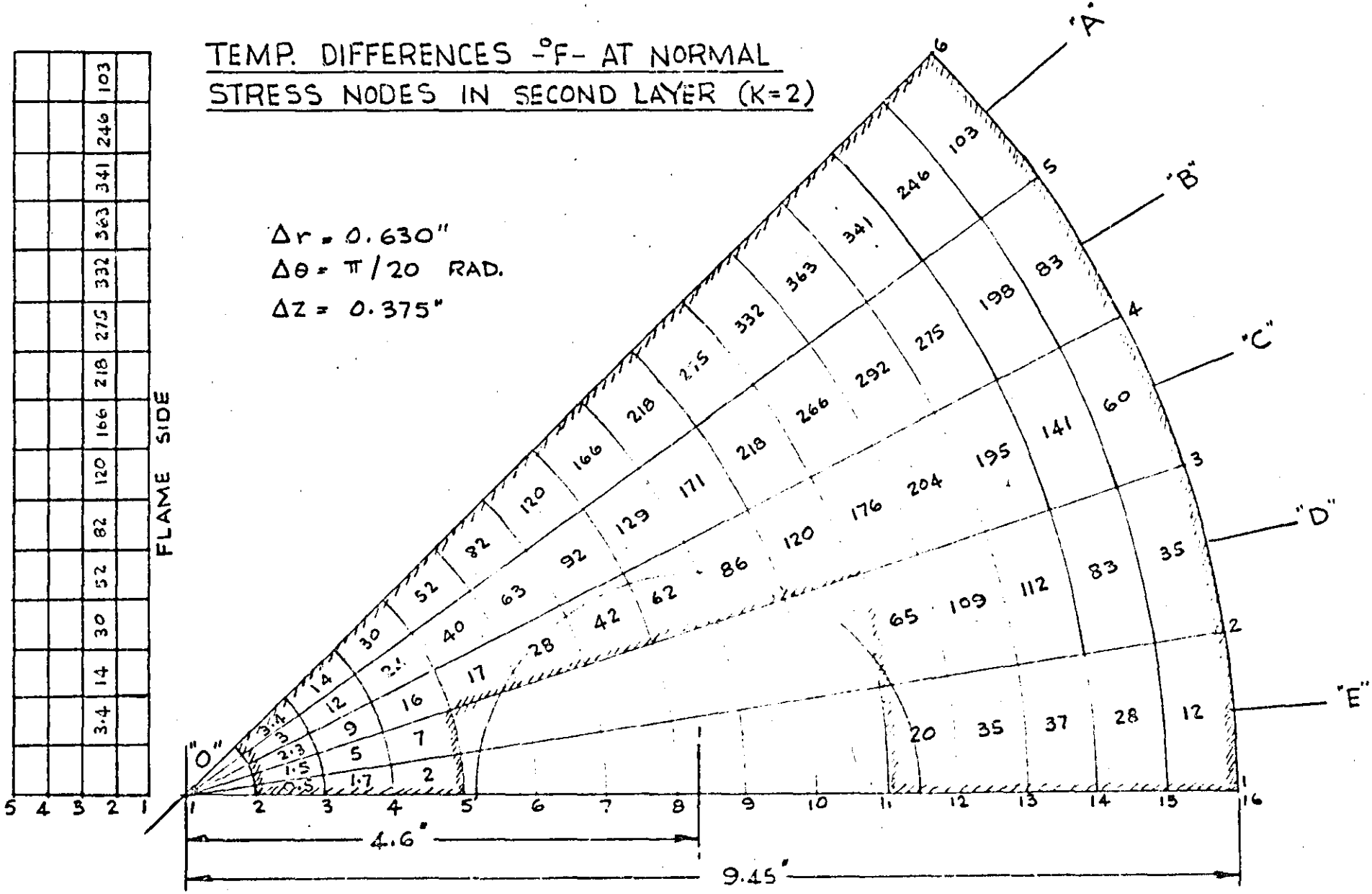
TEMP. DIFFERENCES -°F- AT NORMAL
STRESS NODES IN SECOND LAYER (K=2)
Δr = 0.630"
Δθ = π/20 RAD.
ΔZ = 0.375"
FLAME SIDE
"A"
"B"
"C"
"D"
"E"
"O"
4.6"
9.45"

FIGURE 5.19

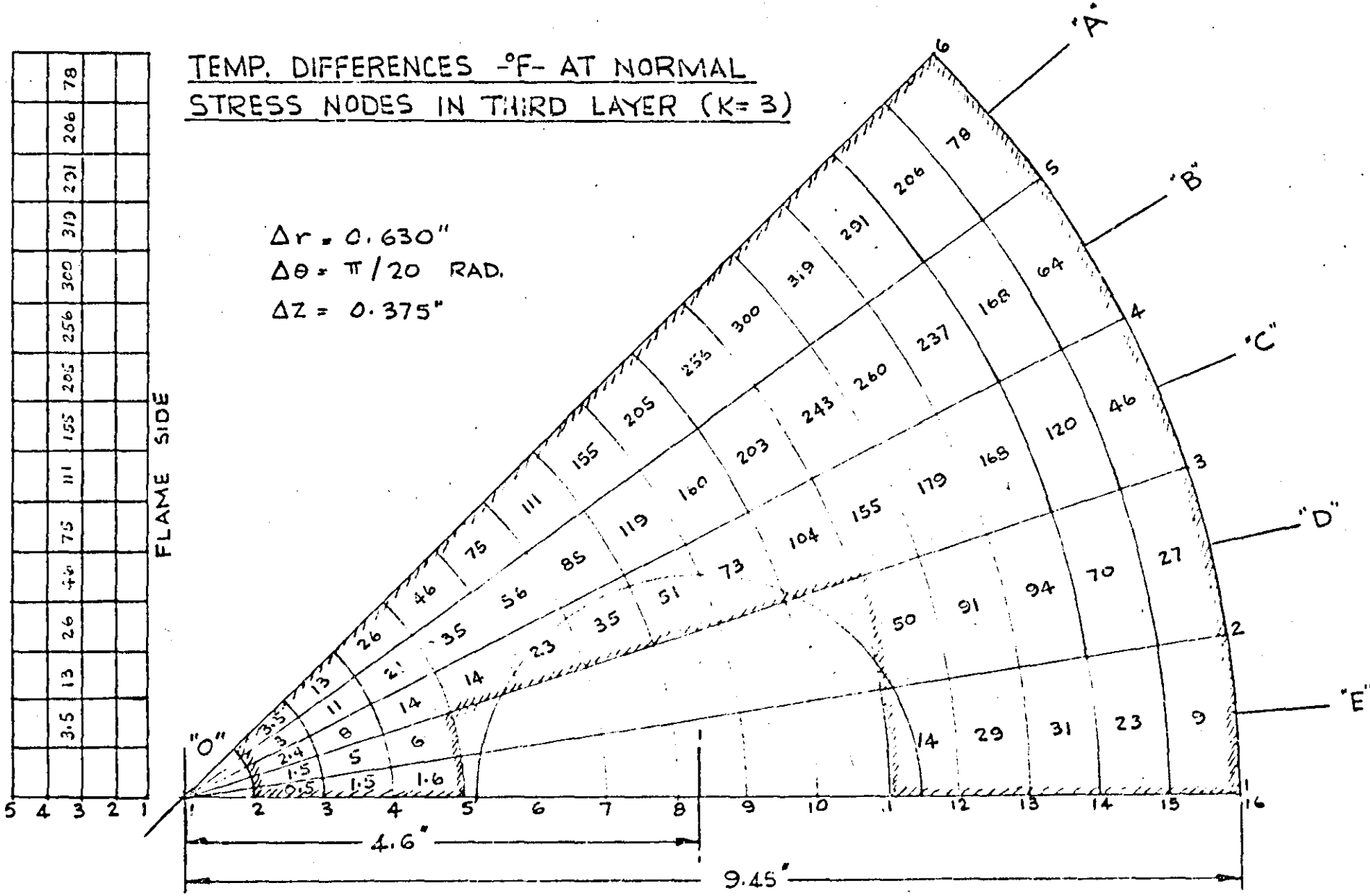
TEMP. DIFFERENCES -°F- AT NORMAL STRESS NODES IN THIRD LAYER (K=3)
Δr = 0.630"
Δθ = π/20 RAD.
ΔZ = 0.375"
FLAME SIDE
"A"
"B"
"C"
"D"
"E"
"O"
4.6"
9.45"

FIGURE 5.20

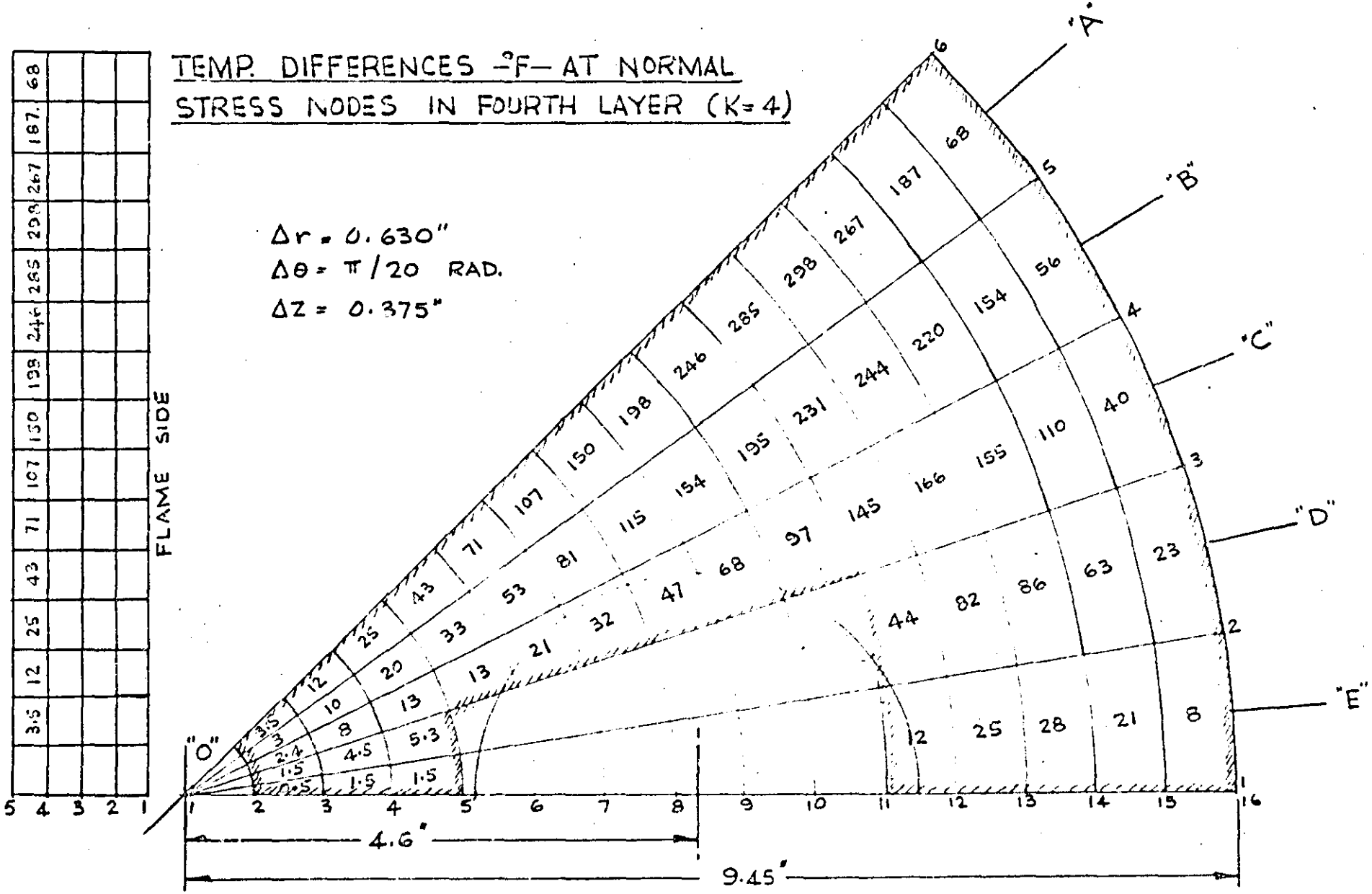
TEMP. DIFFERENCES °F— AT NORMAL STRESS NODES IN FOURTH LAYER (K=4)
Δr = 0.630"
Δθ = π/20 RAD.
ΔZ = 0.375"
FLAME SIDE
68
187
267
299
285
246
198
150
107
71
43
25
12
3.5
"A"
"B"
"C"
"D"
"E"
"O"
4.6"
9.45"

FIGURE 5·21

5.7.2 Thermal Stress Analysis

The programme written for solution No. 2 for the deflection of the flame plate under mechanical load was modified to incorporate the boundary conditions for the thermal stress analysis; the programme is given on pages 261 to 265. The boundary conditions of interest are:

1. All surface stresses are zero, i.e. there are no mechanical loads.
2. The transverse deflection of the plate at the outside diameter is zero on the cold surface, i.e. at I = 15, K = 4, and for all values of J.

The second boundary condition assumes that the plate is simply supported at the outermost mesh on the cold side of the plate. It is also assumed that the plate will deflect downward into the cylinder or away from the cylinder head thus no provision is made for the cylinder head to support the plate except as described above.

The intial conditions with regard to normal stresses have been described. The input data which comes from the thermal analysis was printed out at the begining of the programme as a check to ensure that the correct data had been transferred. The intial conditions with regard to shear stresses, velocities, and displacements are that all of these variables are zero throughout the plate.

The same time increment and damping was used as in the mechanical load analysis, and the running time was approximately 6 hours. The results are given in tables (5.4) to (5.30). The deflection of the cold surface was calculated and is shown in Fig. (5.22) for radial lines O - A and O - E. Tables (5.5) to (5.30) are in semi-pictorial form and the stress distribution can be easily seen.

5.7.2 Analysis of Flame Plate Under Combined Thermal and Gas Pressure Load

The programme used for the thermal stress analysis was modified to include the boundary conditions for the gas pressure load and

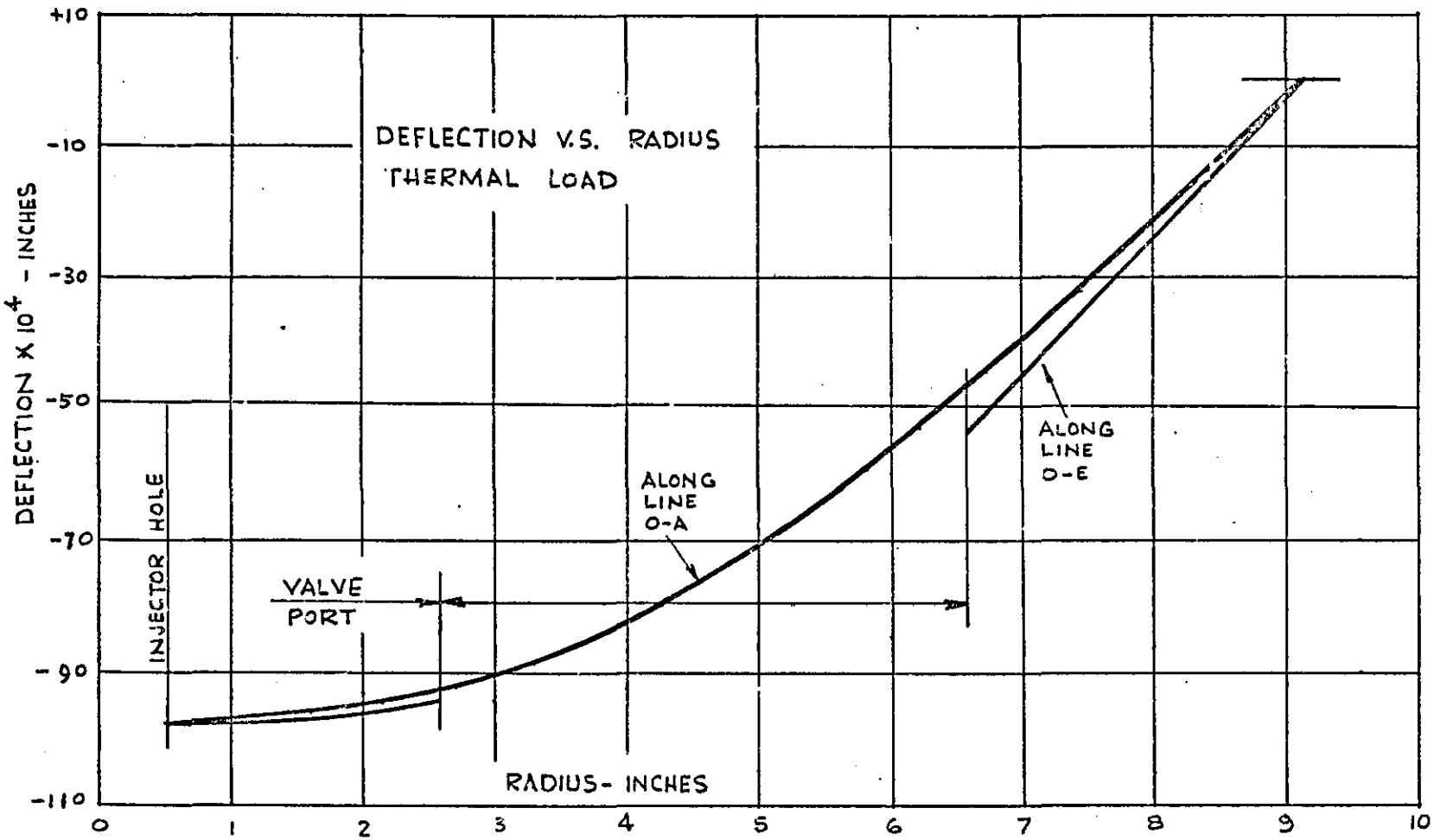
DEFLECTION V.S. RADIUS
THERMAL LOAD
DEFLECTION X 10^4 - INCHES
+10
-10
-30
-50
-70
-90
-110
0
1
2
3
4
5
6
7
8
9
10
RADIUS- INCHES
INJECTOR HOLE
VALVE PORT
ALONG LINE O-A
ALONG LINE O-E

FIGURE 5·22

to incorporate the cylinder head in the calculations as an elastic foundation. It was assumed that the cylinder head would provide a very stiff foundation and in the absence of any factual information regarding the foundation modulus of the head, a modulus of 30×10^6 lb./in.^{3} was assumed. This would correspond to the flame plate resting on a 1 inch thick steel plate which in turn rests on an infinitely stiff foundation. If then under the combined thermal and gas pressure load the flame plate deflects upward, a foundation stress is generated that is proportional to the deflection. Since the foundation is quite stiff relative to the flexural stiffness of the plate, small upward deflections will result in large foundation pressures or stresses and thus the upward deflections will be small in comparison with the flexural displacements under thermal loading.

The need to take this approach of an elastic foundation for the analysis is that the deflected shape of the plate under thermal loading will most likely be incompatible with the deflected shape of the plate under gas pressure load such that under the combined thermal and gas pressure load, the flame plate will not bear uniformly on the cylinder head. By assuming an elastic foundation, which in practice is realistic, the reaction of the cylinder head on the flame plate will be determined automatically and without inducing any additional or extraneous forces or in other words, the flame plate will come to equilibrium with the cylinder head in a natural way.

The boundary conditions for the elastic foundation are that if the deflection on the cold side of the flame plate is upward or positive, then the foundation stress generated is:

$$F_p(I,J) = -W(I,J) \times 30 \times 10^6 \text{ lb./in.}^3$$

If the deflection is zero or is negative, the foundation pressure is zero. Thus in areas where the flame plate makes contact with the cylinder head a foundation stress is generated and in areas where the flame plate does not touch the cylinder head, no surface stress is produced.

The boundary condition for the gas pressure load is simply a surface stress of 1500 lb./in.^{2} and as mentioned, acts over the inside diameter of the gasket face, i.e. the 16.630 in. diameter.

The results of the analysis are presented in tables (5.31) to (5.57). As in the thermal stress analysis, the stresses are given in semi-pictorial tables and the distribution of the stress on different layers can easily be seen. The deflection of the flame plate into the cylinder head is given in table (5.31).

5.8 Discussion of Results of the Analysis of the Flame Plate Under Engine Conditions

From Fig's (5.18) to (5.21) it can be seen that a hot zone exists between the two valve ports and towards the edge of the flame plate. One would normally expect this since this region is remote from the cooling passages and of course the boundary conditions used tend to create this condition. It can also be seen that the temperature gradients through the thickness are quite high in spite of the assumption that there is zero heat flow from the cold surface of the plate. In general, the large mass of material between the valve ports and towards the outside diameter is at a high temperature and high temperature gradients exist through the thickness. Gradients through the thickness of the plate will tend to cause bending in the plate.

Towards the centre of the plate the temperature is much lower due to cooling and the thermal gradients through the thickness are also much lower. Thermal gradients in the radial direction will tend to cause uniform radial and tangential stress through the thickness of the plate.

As previously mentioned, little information with regard to thermal conditions in the plate was available and a great many assumptions had to be made for the analysis and consequently the results are questionable. They do however seem feasible and should serve to illustrate the effects of thermal loading when used in the thermal stress analysis programme.

As shown in Fig. (5.22), under thermal loading and with a simply supported edge, the flame plate deflects downward away from the cylinder head as predicted. The deflection at the edge of the injector hole is approximately 0.01 in. It can also be seen that the deflection along the line O - A is not the same as along line O - B indicating

that bending occurs in the tangential direction as well as the radial direction.

Looking at the stress distribution in the plate, there appears to be three regions of interest. One region is on the rim of the plate between the two valve ports. The tangential stress varies through the thickness between 26,275 and 30,103 lb./in.^{2} The radial, axial, and shear stress are negligible or zero thus the tangential stress is approximately equal to the principal stress. A second region of high stress is in the hot zone. The radial and tangential stresses on the hot face are -10,924 and -28,604 lb./in.^{2} respectively. Again the axial and shear stresses are negligible hence the radial and tangential stress are approximately equal to the principal stresses. The third region is at the edge of the valve port where the radial stress is 21,204 lb./in.^{2} The tangential axial and shear stresses are negligible hence the radial stress is approximately equal to the principal stress. It is possible that this stress is higher than will occur in the actual plate because of the sharp corner that exists in the approximation of the valve port by the dynamic relaxation solution.

Since the plate was not constrained, the stress distribution must be the result of thermal gradients and it would seem reasonable to assert that if the thermal gradients were reduced so the stresses would be reduced. This could likely be achieved by providing cooling in the hot region (in preference to reducing the cooling elsewhere in the plate).

Under the combined thermal and gas pressure load, the stress distribution is altered but not increased as much as was expected. At the rim of the plate the tangential stress was increased from 30,103 to 31,257 lb./in.^{2} in the third layer from the hot side and on the cold side, from 28,516 to 31,716 lb./in.^{2} In the hot zone the radial and tangential stresses were increased on the hot face from -10,924 to -14,961 and from -28,604 to -32,633 lb./in.^{2} respectively. On the cold side of the plate, the radial and tangential stresses were reduced as is usual with bending having taken place. In the third region mentioned above, the stress on the hot side of the plate was reduced from 19,189 to 12,745 and increased on the cold side from 15,612 to 22,102. In general, the negative stresses on the hot side of the plate were

increased by the gas pressure load and the positive stresses are reduced; the stresses referred to are the radial and tangential, the axial stress is of course increased directly by the gas pressure load.

A fourth region of high stress is created under the combined load and is at the edge of the valve port on the radial axis bisecting the valve port. The tangential stress on the hot side is increased from -14,487 to -20,680 lb./in^2 and reduced on the cold side from -13,261 to -7139 lb./in.^{2}

Before concluding the analysis of the flame plate there is one additional point to consider. In the analysis, the gasket loading was neglected and also the four 5/8 in. diameter bolts which are fitted into the water transfer tubes. Both of these features occur in the support of the flame plate and will tend to prevent the downward deflection of the plate. Under the action of the combined thermal and gas pressure load the plate is pushed firmly against the cylinder head so that the forces exerted by the gasket and the four bolts will have little effect in terms of holding the plate against the head as compared with the gas pressure load and neglecting them in this part of the analysis can be justified. By assuming the plate to be simply supported the extremes of two loading conditions are obtained and by comparing the stress distribution under the two loading conditions one can to some degree, separate the effects of radial and tangential thermal gradients from transverse thermal gradients as follows.

Under the action of the gas pressure load, the stress distribution is altered but the maximum stress levels are not greatly increased and in fact the general stress levels are not greatly increased if compared with the maximum stresses in the plate. The impression given is that the high stresses in the plate are due to radial and tangential thermal gradients and that if the plate is laterally constrained the bending stresses induced are small. As mentioned before, reduction of the maximum temperatures will reduce the thermal gradients and in doing so should reduce the overall stress levels.

5.9 Closure

From the analysis of the flame plate under mechanical load, the dynamic relaxation solution gave a deflection at the centre of the plate which was approximately 22 percent greater than the holographic solution and since the holographic solution is assumed to be accurate within 5 percent, the dynamic relaxation solution is pessimistic. A fine mesh solution which gave a better approximation to the valve port boundary did not improve the accuracy of the dynamic relaxation solution.

Under the action of thermal gradients, the flame plate will tend to deflect downward away from the cylinder head; some restraint being provided by the gasket and water transfer tubes. Under gas pressure the plate is forced into contact with the cylinder head hence in operation the plate is subject to a vibratory loading condition which after a period of time could cause a fatigue failure or tend to loosen the plate in the head. Further investigation of the effects of the gasket loading and the constraint provided by the water transfer tubes is is recommended.

The stress level in the plate is not unduly high and one would not expect any problems to arise as a result of high stresses with the exception of reversing stresses however as previously mentioned the lack of temperature information limits the accuracy of any predictions that one might wish to make.

CHAPTER SIX

CONCLUSIONS AND SUGGESTIONS FOR FUTURE WORK

6.1 Conclusions

From the work done in Chapters 3 and 4, in solving two dimensional problems, it is concluded that the method of dynamic relaxation gives an accurate solution when the boundaries of the object coincide with the coordinate system used and can thus be defined exactly without having to approximate them by a series of steps. As described in Chapters 3 and 4, the errors in this type of solution are in the region of 5 percent and it is concluded that errors of this magnitude are the result of the finite difference approximation of the differential equations and the mesh size used. For a complex shaped object, it is reasoned that there are two areas in which the accuracy of the dynamic relaxation solution is degraded one of which is the finite difference approximation of the differential equations and the mesh size used. For example in the solution of the flat circular plate in Chapter 4, the mesh size is 15 x 5 and as described, the dynamic relaxation solution indicates a central deflection 4.3 percent greater than the analytical solution. For the flame plate where the radial and axial mesh is 15 x 4 and, neglecting for the moment the effects of the valve port on the accuracy of the solution, one might estimate an error in the region of 5 percent as a result of the axial mesh being slightly more coarse. This error is considered as inherent in the solution for the mesh size used.

The second area in which the accuracy of the solution will be degraded is in the approximation of complex boundaries which do not fit exactly, the coordinate system being used. In the case of the flame

plate, the valve port is approximated by a stepped boundary. The stepped boundary will tend to cause local stress variations around the valve port which may be reflected in the deflected shape of the plate. As described in Chapter 5 with regard to the holographic solution, a 5 percent discrepancy could exist in the solution as a result of the support reaction occurring towards the inside diameter of the gasket face thus making the deflection smaller than it would be if the support reaction occurred at the centre of the gasket face. Allowing for a 5 percent error inherent in the method of dynamic relaxation because of the mesh size and for a 5 percent experimental error, the error introduced by the approximation of the valve port is 12 percent; the total discrepancy between the holographic solution and dynamic relaxation solution is 22 percent as discussed in Chapter 5. It is felt that a 12 percent error as a result of the valve port approximation is not unduly high and one might postulate that if a plate were built with boundaries identical to those used in the dynamic relaxation solution, the holographic and dynamic relaxation solutions would be in better agreement.

In trying to estimate the magnitude of error that one might expect in solving a problem like the flame plate, a brief literature survey did not reveal any ideally comparative information. Three dimensional work done on arch dams using dynamic relaxation, paper 8 ref. (19), would seem to indicate that an overall discrepancy of 22 percent is not unreasonable however the only similarity between the flame plate and an arch dam is that they are both three dimensional problems with complex boundaries and it is difficult to justify any comparisons. Keeping in mind that the flame plate is a practical problem and not an academic one, it is concluded that an overall discrepancy of 22 percent is notunrealistic.

The need and advantages of combining an experimental solution with a theoretical solution has been demonstrated. In formulating the final dynamic relaxation solution, the dynamic relaxation solution was made to come closer to the holographic solution by altering the shape and size of the valve port cut out. In doing so, it was reasoned that if the deflection of the plate was in good agreement then the stresses, in particular those remote from the valve port, would be more accurate. Thus by having experimental results to compare with the theoretical results, one can refine the theortical solution and at the same time obtain a good estimate of the accuracy of the analysis.

From the work done in Chapters 2 and 4, it is concluded that holographic interferometry is ideally suited to measuring small flexural displacements. For measurement of in-plane displacements, the methods described in (9) and (11) appear theoretically possible however as illustrated in Chapter 2, there are a number of practical difficulties that would first have to be overcome to make the methods attractive for general use. The outstanding features of holographic interferometry are its sensitivity and ease of application. Very little preparation of the subject is required and one can generally work directly with an actual component thus avoiding the need for costly models.

6.2 Suggestions for Future Work

Before attempting to improve on the analysis of the flame plate, more information with regards thermal conditions in the plate is required. Additional analyses might take into account the effects of the gasket loading and the effects of the water transfer tubes. It might be possible to improve the approximation of the valve port boundary by using a different mesh configuration but without greatly increasing the number of mesh points; this might be investigated.

One problem encountered in applying the method of dynamic relaxation is determining the damping constant. A method of determining the optimum damping automatically and within the computer programme is mentioned in (5) and could be investigated further. Another area for investigation is the use of non-orthogonal coordinates. This would allow the use of different shape elements which could provide for a better approximation of complex boundaries.

For holographic interferometry, one might investigate methods of desensitising the method for measuring larger engineering displacements. One might also investigate the design of a system that would allow a rapid and accurate determination of dimensions and fringe order numbers as described in Chapter 2 for measurement of in-plane displacements.

ACKNOWLEDGEMENTS

The author greatfully acknowledges the direction and assistance given by his supervisors Dr. J.H. Butters and Mr. B.P. Holownia of Loughborough University. Thanks are due to the staff and technicians of the Department of Mechanical Engineering and to the staff of the Computer Centre of Loughborough University. The author also wishes to thank Ruston-Hornsby Limited, Lincoln, England, for their cooperation in providing neccessary information and for providing a specimen flame plate for experimental purposes. The author duly thanks Dilworth, Secord, Meagher, and Associates Company Limited, Toronto, Canada, for their financial assistance.

REFERENCES

1. Day, A.S. "An Introduction to Dynamic Relaxation", The Engineer, January 29, 1965, pp 218-221

2. Otter, J.R.H. "Computations for Prestressed Concrete Reactor Pressure Vessels Using Dynamic Relaxation", Nuclear Structural Engineering, 1, 1965, pp 61-75

3. Otter, J.R.H., Cassell, A.C., Hobbs, R.E. "Dynamic Relaxation", Proc. Inst'n Civil Eng'rs, 35, 1965, pp 633-656

4. Rushton, K.R. "The Dynamic Relaxation Method Used For Stress Analysis", Conf. Recent Adv. Stress Analysis, R. Aeronautical Soc., 1968, 3, pp 3.41-3.46

5. Rushton, K.R. "Dynamic Relaxation Solutions of Elastic Plate Problems", Journal of Strain Analysis, Vol. 3, No. 1, 1968, pp 23-32

6. Rushton, K.R. "Dynamic Relaxation Solution for the Large Deflection of Plates With Specified Boundary Stresses", Journal of Strain Analysis, Vol. 4, No. 2, 1969, pp 75-80

7. Cassell, A.C., Kinsey, P.J., Sefton, D.J. "Cylindrical Shell Analysis by Dynamic Relaxation", Proc. Inst'n Civil Eng'rs, Vol. 39, 1968, pp 75-84

8. Ennos, A.E. "Holography and Its Applications", Contemp. Physics, Vol. 8, No. 2, 1967, pp 153-170

9. Ennos, A.E. "Measurement of In-Plane Surface Strain by Hologram Interferometry", Journal of Scientific Instruments, Vol. 1, Series 2, 1968, pp 731-734

10. Haines, K.A., Hildebrand, B.P. "Surface Deformation Measurement Using the Wavefront Reconstruction Technique", Applied Optics, Vol. 5, No. 4, April 1966, pp 595-602

11. Aleksandrov, E.B., Bonch-Bruevich, A.M. "Investigation of Surface Strains by the Hologram Technique", Soviet Physics-Technical Physics, Vol. 12, No. 2, August 1967, pp 258-265

12. Timoshenko, S., Goodier, J.N. "Theory of Elasticity", 2nd ed., McGraw-Hill Book Company, Inc., New York and London, 1951

13. Timoshenko, S., Woinowski-Kreiger, S. "Theory of Plates and Shells, 2nd ed., McGraw-Hill Book Company, Inc., New York and London, 1959

14. Thomson, W.T. "Vibration Theory and Applications", Prentice-Hall, Inc., Englewood Cliffs, N.J., 1965

15. Wylie, C.R. "Advanced Engineering Mathematics", 3rd ed., McGraw-Hill Book Company Inc., 1966

16. Leith, E. "Holography's Practical Dimesion", Electronics, July 25, 1966

17. Otter, J.R.H. "Dynamic Relaxation Compared With Other Iterative Methods", Nuclear Eng. and Design, Vol. 3, 1966, pp 183-185

18. Wood, W.L. "Dynamic Relaxation Compared With Three Other Iterative Methods", The Engineer, November 25, 1967, p 687

19. Chitty, L. (Miss) "A Critical Comparison of the Results From the Methods Presented in Previous Papers", Arch Dams, Inst. of Civil Eng'rs Symp., March 1968, p 141

APPENDIX A

DERIVATION OF FINITE DIFFERENCE EQUATIONS FOR STRESS ANALYSIS USING CYLINDRICAL COORDINATES

The stress-equilibrium equations written in cylindrical coordinates are:

$$\frac{\partial \sigma r}{\partial r} + \frac{1}{r}\frac{\partial \tau r\theta}{\partial \theta} + \frac{\partial \tau rz}{\partial z} + \frac{\sigma r - \sigma \theta}{r} = 0 \qquad (A.1)$$

$$\frac{\partial \tau r\theta}{\partial r} + \frac{1}{r}\frac{\partial \sigma \theta}{\partial \theta} + \frac{\partial \tau z\theta}{\partial z} + 2\frac{\tau r\theta}{r} = 0 \qquad (A.2)$$

$$\frac{\partial \tau rz}{\partial r} + \frac{1}{r}\frac{\partial \tau z\theta}{\partial \theta} + \frac{\partial \sigma z}{\partial z} + \frac{\tau rz}{r} = 0 \qquad (A.3)$$

The damped wave form equilibrium equations are:

$$\frac{\partial \sigma r}{\partial r} + \frac{1}{r}\frac{\partial \tau r\theta}{\partial \theta} + \frac{\partial \tau rz}{\partial z} + \frac{\sigma r - \sigma \theta}{r} = \rho\left(\frac{\partial^2 u}{\partial t^2} + K\frac{\partial u}{\partial t}\right) \qquad (A.4)$$

$$\frac{\partial \tau r\theta}{\partial r} + \frac{1}{r}\frac{\partial \sigma \theta}{\partial \theta} + \frac{\partial \tau z\theta}{\partial z} + 2\frac{\tau r\theta}{r} = \rho\left(\frac{\partial^2 v}{\partial t^2} + K\frac{\partial v}{\partial t}\right) \qquad (A.5)$$

$$\frac{\partial \tau rz}{\partial r} + \frac{1}{r}\frac{\partial \tau z\theta}{\partial \theta} + \frac{\partial \sigma z}{\partial z} + \frac{\tau rz}{r} = \rho\left(\frac{\partial^2 w}{\partial t^2} + K\frac{\partial w}{\partial t}\right) \qquad (A.6)$$

The damped wave equations written in finite difference form and rearranged to provide an expression for the new velocity in terms of the old velocity and stress terms are:

$$\dot{U}(I,J,K) = \dot{U}(I,J,K)\left(\frac{1 - K/2}{1 + K/2}\right) + \rho\frac{\Delta t}{(1+K/2)}\left[\frac{\sigma r(I,J,K) - \sigma r(I-1,J,K)}{\Delta r} + \right.$$

$$\frac{\tau r\theta(I,J+1,K)-\tau r\theta(I,J,K)}{r\Delta\theta}+\frac{\tau rz(I,J,K+1)-\tau rz(I,J,K)}{\Delta z}$$

$$+\frac{\sigma r(I,J,K)+\sigma r(I-1,J,K)-(\sigma\theta(I,J,K)+\sigma\theta(I-1,J,K))}{2r}\Bigg] \qquad (A.7)$$

$$\dot{V}(I,J,K)=\dot{V}(I,J,K)\left(\frac{1-K/2}{1+K/2}\right)+\frac{\Delta t}{\rho(1+K/2)}\Bigg[\frac{\tau r\theta(I+1,J,K)-\tau r\theta(I,J,K)}{\Delta r}$$

$$+\frac{\sigma\theta(I,J,K)-\sigma\theta(I,J-1,K)}{r\Delta\theta}+\frac{\tau z\theta(I,J,K+1)-\tau z\theta(I,J,K)}{\Delta z}$$

$$+2\left(\frac{\tau r\theta(I+1,J,K)+\tau r\theta(I,J,K)}{2r}\right)\Bigg] \qquad (A.8)$$

$$\dot{W}(I,J,K)=\dot{W}(I,J,K)\left(\frac{1-K/2}{1+K/2}\right)+\frac{\Delta t}{\rho(1+K/2)}\Bigg[\frac{\tau rz(I+1,J,K)-\tau rz(I,J,K)}{\Delta r}$$

$$+\frac{\tau z\theta(I,J,K+1)-\tau z\theta(I,J,K)}{r\Delta\theta}+\frac{\sigma z(I,J,K)-\sigma z(I,J,K-1)}{\Delta z}$$

$$+\frac{\tau rz(I+1,J,K)+\tau rz(I,J,K)}{2r} \qquad (A.9)$$

The elasticity or stress strain equations using cylindrical coordinates are:

$$\epsilon r=\frac{\partial u}{\partial r},\quad \epsilon\theta=\frac{1}{r}\frac{\partial v}{\partial\theta}+\frac{u}{r},\quad \epsilon z=\frac{\partial w}{\partial z} \qquad (A.10)$$

$$\gamma r\theta=\frac{1}{r}\frac{\partial u}{\partial\theta}-\frac{v}{r}+\frac{\partial v}{\partial r},\quad \gamma rz=\frac{\partial u}{\partial z}+\frac{\partial w}{\partial r},\quad \gamma z\theta=\frac{\partial v}{\partial z}+\frac{1}{r}\frac{\partial w}{\partial\theta} \qquad (A.11)$$

$$\sigma r=(\lambda+2\mu)\frac{\partial u}{\partial r}+\lambda\frac{u}{r}+\lambda\frac{1}{r}\frac{\partial v}{\partial\theta}+\lambda\frac{\partial w}{\partial z} \qquad (A.12)$$

$$\sigma\theta=(\lambda+2\mu)\frac{1}{r}\frac{\partial v}{\partial\theta}+(\lambda+2\mu)\frac{u}{r}+\lambda\frac{\partial u}{\partial r}+\lambda\frac{\partial w}{\partial z} \qquad (A.13)$$

$$\sigma z=(\lambda+2\mu)\frac{\partial w}{\partial z}+\lambda\frac{\partial u}{\partial r}+\lambda\frac{1}{r}\frac{\partial v}{\partial\theta}+\lambda\frac{u}{r} \qquad (A.14)$$

$$\tau r\theta=\mu\left[\frac{1}{r}\frac{\partial u}{\partial\theta}-\frac{v}{r}+\frac{\partial v}{\partial r}\right] \qquad (A.15)$$

$$\tau rz=\mu\left[\frac{\partial u}{\partial z}+\frac{\partial w}{\partial r}\right] \qquad (A.16)$$

$$\tau z\theta=\mu\left[\frac{\partial v}{\partial z}+\frac{1}{r}\frac{\partial w}{\partial\theta}\right] \qquad (A.17)$$

Differentiating Eq'ns (A.12) through (A.17) with respect to time and using the notation $\dot{u}=\partial u/\partial t$:

$$\frac{\partial\sigma r}{\partial t}=(\lambda+2\mu)\frac{\partial\dot{u}}{\partial r}+\lambda\frac{\dot{u}}{r}+\lambda\frac{1}{r}\frac{\partial\dot{v}}{\partial\theta}+\lambda\frac{\partial\dot{w}}{\partial z} \qquad (A.18)$$

$$\frac{\partial \sigma_\theta}{\partial t} = (\lambda+2\mu)\frac{1}{r}\frac{\partial \dot{v}}{\partial \theta} + (\lambda+2\mu)\frac{\dot{u}}{r} + \lambda\frac{\partial \dot{u}}{\partial r} + \lambda\frac{\partial \dot{w}}{\partial z} \tag{A.19}$$

$$\frac{\partial \sigma_z}{\partial t} = (\lambda+2\mu)\frac{\partial \dot{w}}{\partial z} + \lambda\frac{\partial \dot{u}}{\partial r} + \lambda\frac{1}{r}\frac{\partial \dot{v}}{\partial \theta} + \lambda\frac{\dot{u}}{r} \tag{A.20}$$

$$\frac{\partial \tau_{r\theta}}{\partial t} = \mu\left[\frac{1}{r}\frac{\partial \dot{u}}{\partial \theta} - \frac{\dot{v}}{r} + \frac{\partial \dot{v}}{\partial r}\right] \tag{A.21}$$

$$\frac{\partial \tau_{rz}}{\partial t} = \mu\left[\frac{\partial \dot{u}}{\partial z} + \frac{\partial \dot{w}}{\partial r}\right] \tag{A.22}$$

$$\frac{\partial \tau_{z\theta}}{\partial t} = \mu\left[\frac{\partial \dot{v}}{\partial z} + \frac{1}{r}\frac{\partial \dot{w}}{\partial \theta}\right] \tag{A.23}$$

Equations (A.18) through (A.23) in finite difference form using centred difference notation and rearranged to express the new stress in terms of the old stress and velocity terms are:

$$\sigma r(I,J,K) = \sigma r(I,J,K) + \Delta t\left\{(\lambda+2\mu)\left[\frac{\dot{U}(I+1,J,K) - \dot{U}(I,J,K)}{\Delta r}\right] + \lambda\left[\frac{\dot{U}(I+1,J,K)+\dot{U}(I,J,K)}{2r}\right]\right.$$
$$\left. + \lambda\left[\frac{\dot{V}(I,J+1,K) - \dot{V}(I,J,K)}{r\,\Delta\theta}\right] + \lambda\left[\frac{\dot{W}(I,J,K+1) - \dot{W}(I,J,K)}{\Delta z}\right]\right\} \tag{A.24}$$

$$\sigma\theta(I,J,K) = \sigma\theta(I,J,K) + \Delta t\left\{\lambda\left[\frac{\dot{U}(I+1,J,K)-\dot{U}(I,J,K)}{\Delta r}\right] + (\lambda+2\mu)\left[\frac{\dot{U}(I+1,J,K)+\dot{U}(I,J,K)}{2r}\right]\right.$$
$$\left. + (\lambda+2\mu)\left[\frac{\dot{V}(I,J+1,K)-\dot{V}(I,J,K)}{r\,\Delta\theta}\right] + \lambda\left[\frac{\dot{W}(I,J,K+1)-\dot{W}(I,J,K)}{\Delta z}\right]\right\} \tag{A.25}$$

$$\sigma z(I,J,K) = \sigma z(I,J,K) + \Delta t\left\{\lambda\left[\frac{\dot{U}(I+1,J,K)-\dot{U}(I,J,K)}{\Delta r}\right] + \lambda\left[\frac{\dot{U}(I+1,J,K)+\dot{U}(I,J,K)}{2r}\right]\right.$$
$$\left. + \lambda\left[\frac{\dot{V}(I,J+1,K)-\dot{V}(I,J,K)}{r\,\Delta\theta}\right] + (\lambda+2\mu)\left[\frac{\dot{W}(I,J,K+1)-\dot{W}(I,J,K)}{\Delta z}\right]\right\} \tag{A.26}$$

$$\tau r\theta(I,J,K) = \tau r\theta(I,J,K) + \Delta t\,\mu\left[\frac{\dot{U}(I,J,K)-\dot{U}(I,J-1,K)}{r\,\Delta\theta}\right.$$
$$\left. - \frac{\dot{V}(I,J,K)+\dot{V}(I+1,J,K)}{2r} + \frac{\dot{V}(I,J,K)-\dot{V}(I-1,J,K)}{\Delta r}\right] \tag{A.27}$$

$$\tau rz(I,J,K) = \tau rz(I,J,K) + \Delta t\,\mu\left[\frac{\dot{U}(I,J,K)-\dot{U}(I,J,K-1)}{\Delta z}\right.$$
$$\left. + \frac{\dot{W}(I,J,K)-\dot{W}(I-1,J,K)}{\Delta r}\right] \tag{A.28}$$

$$\tau z\theta(I,J,K) = \tau z\theta(I,J,K) + \Delta t\,\mu\left[\frac{\dot{V}(I,J,K)-\dot{V}(I,J,K-1)}{\Delta z}\right.$$
$$\left. + \frac{\dot{W}(I,J,K)-\dot{W}(I,J-1,K)}{r\,\Delta\theta}\right] \tag{A.29}$$

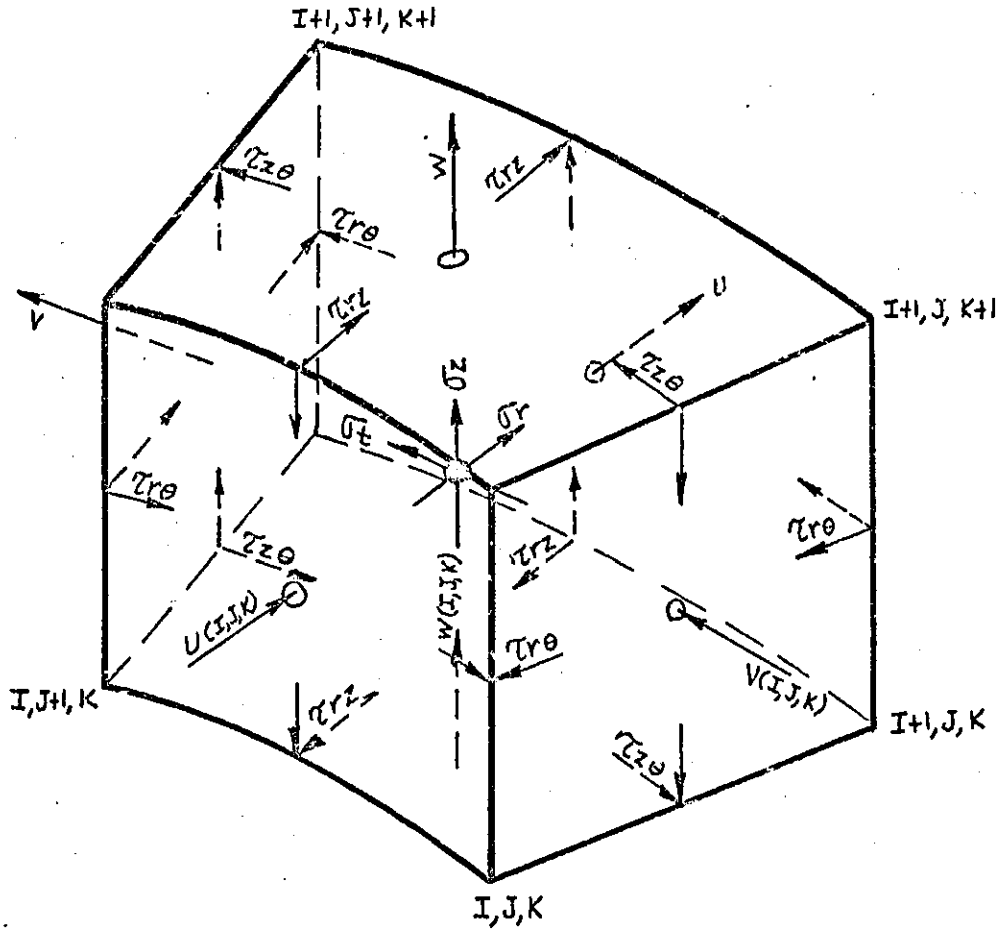

FIGURE A.1

Specification of Stress and Displacement on a Typical Element

APPENDIX B

DERIVATION OF FINITE DIFFERENCE EQUATIONS FOR THE CASE OF PLANE STRESS USING POLAR COORDINATES

The equilibrium equations in polar for for the case of plane stress are:

$$\frac{\partial \sigma r}{\partial r} + \frac{1}{r}\frac{\partial \tau r\theta}{\partial \theta} + \frac{\sigma r - \sigma \theta}{r} = 0 \qquad (B.1)$$

$$\frac{1}{r}\frac{\partial \sigma \theta}{\partial \theta} + \frac{\partial \tau r\theta}{\partial r} + 2\frac{\tau r\theta}{r} = 0 \qquad (B.2)$$

The stress-strain relationships are:

$$\epsilon r = \frac{\partial u}{\partial r}, \quad \epsilon \theta = \frac{1}{r}\frac{\partial v}{\partial \theta} + \frac{u}{r} \qquad (B.3)$$

$$\gamma r\theta = \frac{1}{r}\frac{\partial u}{\partial \theta} + \frac{\partial v}{\partial r} - \frac{v}{r} \qquad (B.4)$$

$$\sigma r = \frac{E}{(1-\nu^2)}\left[\frac{\partial u}{\partial r} + \nu\frac{u}{r} + \nu\frac{1}{r}\frac{\partial v}{\partial \theta}\right] \qquad (B.5)$$

$$\sigma \theta = \frac{E}{(1-\nu^2)}\left[\frac{1}{r}\frac{\partial v}{\partial \theta} + \frac{u}{r} + \nu\frac{\partial u}{\partial r}\right] \qquad (B.6)$$

$$\tau r\theta = \frac{E}{2(1+\nu)}\left[\frac{1}{r}\frac{\partial u}{\partial \theta} + \frac{\partial v}{\partial r} - \frac{v}{r}\right] \qquad (B.7)$$

Using the same procedure as in Appendix A, the finite difference equations for the velocities are:

$$\dot{U}(I,J) = \dot{U}(I,J)\left(\frac{1-K/2}{1+K/2}\right) + \frac{\Delta t}{\rho(1+K/2)}\left[\frac{\sigma r(I,J) - \sigma r(I-1,J)}{\Delta r}\right.$$

$$\left. + \frac{\tau r\theta(I,J+1) - \tau r\theta(I,J)}{r\Delta\theta} + \frac{\sigma r(I,J) + \sigma r(I-1,J) - \left(\sigma\theta(I,J) + \sigma\theta(I-1,J)\right)}{2r}\right] \quad (B.8)$$

$$\dot{V}(I,J) = \dot{V}(I,J)\left(\frac{1-K/2}{1+K/2}\right) + \frac{\Delta t}{\rho(1+K/2)}\left[\frac{\sigma\theta(I,J) - \sigma\theta(I,J-1)}{r\Delta\theta}\right.$$

$$\left. + \frac{\tau r\theta(I+1,J) - \tau r\theta(I,J)}{\Delta r} + \frac{\tau r\theta(I+1,J) + \tau r\theta(I,J)}{r}\right] \quad (B.9)$$

Similarily, the finite difference equations for the stresses are:

$$\sigma r(I,J) = \sigma r(I,J) + \frac{\Delta t E}{1-\nu^2}\left[\frac{\dot{U}(I+1,J) - \dot{U}(I,J)}{\Delta r}\right.$$

$$\left. + \nu\,\frac{\dot{U}(I+1,J) + \dot{U}(I,J)}{2r} + \nu\,\frac{\dot{V}(I,J+1) - \dot{V}(I,J)}{r\Delta\theta}\right] \quad (B.10)$$

$$\sigma\theta(I,J) = \sigma\theta(I,J) + \frac{\Delta t E}{1-\nu^2}\left[\frac{\dot{U}(I+1,J) + \dot{U}(I,J)}{2r}\right.$$

$$\left. + \nu\,\frac{\dot{U}(I+1,J) - \dot{U}(I,J)}{\Delta r} + \frac{\dot{V}(I,J+1) - \dot{V}(I,J)}{r\Delta\theta}\right] \quad (B.11)$$

$$\tau r\theta(I,J) = \tau r\theta(I,J) + \frac{\Delta t E}{2(1+\nu)}\left[\frac{\dot{U}(I,J) - \dot{U}(I,J-1)}{r\Delta\theta}\right.$$

$$\left. + \frac{\dot{V}(I,J) - \dot{V}(I-1,J)}{\Delta r} - \frac{\dot{V}(I,J) + \dot{V}(I-1,J)}{2r}\right] \quad (B.12)$$

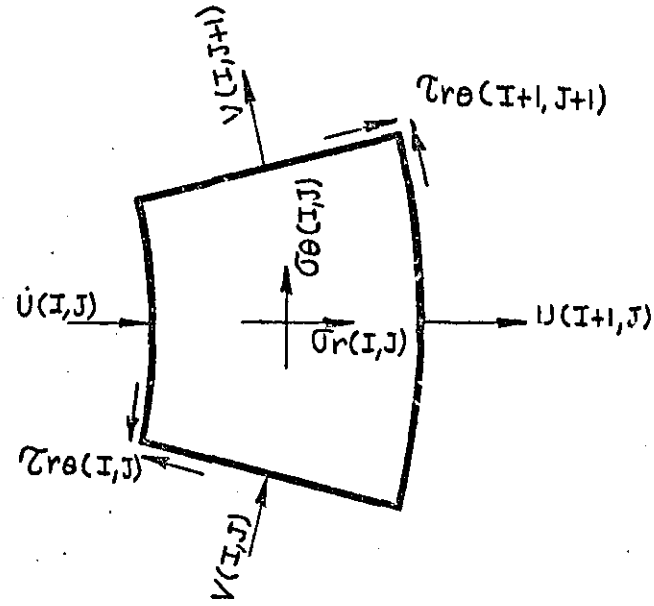

APPENDIX C

DERIVATION OF FINITE DIFFERENCE EQUATIONS FOR THE CASE OF AXIALLY SYMMETRICAL STRESS DISTRIBUTION

The equilibrium equations for axially symmetrical stress distribution are:

$$\frac{\partial \sigma r}{\partial r} + \frac{\partial \tau rz}{\partial z} + \frac{\sigma r - \sigma e}{r} = 0 \qquad (C.1)$$

$$\frac{\partial \tau rz}{\partial r} + \frac{\partial \sigma z}{\partial z} + \frac{\tau rz}{r} = 0 \qquad (C.2)$$

The stress-strain relationships are:

$$\epsilon r = \frac{\partial u}{\partial r}, \quad \epsilon \theta = \frac{u}{r}, \quad \epsilon z = \frac{\partial w}{\partial z} \qquad (C.3)$$

$$\gamma rz = \frac{\partial u}{\partial z} + \frac{\partial w}{\partial r}, \quad \gamma r\theta = \gamma z\theta = 0 \qquad (C.4)$$

$$\sigma r = (\lambda + 2\mu)\frac{\partial u}{\partial r} + \lambda \frac{u}{r} + \lambda \frac{\partial w}{\partial z} \qquad (C.5)$$

$$\sigma \theta = (\lambda + 2\mu)\frac{u}{r} + \lambda \frac{\partial u}{\partial r} + \lambda \frac{\partial w}{\partial z} \qquad (C.6)$$

$$\sigma z = (\lambda + 2\mu)\frac{\partial w}{\partial z} + \lambda \frac{u}{r} + \lambda \frac{\partial u}{\partial r} \qquad (C.7)$$

$$\tau rz = \mu \left[\frac{\partial u}{\partial z} + \frac{\partial w}{\partial r}\right] \qquad (C.8)$$

Using the same procedure as in Appendix A, the finite difference equations for velocity are:

$$\dot{U}(I,K) = \dot{U}(I,K)\left(\frac{1-K/2}{1+K/2}\right) + \frac{\Delta t}{\rho(1+K/2)}\left[\frac{\sigma r(I,K) - \sigma r(I-1,K)}{\Delta r} + \frac{\tau rz(I,K+1) - \tau rz(I,K)}{\Delta z} + \frac{\sigma r(I,K) + \sigma r(I-1,K)}{2r} - \frac{\sigma\theta(I,K) + \sigma\theta(I-1,K)}{2r}\right] \qquad (C.9)$$

$$\dot{W}(I,K) = \dot{W}(I,K)\left(\frac{1-K/2}{1+K/2}\right) + \frac{\Delta t}{\rho(1+K/2)}\left[\frac{\tau rz(I+1,K) - \tau rz(I,K)}{\Delta r} + \frac{\sigma z(I,K) - \sigma z(I,K-1)}{\Delta z} + \frac{\tau rz(I+1,K) + \tau rz(I,K)}{2r}\right] \qquad (C.10)$$

The finite difference equations for the stresses are:

$$\sigma r(I,K) = \sigma r(I,K) + \Delta t\left[(\lambda+2\mu)\frac{\dot{U}(I+1,K) - \dot{U}(I,K)}{\Delta r} + \lambda\frac{\dot{U}(I+1,K) + \dot{U}(I,K)}{2r} + \lambda\frac{\dot{W}(I,K+1) - \dot{W}(I,K)}{\Delta z}\right] \qquad (C.11)$$

$$\sigma\theta(I,K) = \sigma\theta(I,K) + \Delta t\left[(\lambda+2\mu)\frac{\dot{U}(I+1,K) + \dot{U}(I,K)}{2r} + \lambda\frac{\dot{U}(I+1,K) - \dot{U}(I,K)}{\Delta r} + \lambda\frac{\dot{W}(I,K+1) - \dot{W}(I,K)}{\Delta z}\right] \qquad (C.12)$$

$$\sigma z(I,K) = \sigma z(I,K) + \Delta t\left[(\lambda+2\mu)\frac{\dot{W}(I,K+1) - \dot{W}(I,K)}{\Delta z} + \lambda\frac{\dot{U}(I+1,K) + \dot{U}(I,K)}{2r} + \lambda\frac{\dot{U}(I+1,K) - \dot{U}(I,K)}{\Delta r}\right] \qquad (C.13)$$

$$\tau rz(I,K) = \tau rz(I,K) + \mu\,\Delta t\left[\frac{\dot{U}(I,K) - \dot{U}(I,K-1)}{\Delta z} + \frac{\dot{W}(I,K) - \dot{W}(I-1,K)}{\Delta r}\right] \qquad (C.14)$$

APPENDIX D

DERIVATION OF FINITE DIFFERENCE EQUATIONS FOR HEAT CONDUCTION USING CYLINDRICAL COORDINATES

For steady state heat conduction in a solid medium with uniform heat conductivity, the thermal equilibrium equation is:

$$\frac{\partial^2 T}{\partial r^2} + \frac{1}{r}\frac{\partial T}{\partial r} + \frac{1}{r^2}\frac{\partial^2 T}{\partial \theta^2} + \frac{\partial^2 T}{\partial z^2} = 0 \qquad (D.1)$$

Equation (D.1) written as a damped wave equation is:

$$\frac{\partial^2 T}{\partial r^2} + \frac{1}{r}\frac{\partial T}{\partial r} + \frac{1}{r^2}\frac{\partial^2 T}{\partial \theta^2} + \frac{\partial^2 T}{\partial z^2} = \frac{\partial^2 T}{\partial t^2} + K\frac{\partial T}{\partial t} \qquad (D.2)$$

Equation (D.2) can be reduced to four first order partial differential equations in the following manner. Multiplying both sides of Eq. (D.2) by "r" gives:

$$r\frac{\partial^2 T}{\partial r^2} + \frac{\partial T}{\partial r} + \frac{1}{r}\frac{\partial^2 T}{\partial \theta^2} + r\frac{\partial^2 T}{\partial z^2} = r\frac{\partial^2 T}{\partial t^2} + rK\frac{\partial T}{\partial t}$$

or

$$\frac{\partial}{\partial r}\left(r\frac{\partial T}{\partial r}\right) + \frac{1}{r}\frac{\partial}{\partial \theta}\left(\frac{\partial T}{\partial \theta}\right) + r\frac{\partial}{\partial z}\left(\frac{\partial T}{\partial z}\right) = r\frac{\partial^2 T}{\partial t^2} + rK\frac{\partial T}{\partial t} \qquad (D.3)$$

Auxilliary variables u,v, and w are introduced thusly:

$$\text{let} \quad r\frac{\partial T}{\partial t} = \frac{\partial U}{\partial r} + \frac{\partial V}{\partial \theta} + \frac{\partial W}{\partial z} \qquad (D.4)$$

$$\text{let} \quad \frac{\partial U}{\partial t} + KU = r\frac{\partial T}{\partial r} \tag{D.5}$$

$$\text{let} \quad \frac{\partial V}{\partial t} + KV = \frac{1}{r}\frac{\partial T}{\partial \theta} \tag{D.6}$$

$$\text{let} \quad \frac{\partial W}{\partial t} + KW = r\frac{\partial T}{\partial Z} \tag{D.7}$$

Checking these equations, differentiate Eq'ns (D.4), (D.5), (D.6), and (D.7) with respect to t,r,θ, and z, respectively thus:

$$r\frac{\partial^2 T}{\partial t^2} = \frac{\partial U}{\partial r \partial t} + \frac{\partial^2 V}{\partial \theta \partial t} + \frac{\partial^2 W}{\partial z \partial t} \tag{D.8}$$

$$\frac{\partial^2 U}{\partial t \partial r} + K\frac{\partial U}{\partial r} = r\frac{\partial^2 T}{\partial r^2} + \frac{\partial T}{\partial r} \tag{D.9}$$

$$\frac{\partial^2 V}{\partial t \partial \theta} + K\frac{\partial V}{\partial \theta} = \frac{1}{r}\frac{\partial^2 T}{\partial \theta^2} \tag{D.10}$$

$$\frac{\partial^2 W}{\partial t \partial z} + K\frac{\partial W}{\partial z} = r\frac{\partial^2 T}{\partial z^2} \tag{D.11}$$

Multiplying Eq. (D.4) by "k" and adding Eq. (D.8) gives:

$$r\frac{\partial^2 T}{\partial t^2} + K\frac{\partial T}{\partial t} = \frac{\partial^2 U}{\partial r \partial t} + \frac{\partial^2 V}{\partial \theta \partial t} + \frac{\partial^2 W}{\partial z \partial t} + K\left[\frac{\partial U}{\partial r} + \frac{\partial V}{\partial \theta} + \frac{\partial W}{\partial z}\right] \tag{D.12}$$

Adding Eq'ns (D.9), (D.10), and (D.11) gives:

$$\frac{\partial^2 U}{\partial t \partial r} + \frac{\partial^2 V}{\partial t \partial \theta} + \frac{\partial^2 W}{\partial t \partial z} + K\left[\frac{\partial U}{\partial r} + \frac{\partial V}{\partial \theta} + \frac{\partial W}{\partial z}\right] = r\frac{\partial^2 T}{\partial r^2} + \frac{\partial T}{\partial r} + \frac{1}{r}\frac{\partial^2 T}{\partial \theta^2} + r\frac{\partial^2 T}{\partial Z^2} \tag{D.13}$$

Subtracting Eq. (D.13) from (D.12) results in obtaining the original damped wave equation. Equations (D.4) through (D.7) represent the heat conduction equation in separated form. These equations can be written directly in finite difference form thus:

$$T(I,J,K) = T(I,J,K) + \Delta t\left[\frac{U(I+1,J,K) - U(I,J,K)}{r\Delta r}\right.$$

$$\left. + \frac{V(I,J+1,K) - V(I,J,K)}{r\Delta\theta} + \frac{W(I,J,K+1) - W(I,J,K)}{r\Delta z}\right] \tag{D.14}$$

$$U(I,J,K) = U(I,J,K)\frac{1-K/2}{1+K/2} + \frac{\Delta t\, r}{1+K/2}\left[\frac{T(I,J,K) - T(I-1,J,K)}{\Delta r}\right] \tag{D.15}$$

$$V(I,J,K) = V(I,J,K)\frac{1-K/2}{1+K/2} + \frac{\Delta t}{1+K/2}\left[\frac{T(I,J,K) - T(I,J-1,K)}{r\Delta\theta}\right] \tag{D.16}$$

$$W(I,J,K) = W(I,J,K)\frac{1-K/2}{1+K/2} + \frac{\Delta t\, r}{1+K/2}\left[\frac{T(I,J,K) - T(I,J,K-1)}{\Delta z}\right] \tag{D.17}$$

APPENDIX E

THERMAL STRESS-STRAIN RELATIONSHIPS

The strain which results from a uniform temperature change in a body is:

$$\epsilon = \alpha T \tag{E.1}$$

where "T" is the temperature change. This strain must be added to the strain which is caused by the stress distribution in the body thus the stress-strain equations are:

$$\epsilon_x = \frac{1}{E}\left[\sigma_x - \nu\sigma_y - \nu\sigma_z\right] + \alpha T \tag{E.2}$$

$$\epsilon_y = \frac{1}{E}\left[\sigma_y - \nu\sigma_x - \nu\sigma_z\right] + \alpha T \tag{E.3}$$

$$\epsilon_z = \frac{1}{E}\left[\sigma_z - \nu\sigma_x - \nu\sigma_y\right] + \alpha T \tag{E.4}$$

The shear strains are not affected by temperature change since expansion of a small element due to temperature change will not cause angular distortion in an isotropic material.

For dynamic relaxation, thermal stresses are accounted for in the initial conditions by assuming that every element in the body is perfectly constrained hence the strain in every element is zero at time zero. Substituting zero into the L.H.S. of Eq'ns (E.2), (E.3), and (E.4) the stress strain equations become:

$$\sigma_x - \nu(\sigma_y + \sigma_z) = -E\alpha T \tag{E.5}$$

$$\sigma_y - \nu(\sigma_x + \sigma_z) = -E\alpha T \qquad (E.6)$$

$$\sigma_z - \nu(\sigma_y + \sigma_x) = -E\alpha T \qquad (E.7)$$

Solving simultaneously:

$$\sigma_x = -\frac{E\alpha T}{1-2\nu} \qquad (E.8)$$

$$\sigma_y = -\frac{E\alpha T}{1-2\nu} \qquad (E.9)$$

$$\sigma_z = -\frac{E\alpha T}{(1-2\nu)} \qquad (E.10)$$

The stresses given by the above equations define the stress in each element at time zero for an element temperature of "T" degrees above the lowest temperature in the body, for the case of heating, or below the highest temperature for cooling.

For the case of plane stress, the initial stress condition is:

$$\sigma_x = -\frac{E\alpha T}{(1-\nu)} \qquad (E.11)$$

$$\sigma_y = -\frac{E\alpha T}{(1-\nu)} \qquad (E.12)$$

APPENDIX F

EXTRAPOLATION FORMULAE FOR CALCULATING STRESS ON A BOUNDARY WHEN ENTERING AND LEAVING THE BODY IN THE DIRECTION OF ADVANCING SUBSCRIPTS

Newtons divided difference formula is:

$$f(x) = f(x_0) + (x-x_0)\, f(x_0,x_1) + (x-x_0)(x-x_1)\, f(x_0,x_1,x_2)$$
$$+ (x-x_0)(x-x_1)(x-x_2)\, f(x_0,x_1,x_2,x_3)$$
$$+ (x-x_0)(x-x_1)\cdots(x-x_n)\, f(x,x_0,x_1,\cdots x_n) \qquad (F.1)$$

Assuming that f(x) is a polynomial of degree n-1, the last term in the above expression vanishes. Also assuming that $x = h$ = constant, which is the case for a constant mesh width, Eq. (F.1) becomes:

$$f(x) = f_0 + (x-x_0)\frac{\Delta f_0}{h} + (x-x_0)(x-x_0-h)\frac{\Delta^2 f_0}{2!\,h^2}$$
$$+ (x-x_0)(x-x_0-h)(x-x_0-2h)\frac{\Delta^3 f_0}{3!\,h^3} + \cdots \qquad (F.2)$$

If $x = x_0 + rh$, then Eq. (F.2) becomes the "forward Gregory-Newton" interpolation formula thus:

$$f(x) = f_0 + r\frac{\Delta f_0}{1} + r(r-1)\frac{\Delta^2 f_0}{2!} + r(r-1)(r-2)\frac{\Delta^3 f_0}{3!}$$
$$+ r(r-1)(r-2)(r-3)\frac{\Delta^4 f_0}{4!} + \cdots \qquad (F.3)$$

Entering the body in a direction of advancing subscripts, the stress at the first node point is (I). If the boundary coincides with a velocity node, then "r" is -0.5 and Eq. (F.3) becomes:

$$\sigma_b = \sigma(I) - .5\left[\sigma(I+1)-\sigma(I)\right] + \frac{.75}{2}\left[\sigma(I+2)-2\sigma(I+1)+\sigma(I)\right]$$

$$- \frac{1.875}{6}\left[\sigma(I+3)-3\sigma(I+2)+3\sigma(I+1)-\sigma(I)\right] + \cdots \qquad (F.4)$$

For leaving the object in the direction of advancing subscripts, the "backward Newton-Gregory interpolation formula" is used and is:

$$f(x) = f_0 + r\Delta f_{-1} + r(r+1)\frac{\Delta^2 f_{-2}}{2!} + r(r+1)(r+2)\frac{\Delta^3 f_{-3}}{3!}$$

$$+ r(r+1)(r+2)(r+3)\frac{\Delta^4 f_{-4}}{4!} \qquad (F.5)$$

The stress at the first mesh point inside the boundary is $\sigma(I-1)$ and r is +.5. Eqn. (F.5) becomes:

$$\sigma_b = \sigma(I-1) + .5\left[\sigma(I-1)-\sigma(I-2)\right] + \frac{.75}{2}\left[\sigma(I-1)-2\sigma(I-2)+\sigma(I-3)\right]$$

$$+ \frac{1.875}{6}\left[\sigma(I-1)-3\sigma(I-2)+3\sigma(I-3)-\sigma(I-4)\right] + \cdots \qquad (F.6)$$

		Δy	$\Delta^2 y$	$\Delta^3 y$	$\Delta^4 y$	$\Delta^5 y$
x_1	y_1					
		$\frac{y_2 - y_1}{h}$				
x_2	y_2		$\frac{y_3 - 2y_2 + y_1}{2! h^2}$			
		$\frac{y_3 - y_2}{h}$		$\frac{y_4 - 3y_3 + 3y_2 - y_1}{3! h^3}$		
x_3	y_3		$\frac{y_4 - 2y_3 + y_2}{2! h^2}$		$\frac{y_5 - 4y_4 + 6y_3 - 4y_2 + y_1}{4! h^4}$	
		$\frac{y_4 - y_3}{h}$		$\frac{y_5 - 3y_4 + 3y_3 - y_2}{3! h^3}$		$\frac{y_6 - 5y_5 + 10y_4 - 10y_3 + 5y_2 - y_1}{5! h^5}$
x_4	y_4		$\frac{y_5 - 2y_4 + y_3}{2! h^2}$		$\frac{y_6 - 4y_5 + 6y_4 - 4y_3 + y_2}{4! h^4}$	
		$\frac{y_5 - y_4}{h}$		$\frac{y_6 - 3y_5 + 3y_4 - y_3}{3! h^3}$		
x_5	y_5		$\frac{y_6 - 2y_5 + y_4}{2! h^2}$			
		$\frac{y_6 - y_5}{h}$				
x_6	y_6					

Iter'n Number	$\sum \dot{U}^2$	Stress - lb./in.^{2}								
		Node Position								
		1	2	3	4	5	6	7	8	9
1	$.3\times10^{2}$	000	000	000	000	000	000	000	000	773
2	$.2\times10^{2}$	000	000	000	000	000	000	000	597	246
3	$.2\times10^{2}$	000	000	000	000	000	000	461	245	574
4	$.1\times10^{2}$	000	000	000	000	000	357	231	443	414
5	$.1\times10^{2}$	000	000	000	000	275	211	345	383	467
6	$.1\times10^{2}$	000	000	000	213	188	272	343	381	487
7	$.8\times10^{1}$	000	000	164	165	216	301	316	432	438
8	$.8\times10^{1}$	000	127	142	174	260	266	377	379	499
9	$.7\times10^{1}$	98	122	141	222	225	325	332	436	447
10	$.6\times10^{1}$	179	115	188	193	277	291	378	400	487
11	$.5\times10^{1}$	181	216	165	236	255	326	358	428	465
15	$.3\times10^{1}$	267	267	293	295	339	355	387	425	481
20	$.1\times10^{1}$	337	342	353	366	387	408	436	461	482
25	$.6\times10^{0}$	391	395	401	409	422	437	453	473	489
30	$.3\times10^{0}$	426	428	433	440	447	458	468	481	493
35	$.1\times10^{0}$	450	452	455	459	465	471	479	487	496
40	$.6\times10^{-1}$	466	467	469	472	476	481	486	491	497
50	$.1\times10^{-1}$	485	485	486	487	489	491	493	469	499
60	$.2\times10^{-2}$	493	493	494	494	495	496	497	498	499
70	$.5\times10^{-3}$	497	497	497	497	498	498	499	499	500
80	$.1\times10^{-3}$	499	499	499	499	499	499	499	500	500
90	$.2\times10^{-4}$	499	499	499	499	500	500	500	500	500
100	$.5\times10^{-5}$	500	500	500	500	500	500	500	500	500

TABLE 1.1

Stress v.s. Number of

Iterations for k = 0.44

Iter'n Number	$\sum \dot{u}^2$	Stress - lb./in.^{2}								
		Node Position								
		1	2	3	4	5	6	7	8	9
1	$.3\times10^{2}$	000	000	000	000	000	000	000	000	821
2	$.2\times10^{2}$	000	000	000	000	000	000	000	674	226
3	$.3\times10^{2}$	000	000	000	000	000	000	554	251	604
4	$.2\times10^{2}$	000	000	000	000	000	455	260	476	423
5	$.2\times10^{2}$	000	000	000	000	373	258	380	421	460
6	$.2\times10^{2}$	000	000	000	306	248	308	402	379	521
7	$.2\times10^{2}$	000	000	252	233	252	373	321	484	415
8	$.2\times10^{2}$	000	207	216	210	339	280	437	371	533
9	$.1\times10^{2}$	170	197	177	304	248	389	340	475	434
10	$.1\times10^{2}$	318	151	269	224	342	314	419	407	503
11	$.1\times10^{2}$	290	350	203	299	291	368	381	446	470
15	$.5\times10^{1}$	378	362	410	362	444	406	420	428	496
20	$.1\times10^{1}$	440	437	453	446	475	470	503	490	483
25	$.2\times10^{0}$	486	488	487	476	485	487	487	497	495
30	$.3\times10^{-1}$	495	492	499	500	497	500	496	501	497
35	$.2\times10^{-2}$	500	501	500	501	501	501	499	503	500
40	$.1\times10^{-3}$	502	502	501	501	500	500	500	501	499
50	$.6\times10^{-4}$	501	501	501	500	500	500	500	500	500
60	$.6\times10^{-5}$	500	500	500	500	500	500	500	500	500
70	$.2\times10^{-6}$	500	500	500	500	500	500	500	500	500
80	$.1\times10^{-8}$	500	500	500	500	500	500	500	500	500
90	$.3\times10^{-9}$	500	500	500	500	500	500	500	500	500
100	$.4\times10^{-10}$	500	500	500	500	500	500	500	500	500

TABLE 1.2

Stress v.s. Number of

Iterations for k = 0.3

Iter'n Number	$\sum \dot{U}^2$	Stress - lb./in.^{2} Node Position								
		1	2	3	4	5	6	7	8	9
1	$.4x10^{2}$	000	000	000	000	000	000	000	000	858
2	$.3x10^{2}$	000	000	000	000	000	000	000	737	209
3	$.4x10^{2}$	000	000	000	000	000	000	633	254	631
4	$.3x10^{2}$	000	000	000	000	000	543	282	507	428
5	$.3x10^{2}$	000	000	000	000	466	297	413	453	454
6	$.3x10^{2}$	000	000	000	400	302	340	455	375	554
7	$.3x10^{2}$	000	000	343	300	285	442	322	533	389
8	$.3x10^{2}$	000	295	292	242	418	287	497	358	568
9	$.2x10^{2}$	253	281	210	389	264	453	341	514	417
10	$.2x10^{2}$	484	184	357	248	408	330	459	410	519
11	$.2x10^{2}$	416	511	236	363	322	406	403	460	476
15	$.8x10^{1}$	499	457	548	425	584	465	458	424	516
20	$.8x10^{0}$	543	528	563	521	583	528	594	513	472
25	$.2x10^{0}$	579	575	566	510	536	521	510	514	498
30	$.3x10^{0}$	528	511	539	541	528	531	511	517	497
35	$.2x10^{0}$	510	514	507	510	506	505	494	513	497
40	$.4x10^{-1}$	498	494	499	490	498	496	505	497	500
50	$.2x10^{-2}$	496	496	496	496	494	496	497	498	500
60	$.1x10^{-2}$	499	500	500	500	500	499	500	499	501
70	$.1x10^{-4}$	500	501	500	500	500	501	501	500	500
80	$.2x10^{-4}$	500	500	500	500	500	500	500	500	500
90	$.4x10^{-6}$	500	500	500	500	500	500	500	500	500
100	$.3x10^{-6}$	500	500	500	500	500	500	500	500	500

TABLE 1.3

Stress v.s. Iteration

Number for k = 0.2

Stress - lb./in.^{2}										
Iter'n Number	Node Position									
		1	2	3	4	5	6	7	8	9
1	$.3x10^2$	000	000	000	000	000	000	000	000	804
2	$.2x10^2$	000	000	000	000	000	000	000	646	234
3	$.2x10^2$	000	000	000	000	000	000	520	249	593
4	$.2x10^2$	000	000	000	000	000	418	250	464	420
5	$.2x10^2$	000	000	000	000	336	241	367	407	462
6	$.1x10^2$	000	000	000	270	225	294	380	380	508
7	$.1x10^2$	000	000	217	207	239	345	320	464	424
8	$.1x10^2$	000	175	187	197	308	275	414	375	519
9	$.1x10^2$	140	167	164	271	241	364	337	460	440
10	$.1x10^2$	260	137	236	213	317	305	403	405	497
11	$.1x10^2$	246	295	189	274	278	352	372	439	468
15	$.4x10^1$	334	325	362	337	400	386	407	428	489
20	$.1x10^1$	400	401	414	416	439	446	474	479	484
25	$.4x10^0$	450	453	455	453	462	469	475	488	493
30	$.1x10^0$	472	472	476	479	480	485	487	494	496
35	$.3x10^{-1}$	485	486	487	488	490	492	493	497	499
40	$.9x10^{-2}$	493	493	493	494	494	495	497	498	499
50	$.7x10^{-3}$	498	498	498	498	499	499	499	499	500
60	$.5x10^{-4}$	499	499	499	500	500	500	500	500	500
70	$.4x10^{-5}$	500	500	500	500	500	500	500	500	500
80	$.3x10^{-6}$	500	500	500	500	500	500	500	500	500
90	$.2x10^{-7}$	500	500	500	500	500	500	500	500	500
100	$.1x10^{-8}$	500	500	500	500	500	500	500	500	500

TABLE 1.4

Stress v.s. Iteration Number

k = 0.349

Axial Displacement - in.x10^6										
Iter'n	Node Position									
Number	1	2	3	4	5	6	7	8	9	10
1	0.0	0.0	0.0	0.0	0.0	0.0	0.0	0.0	0.0	14.
2	0.0	0.0	0.0	0.0	0.0	0.0	0.0	0.0	11.	15.
3	0.0	0.0	0.0	0.0	0.0	0.0	0.0	9.2	13.	23.
4	0.0	0.0	0.0	0.0	0.0	0.0	7.6	12.	20.	27.
5	0.0	0.0	0.0	0.0	0.0	6.2	11.	17.	24.	32.
6	0.0	0.0	0.0	0.0	5.1	9.2	14.	21.	27.	36.
7	0.0	0.0	0.0	4.2	8.1	12.	19.	24.	32.	39.
8	0.0	0.0	3.4	7.0	11.	16.	21.	28.	34.	43.
9	0.0	2.8	6.1	9.1	14.	18.	25.	30.	38.	46.
10	0.0	5.3	7.8	12.	16.	22.	27.	34.	41.	49.
11	0.0	4.8	11.	14.	19.	24.	30	36.	44.	52.
15	0.0	6.3	12.	19.	25.	33.	39.	46.	54.	62.
20	0.0	7.3	15.	22.	30.	38.	45.	54.	62.	70.
25	0.0	8.1	16.	24.	32.	40.	48.	57.	65.	73.
30	0.0	8.3	16.	25.	33.	41.	50.	58.	66.	75.
35	0.0	8.3	17.	25.	33.	42.	50.	58.	67.	75.
40	0.0	8.4	17.	25.	33.	42.	50.	58.	67.	75.
50	0.0	8.3	17.	25.	33.	42.	50	58.	67.	75.
60	0.0	8.3	17.	25.	33.	42.	50.	58.	67.	75.
70	0.0	8.3	17.	25.	33.	42.	50.	58.	67.	75.
80	0.0	8.3	17.	25.	33.	42.	50.	58.	67.	75.
90	0.0	8.3	17.	25.	33.	42.	50.	58.	67.	75.
100	0.0	8.3	17.	25.	33.	42.	50.	58.	67.	75.

TABLE 1.5

Displacement v.s. Iteration Number $k = 0.3$

Temperature - ^{o}F									
Iter'n	Node Position								
Number	1	2	3	4	5	6	7	8	9
1	000	000	000	000	000	000	000	000	862
2	000	000	000	000	000	000	000	743	119
3	000	000	000	000	000	000	641	103	776
4	000	000	000	000	000	552	88	683	195
5	000	000	000	000	476	76	601	170	721
6	000	000	000	410	66	529	149	645	246
7	000	000	354	57	465	130	576	217	684
8	000	305	49	409	113	515	191	619	281
9	263	42	359	98	459	168	560	250	658
10	263	315	86	410	148	506	222	602	307
11	308	270	365	130	457	198	550	275	640
15	378	351	420	340	474	347	537	308	616
21	452	434	480	427	518	433	520	443	541
25	488	474	487	465	500	463	513	467	524
30	491	495	488	500	491	505	488	509	488
35	499	497	501	496	502	496	503	496	502
40	500	500	500	500	499	501	499	501	499
50	500	500	500	500	500	500	500	500	500
60	500	500	500	500	500	500	500	500	500
80	500	500	500	500	500	500	500	500	500
100	500	500	500	500	500	500	500	500	500

TABLE 1.6

Temperature v.s. Iteration Number k = 0.32

Radial Stress - lb./in.^{2}															
Radius / Angle	.219	.281	.344	.406	.469	.531	.594	.656	.719	.781	.844	.906	.969	1.03	1.09
2.5	-26	186	389	535	638	711	764	805	835	859	879	894	907	917	926
7.5	-22	188	388	531	631	703	755	794	824	848	866	882	894	904	913
12.5	-12	194	385	522	618	686	736	773	802	824	842	857	868	878	886
17.5	2	202	382	510	599	662	709	743	770	790	807	820	831	840	848
22.5	20	212	378	494	574	632	673	704	728	747	762	774	783	791	798
27.5	41	225	373	475	545	595	631	659	679	695	708	718	726	733	739
32.5	65	239	367	454	512	554	583	606	623	636	646	655	662	668	672
37.5	91	254	361	430	477	509	532	549	562	572	580	587	592	596	600
42.5	119	270	355	406	439	462	478	489	498	505	511	515	519	521	524
47.5	147	286	348	381	401	414	423	429	434	437	440	442	444	446	447
52.5	174	302	341	357	363	367	368	369	370	370	371	371	371	371	371
57.5	200	317	335	333	328	322	317	313	309	306	304	302	301	299	298
62.5	224	331	330	312	295	280	269	260	253	248	243	239	236	234	231
67.5	246	343	325	293	266	244	227	214	204	196	189	184	179	176	172
72.5	263	354	320	277	241	213	192	175	162	152	144	137	131	127	123
77.5	277	362	317	265	222	189	164	145	130	118	108	101	94	89	84
82.5	287	367	315	256	209	173	145	124	108	95	84	76	69	63	58
87.5	292	370	314	252	202	165	136	114	97	83	72	63	56	50	44

TABLE 3.1

Analytical Solution

Stress distribution in a flat plate

having a small circular hole at the centre

Tangential Stress - lb./in.^{2}															
Radius / Angle	.219	.281	.344	.406	.469	.531	.594	.656	.719	.781	.844	.906	.969	1.03	1.06
2.5	-437	-71	18	41	44	41	37	33	29	26	23	21	19	17	15
7.5	-398	-47	38	58	60	57	52	48	44	41	38	36	34	32	30
12.5	-320	1	75	92	92	88	83	79	75	71	68	66	64	62	60
17.5	-205	70	130	141	139	134	128	123	119	115	112	110	107	106	104
22.5	-59	159	201	205	199	192	186	180	176	172	169	166	164	162	160
27.5	116	265	286	281	271	262	255	248	243	239	236	233	231	229	227
32.5	314	386	381	366	352	341	332	325	320	315	312	309	307	305	303
37.5	528	516	485	459	441	427	417	409	403	398	394	391	389	387	385
42.5	753	653	594	557	533	517	505	496	490	485	481	478	475	473	471
47.5	981	792	704	656	627	608	595	585	578	573	569	565	562	560	558
52.5	1206	928	813	754	719	698	683	673	665	659	655	652	649	646	644
57.5	1421	1059	916	847	803	783	767	756	748	742	738	734	731	739	727
62.5	1619	1179	1012	932	889	862	845	833	825	818	814	810	807	804	802
67.5	1793	1285	1096	1008	961	932	914	901	892	886	881	877	874	871	869
72.5	1940	1375	1167	1072	1021	991	972	959	949	942	937	933	930	927	925
77.5	2054	1444	1222	1121	1068	1037	1017	1003	993	986	981	977	974	972	969
82.5	2132	1491	1260	1155	1100	1068	1047	1033	1024	1017	1011	1007	1004	1001	999
87.5	2172	1515	1279	1172	1116	1084	1063	1049	1039	1032	1026	1022	1019	1016	1014

TABLE 3.2

Analytical Solution
Stress distribution in a flat plate

having a small circular hole at the centre

Shear Stress - lb./in.^{2}																
Radius / Angle	.187	.250	.312	.375	.437	.500	.562	.625	.687	.750	.812	.875	.937	1.00	1.06	1.12
0.0	0	0	0	0	0	0	0	0	0	0	0	0	0	0	0	0
5.0	0	102	116	114	110	106	103	100	98	97	95	94	93	93	92	91
10.0	0	201	228	224	217	209	203	198	194	190	188	186	184	182	181	180
15.0	0	294	333	328	317	305	296	289	283	278	274	271	269	267	265	263
20.0	0	378	428	422	407	393	381	371	364	358	353	349	346	343	340	339
25.0	0	450	510	503	485	468	454	443	434	426	421	416	412	409	406	403
30.0	0	509	576	568	548	529	513	500	490	482	475	470	466	462	459	456
35.0	0	552	625	617	595	574	557	543	532	523	516	510	505	501	498	495
40.0	0	579	655	646	623	602	584	569	557	548	541	535	529	525	522	519
45.0	0	588	666	656	633	611	593	578	566	557	549	543	538	533	530	527
50.0	0	579	655	646	623	602	584	569	557	548	541	535	529	525	522	519
55.0	0	552	625	617	548	574	557	543	532	523	516	510	505	501	498	495
60.0	0	509	576	568	548	529	513	500	490	482	475	470	466	462	459	456
65.0	0	450	510	503	485	468	454	443	434	426	421	416	412	409	406	403
70.0	0	378	428	422	407	393	381	371	364	358	353	349	346	343	340	339
75.0	0	294	333	328	317	305	296	289	283	278	274	271	269	267	265	263
80.0	0	201	228	224	217	209	203	198	194	190	188	186	184	182	181	180
85.0	0	102	116	114	110	106	103	100	98	97	95	94	93	93	92	91
90.0	0	0	0	0	0	0	0	0	0	0	0	0	0	0	0	0

TABLE 3.3

Analytical Solution
Stress distribution in a flat plate
having a small circular hole at the centre

Radial Stress - lb./in.^{2}															
Radius / Angle	.219	.281	.344	.406	.469	.531	.594	.656	.719	.781	.844	.906	.969	1.03	1.09
2.5	-159	85	329	508	634	725	791	841	880	910	934	953	969	982	993
7.5	-150	91	331	505	628	716	781	830	858	897	920	939	955	968	978
12.5	-131	104	333	499	616	700	762	808	844	872	894	912	926	939	949
17.5	-103	123	337	491	599	677	733	776	809	835	855	871	885	896	906
22.5	-68	147	341	480	577	646	697	735	764	787	805	820	832	842	850
27.5	-25	176	347	467	550	610	653	686	711	730	746	758	768	777	784
32.5	23	208	353	452	521	569	604	630	650	666	678	688	696	703	709
37.5	75	244	360	436	488	524	550	570	585	596	605	613	619	624	628
42.5	129	281	367	420	454	478	494	507	516	523	529	533	537	540	543
47.5	184	318	374	403	420	430	437	442	446	449	451	453	454	455	456
52.5	239	355	381	386	386	379	381	379	377	376	374	373	372	372	371
57.5	291	391	388	371	353	339	328	319	312	306	301	298	294	292	290
62.5	339	423	395	356	323	298	278	263	251	242	234	228	223	218	215
67.5	381	452	400	343	297	262	235	214	198	185	175	166	159	153	148
72.5	417	476	405	332	275	231	198	173	153	137	125	114	106	99	93
77.5	444	495	408	324	258	207	170	141	118	100	86	74	64	56	50
82.5	463	508	411	318	246	191	150	119	94	75	59	47	36	27	20
87.5	473	514	412	315	240	183	140	108	82	62	46	33	22	13	5

TABLE 3.4

Solution by Dynamic Relaxation

Stress distribution in a flat plate

having a small circular hole at the centre

Tangential Stress - lb./in.^{2}															
Radius / Angle	.219	.281	.344	.406	.469	.531	.594	.656	.719	.781	.844	.906	.969	1.03	1.09
2.5	-708	-213	-71	-20	3	17	29	40	53	67	82	99	118	138	160
7.5	-660	-184	-49	-1	21	34	45	56	68	81	96	113	131	150	171
12.5	-566	-128	-5	37	56	67	77	86	97	110	123	139	155	173	193
17.5	-428	-46	53	93	107	116	123	131	140	151	163	177	191	208	225
22.5	-250	60	140	164	173	178	183	189	196	204	214	225	238	252	266
27.5	-39	189	237	249	252	253	254	257	262	268	275	284	293	304	316
32.5	200	328	348	346	341	337	335	335	337	340	344	349	356	363	371
37.5	460	483	467	450	437	428	423	419	418	418	419	421	424	427	432
42.5	723	645	592	560	538	524	514	507	503	499	497	496	495	495	495
47.5	1008	809	720	671	641	621	607	597	589	582	577	572	567	563	559
52.5	1280	971	845	780	742	717	699	685	674	664	655	646	638	631	623
57.5	1539	1126	964	885	839	808	787	769	755	742	730	718	706	695	683
62.5	1778	1268	1074	981	928	893	867	847	829	814	798	784	769	754	739
67.5	1990	1394	1172	1066	1006	967	939	916	896	877	859	842	824	806	788
72.5	2167	1500	1254	1137	1072	1030	999	973	951	930	910	891	871	850	829
77.5	2305	1582	1317	1193	1124	1078	1045	1018	994	972	950	929	907	885	862
82.5	2400	1639	1361	1231	1159	1112	1077	1049	1024	1000	977	955	932	908	884
87.5	2448	1667	1383	1250	1176	1128	1093	1064	1039	1015	991	968	944	920	895

TABLE 3.5

Solution by dynamic relaxation

Stress distribution in a flat plate

having a small circular hole at the centre

Shear Stress - lb./in.^{2}																
Radius / Angle	.187	.250	.312	.375	.437	.500	.562	.625	.687	.750	.812	.875	.937	1.00	1.06	1.12
0.0	0	0	0	0	0	0	0	0	0	0	0	0	0	0	0	0
5.0	0	122	137	134	128	122	116	112	108	104	101	98	95	92	90	87
10.0	0	240	270	264	252	240	229	220	213	206	199	193	188	182	176	171
15.0	0	352	395	386	368	350	335	322	311	301	291	282	274	266	258	250
20.0	0	452	508	496	473	450	431	414	400	386	374	363	352	342	332	321
25.0	0	539	605	591	563	537	514	494	476	461	446	433	420	408	395	383
30.0	0	609	684	668	637	607	581	558	538	521	504	489	475	461	447	433
35.0	0	661	742	725	691	659	630	606	584	565	547	531	515	500	485	470
40.0	0	692	778	759	724	690	660	635	612	592	574	556	540	524	508	492
45.0	0	703	790	771	735	701	671	644	622	601	583	565	548	532	516	500
50.0	0	692	778	759	724	690	660	635	612	592	574	556	540	524	508	492
55.0	0	661	742	725	691	659	630	606	584	565	547	531	515	500	485	470
60.0	0	609	684	668	637	607	581	553	538	521	504	489	475	461	447	433
65.0	0	539	605	591	563	537	514	494	476	461	446	433	420	408	395	383
70.0	0	452	508	496	473	450	431	414	400	386	374	363	352	342	332	321
75.0	0	352	395	386	368	350	335	322	311	301	291	282	274	266	258	250
80.0	0	240	270	264	252	240	229	220	213	206	199	193	188	182	176	171
85.0	0	122	137	134	128	122	116	112	108	104	101	98	95	92	90	87
90.0	0	0	0	0	0	0	0	0	0	0	0	0	0	0	0	0

TABLE 3.6

Solution by Dynamic Relaxation

Stress distribution in a flat plate

having a small circular hole at the centre

Stress - lb./in.^{2}				
	$\alpha = 87.5^\circ$		$\alpha = 2.5^\circ$	
Radius	Tang. Stress	Radial Stress	Tang. Stress	Radial Stress
.219	2490	544	-765	-219
.281	1684	566	-239	39
.344	1391	449	-86	296
.406	1225	342	-30	483
.469	1179	259	-4	616
.531	1129	198	12	711
.594	1093	151	26	781
.656	1063	116	39	833
.719	1037	88	52	874
.781	1012	66	68	905
.844	987	49	84	931
.906	963	35	103	951
.969	938	23	123	968
1.03	912	14	144	981
1.09	886	5	168	993

TABLE 3.7

Stress distribution in a flat plate having a small hole, by dynamic relaxation using Eq. (3.20)

Fringe Number	Distance From Edge Of Support Ring Diameter Number			Average	Mult. By Scale Factor (.625)	Add Distance From Plate Edge (.125)
	1	2	3			
1	0.140	0.220	0.220	0.190	0.119	0.244
2	0.400	0.450	0.460	0.436	0.272	0.397
3	0.660	0.680	0.710	0.684	0.427	0.552
4	0.910	0.920	0.960	0.930	0.581	0.706
5	1.170	1.140	1.200	1.170	0.731	0.856
6	1.430	1.390	1.460	1.428	0.892	1.017
7	1.700	1.630	1.730	1.688	1.052	1.177
8	1.990	1.920	2.020	1.975	1.232	1.357
9	2.320	2.240	2.330	2.295	1.432	1.557
10	2.780	2.700	2.780	2.755	1.720	1.845

TABLE 4.1

Fringe order number v.s. distance from edge of plate - deflection of a flat circular plate by holographic interferometry. Load 55.8 lb.

Fringe Number	Distance From Edge Of Support Ring Diameter Number			Average	Mult. By Scale Factor (.625)	Add Distance From Plate Edge (.125)
	1	2	3			
1	0.150	0.100	0.070	0.107	0.067	0.192
2	0.360	0.320	0.300	0.306	0.191	0.316
3	0.575	0.520	0.520	0.539	0.336	0.461
4	0.780	0.725	0.725	0.744	0.465	0.590
5	0.990	0.940	0.940	0.956	0.598	0.723
6	1.200	1.140	1.150	1.162	0.727	0.852
7	1.410	1.340	1.375	1.375	0.860	0.985
8	1.625	1.560	1.600	1.592	0.996	1.121
9	1.850	1.770	1.840	1.820	1.138	1.263
10	2.110	2.020	2.100	2.078	1.298	1.423
11	2.370	2.290	2.390	2.350	1.470	1.595
12	2.725	2.650	2.740	2.700	1.687	1.812

TABLE 4.2

Load 72.5 lb.

Fringe Number	Distance From Edge Of Support Ring Diameter Number			Average	Mult. By Scale Factor (.610)	Add Distance From Plate Edge (.125)
	1	2	3			
1	0.140	0.075	0.075	0.097	0.059	0.184
2	0.310	0.250	0.250	0.270	0.165	0.290
3	0.475	0.440	0.425	0.446	0.272	0.379
4	0.650	0.625	0.580	0.619	0.377	0.502
5	0.820	0.800	0.750	0.790	0.482	0.607
6	1.000	0.975	0.925	0.966	0.590	0.715
7	1.175	1.150	1.080	1.135	0.692	0.817
8	1.350	1.350	1.250	1.317	0.804	0.929
9	1.525	1.530	1.430	1.429	0.911	1.036
10	1.710	1.725	1.610	1.680	1.025	1.150
11	1.910	1.920	1.800	1.876	1.143	1.268
12	2.120	2.130	2.000	2.083	1.270	1.395
13	2.340	2.360	2.210	2.300	1.405	1.530
14	2.625	2.630	2.470	2.500	1.526	1.651
15	3.075	3.075	2.95	3.030	1.850	1.975

TABLE 4.3

Fringe order number v.s. distance from edge of plate - deflection of a flat circular plate by holographic interferometry.

Load 89.1 lb.

Fringe Number	Distance From Edge Of Support Ring Diameter Number			Average	Mult. By Scale Factor (.625)	Add Distance From Plate Edge (.125)
	1	2	3			
1	0.140	0.150	0.140	0.143	0.090	0.215
2	0.275	0.280	0.300	0.288	0.180	0.305
3	0.410	0.440	0.440	0.430	0.269	0.394
4	0.550	0.580	0.580	0.570	0.356	0.481
5	0.690	0.730	0.730	0.717	0.455	0.580
6	0.820	0.875	0.880	0.857	0.535	0.660
7	0.960	1.040	1.020	1.005	0.629	0.754
8	1.100	1.175	1.170	1.150	0.718	0.843
9	1.240	1.320	1.310	1.290	0.806	0.931
10	1.375	1.475	1.460	1.440	0.900	1.025
11	1.525	1.640	1.625	1.595	0.997	1.122
12	1.675	1.800	1.780	1.752	1.097	1.222
13	1.825	1.975	1.950	1.920	1.200	1.325
14	2.000	2.150	2.125	2.110	1.318	1.443
15	2.175	2.340	2.310	2.305	1.440	1.565
16	2.375	2.550	2.525	2.480	1.551	1.676
17	2.650	2.830	2.790	2.755	1.721	1.846

TABLE 4.4

Fringe order number v.s. distance from edge of plate - deflection of a flat circular plate by holographic interferometry.

Load 106 lb.

Fringe Number	Distance From Edge Of Support Ring Diameter Number			Average	Mult. By Scale Factor (.625)	Add Distance From Edge Of Plate (.125)
	1	2	3			
1	0.075	0.070	0.075	0.073	0.046	0.161
2	0.200	0.200	0.200	0.200	0.125	0.250
3	0.325	0.310	0.340	0.325	0.203	0.328
4	0.440	0.425	0.460	0.442	0.276	0.401
5	0.560	0.540	0.590	0.564	0.352	0.477
6	0.675	0.660	0.700	0.678	0.424	0.549
7	0.790	0.775	0.825	0.798	0.498	0.623
8	0.910	0.890	0.950	0.916	0.573	0.698
9	1.025	1.000	1.075	1.033	0.646	0.771
10	1.150	1.125	1.200	1.158	0.724	0.849
11	1.270	1.240	1.320	1.276	0.797	0.922
12	1.390	1.360	1.450	1.400	0.875	1.000
13	1.510	1.480	1.575	1.522	0.950	1.075
14	1.640	1.610	1.710	1.652	1.032	1.157
15	1.775	1.740	1.850	1.755	1.099	1.224
16	1.920	1.860	2.000	1.929	1.205	1.330
17	2.060	2.010	2.150	2.085	1.304	1.429
18	2.210	2.150	2.310	2.221	1.390	1.515
19	2.375	2.325	2.490	2.395	1.497	1.622
20	2.600	2.525	2.700	2.605	1.629	1.754
21	3.000	2.925	3.100	3.008	1.870	1.995

TABLE 4.5

Fringe order number v.s. distance from edge of plate - deflection of a flat circular plate by holographic interferometry.

Load 122 lb.

Fringe Number	Distance From Edge Of Support Ring Diameter Number			Average	Mult. By Scale Factor (.604)	Add Distance From Edge Of Plate (.125)
	1	2	3			
1	0.110	0.080	0.125	0.105	0.063	0.188
2	0.225	0.190	0.240	0.218	0.132	0.257
3	0.340	0.300	0.360	0.333	0.201	0.326
4	0.450	0.420	0.460	0.444	0.268	0.393
5	0.570	0.525	0.575	0.557	0.336	0.461
6	0.675	0.640	0.680	0.665	0.402	0.527
7	0.790	0.750	0.800	0.780	0.471	0.596
8	0.910	0.875	0.910	0.899	0.544	0.669
9	1.025	0.975	1.020	1.006	0.607	0.732
10	1.140	1.100	1.125	1.122	0.678	0.803
11	1.260	1.210	1.250	1.240	0.749	0.874
12	1.375	1.325	1.350	1.350	0.815	0.940
13	1.490	1.450	1.470	1.470	0.888	1.013
14	1.620	1.570	1.590	1.593	0.962	1.087
15	1.740	1.680	1.710	1.710	1.032	1.157
16	1.860	1.820	1.840	1.840	1.110	1.235
17	2.000	1.960	1.970	1.975	1.192	1.317
18	2.140	2.100	2.110	2.118	1.278	1.403
19	2.280	2.230	2.250	2.255	1.360	1.485
20	2.450	2.400	2.420	2.423	1.462	1.587
21	2.640	2.590	2.600	2.610	1.575	1.700
22	2.900	2.860	2.875	2.880	1.737	1.862

TABLE 4.6

Fringe order number v.s. distance from edge of plate - deflection of a flat circular plate by holographic interferometry.

Load 140 lb.

Fringe Number	Distance From Edge Of Support Ring Diameter Number			Average	Mult. By Scale Factor (.492)	Add Distance From Plate Edge (.125)
	1	2	3			
1	0.130	0.120	0.150	0.133	0.065	0.190
2	0.260	0.230	0.270	0.253	0.125	0.250
3	0.390	0.360	0.400	0.383	0.188	0.313
4	0.525	0.480	0.530	0.511	0.252	0.377
5	0.650	0.625	0.650	0.641	0.316	0.441
6	0.775	0.740	0.780	0.765	0.377	0.502
7	0.900	0.860	0.900	0.880	0.433	0.558
8	1.040	0.980	1.040	1.020	0.502	0.627
9	1.160	1.100	1.150	1.140	0.561	0.686
10	1.275	1.240	1.280	1.265	0.623	0.748
11	1.420	1.360	1.400	1.393	0.687	0.812
12	1.550	1.480	1.540	1.523	0.750	0.875
13	1.675	1.610	1.650	1.645	0.810	0.935
14	1.810	1.740	1.780	1.776	0.875	1.000
15	1.950	1.860	1.925	1.912	0.942	1.067
16	2.080	2.000	2.060	2.050	1.010	1.135
17	2.220	2.140	2.190	2.180	1.072	1.197
18	2.370	2.280	2.350	2.330	1.148	1.273
19	2.520	2.425	2.500	2.482	1.222	1.347
20	2.670	2.575	2.640	2.610	1.285	1.410
21	2.830	2.750	2.810	2.800	1.379	1.504
22	3.025	2.925	2.975	2.975	1.462	1.587
23	3.220	3.125	3.200	3.184	1.569	1.694
24	3.470	3.350	3.430	3.420	1.685	1.810

TABLE 4.7

Fringe order number v.s. distance from edge of plate - deflection of a flat circular plate by holographic interferometry.

Load 156 lb.

Radius	Deflection - Inches x 10^5					
	Distance From Bottom Surface - Inches					
	0.0000	0.0625	0.1250	0.1875	0.2500	0.3125
0.067	0.000	0.0155	0.0252	0.0284	0.0253	0.0166
0.200	1.053	1.065	1.071	1.071	1.065	1.054
0.333	2.110	2.125	2.132	2.132	2.125	2.111
0.467	3.177	3.194	3.203	3.203	3.194	3.177
0.600	4.243	4.264	4.274	4.274	4.264	4.243
0.733	5.300	5.324	5.337	5.337	5.325	5.300
0.867	6.337	6.365	6.380	6.380	6.366	6.337
1.000	7.342	7.375	7.392	7.392	7.375	7.342
1.133	8.301	8.340	8.359	8.359	8.340	8.302
1.267	9.199	9.244	9.266	9.266	9.244	9.199
1.400	10.01	10.07	10.09	10.09	10.07	10.02
1.533	10.71	10.77	10.81	10.82	10.81	10.77
1.667	11.21	11.27	11.30	11.31	11.28	11.22
1.800	11.54	11.60	11.63	11.63	11.60	11.54
1.933	11.70	11.76	11.79	11.79	11.76	11.70

TABLE 4.8

Deflection of a flat circular plate by dynamic relaxation.

Load 55.8 lb.

Radius Inches	Radial Stress - lb/in^2						
	Distance From Bottom Surface - Inches						
	0.000	0.031	0.063	0.156	0.219	0.281	0.313
0.067	-5.0	-4.0	-1.9	0.2	2.3	4.5	5.6
0.200	21.6	20.5	7.6	-1.6	-9.2	-15.6	-19.5
0.333	53.1	42.4	20.9	-0.4	-20.9	-40.6	-50.7
0.467	84.5	67.6	34.1	0.0	-33.8	-67.0	-83.7
0.600	119.5	95.8	48.3	0.0	-48.2	-95.7	-119.5
0.733	159.0	127.3	64.1	-0.1	-64.3	-127.5	-159.5
0.867	203.5	162.8	81.9	-0.3	-82.5	-163.4	-204.0
1.000	254.0	203.6	102.2	-0.6	-103.5	-204.7	-256.2
1.133	314.0	251.7	126.1	-1.4	-128.5	-253.3	-316.0
1.267	388.0	311.2	154.8	-3.4	-159.9	-311.7	-389.0
1.400	486.0	389.2	190.9	-7.0	-202.4	-385.5	-481.0
1.533	605.0	483.8	240.2	10.1	-229.1	-514.8	-642.0
1.667	619.0	495.4	243.8	-3.1	-248.2	-485.0	-606.0
1.800	616.0	493.3	245.3	-1.3	-245.7	-487.5	-609.0
1.933	614.0	492.0	245.8	0.1	-244.8	-489.0	-611.0

TABLE 4.9

Radial stress distribution in a flat circular plate by dynamic relaxation.

Load 55.8 lb.

Radius Inches	Tangential Stress - lb/in^2						
	Distance From Bottom Surface - Inches						
	0.000	0.031	0.094	0.156	0.219	0.281	0.313
0.067	171.0	136.8	65.6	-3.9.	-73.3	-144.2	-179.0
0.200	210.0	167.9	82.9	0.1	-81.9	-164.1	-205.5
0.333	236.5	189.2	94.7	1.1	-92.4	-186.3	-233.0
0.467	265.5	212.5	106.6	1.3	-103.9	-209.8	-262.0
0.600	297.5	238.0	119.3	1.4	-116.5	-235.1	-294.0
0.733	331.5	265.7	133.2	1.6	-130.0	-262.5	-327.5
0.867	370.0	296.0	148.3	1.8	-144.7	-292.4	-365.0
1.000	411.0	392.2	164.9	2.1	-160.7	-325.0	-406.0
1.133	457.5	366.0	183.2	2.6	-178.1	-360.8	-450.0
1.267	507.5	406.5	203.3	3.1	-196.9	-399.5	-499.5
1.400	562.5	450.3	223.9	2.2	-218.3	-440.2	-550.0
1.533	610.0	489.6	237.3	-10.8	-263.9	-534.0	-667.5
1.667	616.0	494.0	243.7	-3.9	-248.5	-486.6	-607.5
1.800	615.0	492.7	245.5	-0.8.	-245.3	-488.1	-610.0
1.933	615.0	492.0	245.8	0.1	-244.8	-489.0	-611.0

TABLE 4.10

Tangential stress distribution in a flat circular plate by dynamic relaxation.
Load 55.8 lb.

Radius	Axial Stress - lb/in^2				
	Distance From Bottom Surface				
Inches	0.031	0.094	0.156	0.219	0.281
0.067	-34.5	-27.1	-16.6	-6.5	0.0
0.200	0.0	-0.9	-1.2	-0.7	0.0
0.133	0.0	0.3	0.3	0.2	0.0
0.467	0.0	0.1	0.2	0.1	0.0
0.600	0.0	0.0	0.0	0.0	0.0
0.733	0.0	0.0	0.0	0.0	0.0
0.867	0.0	0.0	0.0	0.0	0.0
1.000	0.0	0.0	0.1	0.0	0.0
1.133	0.0	0.2	0.3	0.2	0.0
1.267	0.0	0.3	0.3	0.3	0.0
1.400	0.0	-2.8	-5.9	-5.6	0.0
1.533	0.0	-23.6	-59.8	-103.2	-143.0
1.667	0.0	-3.7	-8.0	-7.5	0.0
1.800	0.0	0.5	0.7	0.6	0.0
1.933	0.0	0.7	1.1	0.8	0.0

TABLE 4.11

Axial stress distribution
in a flat circular plate
by dynamic relaxation.
Load 55.8 lb.

Radius Inches	Radial Displacement - Inches x10^6						
	Distance From Bottom Surface - Inches						
	0.000	0.031	0.094	0.156	0.219	0.281	0.313
0.000	11.89	9.509	4.771	0.082	-4.597	-9.301	-11.62
0.133	12.09	9.664	4.831	0.054	-4.715	-9.514	-11.90
0.267	12.25	9.797	4.907	0.059	-4.784	-9.664	-12.09
0.400	12.32	9.861	4.941	0.063	-4.814	-9.732	-12.15
0.533	12.29	9.844	4.932	0.065	-4.802	-9.714	-12.11
0.667	12.15	9.736	4.877	0.067	-4.743	-9.603	-12.00
0.800	11.90	9.524	4.769	0.069	-4.631	-9.386	-11.72
0.933	11.50	9.195	4.603	0.073	-4.457	-9.049	-11.30
1.067	10.90	8.728	4.368	0.079	-4.211	-8.571	-10.71
1.200	10.11	8.096	4.052	0.089	-3.877	-7.925	-9.900
1.333	9.060	7.253	3.634	0.109	-3.427	-7.071	-8.840
1.467	7.650	6.121	3.079	0.135	-2.825	-5.942	-7.420
1.600	5.775	4.620	2.295	-0.005	-2.295	-4.554	-5.690
1.733	3.840	3.073	1.530	-0.007	-1.532	-3.044	-3.800
1.867	1.918	1.534	0.766	-0.001	-0.764	-1.525	-1.905
2.000	0.000	0.000	0.000	0.000	0.000	0.000	0.000

TABLE 4.12

In-plane displacements in a flat circular plate by dynamic relaxation.

Load 55.8 lb.

Radius Inches	Deflection - Inches x10^5					
	Distance From Bottom Surface - Inches					
	0.000	0.063	0.125	0.188	0.250	0.313
0.067	0.000	0.044	0.071	0.080	0.071	0.046
0.200	2.949	2.982	2.999	2.999	2.984	2.952
0.333	5.912	5.953	5.973	5.937	5.953	5.913
0.467	8.898	8.947	8.972	8.972	8.948	8.899
0.600	11.89	11.94	11.97	11.97	11.94	11.89
0.733	14.85	14.92	14.95	14.95	14.92	14.85
0.867	17.75	17.83	17.87	17.87	17.83	17.75
1.000	20.75	20.66	20.71	20.71	20.66	20.57
1.133	23.26	23.36	23.42	23.42	23.36	23.26
1.267	25.77	25.90	25.96	25.96	25.90	25.77
1.400	28.05	28.20	28.27	28.28	28.21	28.06
1.533	30.00	30.17	30.27	30.31	30.28	30.18
1.667	31.41	31.58	31.67	31.67	31.59	31.42
1.800	32.33	32.50	32.59	32.58	32.50	32.33
1.933	32.78	32.96	33.04	33.04	32.95	32.78

TABLE 4.13

Deflection of a flat circular plate by dynamic relaxation.
Load 156 lb.

Radius Inches	Radial Stress - lb/in^2						
	Distance From Bottom Surface - Inches						
	0.000	0.031	0.094	0.156	0.219	0.281	0.313
0.067	-14	-11	-5	1	7	13	16
0.200	73	58	21	-5	-26	-44	-55
0.333	148	118	58	-1	-59	-114	-143
0.467	236	189	95	0	-95	-187	-234
0.600	335	268	135	0	-135	-268	-335
0.733	445	356	179	0	-180	-357	-446
0.867	570	456	229	-1	-231	-458	-572
1.000	713	570	286	-2	-290	-570	-716
1.133	881	705	353	-4	-360	-709	-886
1.267	1089	872	434	-10	-448	-873	-1090
1.400	1362	1090	534	-20	-567	-1079	-1350
1.533	1692	1355	673	28	-641	-1441	-1800
1.667	1732	1387	683	-9	-695	-1358	-1695
1.800	1728	1382	687	-4	-688	-1366	-1705
1.933	1720	1377	688	0	-685	-1370	-1711

TABLE 4.14

Radial stress distribution in a flat circular plate by dynamic relaxation.

Load 156 lb.

Radius Inches	Tangential Stress - lb/in^2						
	Distance From Bottom Surface - Inches						
	0.000	0.031	0.094	0.156	0.219	0.281	0.313
0.067	479	383	184	-11	-205	-404	-504
0.200	600	470	232	0	-229	-459	-574
0.333	663	530	265	3	-259	-522	-652
0.467	743	595	298	4	-291	-587	-734
0.600	833	666	334	4	-326	-658	-823
0.733	929	744	373	4	-364	-735	-918
0.867	1035	829	415	5	-405	-819	-1022
1.000	1150	922	462	6	-450	-910	-1137
1.133	1270	1025	513	7	-499	-1010	-1261
1.267	1420	1138	569	9	-552	-1119	-1397
1.400	1578	1261	627	6	-611	-1233	-1542
1.533	1715	1371	665	-30	-739	-1495	-1869
1.667	1730	1384	683	-11	-696	-1363	-1705
1.800	1725	1380	688	-2	-687	-1367	-1707
1.933	1720	1377	688	0	-685	-1370	-1710

TABLE 4.15

Tangential stress distribution in a flat circular plate by dynamic relaxation.

Load 156 lb.

Radius Inches	Axial Stress - lb/in^2				
	Distance From Bottom Surface - Inches				
	0.031	0.094	0.156	0.219	0.281
0.067	-96.7	-76.0	-46.6	-18.3	0.0
0.200	0.1	-2.7	-3.1	-2.0	0.0
0.333	-0.1	0.7	0.9	0.4	0.0
0.467	0.0	0.3	0.4	0.2	0.1
0.600	0.0	0.1	0.2	0.1	0.1
0.733	0.1	0.1	-0.1	-0.1	0.1
0.867	-0.1	0.0	-0.1	-0.3	0.0
1.000	0.0	0.2	0.2	0.0	0.1
1.133	0.0	0.4	0.6	0.5	0.0
1.267	-0.1	0.8	0.9	0.8	0.1
1.400	0.2	-7.6	-16.4	-15.5	-0.1
1.533	0.0	-65.6	-167.2	-288.4	-399.8
1.667	0.3	-10.3	-22.2	-21.2	-8.1
1.800	-0.1	1.9	2.1	2.0	0.0
1.933	-0.6	1.8	2.9	2.6	0.2

TABLE 4.16

Axial stress distribution in a flat circular plate by dynamic relaxation

Load 156 lb.

Radius	Radial Displacement - Inches x10^6						
	Distance From Bottom Surface - Inches						
	0.000	0.031	0.094	0.156	0.219	0.281	0.313
0.000	33.30	26.62	13.36	0.229	-12.87	-26.04	-32.50
0.133	33.80	27.06	13.53	0.149	-13.20	-26.64	-33.30
0.267	34.35	27.43	13.74	0.166	-13.39	-27.06	-33.80
0.400	34.45	27.61	13.83	0.176	-13.48	-27.25	-34.10
0.533	34.40	27.56	13.81	0.181	-13.45	-27.20	-34.00
0.667	34.10	27.26	13.65	0.186	-13.28	-26.89	-33.62
0.800	33.35	26.67	13.35	0.193	-12.97	-26.28	-32.90
0.933	32.18	25.75	12.89	0.203	-12.48	-25.34	-31.70
1.067	30.55	24.44	12.23	0.220	-11.79	-24.00	-30.00
1.200	28.35	22.67	11.34	0.247	-10.86	-22.19	-27.70
1.333	25.40	20.31	10.18	0.303	-9.598	-19.80	-24.75
1.467	21.42	17.14	8.623	0.376	-7.911	-16.64	-20.80
1.600	16.18	12.94	6.427	-0.014	-6.428	-12.76	-15.95
1.733	10.75	8.607	4.283	-0.020	-4.291	-8.527	-10.68
1.867	5.370	4.296	2.144	-0.004	-2.141	-4.271	-5.340
2.000	0.000	0.000	0.000	0.000	0.000	0.000	0.000

TABLE 4.17

In-plane displacements in a flat circular plate by dynamic relaxation.
Load 156 lb.

Distance from edge of plate	Deflection - Inches x 10^5						
	Load - Pounds						
	55.8	72.5	89.1	106.0	122.0	140.0	156.0
0.067	0.516	0.670	0.823	0.980	1.127	1.294	1.442
0.200	1.551	2.015	2.477	2.947	3.391	3.892	4.337
0.333	2.596	3.373	3.135	4.932	5.677	6.514	7.259
0.467	3.643	4.734	5.818	6.921	7.966	9.141	10.19
0.600	4.683	6.085	7.478	8.897	10.24	11.75	13.09
0.733	5.707	7.415	9.113	10.84	12.48	14.32	15.96
0.867	6.704	8.710	10.70	12.73	14.66	16.82	18.74
1.000	7.661	9.954	12.23	14.55	16.75	19.22	21.42
1.133	8.564	11.13	13.67	16.27	18.72	21.49	23.94
1.267	9.396	12.21	15.00	17.85	20.54	23.57	26.27
1.400	10.13	13.17	16.18	19.25	22.16	25.42	28.33
1.533	10.75	13.96	17.16	20.42	23.50	26.96	30.05
1.667	11.21	14.57	17.90	21.30	24.51	28.13	31.34
1.800	11.52	14.97	18.39	21.88	25.18	28.90	32.20
1.933	11.67	15.17	18.64	22.17	25.52	29.29	32.63

TABLE 4.18

Deflection of a flat circular plate - Analytical Solution

Distance from edge of plate	Stress - lb./in.^{2}			
	Radial Stress		Tangential Stress	
	Load		Load	
	55.8	156	55.8	156
0.067	12.5	35.1	191	534
0.200	38.9	109	215	602
0.333	67.4	189	241	675
0.467	98.6	276	269	753
0.600	133	372	300	838
0.733	171	478	332	929
0.867	214	600	368	1029
1.000	264	738	407	1140
1.133	323	902	450	1260
1.267	395	1103	500	1390
1.400	488	1364	546	1530
1.533	582	1626	582	1626
1.667	582	1626	582	1626
1.800	582	1626	582	1626
1.933	582	1626	582	1626

TABLE 4.19

Radial and tangential stress in a flat circular plate

Analytical Solution

Fringe Number	Bottom Half of Plate			Top Half of Plate		
	Measured Radius Inches	Scaled Radius Inches	Corrected Deflection Inch x 10^4	Measured Radius Inches	Scaled Radius Inches	Corrected Deflection Inch x 10^4
1	.450	1.350	-2.143	.520	1.536	-1.965
2	.550	1.650	-2.018	.640	1.891	-1.840
3	.675	2.025	-1.893	.800	2.364	-1.715
4	.840	2.520	-1.768	.950	2.807	-1.590
5	.975	2.925	-1.643	1.110	3.280	-1.465
6	1.120	3.360	-1.518	1.260	3.723	-1.340
7	1.250	3.750	-1.393	1.400	4.136	-1.215
8	1.390	4.170	-1.268	1.550	4.580	-1.090
9	1.530	4.590	-1.143	1.690	4.993	-0.965
10	1.660	4.980	-1.018	1.830	5.407	-0.840
11	1.790	5.370	-0.893	1.980	5.850	-0.715
12	1.930	5.790	-0.768	2.140	6.323	-0.590
13	2.070	6.210	-0.643	2.320	6.855	-0.465
14	2.220	6.660	-0.518	2.470	7.300	-0.340
15	2.360	7.080	-0.393	2.630	7.770	-0.215
16	2.520	7.560	-0.268	2.790	8.243	-0.090
17	2.680	8.040	-0.143	2.970	8.775	0.035
18	2.850	8.550	-0.018	3.150	9.307	0.160
19	3.020	9.060	0.107	3.300	9.750	0.285
20	3.190	9.570	0.232	-	-	-

TABLE 5.1

Holographic Solution

Load 309 Lb.

Deflection Along Radius O-A

Fringe Number	Bottom Half of Plate			Top Half of Plate		
	Measured Radius Inches	Scaled Radius Inches	Corrected Deflection Inch x 10^4	Measured Radius Inches	Scaled Radius Inches	Corrected Deflection Inch x 10^4
1	.450	1.358	-2.987	.520	1.560	-2.737
2	.550	1.660	-2.862	.600	1.800	-2.612
3	.630	1.902	-2.737	.700	2.100	-2.487
4	.710	2.143	-2.612	.830	2.490	-2.362
5	.820	2.475	-2.487	.940	2.820	-2.237
6	.939	2.807	-2.362	1.060	3.180	-2.112
7	1.040	3.139	-2.237	1.150	3.450	-1.987
8	1.140	3.441	-2.112	1.260	3.780	-1.862
9	1.124	3.743	-1.987	1.370	4.110	-1.737
10	1.340	4.045	-1.862	1.470	4.410	-1.612
11	1.420	4.286	-1.737	1.570	4.710	-1.487
12	1.520	4.588	-1.612	1.670	5.010	-1.362
13	1.610	4.860	-1.487	1.780	5.340	-1.237
14	1.700	5.132	-1.362	1.880	5.640	-1.112
15	1.800	5.433	-1.237	1.980	5.940	-0.987
16	1.900	5.735	-1.112	2.090	6.270	-0.862
17	2.000	6.037	-0.987	2.200	6.600	-0.737
18	2.100	6.339	-0.862	2.320	6.960	-0.612
19	2.210	6.641	-0.737	2.430	7.290	-0.487
20	2.310	6.973	-0.612	2.540	7.620	-0.362
21	2.240	7.305	-0.487	2.650	7.950	-0.237
22	2.530	7.637	-0.362	2.750	8.250	-0.112
23	2.640	7.969	-0.237	2.890	8.670	0.013
24	2.750	8.301	-0.112	3.000	9.000	0.138
25	2.870	8.663	0.013	3.140	9.420	0.263
26	2.990	9.026	0.138	3.250	9.750	0.388
27	3.110	9.388	0.263	-	-	-
28	3.230	9.750	0.388	-	-	-

TABLE 5.2

Holographic Solution

Load 412 Lb.

Deflection Along Radius O-A

Radius Inches	Deflection x 10^5 - Inches				
	Solution No. 1		Solution No. 2		Solution No. 3
	309 lb.	412 lb.	309 lb.	412 lb.	412 lb.
.945	-31.83	-42.50	-26.68	-35.57	-35.61
1.575	-30.59	-40.78	-25.40	-33.87	-33.98
2.205	-29.05	-38.74	-23.93	-31.91	-32.13
2.835	-26.98	-35.97	-22.00	-29.33	-29.73
3.465	-24.35	-32.47	-19.73	-26.30	-26.81
4.095	-21.37	-28.50	-17.26	-23.01	-23.49
4.725	-18.22	-24.29	-14.69	-19.59	-19.98
5.355	-14.98	-19.98	-12.11	-16.15	-16.43
5.985	-11.79	-15.72	-9.56	-12.75	-12.94
6.615	-8.69	-11.59	-7.07	-9.43	-9.55
7.245	-5.70	-7.60	-4.65	-6.20	-6.27
7.875	-2.81	-3.75	-2.29	-3.06	-3.09
8.505	0.00	0.00	0.00	0.00	0.00
9.135	2.71	3.62	2.22	2.96	2.98

TABLE 5.3

Flame Plate Deflection Along
Line O - A
Dynamic Relaxation Solutions
Mechanical Load

Radius Inches	Deflection x -10^4 - Inches				
	Line				
	O - A	O - B	O - C	O - D	O - E
.945	97.81	97.85	97.91	97.97	98.03
1.575	96.58	96.68	96.83	96.97	97.10
2.205	94.69	95.03	95.58	95.72	95.94
2.835	91.59	92.28	93.59	-	-
3.465	87.22	88.31	90.43	-	-
4.095	81.54	83.08	86.12	-	-
4.725	74.57	76.51	80.53	-	-
5.355	66.33	68.54	73.41	-	-
5.985	56.94	59.14	64.36	-	-
6.615	46.59	48.41	52.71	53.78	53.10
7.245	35.56	36.71	38.99	39.70	40.00
7.875	24.08	24.66	25.75	26.16	26.78
8.505	12.26	12.43	12.80	12.94	13.31
9.135	0.00	0.00	0.00	0.00	0.00

TABLE 5.4

Deflection of Flame Plate

Under Thermal Load

Dynamic Relaxation Solution

RADIAL STRESS ON LAYER K = 1
THERMAL LOAD

0.	0.	0.	0.	0.
681.	4560.	4513.	4221.	4024.
2869.	3710.	6458.	6639.	6206.
41.	-90.	11274.	7652.	5498.
0.	0.	10364.	6825.	3608.
0.	0.	11781.	5496.	486.
0.	0.	14005.	4408.	-2723.
0.	0.	16401.	3330.	-5761.
0.	0.	18310.	2165.	-8318.
0	0.	* 19189.	863.	-10119.
-874.	-473.	18407.	-384.	*-10924.
489.	-207.	11354.	-660.	-10386.
913.	-639.	4761.	-1654.	-8751.
257.	-950.	706.	-2009.	-5596.
-293.	-456.	-582.	-989.	-1391.

TABLE 5·5

RADIAL STRESS ON LAYER K = 2
THERMAL LOAD

0.	0.	0.	0.	0.
1022.	3860.	3696.	3347.	3123.
2572.	3121.	5380.	5312.	5220.
67.	-68.	10066.	6600.	4821.
0.	0.	9678.	6166.	3336.
0.	0.	11721.	5135.	601.
0.	0.	14601.	4207.	-2320.
0.	0.	17631.	3199.	-5096.
0.	0.	20106.	2025.	-7407.
0	0.	*21204.	671.	-8918.
-726.	-206.	19917.	-696.	*-9350.
518.	-75.	11018.	-938.	-8497.
961.	-460.	4555.	-1570.	-6820.
390.	-733.	826.	-1734.	-4300.
-255.	-441.	-599.	-1056.	-1485.

TABLE 5·6

RADIAL STRESS ON LAYER K = 3
THERMAL LOAD

0.	0.	0.	0.	0.
5069.	2941.	2806.	2516.	2328.
1992.	2351.	4036.	4068.	3791.
129.	10.	7644.	4782.	3228.
0.	0.	7848.	4477.	1843.
0.	0.	10087.	3680.	-615.
0.	0.	13122.	2861.	-3314.
0.	0.	16234.	1893.	-5877.
0.	0.	18704.	736.	-7938.
0.	0.	*19701.	-545.	-9132.
-715.	-218.	18457.	-1709.	*-9191.
84.	-87.	10176.	-1612.	-8028.
491.	-426.	4192.	-1897.	-6266.
173.	-653.	757.	-1818.	-3949.
-206.	-381.	-544.	-1011.	-1433.

TABLE 5·7

RADIAL STRESS ON LAYER K = 4
THERMAL LOAD

0.	0.	0.	0.	0.
850.	1801.	1776.	1603.	1478.
1122.	1397.	2487.	2348.	1996.
254.	165.	4484.	2251.	792.
0.	0.	5317.	1865.	-713.
0.	0.	7572.	1183.	-3044.
0.	0.	10432.	328.	-5656.
0.	0.	13204.	-728.	-8105.
0.	0.	15145.	-1944.	-9960.
0	0.	*15612.	-3106.	*-10817.
-796.	-393.	14223.	-3755.	-10440.
-744.	-145.	8803.	-2915.	-8893.
-430.	-485.	3659.	-2770.	-6953.
-245.	-644.	508.	-2377.	-4561.
-145.	-308.	-474.	-941.	-1357.

TABLE 5·8

TANGENTIAL STRESS ON LAYER K = 1
THERMAL LOAD

0.	0.	0.	0.	0.
411.	8073.	7504.	7146.	7002.
6505.	5980.	4462.	4553.	4910.
1969.	2495.	3337.	4488.	5355.
0.	0.	1.	2489.	4455.
0.	0.	-4.	2875.	5221.
0.	0.	3.	3236.	5647.
0.	0.	-3.	2530.	4134.
0.	0.	2.	559.	347.
0.	0.	-2.	-3787.	-6965.
*-14487.	-10163.	-2155.	-12431.	-19012.
-8590.	-11575.	-16566.	-22147.	*-28604.
-3737.	-9047.	-16350.	-21352.	-26739.
1960.	-851.	-4297.	-4379.	-4795.
6480.	8812.	10234.	18339.	*26275.

TABLE 5·9

TANGENTIAL STRESS ON LAYER K = 2
THERMAL LOAD

0.	0.	0.	0.	0.
268.	6856.	6189.	5698.	5458.
5760.	5149.	3773.	3667.	3824.
1582.	2098.	3775.	4101.	4478.
0.	0.	2.	2053.	3680.
0.	0.	-2.	2352.	4321.
0.	0.	1.	2522.	4464.
0.	0.	-2.	1800.	2935.
0.	0.	3.	-155.	-778.
0	0.	-2.	-3848.	-7133.
*-11634.	-5444.	3047.	-9472.	-15542.
-5998.	-8108.	-11638.	-16237.	*-21104.
-1776.	-6206.	-11205.	-13827.	-16900.
2440.	161.	-1672.	181.	1502.
5903.	8867.	11479.	21177.	*30215.

TABLE 5·10

TANGENTIAL STRESS ON LAYER K = 3
THERMAL LOAD

0.	0.	0.	0.	0.
491.	5159.	4627.	4233.	4042.
4236.	3734.	2653.	2607.	2770.
739	1203.	2508.	3041.	3519.
0.	0.	2.	1790.	3241.
0.	0.	-2.	2106.	3857.
0.	0.	-0.	2176.	3815.
0.	0.	-5.	1399.	2181.
0.	0.	1.	-550.	-1511.
0	0.	-3.	-3869.	-7256.
*-11496.	-5352.	3492.	-8199.	-13800.
-5975.	-7322.	-10017.	-13420.	*-17275.
-2072.	-5556.	-9314.	-10388.	-12134.
1563.	-99.	-1006.	2047.	4345.
4630.	7590.	10596.	20892.	*30103.

TABLE 5·11

TANGENTIAL STRESS ON LAYER K = 4
THERMAL LOAD

0.	0.	0.	0.	0.
155.	3000.	2740.	2589.	2538.
2046.	1788.	1120.	1374.	1732.
-672.	-282.	101.	1616.	2671.
0.	0.	3.	1763.	3207.
0.	0.	-3.	2162.	3846.
0.	0.	0.	2155.	3628.
0	0.	-4.	1268.	1769.
0.	0.	2.	-809.	-2131.
0.	0.	2.	-4223.	-7854.
*-13261.	-8238.	-480.	-8714.	-13911.
-8026.	-8955.	-11618.	-13458.	*-16735.
-4203.	-6850.	-10257.	-10287.	-11403.
-483.	-1606.	-2221.	1447.	4126.
2733.	5632.	8755.	19309.	*28516.

TABLE 5.12

AXIAL STRESS ON LAYER K = 1
THERMAL LOAD

0.	0.	0.	0.	0.
-23.	-14.	-1.	14.	20.
3.	2.	0.	-2.	-3.
-0.	0.	0.	1.	-1.
0.	0.	1.	1.	0.
0.	0.	1.	0.	1.
0.	0.	-0.	0.	-1.
0.	0.	0.	-1.	0.
0.	0.	1.	-1.	-0.
0.	0.	-0.	1.	-1.
-0.	0.	0.	1.	1.
-0.	1.	0.	1.	1.
0.	0.	-1.	-0.	-0.
1.	-0.	-1.	0.	0.
0.	-1.	0.	-0.	-1.

TABLE 5·13

AXIAL STRESS ON LAYER K = 2
THERMAL LOAD

0.	0.	0.	0.	0.
295.	105.	-63.	-201.	-265.
268.	-49.	-90.	-130.	-135.
-56.	-530.	710.	-42.	-134.
0.	0.	-2.	-52.	-51.
0.	0.	-10.	-26.	-17.
0.	0.	-6.	-22.	-10.
0.	0.	17.	-26.	-8.
0.	0.	98.	-37.	-9.
0	0.	309.	-58.	-12.
-253.	280.	680.	-118.	-17.
141.	-130.	-275.	-62.	-1.
146.	-69.	-85.	4.	29.
55.	-17.	24.	78.	132.
-447.	-161.	-121.	26.	220.

TABLE 5-14

AXIAL STRESS ON LAYER K = 3
THERMAL LOAD

0.	0.	0.	0.	0.
282.	99.	-57.	-186.	-246.
258.	-43.	-84.	-123.	-130.
-61.	-457.	607.	-32.	-124.
0.	0.	7.	-53.	-52.
0.	0.	-9.	-28.	-18.
0.	0.	-7.	-24.	-11.
0.	0.	16.	-25.	-7.
0.	0.	93.	-35.	-9.
0	0.	283.	-56.	-12.
-237.	253.	699.	-113.	-15.
131.	-128.	-265.	-61.	-2.
142.	-66.	-82.	3.	28.
40.	-23.	19.	77.	136.
-767.	-294.	-154.	175.	581.

TABLE 5·15

AXIAL STRESS ON LAYER K = 4
THERMAL LOAD

0.	0	0.	0.	0.
-13.	-9.	-1.	9.	14.
1.	1.	-0.	-1.	-2.
-1.	1.	-0.	1.	0.
0.	0.	-0.	0.	-1.
0.	0.	1.	1.	1.
0.	0.	-1.	0.	-1.
0.	0.	1.	1.	0.
0.	0.	-0.	-0.	-1.
0	0.	0.	-0.	-0.
-0.	0.	1.	0.	0.
0.	0.	-0.	2.	0.
-0.	0.	-1.	-1.	0.
1.	-1.	-1.	-1.	-1.
-850.	-346.	-96.	369.	928.

TABLE 5.16

SHEAR STRESS TRT ON LAYER K = 1

THERMAL LOAD

0	0.	0.	0.	0	0.	
0.	0.	0.	0.	0.	0	
0.	1060.	1733.	1188.	514.	0.	
0.	1645.	3730.	570.	-298.	0.	
0.	0.	0.	-1177.	-1272.	0.	
0	0	0.	-3423.	-2962.	0.	
0.	0	0.	-4971.	-4226.	0.	
0.	0	0.	-6161.	-5042.	0.	
0	0.	0.	-6418.	-4992.	0.	
0	0.	0.	-5285.	-3777.	0.	
0.	0.	0.	-1845.	-1131.	0.	
0	-3789.	-5244.	4783.	2760.	0.	
0	-1254.	-1718.	7047.	5653.	0.	
0	1965.	2191.	8373.	7359.	0.	
0	2938.	3129.	6759.	6170.	0.	
0	0.	0.	0.	0.	0.	

TABLE 5·17

SHEAR STRESS TRT ON LAYER K = 2
THERMAL LOAD

0.	0.	0.	0.	0.	0.	
0.	0.	0.	0.	0.	0.	
0.	962.	1590.	1156.	549.	0	
0.	1400.	3153.	573.	-134.	0.	
0.	0.	0	-618.	-885.	0.	
0	0.	0.	-2814.	-2481.	0.	
0.	0	0.	-4263.	-3638.	0.	
0.	0	0.	-5297.	-4312.	0.	
0	0.	0.	-5481.	-4158	0.	
0	0.	0.	-4398.	-2898.	0.	
0.	0.	0.	-1581.	-420.	0.	
0	-2878.	-4826.	4669.	2906.	0.	
0	-1507.	-2156.	6046.	4901.	0.	
0	582.	572.	6345.	5621.	0.	
0	1324.	1239.	4564.	4209.	0.	
0	0.	0.	0.	0.	0.	

TABLE 5·18

SHEAR STRESS TRT ON LAYER K = 3

THERMAL LOAD

0.	0.	0.	0.	0.	0.	
0.	0.	0.	0.	0.	0.	
0.	743.	1231.	890.	418.	0.	
0.	1077.	2380.	317.	-213.	0.	
0.	0.	0.	-812.	-963.	0.	
0	0	0.	-2710.	-2369.	0.	
0.	0.	0.	-4060.	-3411.	0.	
0.	0.	0.	-4950.	-3943.	0.	
0	0.	0.	-4969.	-3638.	0.	
0.	0.	0.	-3706.	-2252	0.	
0.	0.	0	-879.	198.	0.	
0	-2586.	-4437.	4996.	3186.	0.	
0	-1701.	-2314.	5744.	4615.	0.	
0	-119.	-238.	5398.	4771.	0.	
0	569.	349.	3561.	3293.	0.	
0	0.	0.	0.	0.	0.	

TABLE 5·19

SHEAR STRESS TRT ON LAYER K = 4

THERMAL LOAD

0.	0.	0.	0.	0.	0.	
0.	0.	0.	0.	0.	0.	
0.	470.	763.	482.	183.	0.	
0.	709.	1453.	-226.	-529.	0.	
0.	0.	0.	-1699.	-1466.	0.	
0.	0.	0.	-3146.	-2619.	0.	
0.	0.	0.	-4390.	-3537.	0.	
0.	0.	0.	-5118.	-3908.	0.	
0.	0.	0.	-4850.	-3384.	0.	
0.	0.	0.	-3103.	-1745.	0.	
0.	0.	0.	484.	888.	0.	
0	-2762.	-3822.	6038.	3743.	0.	
0.	-1880.	-2135.	6227.	4815.	0.	
0	-344.	-426.	5353.	4614.	0.	
0.	378.	77.	3342.	3021.	0.	
0.	0.	0.	0.	0.	0.	

TABLE 5·20

SHEAR STRESS TRZ ON LAYER K = 1

THERMAL LOAD

0.	0.	0.	0.	0.	0.														
0.	0.	0.	0.	0.	0.														
0.	0.	0.	0.	0.	0.														
0.	0.	0.	0.	0.	0.														
0	0	0	0.	0.	0.														
0	0.	0.	0.	0.	0.														
0.	0.	0.	0.	0.	0.	0.													
0.	0.	0.	0.	0.	0.	0.													
0.	0.	0.	0.	0.	0.	0.													
0.	0.	0.	0.	0.	0.	0.													
0.	0	0	0.	0.	0.	0.													
0.	0.	0.	0.	0.	0.	0.													
0	0.	0.	0.	0.	0.	0.													
0	0.	0.	0.	0.	0.	0.													
0	0.	0.	0.	0.	0.	0.													
0.	0.	0.	0.	0.	0.	0.													

TABLE 5·21

SHEAR STRESS TRZ ON LAYER K = 2

THERMAL LOAD

0.	0.	0.	0.	0.	0.	
0.	0.	0.	0.	0.	0.	
175.	96.	20.	-49.	-86.	0.	
161.	111.	139.	-26.	-100.	0.	
0.	0.	295.	24.	-24.	0.	
0.	0.	432.	27.	-54.	0.	
0.	0.	541.	-9.	-109.	0.	
0.	0.	616.	-49.	-145.	0.	
0.	0.	613.	-72.	-151.	0.	
0.	0.	463.	-68.	-129.	0.	
0.	0.	-18.	-26.	-98.	0.	
-120.	-228.	-567.	-46.	-80.	0.	
-197.	-88.	-59.	11.	-85.	0.	
-249.	-70.	14.	1.	-126.	0.	
-301.	-133.	-93.	-86.	-227.	0.	
0.	0.	0.	0.	0.	0.	

TABLE 5.22

SHEAR STRESS TRZ ON LAYER K = 3

THERMAL LOAD

0.	0.	0.	0.	0.	0.					
0.	0.	0.	0.	0.	0.					
187.	105.	-29.	-123.	-169.	0.					
346.	208.	-174.	-210.	-204.	0.					
0.	0.	-75.	46.	22.	0.					
0.	0.	74.	-21.	-65.	0.					
0.	0.	216.	-74.	-149.	0.					
0.	0.	308.	-115.	-196.	0.					
0.	0.	333.	-134.	-203.	0.					
0.	0.	293.	-116.	-171.	0.					
0.	0.	216.	-46.	-128.	0.					
-343.	7.	390.	55.	-96.	0.					
-214.	4.	246.	65.	-97.	0.					
-96.	-15.	134.	72.	-86.	0.					
-99.	-66.	58.	119.	52.	0.					
0.	0.	0.	0.	0.	0.					

TABLE 5·23

SHEAR STRESS TRZ ON LAYER K = 4

THERMAL LOAD

0.	0.	0.	0.	0.	0.	
0.	0.	0.	0.	0.	0.	
124.	73.	-51.	-124.	-155.	0.	
378.	211.	-360.	-230.	-207.	0.	
0.	0.	-393.	45.	58.	0.	
0.	0.	-274.	-60.	-46.	0.	
0.	0.	-176.	-109.	-122.	0.	
0.	0.	-115.	-136.	-158.	0.	
0.	0.	-85.	-143.	-161.	0.	
0.	0.	-11.	-118.	-134.	0.	
0.	0.	258.	-53.	-98.	0.	
-336.	233.	1121.	128.	-64.	0.	
-132.	93.	428.	87.	-62.	0.	
102.	49.	188.	103.	-19.	0.	
106.	13.	160.	257.	271.	0.	
0.	0.	0.	0.	0.	0.	

TABLE 5.24

SHEAR STRESS TRZ ON LAYER K = 5

THERMAL LOAD

0.	0	0	0.	0	0.														
0.	0.	0	0.	0.	0.														
0.	0.	0.	0.	0.	0.	0.													
0.	0.	0.	0.	0.	0.	0.													
0	0	0	0.	0.	0.														
0.	0	0.	0.	0.	0.														
0.	0.	0.	0.	0.	0.	0.													
0	0.	0.	0.	0.	0.														
0	0	0.	0.	0.	0.	0.													
0.	0.	0.	0.	0.	0.	0.													
0.	0.	0.	0.	0.	0.	0.													
0.	0.	0.	0.	0.	0.	0.													
0	0.	0.	0.	0.	0.	0.													
0	0.	0.	0.	0.	0.	0.													
0.	0.	0.	0.	0.	0.	0.													
0.	0.	0.	0.	0.	0.	0.													

TABLE 5.25

SHEAR STRESS YZT ON LAYER K = 1
THERMAL LOAD

0.	0.	0.	0.	0.	0.	
0.	0.	0.	0.	0.	0.	
0.	0.	0.	0.	0.	0.	
0.	0.	0.	0.	0.	0.	
0.	0.	0.	0.	0.	0.	
0.	0.	0.	0.	0.	0.	
0.	0.	0.	0.	0.	0.	0.
0.	0.	0.	0.	0.	0.	0.
0.	0.	0.	0.	0.	0.	0.
0.	0.	0.	0.	0.	0.	0.
0.	0.	0.	0.	0.	0.	0.
0.	0.	0.	0.	0.	0.	0.
0.	0.	0.	0.	0.	0.	0.
0.	0.	0.	0.	0.	0.	0.

TABLE 5·26

SHEAR STRESS TZT ON LAYER K = 2

THERMAL LOAD

0.	0.	0.	0.	0.	0.	
0.	-180.	-257.	-239.	-139.	0.	
0.	-198.	-187.	-138.	-107.	0.	
0.	129.	673.	-104.	-90.	0.	
0	0	0.	-148.	-90.	0.	
0.	0.	0	-154.	-87.	0.	
0.	0.	0.	-156.	-72.	0.	
0.	0.	0.	-128.	-43.	0.	
0	0.	0.	-102.	-16.	0.	
0.	0.	0.	-91.	2.	0.	
0.	906.	527.	-404.	-33.	0.	
0.	-263.	-92.	-121.	-30.	0.	
0	-342.	-137.	-6.	-0.	0.	
0	-33.	177.	315.	226.	0.	
0	1047.	1362.	1628.	1344.	0.	
0	0.	0.	0.	0.	0.	

TABLE 5·27

SHEAR STRESS TZT ON LAYER K = 3

THERMAL LOAD

0.	0.	0	0.	0.	0.	
0.	-51.	-81.	-75.	-44.	0.	
0.	-97.	-165.	-96.	-40.	0.	
0.	167.	197.	258.	119.	0.	
0	0.	0.	-114.	-66.	0.	
0	0.	0.	-147.	-92.	0.	
0.	0.	0.	-135.	-76.	0.	
0.	0.	0.	-75.	-37.	0.	
0	0.	0.	17.	9.	0.	
0	0.	0.	140.	45.	0.	
0.	547.	608.	218.	37.	0.	
0	-160.	-158.	20.	-16.	0.	
0	-195.	-165.	20.	1.	0.	
0	78.	211.	374.	262.	0.	
0	1307.	1367.	1622.	1314.	0.	
0	0.	0.	0.	0.	0.	0.

TABLE 5·28

SHEAR STRESS TZT ON LAYER K = 4

THERMAL LOAD

0.	0.	0.	0.	0.	0.	
0.	77.	95.	88.	52.	0.	
0.	31.	-73.	25.	37.	0.	
0.	122.	-203.	436.	247.	0.	
0.	0.	0.	-22.	-10.	0.	
0.	0.	0.	-63.	-51.	0.	
0.	0.	0.	-49.	-43.	0.	
0.	0.	0.	11.	-13.	0.	
0.	0.	0.	119.	28.	0.	
0.	0.	0.	286.	65.	0.	
0.	15.	309.	706.	87.	0.	
0.	-24.	-184.	141.	2.	0.	
0.	9.	-137.	21.	-10.	0.	
0.	114.	110.	217.	142.	0.	
0.	549.	775.	905.	732.	0.	
0.	0.	0.	0.	0.	0.	

TABLE 5·29

SHEAR STRESS TZT ON LAYER K = 5
THERMAL LOAD

0.	0.	0.	0.	0.	0.	
0.	0.	0.	0.	0.	0.	
0.	0.	0.	0.	0.	0.	
0.	0.	0.	0.	0.	0.	
0.	0.	0.	0.	0.	0.	
0.	0.	0.	0.	0.	0.	
0.	0.	0.	0.	0.	0.	0.
0.	0.	0.	0.	0.	0.	
0.	0.	0.	0.	0.	0.	
0.	0.	0.	0.	0.	0.	0.
0.	0.	0.	0.	0.	0.	
0.	0.	0.	0.	0.	0.	0.
0.	0.	0.	0.	0.	0.	0.

TABLE 5·30

Radius Inches	Deflection x 10^6 - Inches				
	Line				
	O - A	O - B	O - C	O - D	O - E
.945	69.39	67.13	62.97	58.39	54.43
1.575	67.85	65.80	62.51	40.44	55.12
2.205	65.63	54.59	44.93	72.61	68.40
2.835	65.89	63.28	59.45	-	-
3.465	62.99	60.17	55.10	-	-
4.095	59.56	54.22	42.71	-	-
4.725	56.71	46.51	20.02	-	-
5.355	54.89	38.56	-23.62	-	-
5.985	53.68	34.43	-77.78	-	-
6.615	50.89	37.44	-94.32	0.28	60.59
7.245	41.89	42.28	19,50	35.12	31.41
7.875	24.02	31.36	33.64	37.49	15.96
8.505	2.81	12.42	20.73	23.35	10.25
9.135	0.0	0.0	0.0	0.0	0.0

TABLE 5.31

Deflection of Flame Plate
Under Combined Loads
Dynamic Relaxation Solution

RADIAL STRESS ON LAYER K = 1
COMBINED LOAD

0.	0.	0.	0.	0.
70.	2557.	2589.	2436.	2314.
825.	2101.	3262.	2990.	2386.
340.	292.	5055.	2535.	424.
0.	0.	5348.	1118.	-2262.
0.	0.	6666.	-126.	-5282.
0.	0.	8390.	-1363.	-8396.
0.	0.	10186.	-2616.	-11292.
0.	0.	11726.	-3763.	-13549.
0.	0.	*12745.	-4694.	-14842.
-1190.	-835.	11929.	-4936.	*-14961.
-569.	-1523.	6940.	-4284.	-13710.
-285.	-1896.	2165.	-4140.	-11191.
-29.	-1206.	-24.	-2814.	-6462.
-180.	-348.	-483.	-897.	-1305.

TABLE 5·32

RADIAL STRESS ON LAYER K = 2
COMBINED LOADS

0.	0.	0.	0.	0.
239.	3131.	3017.	2738.	2553.
2193.	2533.	4209.	4206.	3871.
157.	51.	7670.	4772.	3057.
0.	0.	7997.	4192.	1286.
0.	0.	10042.	3206.	-1415.
0.	0.	12780.	2240.	-4295.
0.	0.	15631.	1182.	-7016.
0.	0.	17996.	20.	-9210.
0.	0.	*19183.	-1199.	-10532.
-826.	-321.	17676.	-2202.	*-10703.
224.	-438.	9562.	-2106.	-9570.
678.	-767.	3777.	-2312.	-7547.
157.	-970.	403.	-2180.	-4766.
-219.	-409.	-573.	-1030.	-1461.

TABLE 5·33

RADIAL STRESS ON LAYER K = 3
COMBINED LOADS

0.	0.	0.	0.	0.
'10.	3546.	3383.	3041.	2826.
:303.	2843.	5042.	5189.	4943.
41.	-103.	9703.	6358.	4740.
0.	0.	9439.	6234.	3621.
0.	0.	11763.	5428.	1135.
0.	0.	14975.	4662.	-1591.
0.	0.	18256.	3748.	-4109.
0.	0.	20788.	2582.	-6350.
0.	0.	*21705.	1178.	-7695.
-603.	-100.	20603.	-316.	*-7957.
417.	333.	11637.	-482.	-7003.
852.	-43.	5059.	-1140.	-5543.
228.	-619.	947.	-1645.	-3778.
-243.	-422.	-585.	-1046.	-1466.

TABLE 5·34

RADIAL STRESS ON LAYER K = 4
COMBINED LOADS

0.	0	0.	0.	0.
372.	3710.	3590.	3264.	3061.
1200.	2957.	5519.	5778.	5573.
-28.	-198.	10529.	7154.	5609.
0.	0.	10196.	7310.	4838.
0.	0.	12612.	6574.	2426.
0.	0.	16019.	5893.	-254.
0.	0.	19469.	5036.	-2828.
0.	0.	21823.	3839.	-4967.
0	0.	*22102.	2325.	-6315.
-481.	-15.	20740.	647.	*-6605.
351.	988.	13137.	495.	-5755.
751.	523.	6040.	-494.	-4679.
245.	-300.	1374.	-1406.	-3489.
-255.	-422.	-581.	-1040.	-1450.

TABLE 5·35

TANGENTIAL STRESS ON LAYER K = 1
COMBINED LOADS

0.	0.	0.	0.	0.
4267.	4153.	3964.	3909.	3938.
2520.	2230.	1536.	1984.	2557.
-972.	-814.	-921.	1423.	3128.
0.	0.	-0.	2372.	4359.
0.	0.	-0.	3009.	5386.
0.	0.	0.	3157.	5480.
0	0.	-0.	1985.	3325.
0.	0.	0.	-731.	-1315.
0	0.	-0.	-6232.	-9599.
*-20680.	-17083.	-10487.	-17054.	-22597.
-14420.	-17869.	-23042.	-26939.	*-32633.
-9040.	-14402.	-21784.	-25900.	-30848.
-2128.	-4832.	-8277.	-7893.	-8081.
2881.	5344.	6898.	15314.	*23408

TABLE S-36

TANGENTIAL STRESS ON LAYER K = 2
COMBINED LOADS

0.	0.	0.	0.	0.
5762.	5446.	4935.	4568.	4399.
4328.	3812.	2735.	2751.	2983.
605.	997.	2142.	2929.	3627.
0.	0.	-0.	1994.	3629.
0.	0.	-0.	2396.	4378.
0.	0.	0.	2502.	4412.
0.	0.	-0.	1630.	2659.
0.	0.	0.	-574.	-1354.
0.	0.	-0.	-4662.	-8049.
*-13654	-7677.	180.	-11052.	-16789.
-7917.	-10196.	-13783.	-17851.	*-22471.
-3479.	-7947.	-12955.	-15283.	-18202.
1171.	-1069.	-2872.	-855.	556.
4769.	7820.	10509.	20315.	*29404

TABLE 5·37

TANGENTIAL STRESS ON LAYER K = 3
COMBINED LOADS

0.	0.	0.	0.	0.
6757.	6350.	5685.	5184.	4936.
5432.	4864.	3522.	3389.	3504.
1591.	2171.	3829.	4019.	4256.
0.	0.	-0.	1851.	3305.
0.	0.	0.	2098.	3846.
0.	0.	0.	2230.	3905.
0	0.	-0.	1592.	2459.
0.	0.	-0.	-135.	-979.
0	0.	-0.	-3086.	-6424.
*-9382.	-3086.	6238.	-6690.	-12667.
-4012.	-5269.	-7963.	-11874.	*-15981.
-277.	-3786.	-7562.	-8858.	-10723.
3186.	1505.	614.	3563.	5813.
5924.	8933.	11913.	22111.	*31257

TABLE 5·38

TANGENTIAL STRESS ON LAYER K = 4
COMBINED LOADS

0.	0.	0.	0.	0.
7118.	6733.	6087.	5615.	5387.
5864.	5360.	3901.	3788.	3919.
2105.	2841.	4273.	4546.	4738.
0.	0.	-0.	1855.	3269.
0.	0.	0.	2028.	3681.
0.	0.	0.	2204.	3767.
0.	0.	0.	1741.	2494.
0.	0.	-0.	383.	-606.
0.	0.	-0.	-1869.	-5394.
* -7139.	-1129.	7906.	-4220.	-10514.
-2181.	-2780.	-5187.	-8838.	* -12841.
1135.	-1651.	-4959.	-5804.	-7284.
4131.	2853.	2320.	5621.	8151.
6481.	9390.	12401.	22675.	*31716.

TABLE 5·39

AXIAL STRESS ON LAYER K = 1
COMBINED LOADS

0.	0.	0.	0.	0.
1500.	-1500.	-1500.	-1500.	-1500.
-1500.	-1500.	-1500.	-1500.	-1500.
-1500.	-1500.	-1500.	-1500.	-1500.
0.	0.	-1500.	-1500.	-1500.
0.	0.	-1500.	-1500.	-1500.
0.	0.	-1500.	-1500.	-1500.
0.	0.	-1500.	-1500.	-1500.
0.	0.	-1500.	-1500.	-1500.
0	0.	-1500.	-1500.	-1500.
-1500.	-1500.	-1500.	-1500.	-1500.
-1500.	-1500.	-1500.	-1500.	-1500.
-1500.	-1500.	-1500.	-1500.	-1500.
-0.	0.	0.	0.	0.
0.	0.	-0.	-0.	-0.

TABLE 5.40

AXIAL STRESS ON LAYER K = 2
COMBINED LOADS

0.	0.	0.	0.	0.
310.	-1497.	-1667.	-1811.	-1880.
1311.	-1637.	-1692.	-1750.	-1772.
-1723.	-2108.	-990.	-1624.	-1745.
0.	0.	-1560.	-1665.	-1690.
0.	0.	-1551.	-1619.	-1637.
0.	0.	-1433.	-1559.	-1598.
0	0.	-1215.	-1488.	-1569.
0.	0.	-970.	-1430.	-1553.
0	0.	-713.	-1423.	-1546.
-1831.	-812.	-431.	-1506.	-1527.
-1210.	-1476.	-1506.	-1486.	-1433.
-989.	-1376.	-1345.	-1253.	-1164.
-127.	-313.	-259.	-137.	-2.
-726.	-439.	-505.	-308.	-82.

TABLE 5·41

AXIAL STRESS ON LAYER K = 3
COMBINED LOADS

0.	0.	0.	0.	0.
363.	-1596.	-1823.	-2018.	-2114.
1404.	-1761.	-1837.	-1935.	-1980.
-1933.	-2372.	-873.	-1745.	-1935.
0.	0.	-1702.	-1825.	-1879.
0.	0.	-1614.	-1738.	-1791.
0.	0.	-1344.	-1606.	-1711.
0	0.	-863.	-1440.	-1647.
0.	0.	-385.	-1288.	-1608.
0	0.	-186.	-1234.	-1585.
-1916.	-271.	233.	-1352.	-1532.
-1000.	-1280.	-1146.	-1381.	-1329.
-615.	-1237.	-1160.	-1048.	-876.
-246.	-574.	-493.	-271.	-21.
-1466.	-986.	-1100.	-656.	-178.

TABLE 5·42

AXIAL STRESS ON LAYER K = 4
COMBINED LOADS

0.	0.	0.	0.	0.
633.	-1752.	-1889.	-2014.	-2082.
1654.	-1813.	-1875.	-1974.	-2035.
-2052.	-2178.	-1348.	-1785.	-1969.
0.	0.	-1784.	-1898.	-1977.
0.	0.	-1653.	-1805.	-1890.
0.	0.	-1281.	-1626.	-1787.
0.	0.	-601.	-1395.	-1701.
0.	0.	0.	-1157.	-1647.
0.	0.	-0.	-1033.	-1610.
-1818.	-8.	-0.	-1123.	-1527.
-942.	-1054.	-585.	-1268.	-1257.
-479.	-1128.	-1009.	-941.	-721.
-307.	-700.	-622.	-372.	-84.
-1896.	-1357.	-1490.	-867.	-218.

TABLE 5·43

FOUNDATION PRESSURE
COMBINED LOADS

0.	0.	0.	0.	0.
633.	-1752.	-1889.	-2014.	-2082.
1654.	-1813.	-1875.	-1974.	-2035.
-2052.	-2178.	-1348.	-1785.	-1969.
0.	0.	-1784.	-1898.	-1977.
0.	0.	-1653.	-1805.	-1890.
0.	0.	-1281.	-1626.	-1787.
0.	0.	-601.	-1395.	-1701.
0.	0.	0.	-1157.	-1647.
0	0.	0.	-1033.	-1610.
-1818.	-8.	0.	-1123.	-1527.
-942.	-1054.	-585.	-1268.	-1257.
-479.	-1128.	-1009.	-941.	-721.
-307.	-700.	-622.	-372.	-84.
-1896.	-1357.	-1490.	-867.	-218.

TABLE 5·44

SHEAR STRESS TRT ON LAYER K = 1
COMBINED LOADS

0.	0.	0.	0.	0.	0.
0.	0.	0.	0.	0.	0.
0.	387.	612.	266.	5.	0.
0.	749.	1471.	-564.	-909.	0.
0.	0.	0.	-2967.	-2427.	0.
0.	0.	0.	-4345.	-3626.	0.
0.	0.	0.	-5654.	-4649.	0.
0.	0.	0.	-6483.	-5170.	0.
0.	0.	0.	-6125.	-4725.	0.
0.	0.	0.	-4104.	-3074.	0.
0.	0.	0.	759.	-82.	0.
0.	-3537.	-3532.	6199.	3615.	0.
0.	-958.	-529.	8163.	6352.	0.
0.	2240.	2927.	9204.	7887.	0.
0.	3187.	3549.	7279.	6502.	0.
0.	0.	0.	0.	0.	0.

TABLE 5.15

SHEAR STRESS TRT ON LAYER K = 2

COMBINED LOADS

0.	0.	0.	0.	0.	0.						
0.	0.	0.	0.	0.	0.						
0.	704.	1164.	810.	360.	0.						
0.	1082.	2353.	213.	-326.	0.						
0.	0.	0.	-1188.	-1267.	0.						
0.	0.	0.	-3083.	-2693.	0.						
0.	0.	0.	-4472.	-3776.	0.						
0.	0.	0.	-5402.	-4356.	0.						
0.	0.	0.	-5385.	-4067.	0.						
0.	0.	0.	-4005.	-2651.	0.						
0.	0.	0.	-700.	-42.	0.						
0.	-2837.	-4251.	5142.	3212.	0.						
0.	-1408.	-1732.	6434.	5143.	0.						
0.	699.	838.	6628.	5796.	0.						
0.	1414.	1380.	4727.	4308.	0.						
0.	0.	0.	0.	0.	0.						

TABLE 5·46

SHEAR STRESS TRT ON LAYER K = 3
COMBINED LOADS

0.	0.	0.	0.	0.	0.						
0.	0.	0.	0.	0.	0.						
0.	942.	1563.	1151.	558.	0.						
0.	1370.	3105.	633.	-53.	0.						
0.	0.	0.	-328.	-638.	0.						
0.	0.	0.	-2490.	-2195.	0.						
0.	0.	0.	-3912.	-3311.	0.						
0.	0.	0.	-4908.	-3932.	0.						
0.	0.	0.	-5082.	-3739.	0.						
0.	0.	0.	-4066.	-2474.	0.						
0.	0.	0.	-1681.	-106.	0.						
0.	-2750.	-4923.	4641.	2979.	0.						
0.	-1816.	-2683.	5485.	4441.	0.						
0.	-165.	-464.	5179.	4620.	0.						
0.	556.	210.	3408.	3183.	0.						
0.	0.	0.	0.	0.	0.						

TABLE 5.47

SHEAR STRESS TRT ON LAYER K = 4
COMBINED LOADS

0.	0.	0.	0.	0.	0.						
0.	0.	0.	0.	0.	0.						
0.	1079.	1785.	1321.	647.	0.						
0.	1552.	3582.	843.	50.	0.						
0.	0.	0.	21.	-362.	0.						
0.	0.	0.	-2263.	-1987.	0.						
0.	0.	0.	-3730.	-3133.	0.						
0.	0.	0.	-4804.	-3788.	0.						
0.	0.	0.	-5128.	-3644.	0.						
0.	0.	0.	-4265.	-2426.	0.						
0.	0.	0.	-2077.	-115.	0.						
0.	-2988.	-5458.	4686.	2946.	0.						
0.	-2130.	-3256.	5185.	4159.	0.						
0.	-547.	-1101.	4563.	4102.	0.						
0.	234.	-313.	2834.	2686.	0.						
0.	0.	0.	0.	0.	0.						

TABLE 5·48

SHEAR STRESS TRZ ON LAYER K = 1
COMBINED LOADS

0.	0.	0.	0.	0.	0.						
0.	0.	0.	0.	0.	0.						
0.	0.	0.	0.	0.	0.						
0.	0.	0.	0.	0.	0.						
0.	0.	0.	0.	0.	0.						
0.	0.	0.	0.	0.	0.						
0.	0.	0.	0.	0.	0.	0.					
0.	0.	0.	0.	0.	0.	0.					
0.	0.	0.	0.	0.	0.	0.					
0.	0.	0.	0.	0.	0.	0.					
0.	0.	0.	0.	0.	0.	0.	0.				
0.	0.	0.	0.	0.	0.	0.	0.				
0.	0.	0.	0.	0.	0.	0.	0.				
0.	0.	0.	0.	0.	0.	0.	0.				
0.	0.	0.	0.	0.	0.	0.	0.	0.			
0.	0.	0.	0.	0.	0.	0.	0.	0.			
0.	0.	0.	0.	0.	0.	0.	0.	0.			
0.	0.	0.	0.	0.	0.	0.	0.	0.			
0.	0.	0.	0.	0.	0.	0.	0.	0.	0.		
0.	0.	0.	0.	0.	0.	0.	0.	0.	0.		
0.	0.	0.	0.	0.	0.	0.	0.	0.	0.	0.	
0.	0.	0.	0.	0.	0.	0.	0.	0.	0.	0.	
0.	0.	0.	0.	0.	0.	0.	0.	0.	0.	0.	0.
0.	0.	0.	0.	0.	0.	0.	0.	0.	0.	0.	0.

TABLE 5·49

SHEAR STRESS TRZ ON LAYER K = 2
COMBINED LOADS

0.	0.	0.	0.	0.	0.	
0.	0.	0.	0.	0.	0.	
66.	101.	203.	233.	234.	0.	
-123.	68.	740.	496.	305.	0.	
0.	0.	1794.	343.	-7.	0.	
0.	0.	1793.	457.	79.	0.	
0.	0.	1798.	481.	135.	0.	
0.	0.	1651.	422.	137.	0.	
0.	0.	1169.	304.	104.	0.	
0.	0.	312.	170.	53.	0.	
0.	0.	-848.	56.	-32.	0.	
-53.	-474.	-1800.	-438.	-218.	0.	
-428.	-629.	-1240.	-615.	-451.	0.	
-1054.	-980.	-1265.	-1020.	-1003.	0.	
-753.	-565.	-755.	-694.	-819.	0.	
0.	0.	0.	0.	0.	0.	

TABLE 5.50

SHEAR STRESS TRZ ON LAYER K = 3
COMBINED LOADS

0.	0.	0.	0.	0.	0.	
0.	0.	0.	0.	0.	0.	
49.	120.	230.	269.	273.	0.	
-22.	160.	689.	512.	347.	0.	
0.	0.	1718.	463.	63.	0.	
0.	0.	1839.	570.	130.	0.	
0.	0.	1860.	590.	183.	0.	
0.	0.	1671.	516.	180.	0.	
0.	0.	1061.	365.	136.	0.	
0.	0.	62.	191.	66.	0.	
0.	0.	-777.	38.	-53.	0.	
-268.	-380.	-1311.	-496.	-299.	0.	
-558.	-751.	-1369.	-797.	-615.	0.	
-1019.	-1066.	-1402.	-1122.	-1091.	0.	
-784.	-717.	-913.	-783.	-851.	0.	
0.	0.	0.	0.	0.	0.	

TABLE 5·51

SHEAR STRESS TRZ ON LAYER K = 4
COMBINED LOADS

0.	0.	0.	0.	0.	0.	
0.	0.	0.	0.	0.	0.	
22.	80.	139.	165.	170.	0.	
59.	146.	304.	273.	209.	0.	
0.	0.	1046.	331.	65.	0.	
0.	0.	1081.	367.	89.	0.	
0.	0.	1093.	380.	122.	0.	
0.	0.	961.	337.	121.	0.	
0.	0.	509.	241.	93.	0.	
0.	0.	-177.	126.	44.	0.	
0.	0.	-558.	14.	-40.	0.	
-286.	-121.	-188.	-306.	-211.	0.	
-381.	-485.	-832.	-550.	-433.	0.	
-558.	-674.	-896.	-717.	-694.	0.	
-460.	-496.	-608.	-476.	-466.	0.	
0.	0.	0.	0.	0.	0.	

TABLE 5.53

SHEAR STRESS TRZ ON LAYER K = 5
COMBINED LOADS

0.	0.	0.	0.	0.	0.
0.	0.	0.	0.	0.	0.
0.	0.	0.	0.	0.	0.
0.	0.	0.	0.	0.	0.
0.	0.	0.	0.	0.	0.
0.	0.	0.	0.	0.	0.
0.	0.	0.	0.	0.	0.
0.	0.	0.	0.	0.	0.
0.	0.	0.	0.	0.	0.
0.	0.	0.	0.	0.	0.
0.	0.	0.	0.	0.	0.
0.	0.	0.	0.	0.	0.
0.	0.	0.	0.	0.	0.
0.	0.	0.	0.	0.	0.
0.	0.	0.	0.	0.	0.
0.	0.	0.	0.	0.	0.

TABLE 5·54

SHEAR STRESS TZT ON LAYER K = 1
COMBINED LOADS

0.	0.	0.	0.	0.	0.						
0.	0.	0.	0.	0.	0.						
0.	0.	0.	0.	0.	0.						
0.	0.	0.	0.	0.	0.						
0.	0.	0.	0.	0.	0.						
0.	0.	0.	0.	0.	0.						
0.	0.	0.	0.	0.	0.	0.					
0.	0.	0.	0.	0.	0.	0.					
0.	0.	0.	0.	0.	0.	0.					
0.	0.	0.	0.	0.	0.	0.					
0.	0.	0.	0.	0.	0.	0.	0.				
0.	0.	0.	0.	0.	0.	0.	0.				
0.	0.	0.	0.	0.	0.	0.	0.				
0.	0.	0.	0.	0.	0.	0.	0.				
0.	0.	0.	0.	0.	0.	0.	0.	0.			
0.	0.	0.	0.	0.	0.	0.	0.	0.			
0.	0.	0.	0.	0.	0.	0.	0.	0.			
0.	0.	0.	0.	0.	0.	0.	0.	0.			
0.	0.	0.	0.	0.	0.	0.	0.	0.	0.		
0.	0.	0.	0.	0.	0.	0.	0.	0.	0.		
0.	0.	0.	0.	0.	0.	0.	0.	0.	0.		
0.	0.	0.	0.	0.	0.	0.	0.	0.	0.		
0.	0.	0.	0.	0.	0.	0.	0.	0.	0.	0.	
0.	0.	0.	0.	0.	0.	0.	0.	0.	0.	0.	
0.	0.	0.	0.	0.	0.	0.	0.	0.	0.	0.	
0.	0.	0.	0.	0.	0.	0.	0.	0.	0.	0.	
0.	0.	0.	0.	0.	0.	0.	0.	0.	0.	0.	0.
0.	0.	0.	0.	0.	0.	0.	0.	0.	0.	0.	0.

TABLE 5.55

SHEAR STRESS TZT ON LAYER K = 2
COMBINED LOADS

0.	0.	0.	0.	0.	0.	
0.	-96.	-129.	-127.	-77.	0.	
0.	-46.	44.	-113.	-109.	0.	
0.	148.	741.	-508.	-374.	0.	
0.	0.	0.	-211.	-159.	0.	
0.	0.	0.	-211.	-133.	0.	
0.	0.	0.	-236.	-145.	0.	
0.	0.	0.	-216.	-156.	0.	
0.	0.	0.	-161.	-176.	0.	
0.	0.	0.	-199.	-240.	0.	
0.	1008.	-78.	-1263.	-401.	0.	
0.	-166.	127.	-628.	-269.	0.	
0.	-339.	67.	-199.	-92.	0.	
0.	-44.	311.	312.	242.	0.	
0.	1122.	1561.	1835.	1488.	0.	
0.	0.	0.	0.	0.	0.	

TABLE 5.56

SHEAR STRESS TZT ON LAYER K = 3
COMBINED LOADS

0.	0.	0.	0.	0.	0.	
0.	5.	7.	-4.	-7.	0.	
0.	87.	131.	-26.	-60.	0.	
0.	183.	503.	-361.	-299.	0.	
0.	0.	0.	-196.	-163.	0.	
0.	0.	0.	-218.	-154.	0.	
0.	0.	0.	-236.	-168.	0.	
0.	0.	0.	-194.	-180.	0.	
0.	0.	0.	-69.	-200.	0.	
0.	0.	0.	-12.	-273.	0.	
0.	701.	-142.	-938.	-447.	0.	
0.	-46.	119.	-656.	-329.	0.	
0.	-205.	98.	-230.	-116.	0.	
0.	66.	397.	376.	287.	0.	
0.	1109.	1623.	1892.	1500.	0.	
0.	0.	0.	0.	0.	0.	

TABLE 5·57

SHEAR STRESS TZT ON LAYER K = 4
COMBINED LOADS

0.	0.	0.	0.	0.	0.	
0.	100.	137.	119.	66.	0.	
0.	144.	135.	60.	9.	0.	
0.	138.	28.	-47.	-89.	0.	
0.	0.	0.	-94.	-87.	0.	
0.	0.	0.	-125.	-98.	0.	
0.	0.	0.	-136.	-112.	0.	
0.	0.	0.	-101.	-124.	0.	
0.	0.	0.	27.	-141.	0.	
0.	0.	0.	159.	-190.	0.	
0.	221.	-298.	-203.	-289.	0.	
0.	49.	67.	-394.	-229.	0.	
0.	-30.	72.	-163.	-89.	0.	
0.	92.	257.	223.	167.	0.	
0.	631.	960.	1115.	874.	0.	
0.	0.	0.	0.	0.	0.	

TABLE 5.58

SHEAR STRESS TZT ON LAYER K = 5
COMBINED LOADS

0.	0.	0.	0.	0.	0.														
0.	0.	0.	0.	0.	0.														
0.	0.	0.	0.	0.	0.														
0.	0.	0.	0.	0.	0.														
0.	0.	0.	0.	0.	0.														
0.	0.	0.	0.	0.	0.														
0.	0.	0.	0.	0.	0.	0.													
0.	0.	0.	0.	0.	0.	0.													
0.	0.	0.	0.	0.	0.	0.													
0.	0.	0.	0.	0.	0.	0.													
0.	0.	0.	0.	0.	0.	0.	0.												
0.	0.	0.	0.	0.	0.	0.	0.												
0.	0.	0.	0.	0.	0.	0.	0.	0.											
0.	0.	0.	0.	0.	0.	0.	0.	0.											
0.	0.	0.	0.	0.	0.	0.	0.	0.	0.										
0.	0.	0.	0.	0.	0.	0.	0.	0.	0.										
0.	0.	0.	0.	0.	0.	0.	0.	0.	0.	0.									
0.	0.	0.	0.	0.	0.	0.	0.	0.	0.	0.									
0.	0.	0.	0.	0.	0.	0.	0.	0.	0.	0.	0.								
0.	0.	0.	0.	0.	0.	0.	0.	0.	0.	0.	0.								
0.	0.	0.	0.	0.	0.	0.	0.	0.	0.	0.	0.	0.							
0.	0.	0.	0.	0.	0.	0.	0.	0.	0.	0.	0.	0.							
0.	0.	0.	0.	0.	0.	0.	0.	0.	0.	0.	0.	0.	0.						
0.	0.	0.	0.	0.	0.	0.	0.	0.	0.	0.	0.	0.	0.						
0.	0.	0.	0.	0.	0.	0.	0.	0.	0.	0.	0.	0.	0.	0.					
0.	0.	0.	0.	0.	0.	0.	0.	0.	0.	0.	0.	0.	0.	0.					
0.	0.	0.	0.	0.	0.	0.	0.	0.	0.	0.	0.	0.	0.	0.	0.				
0.	0.	0.	0.	0.	0.	0.	0.	0.	0.	0.	0.	0.	0.	0.	0.				
0.	0.	0.	0.	0.	0.	0.	0.	0.	0.	0.	0.	0.	0.	0.	0.	0.			
0.	0.	0.	0.	0.	0.	0.	0.	0.	0.	0.	0.	0.	0.	0.	0.	0.			
0.	0.	0.	0.	0.	0.	0.	0.	0.	0.	0.	0.	0.	0.	0.	0.	0.	0.		
0.	0.	0.	0.	0.	0.	0.	0.	0.	0.	0.	0.	0.	0.	0.	0.	0.	0.		
0.	0.	0.	0.	0.	0.	0.	0.	0.	0.	0.	0.	0.	0.	0.	0.	0.	0.	0.	
0.	0.	0.	0.	0.	0.	0.	0.	0.	0.	0.	0.	0.	0.	0.	0.	0.	0.	0.	
0.	0.	0.	0.	0.	0.	0.	0.	0.	0.	0.	0.	0.	0.	0.	0.	0.	0.	0.	0.
0.	0.	0.	0.	0.	0.	0.	0.	0.	0.	0.	0.	0.	0.	0.	0.	0.	0.	0.	0.

TABLE 5.59

```
*FORTRAN NO97.G. GORDON
      MASTER SIMPLE TENSION MEMBER
      DIMENSION SX(9),UD(10),U(10)
      READ(1,100)E,RO,DELX
      WRITE(2,100)E,RO,DELX
      READ(1,101)DELT,DK
      WRITE(2,101)DELT,DK
C CALCULATE CONSTANTS
      P=500.0
      DRX=DELT/DELX/RO
      DX=DELT/DELX
      D1=1.-DK/2.
      D2=1.+DK/2.
      D3=D1/D2
      D4=DRX/D2
      D5=E*DX
C CALCULATE INITIAL CONDITIONS
      IT=0
      DO 1 I=1,9
      SX(I)=0.
    1 CONTINUE
      DO 2 I=1,10
      UD(I)=0.
      U(I)=0.0
    2 CONTINUE
C CALCULATE VELOCITY
  200 IT=IT+1
      DO 3 I=1,10
      IF(I.EQ.1)GO TO 3
      IF(I.EQ.10)UD(I)=UD(I)*D3+2.*D4*(P-SX(I-1))
      IF(I.EQ.10)U(I)=U(I)+UD(I)*DELT
      IF(I.EQ.10)GO TO 3
      UD(I)=UD(I)*D3+(SX(I)-SX(I-1))*D4
      U(I)=U(I)+UD(I)*DELT
    3 CONTINUE
C CALCULATE STRESS
      DO 4 I=1,9
      SX(I)=SX(I)+D5*(UD(I+1)-UD(I))
    4 CONTINUE
C CALCULATE ENERGY
      SUMSQ=0.
      DO 5 I=1,10
      SUMSQ=SUMSQ+UD(I)*UD(I)
    5 CONTINUE
      WRITE(2,103)IT,SUMSQ,SX
      WRITE(2,104)U
      IF(IT.EQ.100)STOP
      GO TO 200
  100 FORMAT(3E12.4)
  101 FORMAT(2F12.4)
  103 FORMAT(1X,I3,F12.4,2X,10F7.0)
  104 FORMAT(16X,10F10.2)
      END
```

```
*FORTRAN N117,G.GORDON
      MASTER HEAT CONDUCTION
      DIMENSION T(9),U(10)
      TE=500.
      DELX=.50
      DK=.34
      DELT=.30
      WRITE(2,100)DELX,DELT,DK
      D1=DELT/DELX
      D2=DELT/(1.+DK/2.)/DELX
      D3=(1.-DK/2.)/(1.+DK/2.)
C CALCULATE INITIAL CONDITIONS
      DO 10 I=1,9
      T(I)=0.0
   10 CONTINUE
      DO 11 I=1,10
      U(I)=0.0
   11 CONTINUE
      IT=0
  200 IT=IT+1
C CALCULATE U
      DO 1 I=1,10
      IF(I.EQ.1)GO TO 1
      IF(I.EQ.10)U(I)=U(I)*D3+2.*D2*(TE-T(I-1))
      IF(I.EQ.10)GO TO 1
      U(I)=U(I)*D3+D2*(T(I)-T(I-1))
    1 CONTINUE
C CALCULATE TEMPERATURE
      DO 2 I=1,9
      T(I)=T(I)+D1*(U(I+1)-U(I))
    2 CONTINUE
      WRITE(2,101)IT,T
      IF(IT.LT.100)GO TO 200
      STOP
  100 FORMAT(3E12.4)
  101 FORMAT(1X,I5,3X,9F7.0)
      END

END OF SEGMENT, LENGTH   270, NAME  HEATCONDUCTION
```

```
FORTRAN COMPILATION BY #XFAS MK 1D    DATE  21/11/69  TIME  13/08/0


*FORTRAN N118,G. GORDON
      NO TRACE
      MASTER PLATE WITH HOLE POLAR COORDINATES
      DIMENSION SR(19,19),ST(19,19),TRT(19,19),UD(19,19),VD(19,19),
     1S1(19,19),S2(19,19),TMAX(19,19),PHI(19,19)
      CALL ITIME(N1)
      NR=19
      NT=19
      E=.30E08
      PR=.300
      RO=.783E-3
      DELR=.0625
      DELTH=3.14159/36.0
      WRITE(2,100)E,PR,RO,DELR,DELTH
      SX=1000.
      READ(1,108)DK,DELT
  300 CONTINUE
      WRITE(2,108)DK,DELT
      D1=(1.-DK/2.)/(1.+DK/2.)
      D2=DELT/RO/(1.+DK/2.)
      D3=D2/DELR
      D4=D2/DELTH
      D5=DELT*E/(1.-PR*PR)
      D6=D5/DELR
      D7=D5/DELTH
      D8=D5*PR
      D9=D8/DELR
      D10=D8/DELTH
      D11=DELT*E/(1.+PR)/2.
      D12=D11/DELR
      D13=D11/DELTH
C INITIAL CONDITIONS
      IT=0
      NIT=100
      DO 1 J=1,NT
      DO 1 I=1,NR
      UD(I,J)=0.
      VD(I,J)=0.
      SR(I,J)=0.
      ST(I,J)=0.
      TRT(I,J)=0.
      S1(I,J)=0.
      S2(I,J)=0.
      TMAX(I,J)=0.
      PHI(I,J)=0.
    1 CONTINUE
C CALCULATE VELOCITIES
  200 IT=IT+1
      DO 2 J=1,NT
      DO 2 I=1,NR
      IF(I.LE.3)GO TO 2
      IF(J.EQ.NT)GO TO 2
      R=DELR*(I-1)
      THETA=DELTH*(J-1)+DELTH/2.
      IF(I.EQ.NR)P=SX*(COS(THETA))**2
```

```
      IF(I.EQ.NR)Q=.5*(3.*ST(I-1,J)-ST(I-2,J))
      IF(I.EQ.NR)UD(I,J)=UD(I,J)*D1-2.*D3*SR(I-1,J)+2.*P*D3
     1+(TRT(I,J+1)-TRT(I,J))*D4/R
     1+(P-Q)*D2/R
      IF(I.EQ.NR)GO TO 2
      IF(I.EQ.4)Q=ST(I,J)-.5*(ST(I+1,J)-ST(I,J))
      IF(I.EQ.4)UD(I,J)=UD(I,J)*D1+2.*D3*SR(I,J)-Q/R*D2
      IF(I.EQ.4)GO TO 2
      UD(I,J)=UD(I,J)*D1+D3*(SR(I,J)-SR(I-1,J))
     1+D4*(TRT(I,J+1)-TRT(I,J))/R+D2*(SR(I,J)+SR(I-1,J)
     1-ST(I,J)-ST(I-1,J))/2./R
    2 CONTINUE
      DO 3 J=1,NT
      DO 3 I=1,NR
      IF(J.EQ.1.OR.J.EQ.NT.OR.I.EQ.NR)GO TO 3
      IF(I.LE.3)GO TO 3
      R=DELR*(I-1)+DELR/2.
      VD(I,J)=VD(I,J)*D1+D4*(ST(I,J)-ST(I,J-1))/R
     1+D3*(TRT(I+1,J)-TRT(I,J))+D2*(TRT(I+1,J)+TRT(I,J))/R
    3 CONTINUE
      SUMSQ=0.
      DO 7 J=1,NT
      DO 7 I=1,NR
      SUMSQ=SUMSQ+UD(I,J)*UD(I,J)+VD(I,J)*VD(I,J)
    7 CONTINUE
C CALCULATE STRESSES
      DO 4 J=1,NT
      DO 4 I=1,NR
      R=DELR*(I-1)+DELR/2.
      IF(I.EQ.NR.OR.J.EQ.NT)GO TO 4
      IF(I.LE.3)GO TO 4
      SR(I,J)=SR(I,J)+D6*(UD(I+1,J)-UD(I,J))
     1+D8*(UD(I+1,J)+UD(I,J))/2./R+D10*(VD(I,J+1)-VD(I,J))/R
    4 CONTINUE
      DO 5 J=1,NT
      DO 5 I=1,NR
      R=DELR*(I-1)+DELR/2.
      IF(I.EQ.NR.OR.J.EQ.NT)GO TO 5
      IF(I.LE.3)GO TO 5
      ST(I,J)=ST(I,J)+D5*(UD(I+1,J)+UD(I,J))/2./R
     1+D7*(VD(I,J+1)-VD(I,J))/R+D9*(UD(I+1,J)-UD(I,J))
    5 CONTINUE
      DO 6 J=1,NT
      DO 6 I=1,NR
      IF(I.LE.4)GO TO 6
      IF(J.EQ.1.OR.J.EQ.NT)GO TO 6
      THETA=DELTH*(J-1)
      IF(I.EQ.NR)TRT(I,J)=-SX*SIN(THETA)*COS(THETA)
      IF(I.EQ.NR)GO TO 6
      R=DELR*(I-1)
      TRT(I,J)=TRT(I,J)+D13*(UD(I,J)-UD(I,J-1))/R
     1+D12*(VD(I,J)-VD(I-1,J))
     1-D11*(VD(I,J)+VD(I-1,J))/2./R
    6 CONTINUE
      WRITE(2,102)IT,SUMSQ,SR(5,5),ST(5,5),TRT(5,5)
      IF(IT.LT.NIT)GO TO 200
      NIT=NIT+100
      WRITE(2,104)
      WRITE(2,107)SR
      WRITE(2,105)
```

```
      WRITE(2,107)ST
      WRITE(2,106)
      WRITE(2,107)TRT
      IF(IT.LT.500)GO TO 200
      CALL ITIME(N2)
      ITIM=N2-N1
      WRITE(2,113)ITIM
      STOP
  100 FORMAT(5E12.4)
  102 FORMAT(1X,I5,3X,E12.4,3F12.2)
  104 FORMAT(///,29H   STRESS IN RADIAL DIRECTION,/)
  105 FORMAT(///,33H   STRESS IN TANGENTIAL DIRECTION,/)
  106 FORMAT(///,15H   SHEAR STRESS,/)
  107 FORMAT(1X,13F7.0)
  108 FORMAT(2E12.4)
  113 FORMAT(1X,7H TIME  ,I10)
      END
```

END OF SEGMENT, LENGTH 1163, NAME PLATEWITHHOLEPOLARCOORDINATES

```
      MASTER FLAT PLATE BENDING
      DIMENSION SR(16,6),ST(16,6),SZ(16,6),TRZ(16,6),
     1UD(16,6),WD(16,6),U(16,6),W(16,6)
      READ(1,100)P
      WRITE(2,100)P
      READ(1,100)P1
      WRITE(2,100)P1
      DELR=.1333
      DELZ=.06250
      DELT=.2500E-6
      DKZ=.010
      DKR=.010
      CLAM=17.3E06
      CMU=11.5E06
      RP=.783E-3
      RA=.783E-3
      NR=16
      NZ=6
      D1=(1.-DKR/2.)/(1.+DKR/2.)
      D2=(1.-DKZ/2.)/(1.+DKZ/2.)
      D3=DELT/RR/(1.+DKR/2.)
      D4=D3/DELR
      D5=D5/DELZ
      D6=DELT/RA/(1.+DKZ/2.)
      D7=D6/DELR
      D8=D6/DELZ
      D9=(CLAM+2.*CMU)*DELT
      D10=D9/DELR
      D11=D9/DELZ
      D12=CLAM*DELT
      D13=D12/DELR
      D14=D12/DELZ
      D15=CMU*DELT
      D16=D15/DELR
      D17=D15/DELZ
C INITIAL CONDITIONS
      IT=0
      NIT=100
      DO 1 K=1,NZ
      DO 1 I=1,NR
      U(I,K)=0.0
      W(I,K)=0.0
      UD(I,K)=0.0
      WD(I,K)=0.0
      SR(I,K)=0.0
      ST(I,K)=0.0
      SZ(I,K)=0.0
      TRZ(I,K)=0.
```

```
    1 CONTINUE
  200 IT=IT+1
      SUMSQ=0.0
      UDSQ=0.0
      WDSQ=0.0
C CALCULATE VELOCITY AND DISPLACEMENT IN RADIAL DIRECTION
      DO 2 K=1,NZ
      DO 2 I=1,NR
      IF(I.EQ.1)GO TO 2
      IF(K.EQ.NZ)GO TO 2
      R=DELR*(I-1)
      IF(I.EQ.NR)UD(I,K)=UD(I,K)*D1-2.*SR(I-1,K)*D4+2.*D4*P
     1-(3.*ST(I-1,K)-ST(I-2,K))/2./R*D3+P/R*D3
      IF(I.EQ.NR)GO TO 3
      UD(I,K)=UD(I,K)*D1+D4*(SR(I,K)-SR(I-1,K))
     1+D5*(TRZ(I,K+1)-TRZ(I,K))+D3*(SR(I,K)+SR(I-1,K))/2./R
     1-D3*(ST(I,K)+ST(I-1,K))/2./R
    3 U(I,K)=U(I,K)+UD(I,K)*DELT
      UDSQ=UDSQ+UD(I,K)*UD(I,K)
    2 CONTINUE
C CALCULATE AXIAL VELOCITY AND DISPLACEMENT
      DO 4 K=1,NZ
      DO 4 I=1,NR
      IF(I.EQ.NR)GO TO 4
      R=DELR*(I-1)+DELR/2.
      IF(I.EQ.15.AND.K.EQ.1)GO TO 4
      IF(I.EQ.4.AND.K.EQ.NZ)WD(I,K)=WD(I,K)*D2
     1-2.*D8*SZ(I,K-1)+2.*P1*D8
      IF(I.EQ.4.AND.K.EQ.NZ)GO TO 5
      IF(K.EQ.1)WD(I,K)=WD(I,K)*D2+2.*SZ(I,K)*D8
      IF(K.EQ.1)GO TO 5
      IF(K.EQ.NZ)WD(I,K)=WD(I,K)*D2-2.*D8*SZ(I,K-1)
      IF(K.EQ.NZ)GO TO 5
      WD(I,K)=WD(I,K)*D2+D7*(TRZ(I+1,K)-TRZ(I,K))
     1+D8*(SZ(I,K)-SZ(I,K-1))+D6*(TRZ(I+1,K)+TRZ(I,K))/2./R
    5 W(I,K)=W(I,K)+WD(I,K)*DELT
      WDSQ=WDSQ+WD(I,K)*WD(I,K)
    4 CONTINUE
      SUMSQ=UDSQ+WDSQ
C CALCULATE RADIAL STRESS
      DO 6 K=1,NZ
      DO 6 I=1,NR
      IF(I.EQ.NR.OR.K.EQ.NZ)GO TO 6
      R=DELR*(I-1)+DELR/2.
      SR(I,K)=SR(I,K)+D10*(UD(I+1,K)-UD(I,K))
     1+D12*(UD(I+1,K)+UD(I,K))/2./R
     1+D14*(WD(I,K+1)-WD(I,K))
    6 CONTINUE
```

```
C CALCULATE HOOP STRESS
      DO 7 K=1,NZ
      DO 7 I=1,NR
      IF(I.EQ.NR.OR.K.EQ.NZ)GO TO 7
      R=DELR*(I-1)+DELR/2.
      ST(I,K)=ST(I,K)+D9*(UD(I+1,K)+UD(I,K))/2./R
     1+D13*(UD(I+1,K)-UD(I,K))+D14*(WD(I,K+1)-WD(I,K))
    7 CONTINUE
C CALCULATE SHEAR STRESS
      DO 8 K=1,NZ
      DO 8 I=1,NR
      IF(I.EQ.1.OR.I.EQ.NR.OR.K.EQ.1.OR.K.EQ.NZ)GO TO 8
      TRZ(I,K)=TRZ(I,K)+D17*(UD(I,K)-UD(I,K-1))
     1+D16*(WD(I,K)-WD(I-1,K))
    8 CONTINUE
C CALCULATE AXIAL STRESS
      DO 9 K=1,NZ
      DO 9 I=1,NR
      IF(I.EQ.NR.OR.K.EQ.NZ)GO TO 9
      R=DELR*(I-1)+DELR/2.
      SZ(I,K)=SZ(I,K)+D13*(UD(I+1,K)-UD(I,K))
     1+D12*(UD(I+1,K)+UD(I,K))/2./R
     1+D11*(WD(I,K+1)-WD(I,K))
    9 CONTINUE
      WRITE(2,101)IT,SUMSQ,UDSQ,WDSQ,W(9,1),SR(5,1),ST(5,1),TRZ(5,3)
      IF(IT-NIT)200,10,10
   10 NIT=NIT+100
      WRITE(2,102)
      WRITE(2,110)SR
      WRITE(2,103)
      WRITE(2,110)ST
      WRITE(2,104)
      WRITE(2,110)SZ
      WRITE(2,105)
      WRITE(2,110)TRZ
      WRITE(2,106)
      WRITE(2,108)U
      WRITE(2,107)
      WRITE(2,108)W
      IF(IT.EQ.2000)STOP
      GO TO 200
  100 FORMAT(E12.4)
  101 FORMAT(I5,7E12.4)
  102 FORMAT(//,16H   RADIAL STRESS,//)
  103 FORMAT(//,20H   TANGENTIAL STRESS,//)
  104 FORMAT(//,15H   AXIAL STRESS,//)
  105 FORMAT(//,15H   SHEAR STRESS,//)
  106 FORMAT(//,22H   RADIAL DISPLACEMENT,//)
  107 FORMAT(//,21H   AXIAL DISPLACEMENT,//)
  108 FORMAT(1X,9E12.4)
  110 FORMAT(1X,16F7.1)
      END

END OF SEGMENT, LENGTH  1269, NAME  FLATPLATEBENDING
```

```
      MASTER FLAME PLATE BENDING SIMPLE HOLE
      DIMENSION SR(15,5,4),ST(15,5,4),SZ(15,5,4),
     1TRT(16,6,5),TRZ(16,6,5),TZT(16,6,5),
     1UD(16,5,4),VD(15,6,4),WD(15,5,5),
     1W(15,5)
      CALL ITIME (N1)
      NR=16
      NT=6
      NZ=5
      DKR=.0038
      DKT=.0038
      DKZ=.0038
      DELR=.630
      DELTH=3.14159/20.0
      DELZ=.375
      CLAM=17.3E06
      CMU=11.5E06
      AL=.65E-5
      RR=.732E-3
      RT=.732E-3
      RA=.732E-3
      WRITE(2,100)CLAM,CMU,RR,RT,RA,AL
      READ(1,116)DELT
  501 CONTINUE
      WRITE(2,101)DKR,DKT,DKZ,DELR,DELTH,DELZ,DELT
      WA=3.14159/4.0*5.25*100.0
      P=WA/(6.28*1.5*DELR*DELR)
      D1=(1.-DKR/2.)/(1.+DKR/2.)
      D2=(1.-DKT/2.)/(1.+DKT/2.)
      D3=(1.-DKZ/2.)/(1.+DKZ/2.)
      D4=DELT/RR/(1.+DKR/2.)
      D5=D4/DELR
      D6=D4/DELTH
      D7=D4/DELZ
      D8=DELT/RT/(1.+DKT/2.)
      D9=D8/DELR
      D10=D8/DELTH
      D11=D8/DELZ
      D12=DELT/RA/(1.+DKZ/2.)
      D13=D12/DELR
      D14=D12/DELTH
      D15=D12/DELZ
      D16=(CLAM+2.*CMU)*DELT
      D17=D16/DELR
      D18=D16/DELTH
      D19=D16/DELZ
      D20=CLAM*DELT
      D21=D20/DELR
      D22=D20/DELTH
      D23=D20/DELZ
      D24=CMU*DELT
      D25=D24/DELR
      D26=D24/DELTH
      D27=D24/DELZ
C INITIAL CONDITIONS
      M=1
      IF(M)30,30,31
   30 CONTINUE
```

```
      DO 1 K=1,NZ-1
      DO 1 J=1,NT-1
      DO 1 I=1,NR-1
      SR(I,J,K)=0.0
      ST(I,J,K)=0.0
      SZ(I,J,K)=0.0
    1 CONTINUE
      DO 2 K=1,NZ
      DO 2 J=1,NT
      DO 2 I=1,NR
      TRT(I,J,K)=0.
      TRZ(I,J,K)=0.
      TZT(I,J,K)=0.
    2 CONTINUE
      DO 22 K=1,NZ
      DO 22 J=1,NT-1
      DO 22 I=1,NR-1
      WD(I,J,K)=0.
      W(I,J)=0.0
   22 CONTINUE
      DO 23 K=1,NZ-1
      DO 23 J=1,NT-1
      DO 23 I=1,NR
      UD(I,J,K)=0.
   23 CONTINUE
      DO 24 K=1,NZ-1
      DO 24 J=1,NT
       DO 24 I=1,NR-1
      VD(I,J,K)=0.
   24 CONTINUE
      IT=0
      NIT=500
      GO TO 32
   31 CONTINUE
      REWIND 3
      READ(3)SR
      READ(3)ST
      READ(3)SZ
      READ(3)TRT
      READ(3)TRZ
      READ(3)TZT
      READ(3)UD
      READ(3)VD
      READ(3)WD
      READ(3)W
      READ(3)IT
      READ(3)NIT
      REWIND 3
   32 CONTINUE
  200 IT=IT+1
      SUMSQ=0.
      UDSQ=0.
      VDSQ=0.
      WDSQ=0.
C CALCULATE VELOCITY IN RADIAL DIRECTION
      DO 4 K=1,NZ-1
      DO 4 J=1,NT-1
      DO 4 I=1,NR
      IF(I.EQ.1)GO TO 4
      IF(I.LE.10.AND.I.GE.6.AND.J.LE.2)GO TO 4
      R=DELR*(I-1)
      IF(I.EQ.2)GO TO 45
      IF(I.EQ.11.AND.J.LE.2)GO TO 45
```

```
      IF(I.EQ.NR)GO TO 46
      IF(I.EQ.5.AND.J.LE.2)GO TO 46
      UD(I,J,K)=UD(I,J,K)*D1+D5*(SR(I,J,K)-SR(I-1,J,K))
     1+D6*(TRT(I,J+1,K)-TRT(I,J,K))/R+D7*(TRZ(I,J,K+1)-TRZ(I,J,K))
     1+D4*(SR(I,J,K)+SR(I-1,J,K)-(ST(I,J,K)+ST(I-1,J,K)))/2./R
      GO TO 44
   45 UD(I,J,K)=UD(I,J,K)*D1+2.*D5*SR(I,J,K)
     1-.5*(3.*ST(I,J,K)-ST(I+1,J,K))*D4/R
      GO TO 44
   46 UD(I,J,K)=UD(I,J,K)*D1-2.*D5*SR(I-1,J,K)
     1-.5*(3.*ST(I-1,J,K)-ST(I-2,J,K))*D4/R
   44 UDSQ=UDSQ+UD(I,J,K)*UD(I,J,K)
    4 CONTINUE
C CALCULATE VELOCITY IN TANGENTIAL DIRECTION
      DO 6 K=1,NZ-1
      DO 6 J=1,NT
      DO 6 I=1,NR-1
      IF(J.EQ.1.OR.J.EQ.NT)GO TO 6
      IF(I.EQ.1)GO TO 6
      IF(I.LE.10.AND.I.GE.5.AND.J.EQ.2)GO TO 6
      R=DELR*(I-1)+DELR/2.
      IF(I.LE.10.AND.I.GE.5.AND.J.EQ.3)GO TO 67
      VD(I,J,K)=VD(I,J,K)*D2+D9*(TRT(I+1,J,K)-TRT(I,J,K))
     1+D10*(ST(I,J,K)-ST(I,J-1,K))/R+D11*(TZT(I,J,K+1)-TZT(I,J,K))
     1+D8*(TRT(I+1,J,K)+TRT(I,J,K))/R
      GO TO 66
   67 VD(I,J,K)=VD(I,J,K)*D2+2.*D10*ST(I,J,K)/R
   66 VDSQ=VDSQ+VD(I,J,K)*VD(I,J,K)
    6 CONTINUE
C CALCULATE VELOCITY IN AXIAL DIRECTION
      DO 8 K=1,NZ
      DO 8 J=1,NT-1
      DO 8 I=1,NR-1
      IF(I.EQ.1)GO TO 8
      IF(I.LE.10.AND.I.GE.5.AND.J.LE.2)GO TO 8
      IF(I.EQ.14.AND.K.EQ.NZ)GO TO 8
      IF(I.EQ.2.AND.K.EQ.1)WD(I,J,K)=WD(I,J,K)*D3+2.*D15*(SZ(I,J,K)-P
      IF(I.EQ.2.AND.K.EQ.1)GO TO 88
      IF(K.EQ.1)WD(I,J,K)=WD(I,J,K)*D3+2.*SZ(I,J,K)*D15
      IF(K.EQ.1)GO TO 88
      IF(K.EQ.NZ)WD(I,J,K)=WD(I,J,K)*D3-2.*SZ(I,J,K-1)*D15
      IF(K.EQ.NZ)GO TO 89
      R=DELR*(I-1)+DELR/2.
      WD(I,J,K)=WD(I,J,K)*D3+D13*(TRZ(I+1,J,K)-TRZ(I,J,K))
     1+D14*(TZT(I,J+1,K)-TZT(I,J,K))/R+D15*(SZ(I,J,K)-SZ(I,J,K-1))
     1+D12*(TRZ(I+1,J,K)+TRZ(I,J,K))/2./R
      GO TO 89
   88 W(I,J)=W(I,J)+WD(I,J,K)*DELT
   89 WDSQ=WDSQ+WD(I,J,K)*WD(I,J,K)
    8 CONTINUE
      SUMSQ=UDSQ+VDSQ+WDSQ
C CALCULATE NORMAL STRESSES
      DO 10 K=1,NZ-1
      DO 10 J=1,NT-1
      DO 10 I=1,NR-1
      IF(I.EQ.1)GO TO 10
      IF(I.LE.10.AND.I.GE.5.AND.J.LE.2)GO TO 10
      R=DELR*(I-1)+DELR/2.
C CALCULATE RADIAL STRESS
      SR(I,J,K)=SR(I,J,K)+D17*(UD(I+1,J,K)-UD(I,J,K))
     1+D20*(UD(I+1,J,K)+UD(I,J,K))/2./R
     1+D22*(VD(I,J+1,K)-VD(I,J,K))/R+D23*(WD(I,J,K+1)-WD(I,J,K))
C CALCULATE TANGENTIAL STRESS
```

```
      ST(I,J,K)=ST(I,J,K)+D21*(UD(I+1,J,K)-UD(I,J,K))
     1+D18*(VD(I,J+1,K)-VD(I,J,K))/R+D23*(WD(I,J,K+1)-WD(I,J,K))
     1+D16*(UD(I+1,J,K)+UD(I,J,K))/2./R
C CALCULATE AXIAL STRESS
      SZ(I,J,K)=SZ(I,J,K)+D21*(UD(I+1,J,K)-UD(I,J,K))
     1+D20*(UD(I+1,J,K)+UD(I,J,K))/2./R
     1+D22*(VD(I,J+1,K)-VD(I,J,K))/R+D19*(WD(I,J,K+1)-WD(I,J,K))
   10 CONTINUE
C CALCULATE SHEAR STRESS ON RZ PLANE TRT
      DO 16 K=1,NZ
      DO 16 J=1,NT
      DO 16 I=1,NR
      IF(I.EQ.2)GO TO 16
      IF(I.EQ.1.OR.I.EQ.NR.OR.J.EQ.1.OR.J.EQ.NT.OR.K.EQ.NZ)GO TO 16
      IF(I.LE.11.AND.I.GE.5.AND.J.LE.3)GO TO 16
      R=DELR*(I-1)
      TRT(I,J,K)=TRT(I,J,K)+D26*(UD(I,J,K)-UD(I,J-1,K))/R
     1-D24*(VD(I,J,K)+VD(I-1,J,K))/2./R+D25*(VD(I,J,K)-VD(I-1,J,K))
   16 CONTINUE
C CALCULATE SHEAR STRESS TRZ
      DO 18 K=1,NZ
      DO 18 J=1,NT
      DO 18 I=1,NR
      IF(I.EQ.2)GO TO 18
      IF(I.EQ.1.OR.I.EQ.NR.OR.K.EQ.1.OR.K.EQ.NZ.OR.J.EQ.NT)GO TO 18
      IF(I.LE.11.AND.I.GE.5.AND.J.LE.2)GO TO 18
      TRZ(I,J,K)=TRZ(I,J,K)+D27*(UD(I,J,K)-UD(I,J,K-1))
     1+D25*(WD(I,J,K)-WD(I-1,J,K))
   18 CONTINUE
C CALCULATE TZT
      DO 20 K=1,NZ
      DO 20 J=1,NT
      DO 20 I=1,NR
      IF(I.EQ.1)GO TO 20
      IF(K.EQ.1.OR.K.EQ.NZ.OR.I.EQ.NR.OR.J.EQ.1.OR.J.EQ.NT)GO TO 20
      IF(I.LE.10.AND.I.GE.5.AND.J.LE.3)GO TO 20
      R=DELR*(I-1)+DELR/2.
      TZT(I,J,K)=TZT(I,J,K)+D27*(VD(I,J,K)-VD(I,J,K-1))
     1+D26*(WD(I,J,K)-WD(I,J-1,K))/R
   20 CONTINUE
      WRITE(2,102)IT,SUMSQ,UDSQ,VDSQ,WDSQ,W(2,3),SR(5,4,1),
     1ST(5,4,1),SZ(5,4,1),TRT(5,4,1)
      IF(IT-NIT)200,21,21
   21 NIT=NIT+500
      WRITE(2,103)
      WRITE(2,115)SR
      WRITE(2,104)
      WRITE(2,115)ST
      WRITE(2,105)
      WRITE(2,115)SZ
      WRITE(2,106)
      WRITE(2,118)TRT
      WRITE(2,107)
      WRITE(2,118)TRZ
      WRITE(2,108)
      WRITE(2,118)TZT
      WRITE(2,111)
      WRITE(2,115)W
      REWIND 4
      WRITE(4)SR
      WRITE(4)ST
      WRITE(4)SZ
```

```
      WRITE(4)TRT
      WRITE(4)TRZ
      WRITE(4)TZT
      WRITE(4)UD
      WRITE(4)VD
      WRITE(4)WD
      WRITE(4)W
      WRITE(4)TT
      WRITE(4)NIT
      REWIND 4
      CALL ITIME (N2)
      ITIM=N2-N1
      WRITE(2,119)ITIM
      STOP
  100 FORMAT(1X,6E12.4,/)
  101 FORMAT(7F12.3)
  102 FORMAT(I5,2X,9E12.3)
  103 FORMAT(///.16H   RADIAL STRESS,/)
  104 FORMAT(///.20H   TANGENTIAL STRESS,/)
  105 FORMAT(///.15H   AXIAL STRESS,/)
  106 FORMAT(///.23H   SHEAR STRESS R-THETA,/)
  107 FORMAT(///.19H   SHEAR STRESS R-Z,/)
  108 FORMAT(///.23H   SHEAR STRESS Z-THETA,/)
  111 FORMAT(///.21H   AXIAL DISPLACEMENT,/)
  115 FORMAT(1X,9E12.4)
  116 FORMAT(E12.4)
  118 FORMAT(1X,9E12.4)
  119 FORMAT(//,2X,7H  TIME ,I6)
      END
```

NT. LENGTH 2510. NAME FLAMEPLATEBENDINGSIMPLEHOLE

```
      MASTER FLAME PLATE TEMPERATURE
      DIMENSION T(15,5,4),SR(15,5,4),U(16,5,4),V(15,6,4),W(15,5,5),
     1TRUS(15),TS(15,10)
      NR=16
      NT=6
      NZ=5
      TR=0.0
      TH=0.0
      READ(1,105)TRUS
      WRITE(2,105)TRUS
      DK=.050
      DELR=.630
      DELTH=3.14159/20.0
      DELZ=.3750
      READ(1,103)DELT
      WRITE(2,100)DELR,DELTH,DELZ,DK,DELT
      E=30.E06
      AL=.65E-5
      PR=.3
      TSC=-E*AL/(1.-2.*PR)
      D1=(1.-DK/2.)/(1.+DK/2.)
      D2=DELT/DELR/(1.+DK/2.)
      D3=DELT/DELTH/(1.+DK/2.)
      D4=DELT/DELZ/(1.+DK/2.)
      D5=DELT/DELR
      D6=DELT/DELTH
      D7=DELT/DELZ
C INITIAL CONDITIONS
      CALL ITIME(N1)
      IT=0.
      NIT=100
      DO 1 K=1,NZ-1
      DO 1 J=1,NT-1
      DO 1 I=1,NR-1
      T(I,J,K)=0.0
    1 CONTINUE
      DO 2 K=1,NZ-1
      DO 2 J=1,NT-1
      DO 2 I=1,NR-1
      SR(I,J,K)=0.0
    2 CONTINUE
      DO 3 K=1,NZ-1
      DO 3 J=1,NT-1
      DO 3 I=1,NR
      U(I,J,K)=0
    3 CONTINUE
      DO 4 K=1,NZ-1
      DO 4 J=1,NT
```

```
      DO 4 I=1,NR-1
      V(I,J,K)=0.
    4 CONTINUE
      DO 5 K=1,NZ
      DO 5 J=1,NT-1
      DO 5 I=1,NR-1
      W(I,J,K)=0
    5 CONTINUE
  200 IT=IT+1
C CALCULATE U
      DO 6 K=1,NZ-1
      DO 6 J=1,NT-1
      DO 6 I=1,NR
      R=DELR*(I-1)
      IF(I.EQ.1)GO TO 6
      IF(I.EQ.2)U(I,J,K)=U(I,J,K)*D1+2.*R*D2*(T(I,J,K)-TW)
      IF(I.EQ.2)GO TO 6
      IF(I.EQ.NR)U(I,J,K)=U(I,J,K)*D1+2.*R*D2*(TR-T(I-1,J,K))
      IF(I.EQ.NR)GO TO 6
      IF(I.LE.10 AND.I.GE 6.AND.J.LE.2)GO TO 6
      IF(I.EQ.11 AND.J.LE 2)GO TO 66
      IF(I.EQ.5.AND.J.LE.2)GO TO 67
   61 U(I,J,K)=U(I,J,K)*D1+D2*R*(T(I,J,K)-T(I-1,J,K))
      GO TO 6
   66 U(I,J,K)=U(I,J,K)*D1+D2*R*2.*T(I,J,K)
      GO TO 6
   67 U(I,J,K)=U(I,J,K)*D1-D2*2.*R*T(I-1,J,K)
    6 CONTINUE
C CALCULATE V
      DO 7 K=1,NZ-1
      DO 7 J=1,NT
      DO 7 I=1,NR-1
      IF(J.EQ.NT)GO TO 7
      IF(I.EQ.1)GO TO 7
      IF(I.LE.10.AND.I.GE.5.AND.J.LE.2)GO TO 7
      R=DELR*(I-1)+DELR/2.
      IF(J.EQ.1)GO TO 77
      IF(I.LE.10 AND.I.GE.5.AND.J.EQ.3)GO TO 77
   71 V(I,J,K)=V(I,J,K)*D1+D3*(T(I,J,K)-T(I,J-1,K))/R
      GO TO 7
   77 V(I,J,K)=V(I,J,K)*D1+2.*D3*T(I,J,K)/R
    7 CONTINUE
C CALCULATE W
      DO 8 K=1,NZ
      DO 8 J=1,NT-1
      DO 8 I=1,NR-1
      R=DELR*(I-1)+DELR/2.
      IF(K.EQ.NZ)GO TO 8
```

```
      IF(I.EQ.1)GO TO 8
      IF(I.LE.10 AND.I.GE.5.AND.J.LE.2)GO TO 8
      TS(I,J)=(TRUS(I)-260.)/(R*(.785-DELTH))
     1*(DELTH*(J-1)+DELTH/2.)*R
      IF(K.EQ.1)W(I,J,K)=W(I,J,K)*D1+2.*D4*R*(T(I,J,K)-TS(I,J))
      IF(K.EQ.1)GO TO 8
   81 W(I,J,K)=W(I,J,K)*D1+D4*R*(T(I,J,K)-T(I,J,K-1))
    8 CONTINUE
      DO 10 K=1,NZ-1
      DO 10 J=1,NT-1
      DO 10 I=1,NR-1
      IF(I.EQ.1)GO TO 10
      R=DELR*(I-1)+DELR/2.
      IF(I.LE.10 AND.I.GE.5.AND.J.LE.2)GO TO 10
   11 T(I,J,K)=T(I,J,K)+D5*(U(I+1,J,K)-U(I,J,K))/R
     1+D6*(V(I,J+1,K)-V(I,J,K))/R
     1+D7*(W(I,J,K+1)-W(I,J,K))/R
   10 CONTINUE
      WRITE(2,101)IT,T(12,7,1)
      IF(IT-NIT)200,9,9
    9 NIT=NIT+100
      WRITE(2,104)
      WRITE(2,102)T
      IF(IT.EQ.300)GO TO 300
      GO TO 200
  300 DO 12 K=1,NZ-1
      DO 12 J=1,NT-1
      DO 12 I=1,NR-1
      SR(I,J,K)=T(I,J,K)*TSC
   12 CONTINUE
      REWIND 4
      WRITE(4)SR
      REWIND 4
      CALL ITIME(N2)
      NTIM=N2-N1
      WRITE(2,301)NTIM
      STOP
  100 FORMAT(1X,5E12.4)
  101 FORMAT(1X,I5,5X,E12.4)
  102 FORMAT(1X,15F7.1)
  103 FORMAT(E12.4)
  104 FORMAT(//,14H    TEMPERATURE,//)
  105 FORMAT(15F5.0)
  301 FORMAT(//,6H TIME ,I10)
      END
```

LENGTH 1203, NAME FLAMEPLATETEMPERATURE

```
      MASTER FLAME PLATE THERMAL STRESS
      DIMENSION SR(15,5,4),ST(15,5,4),SZ(15,5,4),
     1TRT(16,6,5),TRZ(16,6,5),TZT(16,6,5),
     1UD(16,5,4),VD(15,6,4),WD(15,5,5),
     1W(15,5)
      CALL ITIME (N1)
      NR=16
      NT=6
      NZ=5
      DKR=.0037
      DKT=.0037
      DKZ=.0037
      DELR=.630
      DELTH=3.14159/20.0
      DELZ=.375
      CLAM=17.3E06
      CMU=11.5E06
      AL=.65E-5
      RR=.732E-3
      RT=.732E-3
      RA=.732E-3
      WRITE(2,100)CLAM,CMU,RR,RT,RA,AL
      READ(1,116)DELT
      WRITE(2,101)DKR,DKT,DKZ,DELR,DELTH,DELZ,DELT
      P=0.0
      D1=(1.-DKR/2.)/(1.+DKR/2.)
      D2=(1.-DKT/2.)/(1.+DKT/2.)
      D3=(1.-DKZ/2.)/(1.+DKZ/2.)
      D4=DELT/RR/(1.+DKR/2.)
      D5=D4/DELR
      D6=D4/DELTH
      D7=D4/DELZ
      D8=DELT/RT/(1.+DKT/2.)
      D9=D8/DELR
      D10=D8/DELTH
      D11=D8/DELZ
      D12=DELT/RA/(1.+DKZ/2.)
      D13=D12/DELR
      D14=D12/DELTH
      D15=D12/DELZ
      D16=(CLAM+2.*CMU)*DELT
      D17=D16/DELR
      D18=D16/DELTH
      D19=D16/DELZ
      D20=CLAM*DELT
      D21=D20/DELR
      D22=D20/DELTH
      D23=D20/DELZ
      D24=CMU*DELT
      D25=D24/DELR
      D26=D24/DELTH
      D27=D24/DELZ
C INITIAL CONDITIONS
      M=1
      IF(M)30,30,31
   30 CONTINUE
      REWIND 3
      READ(3)SR
      REWIND 3
      WRITE(2,115)SR
```

```
      DO 1 K=1,NZ-1
      DO 1 J=1,NT-1
      DO 1 I=1,NR-1
      ST(I,J,K)=SR(I,J,K)
      SZ(I,J,K)=SR(I,J,K)
    1 CONTINUE
      DO 2 K=1,NZ
      DO 2 J=1,NT
      DO 2 I=1,NR
      TRT(I,J,K)=0.
      TRZ(I,J,K)=0.
      TZT(I,J,K)=0.
    2 CONTINUE
      DO 22 K=1,NZ
      DO 22 J=1,NT-1
      DO 22 I=1,NR-1
      WD(I,J,K)=0.
      W(I,J)=0.0
   22 CONTINUE
      DO 23 K=1,NZ-1
      DO 23 J=1,NT-1
      DO 23 I=1,NR
      UD(I,J,K)=0.
   23 CONTINUE
      DO 24 K=1,NZ-1
      DO 24 J=1,NT
       DO 24 I=1,NR-1
      VD(I,J,K)=0.
   24 CONTINUE
      IT=0
      NIT=500
      GO TO 32
   31 CONTINUE
      REWIND 3
      READ(3)SR
      READ(3)ST
      READ(3)SZ
      READ(3)TRT
      READ(3)TRZ
      READ(3)TZT
      READ(3)UD
      READ(3)VD
      READ(3)WD
      READ(3)W
      READ(3)IT
      READ(3)NIT
      REWIND 3
   32 CONTINUE
  200 IT=IT+1
      SUMSQ=0.
      UDSQ=0.
      VDSQ=0.
      WDSQ=0.
C CALCULATE VELOCITY IN RADIAL DIRECTION
```

```
      DO 4 K=1,NZ-1
      DO 4 J=1,NT-1
      DO 4 I=1,NR
      IF(I.EQ.1)GO TO 4
      IF(I.LE.10 AND.I.GE.6.AND.J.LE.2)GO TO 4
      R=DELR*(I-1)
      IF(I.EQ.2)GO TO 45
      IF(I.EQ.11.AND.J.LE.2)GO TO 45
      IF(I.EQ.NR)GO TO 46
      IF(I.EQ.5.AND.J.LE.2)GO TO 46
      UD(I,J,K)=UD(I,J,K)*D1+D5*(SR(I,J,K)-SR(I-1,J,K))
     1+D6*(TRT(I,J+1,K)-TRT(I,J,K))/R+D7*(TRZ(I,J,K+1)-TRZ(I,J,K))
     1+D4*(SR(I,J,K)+SR(I-1,J,K)-(ST(I,J,K)+ST(I-1,J,K)))/2./R
      GO TO 44
   45 UD(I,J,K)=UD(I,J,K)*D1+2.*D5*SR(I,J,K)
     1-.5*(3.*ST(I,J,K)-ST(I+1,J,K))*D4/R
      GO TO 44
   46 UD(I,J,K)=UD(I,J,K)*D1-2.*D5*SR(I-1,J,K)
     1-.5*(3.*ST(I-1,J,K)-ST(I-2,J,K))*D4/R
   44 UDSQ=UDSQ+UD(I,J,K)*UD(I,J,K)
    4 CONTINUE
C CALCULATE VELOCITY IN TANGENTIAL DIRECTION
      DO 6 K=1,NZ-1
      DO 6 J=1,NT
      DO 6 I=1,NR-1
      IF(J.EQ.1.OR.J.EQ.NT)GO TO 6
      IF(I.EQ.1)GO TO 6
      IF(I.LE.10.AND.I.GE.5.AND.J.EQ.2)GO TO 6
      R=DELR*(I-1)+DELR/2.
      IF(I.LE.10.AND.I.GE.5.AND.J.EQ.3)GO TO 67
      VD(I,J,K)=VD(I,J,K)*D2+D9*(TRT(I+1,J,K)-TRT(I,J,K))
     1+D10*(ST(I,J,K)-ST(I,J-1,K))/R+D11*(TZT(I,J,K+1)-TZT(I,J,K))
     1+D8*(TRT(I+1,J,K)+TRT(I,J,K))/R
      GO TO 66
   67 VD(I,J,K)=VD(I,J,K)*D2+2.*D10*ST(I,J,K)/R
   66 VDSQ=VDSQ+VD(I,J,K)*VD(I,J,K)
    6 CONTINUE
C CALCULATE VELOCITY IN AXIAL DIRECTION
      DO 8 K=1,NZ
      DO 8 J=1,NT-1
      DO 8 I=1,NR-1
      IF(I.EQ.1)GO TO 8
      IF(I.LE.10.AND.I.GE.5.AND.J.LE.2)GO TO 8
      IF(I.EQ.15.AND.K.EQ.NZ)GO TO 8
      IF(K.EQ.1)WD(I,J,K)=WD(I,J,K)*D3+2.*D15*SZ(I,J,K)-2.*P*D15
      IF(K.EQ.1)GO TO 89
      IF(K.EQ.NZ)WD(I,J,K)=WD(I,J,K)*D3-2.*SZ(I,J,K-1)*D15
      IF(K.EQ.NZ)GO TO 88
      R=DELR*(I-1)+DELR/2.
      WD(I,J,K)=WD(I,J,K)*D3+D13*(TRZ(I+1,J,K)-TRZ(I,J,K))
     1+D14*(TZT(I,J+1,K)-TZT(I,J,K))/R+D15*(SZ(I,J,K)-SZ(I,J,K-1))
     1+D12*(TRZ(I+1,J,K)+TRZ(I,J,K))/2./R
      GO TO 89
   88 W(I,J)=W(I,J)+WD(I,J,K)*DELT
   89 WDSQ=WDSQ+WD(I,J,K)*WD(I,J,K)
    8 CONTINUE
      SUMSQ=UDSQ+VDSQ+WDSQ
C CALCULATE NORMAL STRESSES
```

```
      DO 10 K=1,NZ-1
      DO 10 J=1,NT-1
      DO 10 I=1,NR-1
      IF(I.EQ.1)GO TO 10
      IF(I.LE.10.AND.I.GE.5.AND.J.LE.2)GO TO 10
      R=DELR*(I-1)+DELR/2.
C CALCULATE RADIAL STRESS
      SR(I,J,K)=SR(I,J,K)+D17*(UD(I+1,J,K)-UD(I,J,K))
     1+D20*(UD(I+1,J,K)+UD(I,J,K))/2./R
     1+D22*(VD(I,J+1,K)-VD(I,J,K))/R+D23*(WD(I,J,K+1)-WD(I,J,K))
C CALCULATE TANGENTIAL STRESS
      ST(I,J,K)=ST(I,J,K)+D21*(UD(I+1,J,K)-UD(I,J,K))
     1+D18*(VD(I,J+1,K)-VD(I,J,K))/R+D23*(WD(I,J,K+1)-WD(I,J,K))
     1+D16*(UD(I+1,J,K)+UD(I,J,K))/2./R
C CALCULATE AXIAL STRESS
      SZ(I,J,K)=SZ(I,J,K)+D21*(UD(I+1,J,K)-UD(I,J,K))
     1+D20*(UD(I+1,J,K)+UD(I,J,K))/2./R
     1+D22*(VD(I,J+1,K)-VD(I,J,K))/R+D19*(WD(I,J,K+1)-WD(I,J,K))
   10 CONTINUE
C CALCULATE SHEAR STRESS ON RZ PLANE TRT
      DO 16 K=1,NZ
      DO 16 J=1,NT
      DO 16 I=1,NR
      IF(I.EQ.2)GO TO 16
      IF(I.EQ.1.OR.I.EQ.NR.OR.J.EQ.1.OR.J.EQ.NT.OR.K.EQ.NZ)GO TO 16
      IF(I.LE.11.AND.I.GE.5.AND.J.LE.3)GO TO 16
      R=DELR*(I-1)
      TRT(I,J,K)=TRT(I,J,K)+D26*(UD(I,J,K)-UD(I,J-1,K))/R
     1-D24*(VD(I,J,K)+VD(I-1,J,K))/2./R+D25*(VD(I,J,K)-VD(I-1,J,K))
   16 CONTINUE
C CALCULATE SHEAR STRESS TRZ
      DO 18 K=1,NZ
      DO 18 J=1,NT
      DO 18 I=1,NR
      IF(I.EQ.2)GO TO 18
      IF(I.EQ.1.OR.I.EQ.NR.OR.K.EQ.1.OR.K.EQ.NZ.OR.J.EQ.NT)GO TO 18
      IF(I.LE.11.AND.I.GE.5.AND.J.LE.2)GO TO 18
      TRZ(I,J,K)=TRZ(I,J,K)+D27*(UD(I,J,K)-UD(I,J,K-1))
     1+D25*(WD(I,J,K)-WD(I-1,J,K))
   18 CONTINUE
C CALCULATE TZT
      DO 20 K=1,NZ
      DO 20 J=1,NT
      DO 20 I=1,NR
      IF(I.EQ.1)GO TO 20
      IF(K.EQ.1.OR.K.EQ.NZ.OR.I.EQ.NR.OR.J.EQ.1.OR.J.EQ.NT)GO TO 20
      IF(I.LE.10.AND.I.GE.5.AND.J.LE.3)GO TO 20
      R=DELR*(I-1)+DELR/2.
      TZT(I,J,K)=TZT(I,J,K)+D27*(VD(I,J,K)-VD(I,J,K-1))
     1+D26*(WD(I,J,K)-WD(I,J-1,K))/R
   20 CONTINUE
      WRITE(2,102)IT,SUMSQ,UDSQ,VDSQ,WDSQ,W(2,3),SR(5,4,1),
     1ST(5,4,1),SZ(5,4,1),TRT(5,4,1)
      IF(IT-NIT)200,21,21
   21 NIT=NIT+500
      WRITE(2,103)
      WRITE(2,115)SR
      WRITE(2,104)
      WRITE(2,115)ST
      WRITE(2,105)
      WRITE(2,115)SZ
      WRITE(2,106)
      WRITE(2,118)TRT
      WRITE(2,107)
      WRITE(2,118)TRZ
      WRITE(2,108)
      WRITE(2,118)TZT
      WRITE(2,111)
```

```
      WRITE(2,115)W
      REWIND 4
      WRITE(4)SR
      WRITE(4)ST
      WRITE(4)SZ
      WRITE(4)TRT
      WRITE(4)TRZ
      WRITE(4)TZT
      WRITE(4)UD
      WRITE(4)VD
      WRITE(4)WD
      WRITE(4)U
      WRITE(4)IT
      WRITE(4)NIT
      REWIND 4
      CALL ITIME (N2)
      ITIM=N2-N1
      WRITE(2,119)ITIM
      STOP
  100 FORMAT(1X,6E12.4,/)
  101 FORMAT(7E12.3)
  102 FORMAT(I5,2X,9E12.3)
  103 FORMAT(///,16H   RADIAL STRESS,/)
  104 FORMAT(///,20H   TANGENTIAL STRESS,/)
  105 FORMAT(///,15H   AXIAL STRESS,/)
  106 FORMAT(///,27H   SHEAR STRESS R-THETA,/)
  107 FORMAT(///,19H   SHEAR STRESS R-Z,/)
  108 FORMAT(///,27H   SHEAR STRESS Z-THETA,/)
  111 FORMAT(///,21H   AXIAL DISPLACEMENT,/)
  115 FORMAT(1X,9E12.4)
  116 FORMAT(E12.4)
  118 FORMAT(1X,9E12.4)
  119 FORMAT(//,2X,7H  TIME ,I6)
      END

, LENGTH  2476, NAME  FLAMEPLATETHERMALSTRESS
```

```
      MASTER FLAME PLATE COMBINED STRESS ELASTIC FOUNDATION
      DIMENSION SR(15,5,4),ST(15,5,4),SZ(15,5,4),
     1TRT(16,6,5),TRZ(16,6,5),TZT(16,6,5),
     1UD(16,5,4),VD(15,6,4),WD(15,5,5),
     1W(15,5),FP(15,5)
      CALL ITIME (N1)
      NR=16
      NT=6
      NZ=5
      DKR=.04
      DKT=.04
      DKZ=.04
      EM=30.E06
      WRITE(2,120)EM
      DELR=.630
      DELTH=3.14159/20.0
      DELZ=.375
      CLAM=17.3E06
      CMU=11.5E06
      AL=.65E-5
      RR=.732E-3
      RT=.732E-3
      RA=.732E-3
      WRITE(2,100)CLAM,CMU,RR,RT,RA,AL
      READ(1,116)DELT
  501 CONTINUE
      WRITE(2,101)DKR,DKT,DKZ,DELR,DELTH,DELZ,DELT
      P=-1500.
      WRITE(2,121)P
      D1=(1.-DKR/2 )/(1.+DKR/2.)
      D2=(1.-DKT/2 )/(1.+DKT/2.)
      D3=(1.-DKZ/2.)/(1.+DKZ/2.)
      D4=DELT/RR/(1.+DKR/2.)
      D5=D4/DELR
      D6=D4/DELTH
      D7=D4/DELZ
      D8=DELT/RT/(1.+DKT/2.)
      D9=D8/DELR
      D10=D8/DELTH
      D11=D8/DELZ
      D12=DELT/RA/(1.+DKZ/2.)
      D13=D12/DELR
      D14=D12/DELTH
      D15=D12/DELZ
      D16=(CLAM+2.*CMU)*DELT
      D17=D16/DELR
      D18=D16/DELTH
      D19=D16/DELZ
      D20=CLAM*DELT
      D21=D20/DELR
      D22=D20/DELTH
      D23=D20/DELZ
      D24=CMU*DELT
      D25=D24/DELR
      D26=D24/DELTH
      D27=D24/DELZ
C     INITIAL CONDITIONS
      M=1
      IF(M)30,30,31
   30 CONTINUE
      REWIND 3
      READ(3)SR
      REWIND 3
```

```
      DO 1 K=1,NZ-1
      DO 1 J=1,NT-1
      DO 1 I=1,NR-1
      ST(I,J,K)=SR(I,J,K)
      SZ(I,J,K)=SR(I,J,K)
    1 CONTINUE
      DO 2 K=1,NZ
      DO 2 J=1,NT
      DO 2 I=1,NR
      TRT(I,J,K)=0.
      TRZ(I,J,K)=0
      TZT(I,J,K)=0.
    2 CONTINUE
      DO 22 K=1,NZ
      DO 22 J=1,NT-1
      DO 22 I=1,NR-1
      WD(I,J,K)=0.
      W(I,J)=0.0
   22 CONTINUE
      DO 23 K=1,NZ-1
      DO 23 J=1,NT-1
      DO 23 I=1,NR
      UD(I,J,K)=0.
   23 CONTINUE
      DO 24 K=1,NZ-1
      DO 24 J=1,NT
      DO 24 I=1,NR-1
      VD(I,J,K)=0.
   24 CONTINUE
      IT=0
      NIT=500
      GO TO 32
   31 CONTINUE
      REWIND 3
      READ(3)SR
      READ(3)ST
      READ(3)SZ
      READ(3)TRT
      READ(3)TRZ
      READ(3)TZT
      READ(3)UD
      READ(3)VD
      READ(3)WD
      READ(3)W
      READ(3)IT
      READ(3)NIT
      REWIND 3
      NIT=1500
   32 CONTINUE
  200 IT=IT+1
      SUMSQ=0.
      UDSQ=0.
      VDSQ=0.
      WDSQ=0.
C CALCULATE VELOCITY IN RADIAL DIRECTION
      DO 4 K=1,NZ-1
      DO 4 J=1,NT-1
      DO 4 I=1,NR
      IF(I.EQ.1)GO TO 4
      IF(I.LE.10.AND.I.GE.6.AND.J.LE.2)GO TO 4
      R=DELR*(I-1)
      IF(I.EQ.2)GO TO 45
      IF(I.EQ.11.AND.J.LE.2)GO TO 45
```

```
      IF(I.EQ.NR)GO TO 46
      IF(I.EQ.5.AND.J.LE.2)GO TO 46
      UD(I,J,K)=UD(I,J,K)*D1+D5*(SR(I,J,K)-SR(I-1,J,K))
     1+D6*(TRT(I,J+1,K)-TRT(I,J,K))/R+D7*(TRZ(I,J,K+1)-TRZ(I,J,K))
     1+D4*(SR(I,J,K)+SR(I-1,J,K)-(ST(I,J,K)+ST(I-1,J,K)))/2./R
      GO TO 44
   45 UD(I,J,K)=UD(I,J,K)*D1+2.*D5*SR(I,J,K)
     1-.5*(3.*ST(I,J,K)-ST(I+1,J,K))*D4/R
      GO TO 44
   46 UD(I,J,K)=UD(I,J,K)*D1-2.*D5*SR(I-1,J,K)
     1-.5*(3.*ST(I-1,J,K)-ST(I-2,J,K))*D4/R
   44 UDSQ=UDSQ+UD(I,J,K)*UD(I,J,K)
    4 CONTINUE
C CALCULATE VELOCITY IN TANGENTIAL DIRECTION
      DO 6 K=1,NZ-1
      DO 6 J=1,NT
      DO 6 I=1,NR-1
      IF(J.EQ.1.OR.J.EQ.NT)GO TO 6
      IF(I.EQ.1)GO TO 6
      IF(I.LE.10.AND.I.GE.5.AND.J.EQ.2)GO TO 6
      R=DELR*(I-1)+DELR/2.
      IF(I.LE.10.AND.I.GE.5.AND.J.EQ.3)GO TO 67
      VD(I,J,K)=VD(I,J,K)*D2+D9*(TRT(I+1,J,K)-TRT(I,J,K))
     1+D10*(ST(I,J,K)-ST(I,J-1,K))/R+D11*(TZT(I,J,K+1)-TZT(I,J,K))
     1+D8*(TRT(I+1,J,K)+TRT(I,J,K))/R
      GO TO 66
   67 VD(I,J,K)=VD(I,J,K)*D2+2.*D10*ST(I,J,K)/R
   66 VDSQ=VDSQ+VD(I,J,K)*VD(I,J,K)
    6 CONTINUE
C CALCULATE VELOCITY IN AXIAL DIRECTION
      DO 8 K=1,NZ
      DO 8 J=1,NT-1
      DO 8 I=1,NR-1
      IF(I.EQ.1)GO TO 8
      IF(I.LE.10.AND.I.GE.5.AND.J.LE.2)GO TO 8
      IF(I.EQ.14.AND.K.EQ.1)WD(I,J,K)=WD(I,J,K)*D3+2.*D15*BZ(I,J,K)
      IF(I.EQ.14.AND.K.EQ.1)GO TO 8
      IF(I.EQ.15.AND.K.EQ.1)WD(I,J,K)=WD(I,J,K)*D3+2.*D13*BZ(I,J,K)
      IF(I.EQ.15.AND.K.EQ.1)GO TO 8
      IF(I.EQ.15.AND.K.EQ.NZ)GO TO 8
      IF(K.EQ.1)WD(I,J,K)=WD(I,J,K)*D3+2.*D15*(SZ(I,J,K)-P)
      IF(K.EQ.1)GO TO 89
      IF(W(I,J).GT.0.0)FP(I,J)=-W(I,J)*FM
      IF(W(I,J).LE.0.0)FP(I,J)=0.0
      IF(K.EQ.NZ)WD(I,J,K)=WD(I,J,K)*D3-2.*SZ(I,J,K-1)*D15
     1+2.*FP(I,J)*D15
      IF(K.EQ.NZ)GO TO 88
      R=DELR*(I-1)+DELR/2.
      WD(I,J,K)=WD(I,J,K)*D3+D13*(TRZ(I+1,J,K)-TRZ(I,J,K))
     1+D14*(TZT(I,J+1,K)-TZT(I,J,K))/R+D15*(SZ(I,J,K)-SZ(I,J,K-1))
     1+D12*(TRZ(I+1,J,K)+TRZ(I,J,K))/2./R
      GO TO 89
   88 W(I,J)=W(I,J)+WD(I,J,K)*DELT
   89 WDSQ=WDSQ+WD(I,J,K)*WD(I,J,K)
```

```
    8 CONTINUE
      SUMSQ=UDSQ+VDSQ+WDSQ
C CALCULATE NORMAL STRESSES
      DO 10 K=1,NZ-1
      DO 10 J=1,NT-1
      DO 10 I=1,NR-1
      IF(I.EQ.1)GO TO 10
      IF(I.LE.10.AND.I.GE.5.AND.J.LE.2)GO TO 10
      R=DELR*(I-1)+DELR/2.
C CALCULATE RADIAL STRESS
      SR(I,J,K)=SR(I,J,K)+D17*(UD(I+1,J,K)-UD(I,J,K))
     1+D20*(UD(I+1,J,K)+UD(I,J,K))/2./R
     1+D22*(VD(I,J+1,K)-VD(I,J,K))/R+D23*(WD(I,J,K+1)-WD(I,J,K))
C CALCULATE TANGENTIAL STRESS
      ST(I,J,K)=ST(I,J,K)+D21*(UD(I+1,J,K)-UD(I,J,K))
     1+D18*(VD(I,J+1,K)-VD(I,J,K))/R+D23*(WD(I,J,K+1)-WD(I,J,K))
     1+D16*(UD(I+1,J,K)+UD(I,J,K))/2./R
C CALCULATE AXIAL STRESS
      SZ(I,J,K)=SZ(I,J,K)+D21*(UD(I+1,J,K)-UD(I,J,K))
     1+D20*(UD(I+1,J,K)+UD(I,J,K))/2./R
     1+D22*(VD(I,J+1,K)-VD(I,J,K))/R+D19*(WD(I,J,K+1)-WD(I,J,K))
   10 CONTINUE
C CALCULATE SHEAR STRESS ON RZ PLANE TRT
      DO 16 K=1,NZ
      DO 16 J=1,NT
      DO 16 I=1,NR
      IF(I.EQ.2)GO TO 16
      IF(I.EQ.1.OR.I.EQ.NR.OR.J.EQ.1.OR.J.EQ.NT.OR.K.EQ.NZ)GO TO 16
      IF(I.LE.11.AND.I.GE.5.AND.J.LE.3)GO TO 16
      R=DELR*(I-1)
      TRT(I,J,K)=TRT(I,J,K)+D26*(UD(I,J,K)-UD(I,J-1,K))/R
     1-D24*(VD(I,J,K)+VD(I-1,J,K))/2./R+D25*(VD(I,J,K)-VD(I-1,J,K))
   16 CONTINUE
C CALCULATE SHEAR STRESS TRZ
      DO 18 K=1,NZ
      DO 18 J=1,NT
      DO 18 I=1,NR
      IF(I.EQ.2)GO TO 18
      IF(I.EQ.1.OR.I.EQ.NR.OR.K.EQ.1.OR.K.EQ.NZ.OR.J.EQ.NT)GO TO 18
      IF(I.LE.11.AND.I.GE.5.AND.J.LE.2)GO TO 18
      TRZ(I,J,K)=TRZ(I,J,K)+D27*(UD(I,J,K)-UD(I,J,K-1))
     1+D25*(UD(I,J,K)-WD(I-1,J,K))
   18 CONTINUE
C CALCULATE TZT
      DO 20 K=1,NZ
      DO 20 J=1,NT
      DO 20 I=1,NR
      IF(I.EQ.1)GO TO 20
```

```
      IF(K.EQ.1.OR.K.EQ.NZ.OR.I.EQ.NR.OR.J.EQ.1.OR.J.EQ.NT)GO TO 20
      IF(I.LE.10.AND.I.GE.5.AND.J.LE.3)GO TO 20
      R=DELR*(I-1)+DELR/2.
      TZT(I,J,K)=TZT(I,J,K)+D27*(VD(I,J,K)-VD(I,J,K-1))
     1+D26*(WD(I,J,K)-WD(I,J-1,K))/R
   20 CONTINUE
      WRITE(2,102)IT,SUMSQ,UDSQ,VDSQ,WDSQ,W(2,3),SR(5,4,1),
     1ST(5,4,1),SZ(5,4,1),TRT(5,4,1)
      IF(IT-NIT)200,21,21
   21 NIT=NIT+500
      WRITE(2,103)
      WRITE(2,115)SR
      WRITE(2,104)
      WRITE(2,115)ST
      WRITE(2,105)
      WRITE(2,115)SZ
      WRITE(2,106)
      WRITE(2,118)TRT
      WRITE(2,107)
      WRITE(2,118)TRZ
      WRITE(2,108)
      WRITE(2,118)TZT
      WRITE(2,111)
      WRITE(2,115)W
      REWIND 4
      WRITE(4)SR
      WRITE(4)ST
      WRITE(4)SZ
      WRITE(4)TRT
      WRITE(4)TRZ
      WRITE(4)TZT
      WRITE(4)UD
      WRITE(4)VD
      WRITE(4)WD
      WRITE(4)W
      WRITE(4)IT
      WRITE(4)NIT
      WRITE(4)FP
      REWIND 4
      WRITE(2,122)
      WRITE(2,113)FP
      CALL ITIME (N2)
      ITIM=N2-N1
      WRITE(2,119)ITIM
      STOP
  100 FORMAT(1X,6E12.4,/)
  101 FORMAT(7E12.3)
  102 FORMAT(I5,2X,9E12.3)
  103 FORMAT(///,16H   RADIAL STRESS,/)
  104 FORMAT(///,20H  TANGENTIAL STRESS,/)
  105 FORMAT(///,15H   AXIAL STRESS,/)
  106 FORMAT(///,23H   SHEAR STRESS R-THETA,/)
  107 FORMAT(///,19H  SHEAR STRESS R-Z,/)
  108 FORMAT(///,23H  SHEAR STRESS Z-THETA,/)
  111 FORMAT(///,21H   AXIAL DISPLACEMENT,/)
  115 FORMAT(1X,9E12.4)
  116 FORMAT(E12.4)
  118 FORMAT(1X,9E12.4)
  119 FORMAT(//,2X,7H TIME=,I6)
  120 FORMAT(2X,19HFOUNDATION MODULUS=,E12.4)
  121 FORMAT(2X,23HENGINE FIRING PRESSURE=,E12.4)
  122 FORMAT(//,2X,19HFOUNDATION PRESSURE,//)
      END
```